THE INFLUENCE OF THE INTERACTION OF CARBON BASED MATERIALS WITH

IONIC LIQUID ON THE TRIBOLOGICAL PERFORMANCE OF LUBRICATING GREASE

AND OIL

by

KIMAYA VYAVHARE

Presented to the Faculty of the Graduate School of

The University of Texas at Arlington in Partial Fulfillment

of the Requirements

for the Degree of

MASTER OF SCIENCE IN MATERIALS SCIENCE AND ENGINEERING

THE UNIVERSITY OF TEXAS AT ARLINGTON

December 2016

Acknowledgment

Abstract

THE INFLUENCE OF THE INTERACTION OF CARBON MATERIALS AND IONIC

LIQUIDS ON THE TRIBOLOGICAL PERFORMANCE OF LUBRICATING OIL AND

GREASE

Kimaya Vyavhare, MS

The University of Texas at Arlington, 2016

Supervising Professor: Pranesh B. Aswath

Stringent government regulation on environment emissions and demand to develop energy efficient and durable modern mechanical systems has imposed a significant challenge on the lubricant additive manufacturer to develop environment friendly and high performance additives for the lubricating medias like oil and grease. The current industrial additive technology is dominated by phosphorus and sulfur containing the liquid antiwear additive, Zinc dialkyl dithiophosphate and extreme pressure solid additives like Graphite, Molybdenum disulfide. This current additive package possesses harm to the environment and has already met performance limit for applications working under severe operating condition. A proposed solution to combat with this problem is the use of ionic liquid as the next generation green lubricant additive. The unique properties of the ionic liquids such as negligible volatility, nonflammability, and high thermal stability make them potential candidate as an antiwear additive. Also, with the advent of nanotechnology, nanoparticles have recognized considerable attention as solid additives in lubricating oils and greases.

In this research study, the nature of the interaction between ionic liquids and carbonaceous materials like carbon nanotube and soot is considered and is correlated with the tribological performance of the lubricating media, engine oil, and grease. This thesis work is divided into two

main section, first section deals with the tribological performance of the combined solid and liquid additive chemistry of multi-walled carbon nanotube (MWCNT) and ionic liquid in lithium lubricating greases, while, the second section is about evaluating the potential of ionic liquid in minimizing the detrimental effect of the increased soot contamination in the engine oil.

As an attempt to study the interaction of MWCNT and ionic liquids, the first approach was to determine the optimal concentration of MWCNT as an antiwear additive in lithium based grease is investigated by analyzing the friction and wear results generated during four ball standard ASTM D2266 test. The results indicate the MWCNTs at optimal concentration of 1wt% decreases the wear by 25% and friction by 39%. Secondly, the antiwear and antifriction performance of the four different ionic liquids in lithium grease was investigated. The excellent antiwear property of the ionic liquid is attributed to the formation of protective phosphate tribofilms on the interacting surfaces. In addition, ionic liquids were blended with the MWCNT to study the synergism between novel solid-liquid combined chemistry. The addition of hydroxyl functionalized MWCNT at 1wt% with the ionic liquid having phosphonium cation and dithiophosphate anion results in the comparable tribological behavior to the grease blends with the MWCNT and ionic liquid alone.

Second Section of the thesis describes the influence of the increased soot contamination on the diesel engine wear. First, the abrasive nature of the soot was examined by using X-ray absorption near edge spectroscopy and high temperature X-ray diffraction. Then the oil formulations were prepared by dispersing the diesel engine soot with three different antiwear additives, namely, ashed Zinc dialkyldithiophosphate, ashless alkyl dithiophospahte and an ionic liquid. The soot concentration at 10wt% exhibits the extremely high wear in the presence of all the three additives. The soot abrades the protective tribofilms formed by antiwear additives and results in sever wear.

Table of Contents

List of Illustrations

List of Tables

1. Introduction

The lubrication industry is striving hard to keep up with the growing demand of increase in the efficiency and durability of the modern machineries. For any machine to operate smoothly, some energy must be provided for the sole purpose of overcoming friction. Minimizing energy loss through friction increases the efficiency of machines. Recent studies have indicated that advances in tribology could lead to savings of approximately 11% of total annual energy loss in three major areas: power generation, transportation, and industrial processes [1]. Therefore, in the context of energy efficiency, an effective lubrication is very crucial in reducing the friction and wear.

Lubricant additives have an important influence on the performance of lubricants. Additives are required to enhance or impart a required operational capability to a specific lubricating media (oil/grease), which is not provided by the base fluid alone. The increased demand for improved fuel economy and the need for enhanced durability has compelled the lubricant additive manufacturers to develop new lubricant additives capable of overcoming the performance limit of the existing lubricant additives. In addition to this, industry is also facing increasingly rigorous environmental regulations. As the use of traditional organic lubricant additives that contain P, S and Cl elements possess harm to the environment and human health, the research for the novel lubricant additives with good tribological properties and low environmental impact becomes very important [2].

Recently, ionic liquids have gained considerable attention as the "green solvents". Ionic liquids (ILs) are salts with a melting point lower than room temperature. Ionic liquids have some unique characteristics including negligible volatility, non-flammability, high thermal stability, low melting point, broad liquid range, and controlled miscibility with organic compounds, which are highly desirable for tribological applications. Many authors have proposed the applications of ionic liquids as lubricants/lubricant additives [3,4,5,6]. Recent progress in ionic liquid lubrication is being made in three directions: tailoring the molecular structures to achieve good miscibility in non-polar

oils [7,8,9], investigating the tribochemical interactions between ionic liquids and contact surfaces to understand the lubricating mechanism [10,11,12], and using ionic liquids to modify the surface of nanostructured materials to obtain synergistic effect [13,14].

The present quest for the design of novel and superior lubricant additives has expanded the realms of research towards the use of nanoparticles or nanomaterials as the additive in lubricating media like oil or grease. Instead of traditional materials, new nanomaterials and nanoparticles have been recently under investigation as lubricants or lubricant additives because of their unusual properties. In literature, a variety of nanoparticles have been used as lubricant additives with potentially interesting friction and wear properties. Carbon based nanomaterials family is one of them. All carbon based materials have demonstrated the ability to reduce the adhesion and friction under the dry and lubrication condition. Carbon based material such as graphite is the dominant friction modifier for the high temperature applications since many decades. Other similar carbon-based materials are the newest durable lubricant. Carbon nanotubes (CNTs) are presently being investigated for lubrication applications. Due to superior physical and mechanical properties, carbon nanotubes have found its place in many critical applications. Due to its tubular structures and higher mechanical properties it can be predicted that CNTs may work as rolling bearings without getting broken between two mating parts which may reduce the frictional coefficient and increase the load bearing capacity of the CNT based lubricant. The CNTs are still in the early stages of development in the field of tribology, and it will be some time before practical tribological usage is realized. Tribology applications may emerge that can take full advantage of intrinsic structures and properties of carbon-based nanomaterials and films in such areas as solid films for dry lubrication, additives for liquid lubricants and composites for wear parts [15].

CNTs have a strong tendency to aggregate because of their nanosize and respective high surface energy, which greatly limits their uniform dispersion in the lubricant. Recent studies have shown the ability of amphiphilic characteristic of ionic liquid can minimize this problem by

dispersing and chemically modifying carbon nanotubes [16,17,18]. It is proposed that ionic liquid interacts with CNTs through weak van der Waals interaction and shields the stacking interaction among themselves [19]. It is important to note that these studies have been focused on the application of covalently modified CNTs as additives in ionic liquid and thermoplastics. Also, the most of single walled and multi-walled carbon nanotubes studies were performed in oil soluble single phase system. As per authors knowledge, systematic information on the optimal concentration of the multi-walled carbon nanotube (MWCNT) as an antiwear and extreme pressure additive in the lubricating grease is not available. Also, no information is reported on the effect of the MWCNT-ionic liquid combination for antiwear and extreme pressure characteristics in the grease.

This thesis work focusses on evaluating the potential of multi-walled carbon nanotube as antiwear and extreme pressure additive in lithium based lubricating grease. It also deals with the understanding the nature of the MWCNT-ionic liquid interaction in the grease.

1.1 Motivation

A lubricating grease is a semi-fluid to solid product of a dispersion of a thickener in a liquid lubricant Dripping and spattering are nearly eliminated. The principal advantage of choosing grease over conventional lubricating oil in certain applications is the grease's ability to remain in contact with the desired moving surfaces. Greases will generally not leak away from the point of application. Thickeners in the grease are designed to reduce any migration caused by gravity, pressure, or centrifugal action. Lubricating greases are subjected to harsh operating conditions like high- low temperature, high-low speed, etc. The additive package of grease normally consists of oxidation stabilizer, corrosion inhibitor, friction modifier and extreme pressure/antiwear additives. Rigorous operating conditions demands to the development of advanced lubricant additives with the comparable or better performance than the conventional MoS_2, graphite and PTFE additives. In recent years, nano-sized materials have emerged as a new alternative to the existing solid lubricant

additives. There have been many investigations on the addition of nanoparticles with the typical size in the range of 2–120 nm to lubricants as friction modifiers for efficiently reducing friction and wear. In particular, nanoparticles based on carbon compound, metal, metal oxide, metal sulfide, metal borate, metal carbonate, rare earth compound and SiO2 have been investigated. The antifriction and antiwear properties of the solid nano-materials have been attributed to the mechanisms like mending effect, rolling effect, ball bearing effect, colloidal effect, protective film, and third body material transfer. The major drawback of solid nanomaterial lubricant additives, the intrinsic poor stability in liquid base lubricant systems, has considerably restrained them from applications [20].

The short comings of the solid lubricant additives can be overcome by their liquid counterparts, however, much tighter emission control strategies and environmental mandates imposed by various government agencies have been discouraging the use of certain types of liquid additives like zinc dialkyldithiophosphates. The new developed ashless environment friendly additives also failed to meet the desired tribological performance under some severe environment. Overall, it looks like in near future, experts in the solid and lubrication fields will have to work together to bridge the gap that exists between these two-lubrication media and come up with novel solid-liquid formulations that can safely meet the increasingly harsher application conditions that will be demanded by the future mechanical systems. In short, combining the potentials of solid and liquid lubricants in one package sounds like the most logical next step for achieving better performance and efficiency in future tribological systems.

1.2 Objective

Nano-additives open new ways to maximizing lubricant performance. For tribology applications, nanoparticles as additives in base oil have been investigated [21,22]. These studies refer to synthesis and preparation of nanoscale particles, and their tribological properties and

mechanisms. It has been found that when the nanoparticles were added to base oil, the extreme-pressure property and load-carrying capacity were improved and friction coefficient was decreased. The results of these studies indicate that nanoparticles using as lubricating oil additive can improve the tribological properties of base oils.

The main objective of this study is to assess the capability of multi-walled carbon nanotubes (MWCNT) as an antiwear and extreme pressure additive in the lithium lubricating greases under boundary lubrication regime. To achieve this goal, first approach was to find the optimum concentration of the MWCNT additive by performing the extreme pressure ASTM D2266 four ball wear test. The grease blends were formulated by adding the varying concentration of MWCNT in lithium complex grease. The tribological performance of the grease blends were then evaluated by measuring wear scar diameter and coefficient of friction developed during four ball wear test. The morphology and chemistry of the worn surfaces were studied to understand the wear mechanism and lubrication mechanism of the MWCNT. The wear scar analysis was carried out by using scanning electron microscope (SEM) and energy dispersive spectroscopy (EDS).

Second part of this research work involves the study of the antifriction and antiwear property of the ionic liquids in lithium grease. Four different ionic liquids containing phosphorus and sulfur with different cation and anion moieties were used. Diversity in the ionic liquid chemistries enables to examine the influence of different cations, anions and chain length on the wear protection. The grease blends with different ionic liquids were tested under severe boundary lubrication conditions using four ball tribometer. SEM characterization of the wear surfaces helped to understand the wear mechanism taking place in the presence of ionic liquid. The antiwear mechanism of ionic liquids by the formation of tribofilms was studied using EDS elemental spectrum and mapping analysis.

The final approach was to combine the MWCNT and ionic liquids at the optimum concentrations achieved from the previous tests. The combination of solid-liquid was thought to

give bifold benefits. First, the polar nature of the ionic liquid will assist the stability of MWCNT in the lubricant system. Second, the addition of the two different additives having different lubrication mechanism will complement each other and enhance the friction and wear resistance of the lubricating grease. The evaluation of tribological property was carried by using four ball tribometer. The effect of the MWCNT-ionic liquid interaction was further studied by using SEM-EDS characterization of the worn surfaces developed by grease formulations during the tribotest. Hypothesis…..

The most known natural carbon structure is graphite and is used as solid lubricant additive mainly in greases. Graphite has been studied for its tribological properties since 1950 [23]. In the macroscopic scale, the friction coefficient of 0.1 was obtained with graphite, without any other lubricant and even at high temperatures [24]. The excellent low friction characteristic of the graphite is attributed to its unique layered crystal structure. The crystal structure of graphite consists of parallel layers of the condensed C_6 rings as shown in the figure 1.1. Each carbon atom is strongly covalent bonded with the neighboring atom while the parallel layers are pinned through weak van der waals forces. When the graphite particles get adsorbed on the sliding surfaces, the atomic layers in these solids align themselves parallel to the direction of relative motion and slide over one another with relative ease to provide low friction.

Graphite structure
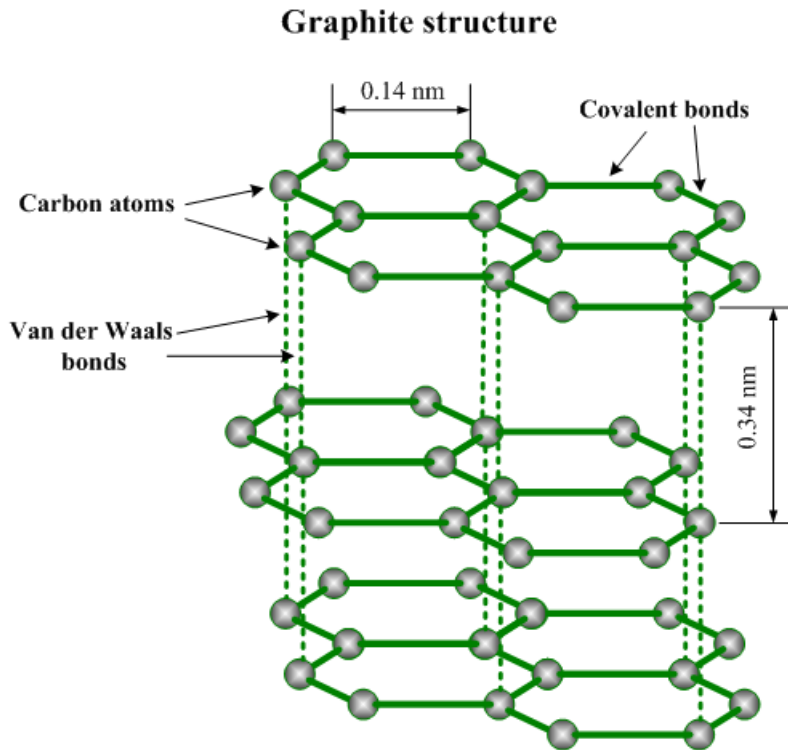
Figure 1.1 Schematic representation of layered lattice structure of graphite. [25]

Author postulate that similar to the graphite, carbon nanotubes (CNTs) has the potential as the extreme pressure solid lubricant additive due to their unique structure. A CNT is often described as a honeycomb lattice rolled into a cylinder. CNTs consist of graphene cylinders closed at either end with caps containing pentagonal rings. They are part of the fullerene family: essentially buckyballs expanded from the center into cylinders. CNTs may be either single- or multiwalled. Both types possess remarkable physical, electronic, and thermal properties. For example, the Young's modulus of single-walled carbon nanotubes lies close to 1 TPa, and the maximum tensile strength is close to 30 GPa [26], with values for multi-walled carbon nanotubes being somewhat less. The precise values depend upon the CNT diameter, length, chirality, and number of walls and

defects. Their intriguing structures have sparked much excitement in recent years, and a large amount of research has been dedicated to understanding them.

It is hypothesized that the carbon nanotubes can act as the third body between the interfacing surfaces under the boundary lubrication condition regime. The high Young's modulus of the carbon nanotube and their unique tubular structure will help them to reduce the frictional resistance through low shearing by either sliding or rolling between the contacting surfaces. In addition to the reduction in coefficient of friction, carbon nanotubes can also increase the load bearing capacity of the lubricant.

1.3 Outline of the Research Work

This thesis is presented in a total of five chapters. Following is a list of the chapters with a brief outline of contents presented.

Chapter 1: This chapter gives the reader a broad overview of the research work carried out. It also highlights the objectives and motivation for the research.

Chapter 2: This is a background chapter and explains in depth all the fundamentals related to tribology and lubrication. It also briefs the additives and chemistries used throughout the research work. It gives information on their background, their known properties and tribological research work on them till date.

Chapter 3: This chapter deals with the evaluation of the tribological performance of the multi-walled carbon nanotubes as the antiwear and extreme pressure additives in the lithium based lubricating greases.

Chapter 4: This chapter involves the examination of the potential of ionic liquids in enhancing the friction and wear resistance of the lithium based lubricating greases.

Chapter 5: This chapter outlines the thorough study carried out in assessing the tribological performance of the lubricating grease containing the combined multi-wall carbon nanotubes and ionic liquid additive mixture.

2. Background

2.1 Introduction to Tribology

Tribology is the science of relative motion. The word tribology comes from the Greek tribos, meaning rubbing. Tribology is the art of applying operational analyses to problems of great economic significance, namely, reliability, maintenance, and wear of technical equipment, ranging from spacecraft to household appliances. Surface interactions in a tribological interface are highly complex, and their understanding requires knowledge of various disciplines, including physics, chemistry, applied mathematics, solid mechanics, fluid mechanics, thermodynamics, heat transfer, materials science, rheology, lubrication, machine design, performance and reliability.

It is the only name which is new but the roots of the tribology concepts come from deep historical background. Early civilizations developed quite sophisticated tribological devices such as potter's wheels, door hinges and wheeled carriages. Military engineers rose to prominence in the days of the Roman Empire by devising both war machinery and methods of fortification using tribological principles. It was the renaissance engineer-artist, Leonardo da Vinci (1452-1519), celebrated engineer, painter, and sculptor, who discovered that the tangential force of friction between moving solid bodies is proportional to the normal force. His notebooks show many designs for moving parts and machines that show a remarkable similarity to those in use today. The coming of the computer age has provided new challenges for tribologists. The interface between the reading head and the magnetic disk in a computer hard disk requires careful design and lubrication to minimize friction and reduce the likelihood of disk crashes and damage.

Tribology comprises the fields of friction, wear and lubrication. It aims at the functional, economic and ecological optimization of motion systems. The implementation of tribological knowledge results in a reduction of wear and an optimization of friction systems. The operational

reliability of machines and installations is increased, production costs are reduced, resources and energy are saved and emissions are decreased.

2.2 Friction

The surfaces of the body are never perfectly smooth. A microscopic image reveals the roughness and irregularities present on even smooth and polished surfaces, such irregularities are called as surface asperities. If a block of one substance is placed over the other, a certain degree of interlocking or touching of the surface asperities takes place. As long as the block is stationary no force is acting on the system. But, whenever, block moves or tends to move tangentially with respect to the bottom, the interlocking property of the minute particles opposes the movement of the upper block. This opposing force is called as the friction force. Figure 2.1 shows the tangential frictional force acting on the bodies in sliding and rolling motion.
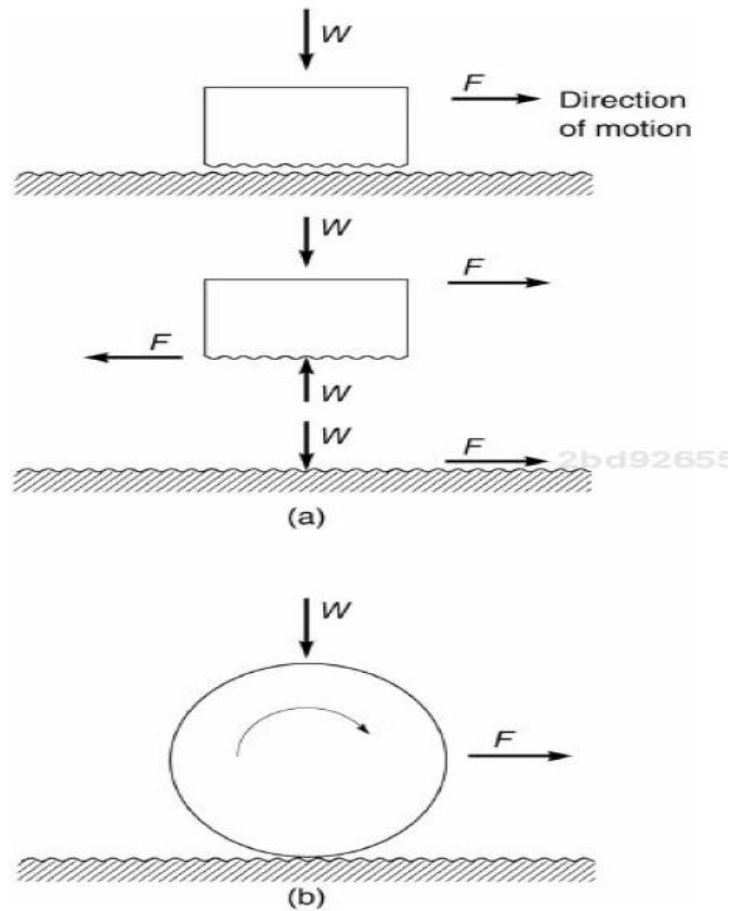
Figure 2-1 Schematic illustration of (a) a body sliding on a surface with a free body diagram (b) a

body rolling on a horizontal surface; W is the normal load (force) and F is the friction force [1].

Friction can be defined as a resisting force that acts tangential to the interface between two bodies when, under the action of external force one body moves or tends to move relative to the other. Also, The ASTM D 996 definition of friction is "resistance to relative motion of two bodies in contact." The force (F) that must be applied to an object to initiate and maintain relative motion is proportional to the applied load (N). The proportionality constant is the coefficient of friction (μ):

$$F = \mu N$$

There are two values reported for the coefficient of friction. The static co-efficient of friction is used in reference to the initial movement of the object from the rest position and is defined by ASTM D 996 as "the ratio of force required to move one surface over another, to the total force applied normal to those surfaces, at the instant motion starts." The kinetic coefficient of friction is used for two surfaces in relative motion and is defined by ASTM D 996 as "the ratio of force required to move one body over another, to the total force applied normal to those surfaces, once that motion is in progress." Types of friction can be further classified as (a) Boundary friction (b) Film friction

2.2.1 Boundary Friction*:

Boundary friction is the type of friction experienced by two rubbing surfaces, when a very thin lubricant film exists between the two surfaces. The thickness of this layer is of the molecular dimension. Boundary friction occurs when a surface is at least partially wet, but not so lubricated that there is no direct friction between two surfaces. When two consistent, unlubricated surfaces slide against each other, there is a specific, predictable amount of friction that occurs. This amount increases as velocity does, but only up to a certain point. That increase generally follows what is known as a Stribeck curve, after Richard Stribeck. On the other hand, if the two surfaces are completely lubricated, there is no direct friction or rubbing at all. In real life, though, there is often a situation where the surfaces are not completely dry, but also not so lubricated that they do not touch. This "boundary friction" produces various effects, like an increase in lubrication through the generation of shearing forces, or an oscillation effect during motion, as the friction increases and decreases. For example, one can experience vibration when trying to break on a partially damp road, or a cold glass that is slowly condensing moisture can be lifted until it spontaneously slides across the surface it is resting on. The boundary friction follows the laws of solid friction:

1. The force of friction is directly proportional to the normal load between surfaces.

2. The force of friction depends upon the material of which the contact surfaces are made.

3. The force of friction is independent of the velocity of sliding of one body relative to the other body.

2.2.2 Fluid Friction

It is the friction experienced between the rubbing surfaces, when the surfaces have a thick layer of the lubricant. In this case, the surfaces do not come in actual contact and thus does not rub against each other. It is thus obvious that fluid friction is not due to the surfaces in contact but it is due to the viscosity and oiliness of the lubricant. Fluid friction follows the laws of fluid friction:

1. The force of friction is almost independent of the load.

2. The force of friction reduces with the increase of the temperature of the lubricant.

3. The force of friction is independent of the substances of the bearing surfaces.

4. The force of friction is different for different lubricants.

2.3 Wear

2.3.1 Introduction

Wear is known as the progressive removal and deformation of material on a surface in a sliding, rolling or impact motion against its counterpart. In most of the cases, wear is not desired, since it may result in shrink in durability of machinery components, reduction of reliability and cost of replacement for failed machinery parts. Therefore, it is of great interest for industry to carry out research on characterizing and minimizing wear.

Like friction, wear is not a material property. Wear of a system depends on many factors, such as working environment, type of motion, speed of motion, load, temperature, contact geometry, properties of the contact surfaces and so on. Wear of a system is independent from the friction performance to some extent. High friction can be companied with little wear, and low friction does not necessarily suggest insignificant wear.

2.3.2 Wear Mechanism

2.3.2.1 Adhesive wear

Adhesive wear occurs when surface asperities come into sliding contact under a load. If sufficient heat is generated, micro welding of the two contacting asperities with subsequent shearing and material transfer will be observed. When two interacting surfaces are not sufficiently lubricated, adhesive transfer or removal of near-surface material may be observed. Surface adhesion is dependent on the nature of the contacting surface. Wear material transfer in this region has been called "solid-phase welding" (also known as the micro and macro-welding process) which occurs at asperity contacts. Smearing and galling are the well-known forms of adhesive wear. Adhesive wear can be reduced by the proper selection of material pairs and sufficient lubrication to provide a protective surface and EHD/micro-EHD film.
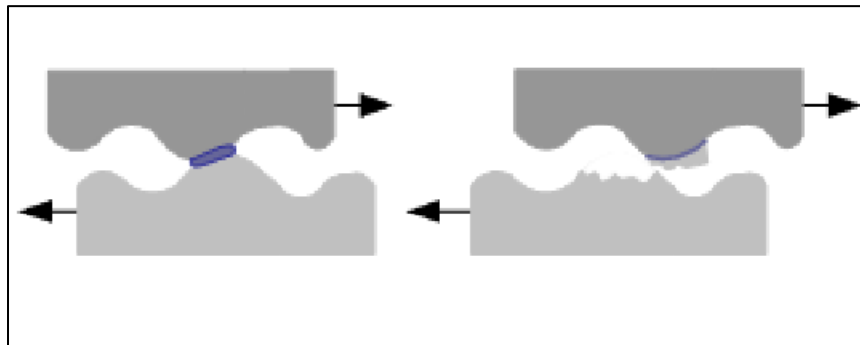
Figure 2-2 Schematic diagram of adhesive wear mechanism [27].

2.3.2.2 Abrasive wear

Abrasive wear refers to the cutting of a metal by a hard particle or a rough surface by a ploughing or microcutting (scratching) mechanism [27]. ASTM G 40 defines spalling as: "the separation of macroscopic particles from a surface in the form of flakes, or chips, usually associated with rolling element bearings and gear teeth, but also resulting from impact events."

The abrasive wear mechanism involves the penetration of a surface by a hard particle that is subsequently embedded into one of the wear surfaces. Abrasive wear occurs when one of the contacting surfaces is harder than the other. The observed wear behavior involves plastic

deformation and material displacement during ploughing or smearing. Ploughing was described in the friction due to ploughing section. This results in surface-initiated fatigue spalling. EHD and micro-EHD films reduce or eliminate local surface plastic flow. When abrasive wear is caused by a hard particle between two surfaces, it is called three-body wear, as illustrated in Figure 2.3. Hard particles causing three-body wear may be introduced into a system from the manufacturing process, generated internally as wear debris, introduced as a contaminant with the lubricant being tested, or possibly by all three introduction mechanisms. Two-body wear is caused by a harder surface with asperity dimensions sufficiently large enough to penetrate the lubricating oil film, causing a ploughing or microcutting (scratching) action on the softer metal surface of the wear contact, which is in relative motion. Although two- and three-body abrasion are sometimes difficult to distinguish visually, embedded particles are indications of three-body abrasion. Also, the amount of wear observed in three-body abrasion is typically one order of magnitude lower than that observed in two-body abrasion [28].
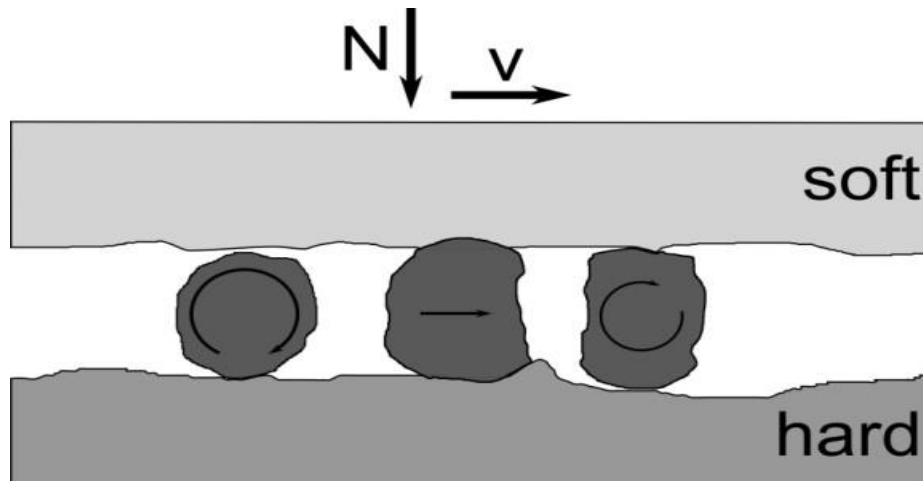
Figure 2-3 Schematic representation of the third-body abrasive wear process. The upper surface slides with a velocity v to the right at a normal force N, causing third bodies to roll or slide and generate local wear to the surfaces [28].

2.3.2.3 Corrosive Wear

Corrosive wear is caused by a removal of layers of materials which are being continually formed on rubbing surfaces by chemical reaction. Corrosive wear takes place when surfaces are slide in a corrosive lubricant system or a lubricant system contains corrosive species such as water, oxygen, carbon dioxide, sulphur and other types of lubricant additives. The reaction product generated from chemical or electrochemical interactions is often weaker than the substrate material. Although the resultant usually prevents or reduces adhesive wear, it can be easily abraded away. As the fresh surface exposes, the reaction continues. Since the chemical reaction is the dominant mechanism for corrosive wear, the wear rate is controlled by the rate of chemical reaction.

2.4.4 Fatigue Wear

As the name suggests, fatigue wear is a type of material failure caused by repeated stress cycles on an asperity contact. The repeated loading and unloading cycles that the materials are experiencing may induce cracks on surface or underneath surface. Cracks can be initiated and propagated by fatigue wear even when the sliding is relatively too mild to prompt adhesive wear and abrasive wear. As shown in Figure 2.4, when these cracks reach a critical size, the top material will be removed and catastrophic wear will take place [29].

In a system, the dominant wear mode may not be constant at all time. There are a number of factors that may influence the transition of wear mode such as:

- A change of contact geometry
- Altering of the properties of the rubbing surfaces
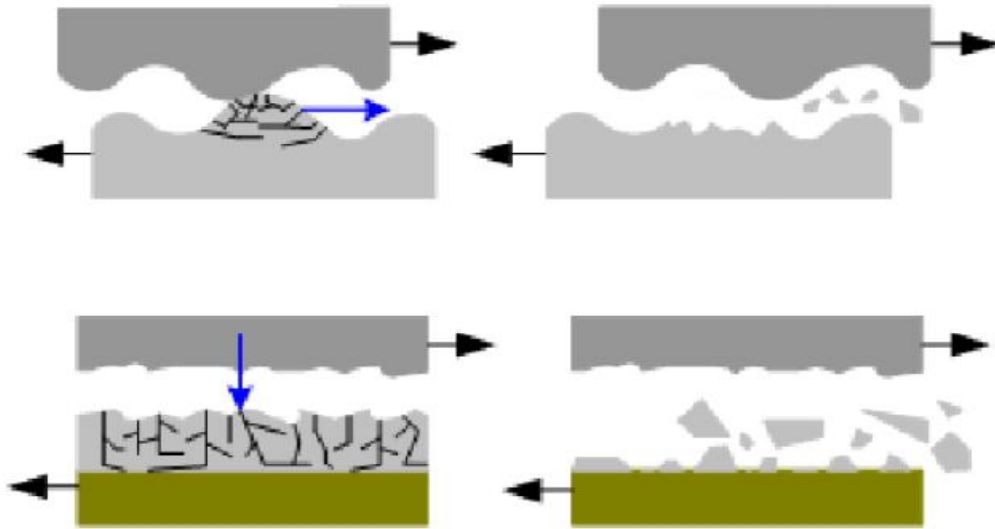
Figure 2-4 Schematic of the fatigue wear (27)

2.4 Lubrication

Lubrication can be defined as a process or a technique employed to reduce wear on the interacting surfaces by using a lubricant. The lubricant present in between the interacting surfaces carries the load and the additives present in the lubricant help in improvement of properties like weld load, EP, rust and corrosion inhibition.

2.4.1 Lubrication regimes

Three distinguishing lubrication regimes can be observed when two rubbing counterparts are lubricated by liquid lubricants. These three lubrication regimes are defined by a relative thickness of the lubricant film formed between the rubbing components to the roughness of the component surface:

Hydrodynamic or fluid film lubrication is the condition when the load carrying surfaces are separated by a relatively thick film of lubricant. This is a stable regime of lubrication and metal-to-metal contact does not occur during the lubrication since the thickness of the lubricant film is bigger than the roughness of the surfaces. The lubricant pressure is self-generated by the moving

surfaces and the lubricant is entrapped into the wedge formed by the moving surfaces at a sufficient velocity to generate the pressure to completely separate the surfaces and support the applied load [30].

Mixed lubrication is the condition when a lubricant film formed between two surfaces is thick enough to avoid most of the asperities in contact but not sufficiently thick to prevent the contact completely as in hydrodynamic lubrication regime. During this type of lubrication, the tallest asperities of the bounding surfaces will protrude through the film and occasionally come in contact. This lubrication regime often occurs at high load condition when insufficient entrainment speed and lubricant with low viscosity are applied [31].

Boundary lubrication is the condition when the fluid films are so thin and there are considerable asperities in contact. Compared with the other two lubrication regimes, boundary lubrication generally occurs at relatively severe operating conditions. Very low entrainment speed, very high load and the employment of lubricant with very low viscosity could all result in boundary lubrication [32].

A boundary film can be formed during boundary lubrication, and the physical and chemical properties of thin surface films are of significant importance. Lubricant additives can have important influence to the properties and the formation of boundary films. Therefore, in boundary lubrication it is important to understand the characteristics of the lubricant additives and the boundary films. The morphology of boundary films is very random and depends on the lubrication condition. The boundary films can be either patchy or continuous [34].

2.4.2 Stribeck Curve

Stribeck curve is often used to present the transitions between different lubrication regimes [33,32]. In a Stribeck curve, as shown in Figure 2.5, friction coefficient is presented as a function of viscosity, speed and load. Stribeck curve can also be used to show how friction coefficient

develops with a variation of lubricant film thickness since these are the parameters that control the lubricant film thickness.

Many sliding components are attempted to be designed to operate in hydrodynamic and mixed lubrication regimes, in which low friction coefficient and wear can be obtained due to the good separation of sliding surfaces by a lubricant film. However, for some components enduring very high pressure, especially in starting and stopping stage, boundary lubrication can be the dominant regime in which the system is operating and high friction and wear are expected in these circumstances. In boundary lubrication, a monolayer of adsorbed molecules could make a noticeable difference on the antiwear performance of a component. The performance of sliding components in boundary lubrication becomes crucial since it sometimes controls the durability of the components [33].
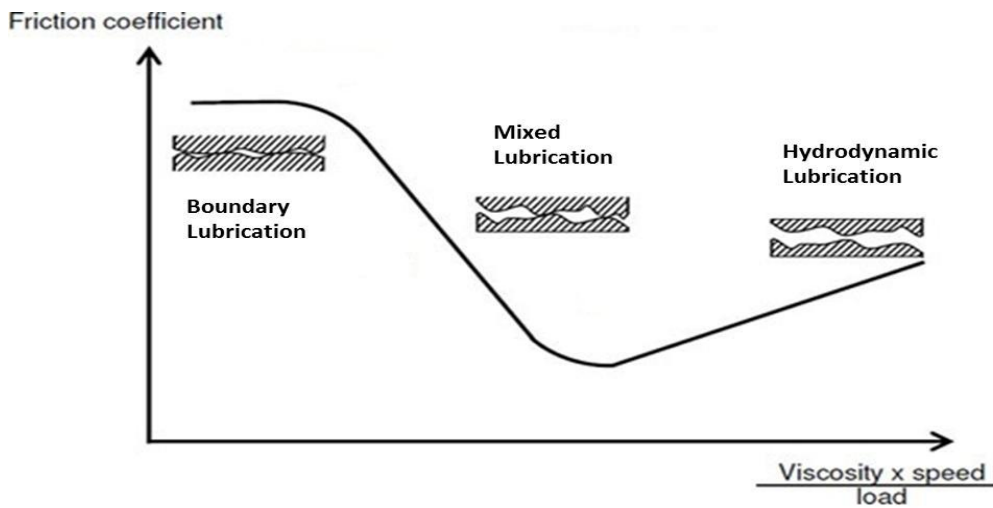
Figure 2-5 Stribeck Curve [33]

2.5 Greases and Additives

The essential function of any lubricant is to prolong the life and increase the efficiency of mechanical devices by reducing friction and wear. Secondary functions include heat dissipation, corrosion protection, power transmission, and contaminant removal. Generally, fluid lubricants are

difficult to retain at the point of application and must be replenished frequently. If, however, a fluid lubricant is thickened, its retention is improved, and lubrication intervals can be extended. A lubricating grease is simply a lubricating fluid which has been gelled with a thickening agent so that the lubricant can be retained more readily in the required area. This is not to say that the thickener does not play a part in the lubrication. Depending on the type of thickener being used and the lubricating regime, some thickeners will contribute in the lubrication. Lubricating greases have a number of advantages over lubricating fluids. Some of these are:

- Dripping and spattering are nearly eliminated

- Less frequent applications are required

- Greases are easier to handle

- Less expensive seals can be used

- They adhere better to surfaces

- They reduce noise and vibration

The liquid lubricant or base oil in grease usually accounts for 70–95% of the grease. The base oil may be mineral oil, synthetic oil, or natural oil such as a vegetable oil. Oils from animal sources are generally not used today. Generally, thickening agents constitute between 5 and 25% of the grease composition. The most common thickeners in use today are metallic soaps, particularly lithium soaps, which account for >60% of the grease market. Silica, expanded graphite, or clays (bentonite or hectorite) are sometimes used as thickeners. Additives, required to improve certain properties of the grease such as oxidative stability, wear protection, and corrosion inhibition are used in 0.5–10% of the grease depending on the grease type and application. When grease is to be used under more severe conditions, it generally contains a more enhanced additive package. These additives are often the same additives used in liquid lubricants. Exceptions are solid additives such as graphite and molybdenum disulfide, which are typically used as antifriction and extreme-pressure (EP) additives.

2.6 MWCNT

2.6.1 Introduction

Carbon nanotubes (CNTs) describe a family of nanomaterials made up entirely of carbon. In this family, Single-walled carbon nanotubes (SWNTs) and Multi-walled carbon nanotubes (MWCNTs) are the two types; which are similar in certain respects but they also have striking differences. SWNTs are an allotrope of sp^2 hybridized carbon structurally a cylindrical tube including six-membered carbon rings similar to graphite. MWCNTs are of special interest for the industry as structurally MWCNTs consist of multiple layers in concentric cylinders of graphite superimposed and rolled in on themselves to form a tubular shape. The diameter of MWNTs may reach upto 30 nm as related to 0.7–2.0 nm for typical SWNTs [37].

2.6.2 Properties of MWNTs

MWNTs have excellent properties and are being employed in a large number of commercial applications. The properties of MWNTs are [37]:

1. Electrical: The cylindrical graphitic polymeric structures have novel or improved properties that makes MWCNT potentially useful in a wide variety of applications in electronics, optics and other fields of materials science. MWNTs are highly conductive when properly integrated into a composite structure. Here, only the outer wall alone is conducting, the inner walls are not conductive.

2. Morphology: MWNTs have a high aspect ratio with lengths typically more than 100 times or greater the diameter. Their performance and application is based on aspect ratio, degree of entanglement and the straightness of the tubes, which is a function of the degree and dimension of defects in the tubes.

3. Physical: MWCNTs can be combined with different materials to enhance their properties. For example, MWNTs have an excellent tensile strength as an defect–free, individual material also when integrated into a composite, such as a thermoplastic or thermoset

compounds, can considerably increase its strength. Carbon nanotubes are endowed with exceptionally high material properties, very close to their theoretical limits, such as electrical and thermal conductivity, strength, stiffness, and toughness.

4. Thermal: Considering the factors like level of defects and on the purity as residual catalyst in the product which can also catalyze decomposition, MWNTs displays a thermal stability more than 600 °C.

2.6.3 Application

Because of the above properties of MWCNTs, there is a huge domain of applications open for MWCNTs. They are listed below on their physico- chemical strength applications:
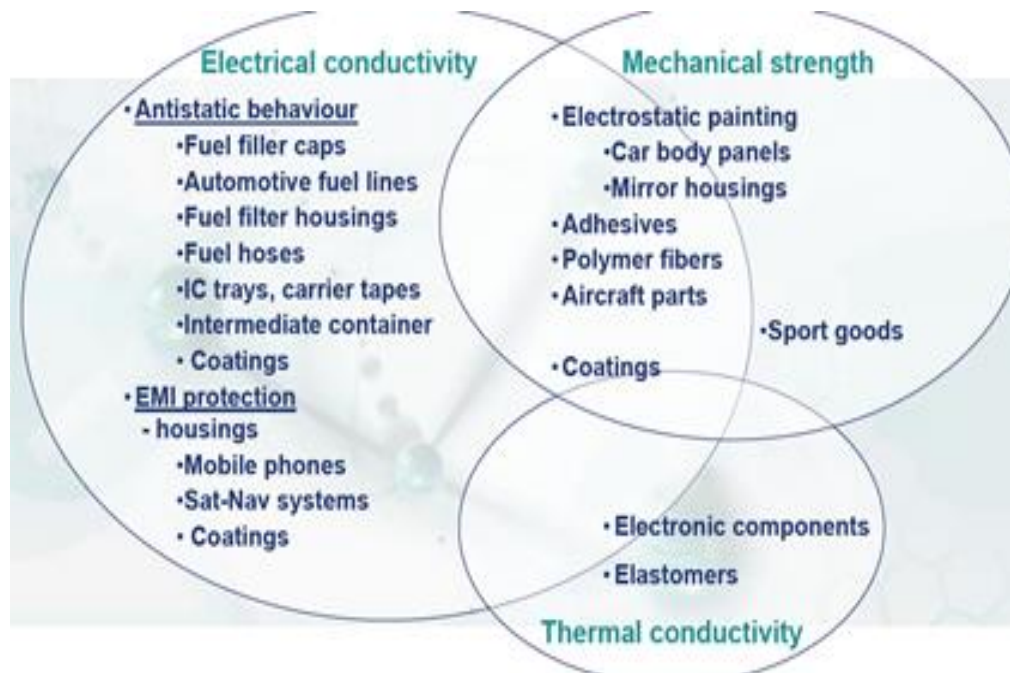
Figure 2.7 Key properties of MWCNTs give rise to a number of potential application fields [38].

Depending on the duration of development of the application, MWCNT applications can be divided in three categories as short term which available shortly, expected shortly and still in R&D phase as Long term.

2.6.4 Current Understanding:

By the discovery of MWCNT was done in 1991 by Iijima, new era opened up in physics and chemistry [39]. One of the features of this MWCNTs was found that it could be grown without magnetic catalyst particles, which causes magnetic and thus transport measurement disturbances. The larger diameters of MWCNTs allows scope for different studies. It was found that they are useful in scanning probe tip applications, as the Russian- doll structure model facilitates understanding of the required rigidity and mechanical stability. Its individual metallic or semiconducting shells are made of SWNTs. In the Parchment model description, a single sheet of graphite is rolled in around itself, resembling a scroll of parchment or a rolled newspaper. The interlayer distance in multi-walled nanotubes is close to the distance between graphene layers in graphite, approximately 3.4 Å. The MWNT is a zero-gap metal due to restrictions on diameters of tubes. Work was done on filling the nanotubes by chemical methods or physical methods. Thus, the capillary action depends on the diameter of the inner cavity of the wall; thus on radius of curvature of the tubes. The filled MWCNTs show good structure for electronic studies. Institutes like NASA are working on finding out next generation MWCNTs composites to be used in applications like space-crafts. Research has started to expand in tribology applications of MWCNTs [35].

2.7 Ionic Liquids

The last few years has fueled growth of studies on ionic liquids for their diverse applications as catalyst, liquid crystals, green solvent in organic synthesis, and in separations, electrochemistry, photochemistry, CO_2 storage devices, etc. Ionic liquids come from a nonconventional class of novel solvents. They are successfully used as media for green synthesis and many such profound reactions is due to their properties. Ionic liquids have negligible volatility and high thermal stability. They are nonflammable and have low melting point. They have broad liquid range and showcase miscibility with organic compounds, especially with many heterocyclic

compounds, thus making them favorable to be used as lubricants, especially in space. Generally, they are composed of ion pairs containing bulky, asymmetric cations and anions. Mainly, super-refined mineral oils such as polyol ester, perfluoropolyether (PFPE) and the multiply-alkylated cyclopentane (Pennzane) are used in space applications. However, these lubricants have disadvantages that can limit their lifetimes in a vacuum environment: catalytic degradation of PFPE on metal surfaces, high vapor pressure of mineral oils at high temperature; dewetting problems of Pennzane. Lately, it was researched that alkylimidazolium ionic liquid was suitable as versatile lubricant for different sliding pairs and exhibited excellent friction-reduction, anti-wear performance and high load-carrying capacity.

In order, for traditional lubricant systems to be replaced by other more efficient and/or more environmentally friendly alternatives, the cost of the new lubricants is a significant consideration. Currently, ILs are expensive in comparison to mineral base oils and synthetic base oils, such as polyalphaolefins, and they are not yet made in large volumes. Therefore, their use as neat lubricants may be limited to critical applications, such as low-pressure environments or micro-electro mechanical machines. On the other hand, there is much more scope for their use as a lubricant additive in which a small amount of IL in a base oil could make a large difference to the friction and wear. As mentioned in the introduction, there is always a need to improve existing additives in order to further improve the friction coefficient and wear rates for common combinations, such as steel/steel. Of even greater interest is the development of new technology that will facilitate new applications for difficult to lubricate systems, such as aluminium/steel. There is also a drive for additives that are low in or free from sulphated ash, phosphorus and sulphur (SAPS). Given the breadth of chemistries available for ILs, these offer significant possibilities. Research thus far has concentrated on fluorine and phosphorus based anions, however, there has also been some work on borates as environmentally friendly IL lubricant additives.

Ionic liquids have been added to a number of base oils, such as hydrocarbons, polyethylene glycol (PEG), polyalphaolefins (PAO) propylene glycol dioleate (PGDO) and glycerol. The amount of IL added to base oils has varied from 0.3 wt% to 10 wt%, with the proportion depending on the solubility and the amount required to give the best performance. It has been found that ILs usually have low solubility in non-polar base oils, such as mineral oils and PAO, and this has been attributed to the ILs polar nature. Some researchers have improved the solubility by using more polar base oils, such as PEG and PGDO while others have tested the IL/base oil as an emulsion. Mistry et al. used a succinimide dispersant and sulphonate detergent to increase the solubility of an imidazolium IL in a group III base oil, but otherwise little work has been done on improving the solubility of ILs in base oils [48]. As an additive, the ILs that performed well in neat form did not always perform well when blended into a base oil. In fact, Jiminez et al. tested a series of imidazolium ILs and found two that caused tribocorrosion in the neat state, resulting in high wear and friction, led to the lowest wear as an additive in mineral oil [61]. They found that the short alkyl chain ILs that caused tribocorrosion in the neat state had better miscibility in the mineral oil than the longer alkyl chain ILs. It was suggested that this low miscibility may prevent the formation of a lubricating adsorbed layer.

Recently, two phosphonium ILs, trihexyl(tetradecyl)phosphonium bis(2-ethylhexyl)phosphate and trihexyl(tetradecyl)phosphonium bis(2,4,4-trimethylpentyl)phosphinate, were found to be fully miscible in a mineral oil and PAO. The solubility was attributed to the long alkyl chains on both the anions and cations. Both of the IL additives resulted in reduced friction and wear for a simulated engine wear test, as compared to traditional additives.

3. Tribological Performance of Multi-walled carbon nanotubes based grease.

3.1 Introduction

There is an increasing demand for the development of high performance lubricating materials for different mechanical systems in the fields of aerospace, nuclear energy, aviation and microelectronics [34]. The lubricating material used in these fields must be capable of combating against the extreme pressure conditions like high/low temperature, unfavorable atmosphere and corrosive environments, etc. However, the failure of conventional lubricating materials towards these intense requirements drive an urge towards improvement and development of the special additive species [35].

In recent years, with the development of nanomaterials and nanotribology, more and more material scientists pay attention to the tribological properties of nanomaterials. Nanomaterials and nanostructures, because of their special dimensions, reveal totally different tribological and mechanical properties compared with traditional materials. Some of the advantages of using nano-additives over conventional additives are suitable size effect, surface and interface effects, thermal stability and variety of particle chemistries. Many studies have shown that the use of organic or inorganic nano-additives can effectively reduce friction and wear of the lubricants. Although there is no established mechanism behind the excellent tribological performance of nano-materials, some of the suggested and widely accepted friction modifying mechanisms are rolling effect, ball bearing effect, colloidal effect, protective film, and third body material transfer [40].

Various studies have stated that the addition of nanoparticles, such as metal [41], metal oxide [42,43], metal sulfides[44], carbonate [45], borate [46], carbon materials [47], organic materials [49] and rare earth compound [50] to lubricants is effective in decreasing both friction and wear. Unfortunately, most of the reported nanomaterials contain phosphorous, sulfur or heavy

metals and are considered as threat to environment. Therefore, environment concerns drive the attention of lubrication engineers to carbonaceous nanomaterial.

Since 1950, initially, carbonaceous nanomaterials, specially graphite were used as dry lubricants in very harsh environment such as high temperature applications, where organic lubricants are considered to be unsuitable. The low-friction performance is attributed to their low resistance to shear between neighboring atomic layers of these materials. Some essential characteristics of lamellar solids that ensure full benefit of graphite as lubricating additives include: (i) The lamellar structure can be deformed, even at low level of shear stress; (ii) The lamellar solid adhere to the worn surface strongly; and (iii) There is no composition or other forms of chemical degradation of the lamellar solid at the operating temperature and in the environment. Considerable work has shown that graphite serves as excellent solid lubricant. Chang-gun lee et al showed the physical and tribological performance of graphite based nano lubricants using disk on disk tribometer. They proposed that the presence of graphite nano particles between the friction surfaces reduced the contact between the surfaces by acting as the ball-bearing spacers and helped to reduce friction and wear [20]. Antony et al studied the synergy between graphite and MoS_2 additive interaction and proposed both solid lubricant additive enhanced the tribological property by imposing as a thin interfacial layer which shears easily with the rubbing action. The synergy was observed to be dependent on the ratio of graphite and MoS_2 added in the grease [65].

Recently, carbon nanotubes are gaining attention as nano-additives for lubricating oil. Nanotubes unique structure make them a promising candidate as extreme pressure lubricant additive. The dimension of nanotubes allows them to be easily active in the contact area, without dangling bonds confers them a chemical inertness. Kobayashi et al compared the tribological properties of greases containing carbon materials like graphite, cluster diamond with the grease having carbon nanohorn as extreme pressure additive and found that all carbon material containing greases resulted in improved friction and wear behavior of lithium based grease [51]. Cursaru et al.

reported that Co-based single-walled carbon nanotubes (SWCNTs) can be used as an additive for mineral base oils with friction reduction, and a synergistic effect was observed when SWCNTs were used combined with the commercial additive [52]. Mohamed et al added electric arc discharged carbon nanotubes (CNTs) with 10nm average diameter and 5µm in length as an additive in lithium grease and evaluate its tribological performance with four ball Tribo-tester. They showed that addition of CNTs to only 1wt% decreased the wear scar diameter about 63%, decrease friction coefficient about 81.5wt%, and increase load carrying capacity about 52% [53]. Chen et al. studied the multi-walled carbon nanotubes (MWCNTs) as an oil additive. They modified MWCNTs by performing treatments using sulfuric and nitric acids, and refluxing with stearic acid to enhance the tribological properties. They proved that the ability of nano-lubricant for wear and friction reduction depended not only on the tribological behavior of the nanoparticles, but also on the dispersion pattern of particles in oil [72].

Many studies have shown the capability of carbon nanotube to be an extreme pressure or antiwear additive in lubricating oils. However, as per author's knowledge no work has been focused on evaluating tribological performance of the multi-wall carbon nanotube (MWCNT) as an additive in lubricating grease. The main objective of this work is to evaluate the tribological behavior of MWCNTs as an additive on lithium grease to exhibit good performance in antiwear and friction reduction.

3.2 Experimental Approach

3.2.1 Base grease and additive chemistries

Base grease used for this study was commercially purchased lithium complex thickener. This grease was obtained from the supplier by removing a pail during the grease making process before adding any type of additives. This type of grease assist in correlating the role of additives directly with the tribological test results. As this test base grease had been pulled out early in the process, remaining base oil had to be added manually to achieve the desired consistency of NLGI 2

grade of medium viscosity. Base oil used was product of Shell manufactured under brand name Shell 46 Rotella T Triple Protection 15W-40. It is basically used as engine oil. It is highly refined mineral oil. It has outstanding shear stability for viscosity control. Typical physical characteristics are shown in table below.

Properties			Method	Shell Rotella T Triple Protection 15W-40 (CJ-4)
SAE Viscosity Grade				15W-40
Kinematic Viscosity	@40°C	mm²/s	ASTM D445	120
Kinematic Viscosity	@100°C	mm²/s	ASTM D445	15.5
Viscosity Index			ASTM D2270	135
density	@15°C	kg/l	ASTM D4052	0.879
Sulfated Ash		%	ASTM D874	1.0
Total Base Number		mg KOH/g	ASTM D2896	10.1
Flash Point (COC)			ASTM D92	204
Pour Point		°C	ASTM D97	-30

Figure 3-1 Properties of Base Oil Rotella 15W-40 [54]

Multiwall carbon nanotubes (MWCNTs) were used as the antiwear and friction additives for this study. Industrial grade MWCNTs were commercially purchased from Cheap Tubes Inc, USA. This MWCNTs were made by combustion chemical vapor deposition (CCVD) and purified using concentrated acid chemistry. Both type and diameter are important for MWCNTs selection. The wider the diameter of the carbon nanotube (CNTs), the more it behaves like graphite. The narrower the diameter of the Carbon Nanotubes (CNTs), the more its intrinsic properties depends upon its specific type. The diameter of MWCNTs used was 20-30nm. Also, COOH and OH functionalized MWCNTs were used to check the influence of functionality on the tribological behavior. Table 1 below gives the specification of all the MWCNTs used:

Table 1 Industrial Grade Multiwalled Carbon Nanotubes Specifications

Purity	>90wt%
Outer Diameter	20-40 nm
Inner Diameter	5-10 nm
Length	10-30 nm
Ash	<1.5wt%

3.2.2 Grease Blends Formulations

Blend formulations prepared to examine the optimum concentration of MWCNTs are as shown in the table 1-2. Initial blends were formulated using varying concentration of 0.5, 1 and 1.5 wt% of MWCNT so as to get effective concentration value capable of imparting better tribological properties. For the comparison purpose, baseline grease blend was prepared by maintaining 100:30 ratio of thickener and synthetic base oil.

Table 2 Formulation of Grease Blends with MWCNTs

Blend Code	Base Grease	Additives	Additive Treat Level
MWCNT_00	Lithium Complex NLGI#2	-	0 wt%
MWCNT_01	Lithium Complex NLGI#2	MWCNT	0.5wt%
MWCNT_02	Lithium Complex NLGI#2	MWCNT	1wt%
MWCNT_03	Lithium Complex NLGI#2	MWCNT	1.5wt%

MWCNT_COOH	Lithium Complex NLGI#2	MWCNT-COOH	1wt%
MWCNT_OH	Lithium Complex NLGI#2	MWCNT-OH	1wt%

The blends were formulated using a Kitchen-Aid Mixer. The electrical specifications of the mixer were, 120 Volts, power rating of 250 W. Each formulation was blended for 2 hours with hand mixing at every 25 minutes. Initially calculations were carried out for 100:30 ratio of thickner and synthetic base oil for 100 grams of total blend. Then the base oil and MWCNT additive was measured and hand mixed in the steel container. About 30-40gms of base grease was initially added to the mixture of base oil and MWCNT and hand mixed and later the complete mixture was mixed in the Kitchen-Aid at a speed of 100 rpm. Figure 3-2 shows the Kitchen Aid in the TLCL used for grease blends formulations.

Figure 3-2 Figure Kitchen Aid Mixer

The blended greases are tested further in a Plint Four-Ball Tribometer. They are evaluated for wear and friction performance. If the blended grease is not used over a period of time there is high probability of oil separation. Before every use the grease is mixed using a spatula manually.

3.2.3 Four Ball Tribometer Tests

The four ball tribometer tests were carried by following standard ASTM D2266 test conditions of 40Kg load, 1200 rpm and 75˚C temperature for one hour. This test conditions ensure the continuous sliding mode under boundary lubrication regime. Tribological tests were carried out using the Plint TE-92 Rotary Tribometer procured from Phoenix Tribology (London, UK). About 10-15gms grease was loaded in the steel cup. Three E52100 ½" steel balls were taken in the cup, which were fixed with the help of a holding cup and a hexagonal nut (Lower Loading assembly). The fourth ball was taken in the chuck and fixed to the top rotating spindle. The spindle ball was normally loaded (0.39 kN) against the three base balls to create a point contact and heated (upto test condition). The spindle and the top ball were rotated at speed of 1200rpm for 72000 cycles. The lubricating medium ran between the top ball and base balls, thus evaluating its tribological properties. The friction coefficient is measured using a load cell attached to the lower loading assembly and another load cell attached such as to measure the torque sensed by the lower assembly which could freely rotate over a centre spindle. All the tests were repeated thrice to ensure repeatability.

The friction values after the test are measured by the formula as described in the ASTM D5183 and using the torque and load values generated during tests from the Compend X software assisting the four ball tribometer. After the termination of every test, the three stationary steel balls were retrieved and analyzed to determine the WSD (Wear Scar Diameter) using stereo-optical microscope and image J software.

3.2.4 Stere-optical microscope

Stereo-Optical microscope (model type: Nikon SMZ 1500) was used to image the wear scars formed on the three stationary steel balls after the four ball tests. The steel balls were cleaned using hexane and were mounted on a home-made sample holder; which were then imaged at a magnification of 100X on the microscope. The images were analyzed using the Image J software. The software comprised of measuring tools & Pixel-counter which was used to document the WSD for all the three steel balls and an average value was reported. Wear Scar Diameter for each blend was determined using an average of 18 readings on 9 samples from a total of three repeat runs. Each reading represents the average value of longest horizontal striation and longest vertical striation. Imaging all the samples ensured machine repeatability and normal loading of the samples by the spindle.

3.2.5 Scanning Electron Microscopy (SEM) and Energy Dispersive Spectroscopy (EDX)

SEM (model type: Hitachi S-3000N) was used in the SE (Secondary Electron) mode to image the wear surfaces developed on the stationary steel balls. Images were taken at an accelerating voltage of 15-20 kV was used in all the cases. Carbon tape was used to maintain good electrical contact in between the steel balls and sample holder. The wear mechanism in play on the surface formed on the surface was evaluated by observing images at 100X and 500X. Specific areas on the surface showing distinct wear tracks and surface morphology were imaged at a higher magnification of 1000X to understand the wear mechanism.

EDX spectrums were collected for the wear test samples. The spectrums were for the magnification of the 1000x, the voltage was charged down to 15kV to reduce the penetration depth. The spectrum was collected in order understand the carbon percentage on the worn surfaces. EDX maps were also collected. EDX elemental mapping helps to understand the antiwear protection of MWCNT towards severe wear of the surfaces.

3.3 Results

3.3.1 Friction Results

The coefficient of friction (COF) values are obtained using the procedure described in ASTM D5183-05. The procedure involves use of normalization factor [68]. Coefficient of friction values are derived using following formula:

$$COF = (0.2227 * Torque)/Load$$

The absolute torque and load values were received from the tests conducted using the Four-ball tribometer. Figure (3-3 (a)) exhibits the change in COF values during the test run for the grease blends with increased MWCNT concentration and with functionalized MWCNTs respectively. Observation of COF variation will help to understand the effectiveness of the MWCNTs as the friction modifier with the test duration.
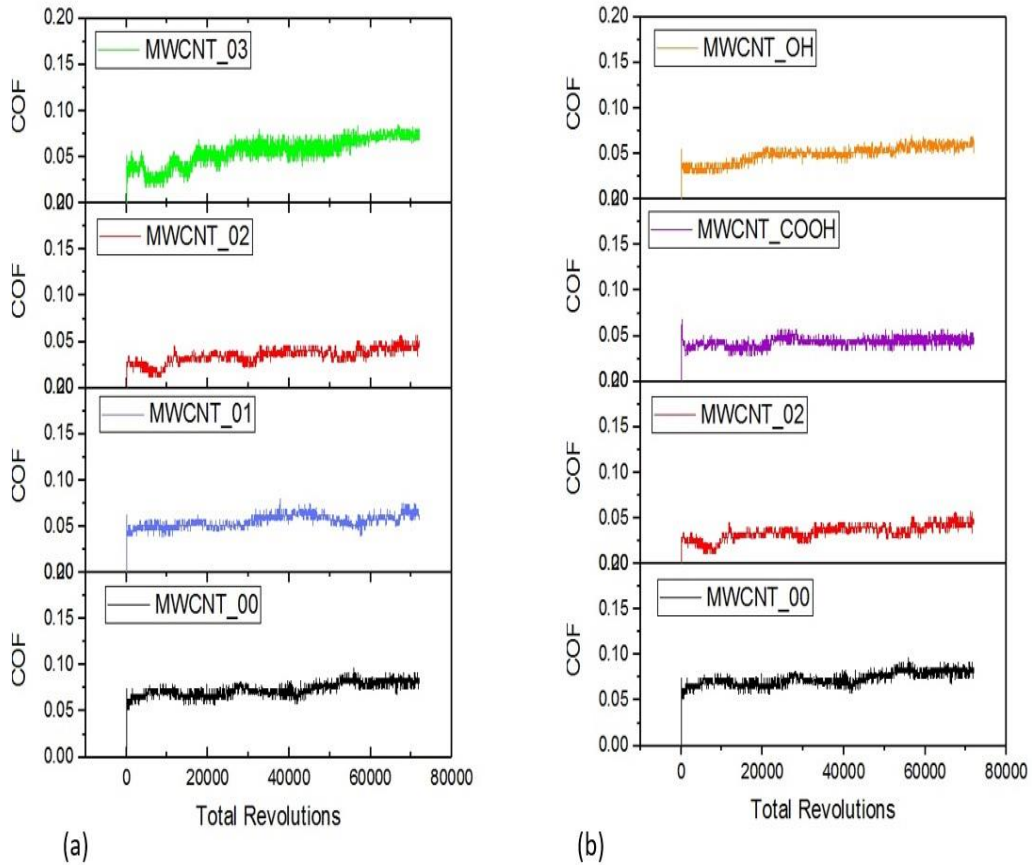
Figure 3-3 (a) Effect of MWCNT concentration on COF (b) Effect of functionalized MWCNT on COF

Base Grease blend (MWCNT_00) shows a high COF value which seems to increase gradually with the test. Addition of MWCNT by 0.05wt % results in slight decrease of COF value. MWCNT_01 shows variation in COF values near 40000 revolutions. MWCNT_02 grease blend with 1 wt% of soot demonstrate interesting behavior. At the beginning of the test stable COF value is observed which is further followed by the short drop. This pattern is continued till the end of the test. It is important to note that the MWCNT_01 shows the least variation and increase in the COF value. These changes in COF values indicates that initially thin layer of MWCNTs are formed between the interfacial surfaces and with the continuation of the test these films are removed due to build up frictional force exerted normally by the top rotating steel ball. Slight increase and stability

in COF values for MWCNT_01 grease blend signifies the effective antifriction behavior of MWCNTs. MWCNT_02 grease blend shows the continuous increase in COF values with the test duration. Gradual increase in COF value also indicates the continued removal of adsorbed MWCNTs. The figure (3-4) also demonstrate the effect of MWCNTs concentration on the antifriction behavior of the grease blends. COF values plotted in the following column chart are the averages of the COF values obtained from three runs performed for each blend. Addition of MWCNTs results in decrease of COF values till 1wt%. However, further increase in concentration of MWCNTs affects the friction performance of the lubricating grease.
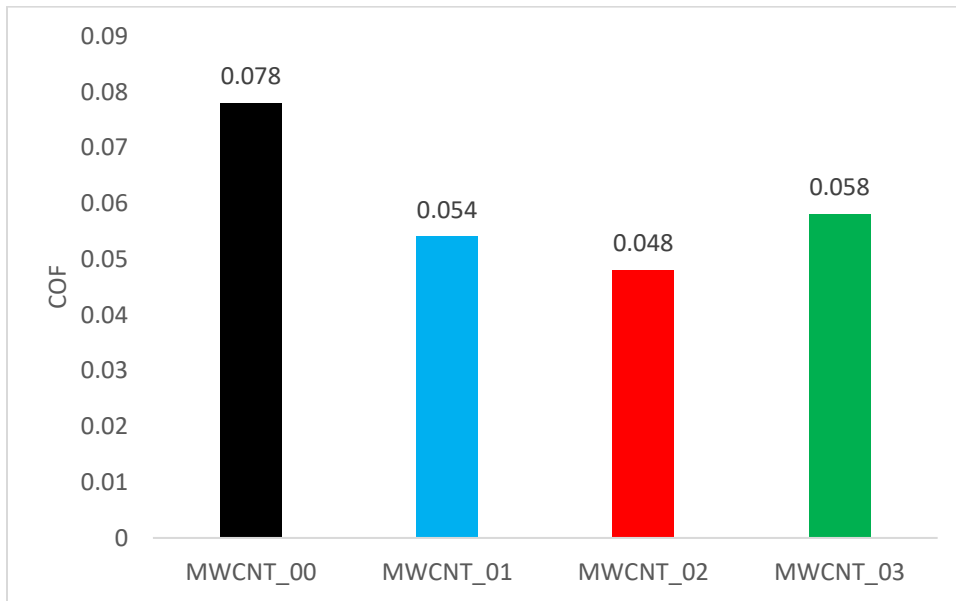
Figure 3-4 Friction results of the grease blends containing different MWCNTs concentration.

Figure (3-3 (b)) also shows the friction performance of the grease blends containing functionalized MWCNTs. Grease blends with Carboxylic functionality exhibits stable friction performance for some duration of the test while the grease blend with hydroxyl functionality shows some variation at the same duration. Also, at the end of the test COF value for MWCNT-OH increases considerably. Comparison of the antifriction behavior of functionalized MWCNTs grease

blends in terms of the average COF value is shown in figure (3-5). MWCNT_COOH shows slightly better COF value than the MWCNT_OH.
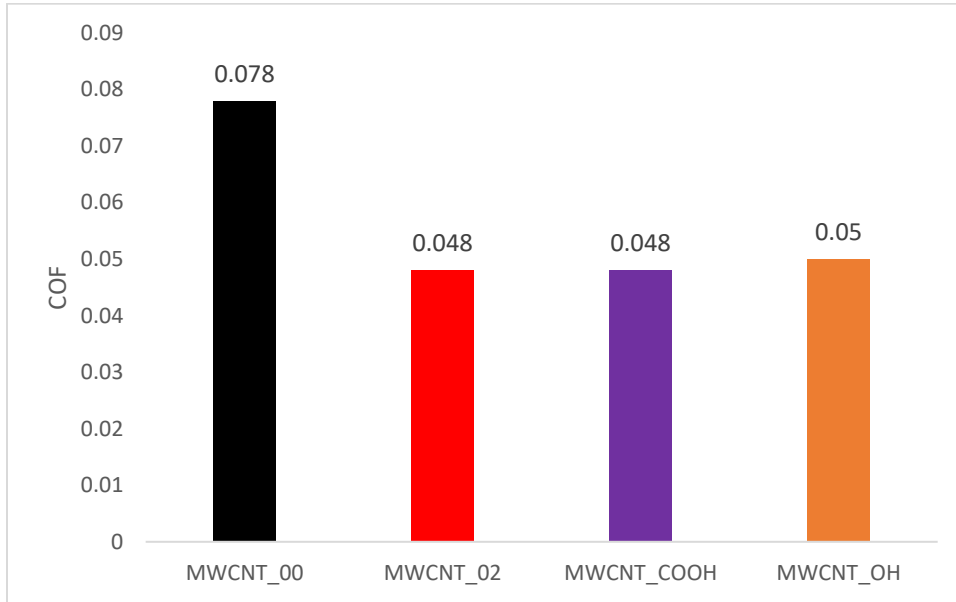
Figure 3-5 Friction results of the grease blends containing functionalized MWCNTs

3.3.2 Wear Results

It is observed from the Figure 3.6 that there is substantial decrease in the wear of the stationary steel ball surface when MWCNTs is used as solid additive. The minimum wear is observed at the 1wt% of MCNT. The grease blend with 1.5wt% MWCNT displays higher wear than the base grease without any additives. These observations indicate 1wt% of CNT provides the minimum wear rate. The estimation of the desired percent of CNT for various operating conditions requires exhaustive experimental investigations.
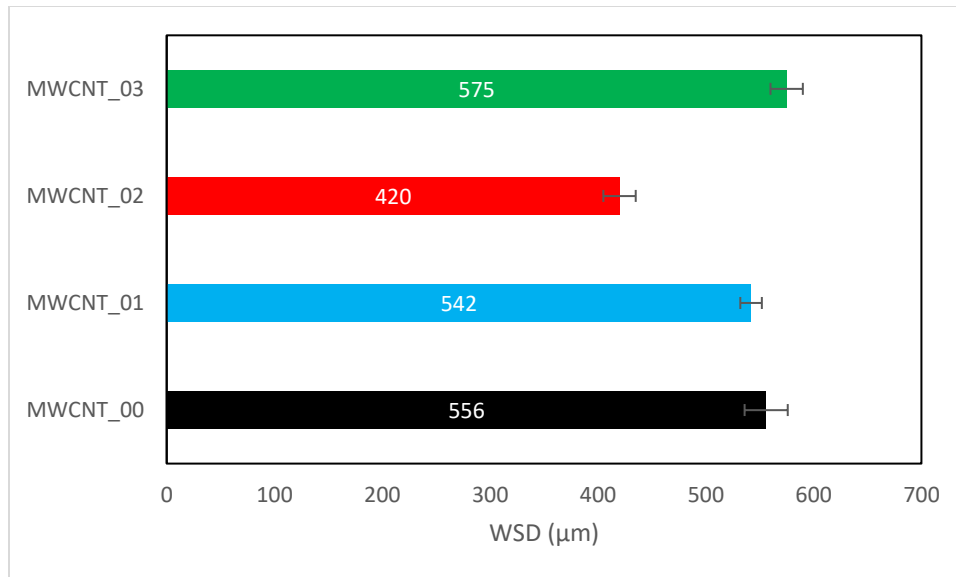
Figure 3-6 Wear results for the grease blends with different MWCNT concentration.

Addition of MWCNT at a certain concentration exhibits effective antiwear properties. MWCNTs get adsorbed on the interacting tribosurfaces forming thin layer. These layers minimize the sliding resistance and hence reduces the wear between contacting surfaces. As the concentration of MWCNTs increase the non-adherent particles having high surface energy tend to form large agglomerates. Agglomerates may result in degradation of antiwear properties of MWCNTs. Figure 3.7 shows the wear performance of the grease blends having functionalized MWCNTs. Presence of Carboxyl and hydroxyl functional groups doesn't show a significant decrease in wear scar diameter as compared to un-functionalized MWCNTs. It was hypothesized that functional groups may increase propensity of MWCNTs towards adsorption on steel surfaces. However, at such rigorous test conditions all the MWCNTs are showing similar antiwear performance. Figure 3.8 shows the variation in wear scar diameter with the MWCNT concentration with the help of low magnification scanning electron images.
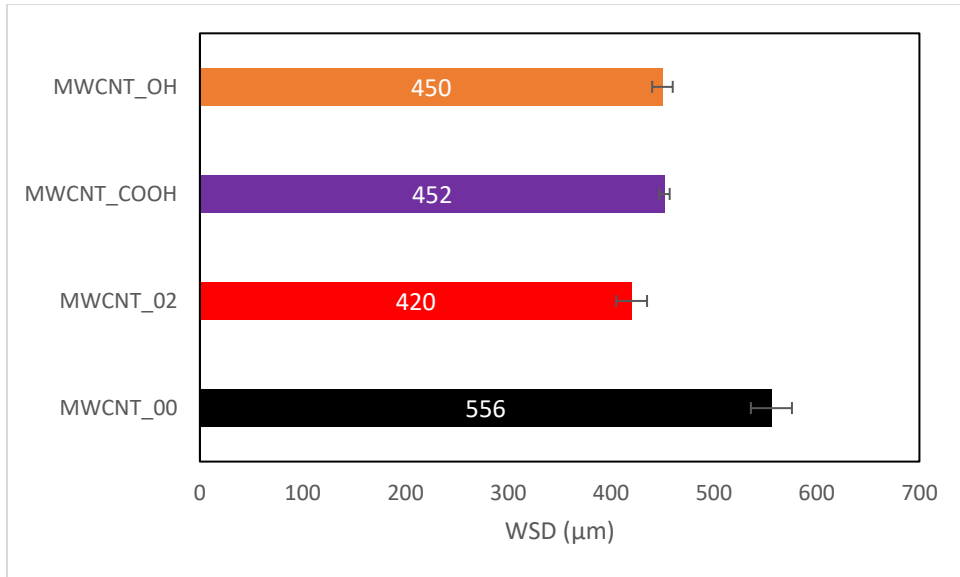
Figure 3-7 Wear results for the grease blends containing functionalized MWCNTs.
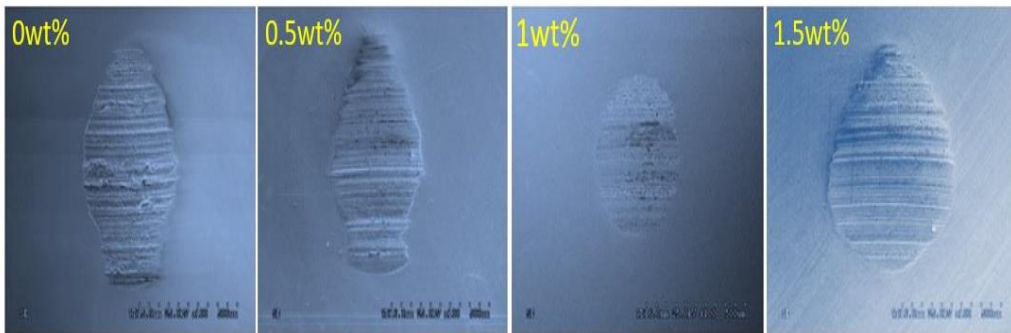
Figure 3-8 Low magnification SEM images of the grease blends with different MWCNT concentration.

3.3.3 Scanning Electron Microscope (SEM)

Scanning electron microscopy (SEM) using secondary electrons was used to examine the local morphology of wear scars of all the grease blends. The morphology and characteristics of the wear track provide significant information about the wear behavior of the various chemistries. Figure 3.9-3.12 shows a typical wear scar for the base grease blend having MWCNT concentration of 0wt%, 0.5 wt%, 1wt% and 1.5wt%.
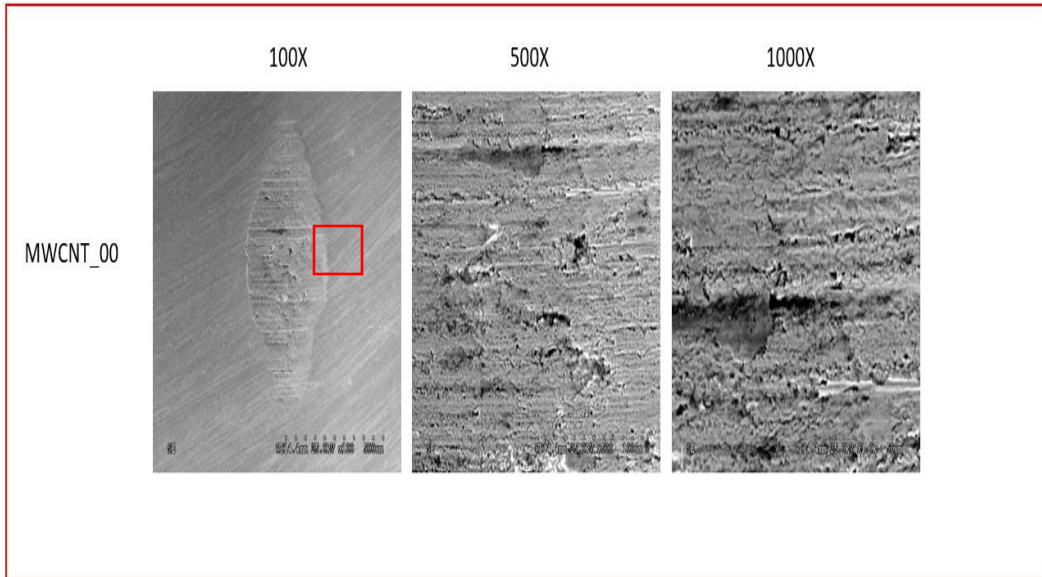
Figure 3-9 SEM image for grease blend MWCNT_00 at 100X, 500X, 1000X.
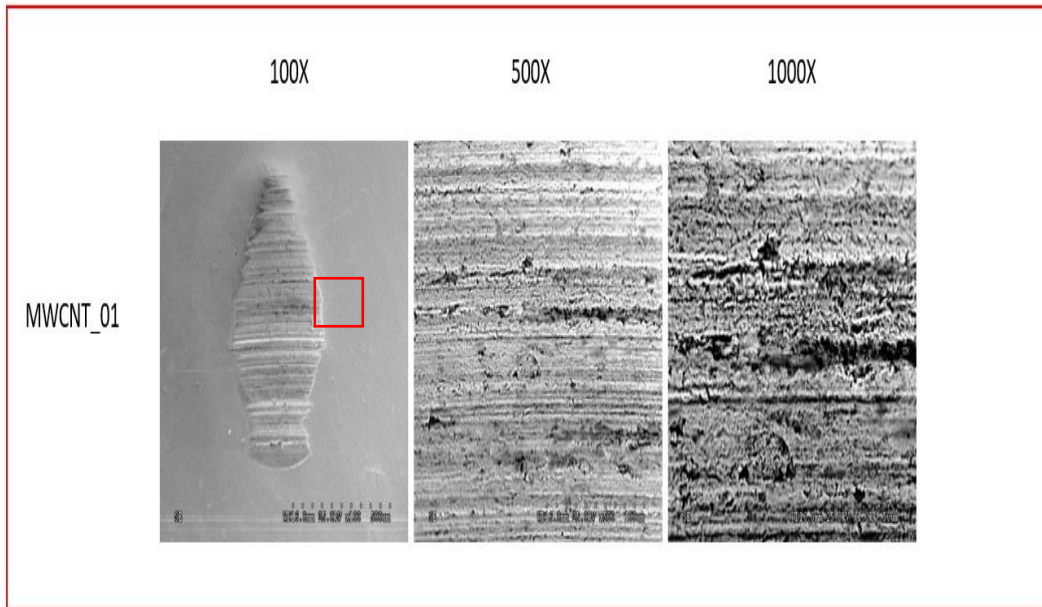
Figure 3-10 SEM image for grease blend MWCNT_01 at 100X, 500X, 1000X.
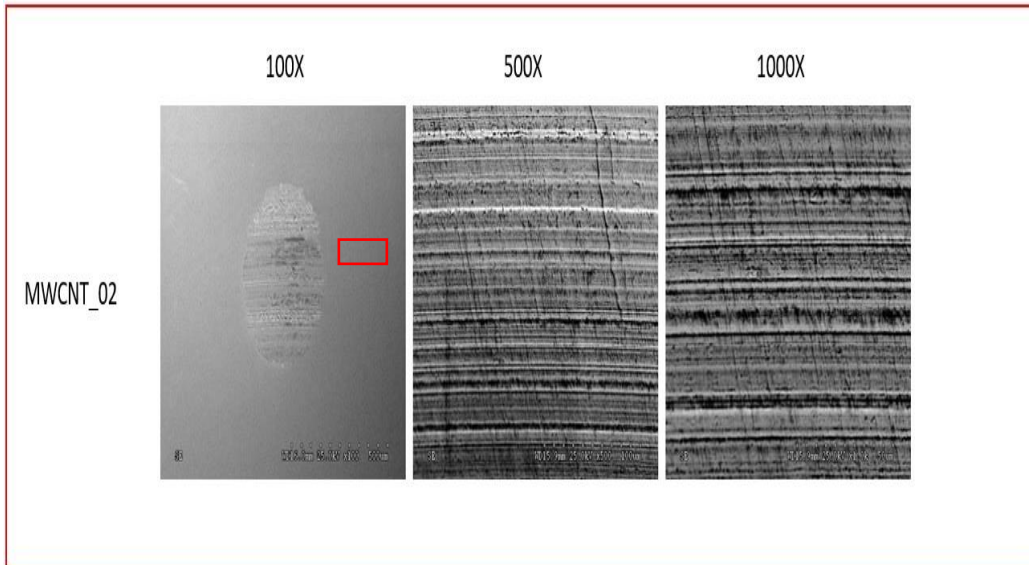
Figure 3-11 SEM image for grease blend MWCNT_02 at 100X, 500X, 1000X.
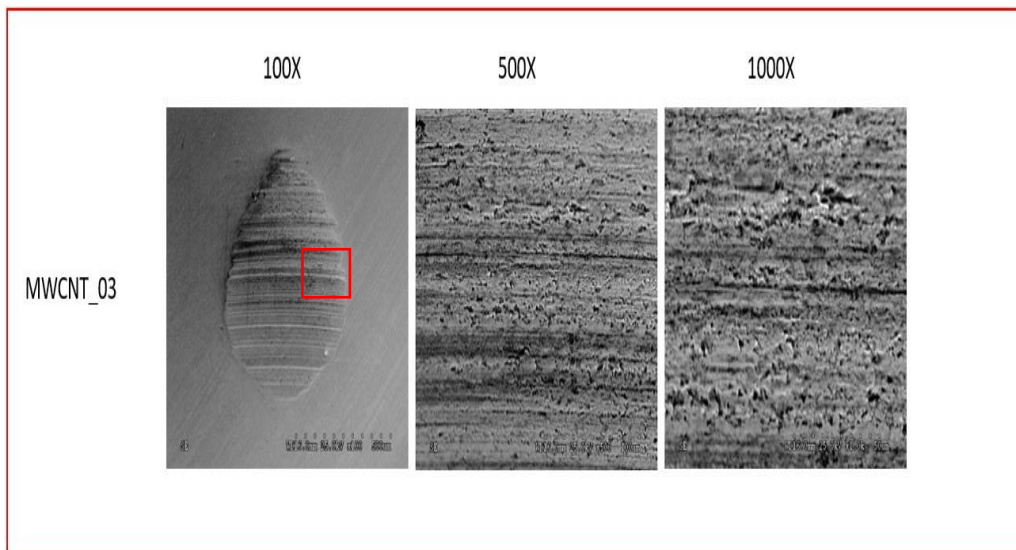
Figure 3-12 SEM image for grease blend MWCNT_03 at 100X, 500X, 1000X.

SEM images of the wear scar for blend MWCNT_00 exhibits severe ploughing groves and adhesive wear surfaces. As there were no additives present in the grease, direct metal to metal contact resulted in heavy wear. Wear scar of the MWCNT_01 grease blend with 0.5wt% MWCNT suggests 0.5wt% of MWCNT was not sufficient to protect the stationary surface against the high

frictional force. However, wear scar of MWCNT_01 shows some smooth polished area with few deep ploughing grooves as compared to MWCNT_00. MWCNT_02 has the smallest wear scar among all the grease blends formulation. Wear scar morphology exhibits deep abrasive grooves with some amount of polishing wear. Also, the black color deposition can be seen near abrasive grooves in the SEM image taken at 1000X magnification. Chemical composition analysis of this wear scar surface will help to figure out the reason behind the smallest wear scar diameter. Figure 3.12 displays the morphology of the wear scar formed during tribotesting of the grease blend containing 1.5 wt% of MWCNTs. Wear scar shows heavy metal scuffing at the top mart and abrasive grooves at the center. Such a wear scar surface features justifies the higher wear scar diameter of the grease blend MWCNT_03.

SEM images of the wear scar surface developed on the stationary steel ball during four ball tribometer for the grease blends containing functionalized MWCNTs are shown in the figure (3.13).
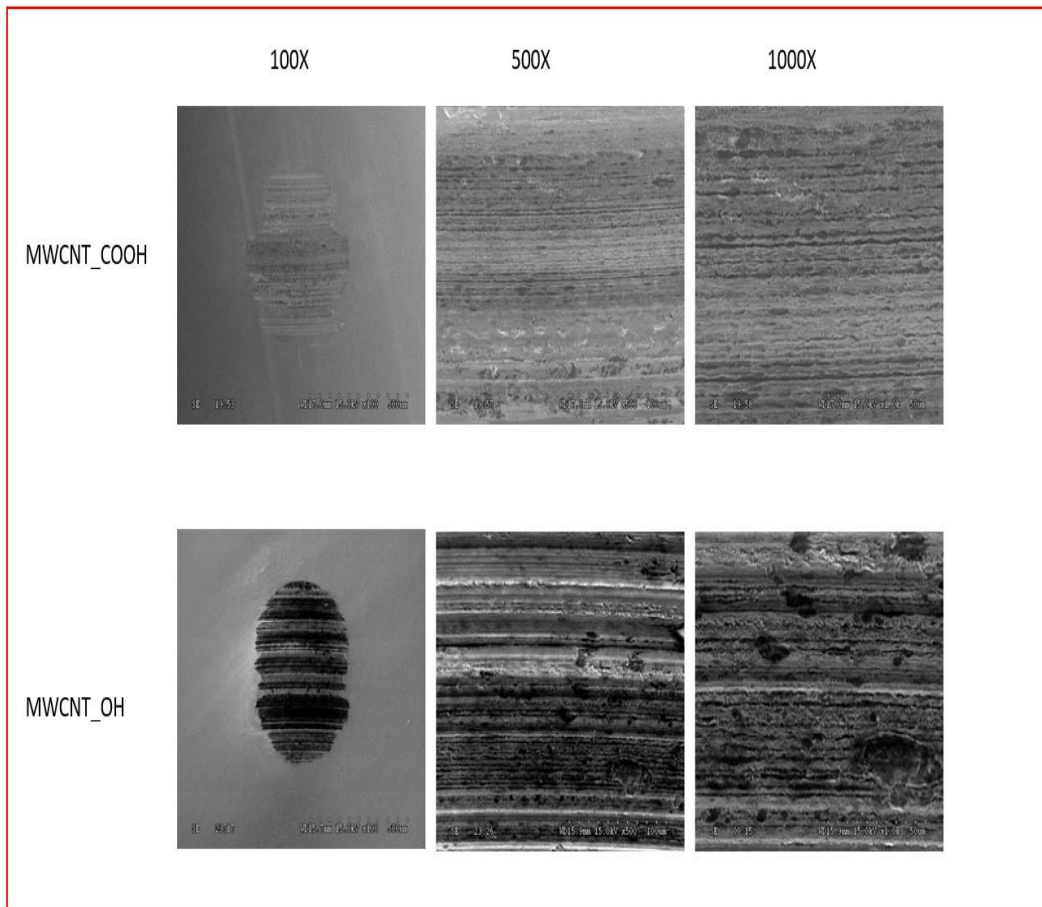
Figure 3-13 SEM image for grease blend MWCNT_COOH and at 100X, 500X, 1000X.

Study of functionalized MWCNTs blended lubricating greases will help to recognize the effect of functionality groups on minimizing the wear. Unfortunately, under the used test conditions wear scar diameter of MWCNT_COOH and MWCNT_OH showed almost similar wear performance to that of un-functionalized MWCNT. This effect can be further consolidated by careful examination of the wear scars. Wear scar of MWCNT_COOH is very light and not seems to be not well developed. Wear scar surface shows the deep metal cut and abrasive grooves. Wear scar developed by grease blend MWCNT_0H exhibits smooth areas between the abrasive grooves. Also, some amount of adhesive wear is also observed with MWCNT_OH.

3.3.4 Energy Dispersive Spectroscopy (EDS)

As stated earlier it is important to analyze the chemistry of the worn surfaces. EDS element spectrum characterization was carried out to see the MWCNTs contribution towards the wear protection. This helps to interpret the role of MWCNTs and form a tentative understanding of the mechanism resulting in wear.
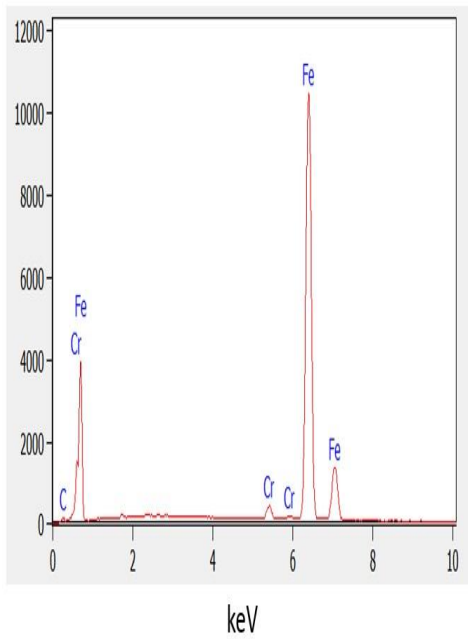
Element	Atomic %
Carbon	4.10
Iron	94.13

Figure 3-14 EDS spectrum analysis of grease blend MWCNT_00 at 1000X.
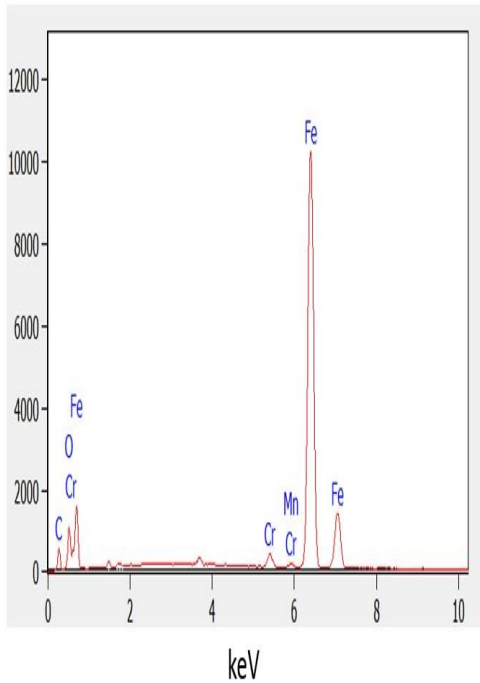
Element	Atomic %
Carbon	18.56
Iron	80.13

Figure 3-15 EDS spectrum analysis of grease blend MWCNT_02 at 1000X.

Figures 3-14 and 3-15 shows the EDS obtained from the worn scar on the steel balls lubricated by grease blends, MWCNT_00 containing base grease and MWCNT_02 containing 1 wt% MWCNTs respectively. It can be seen that the element of C was present on the worn scar surface lubricated by lithium grease containing 1 wt.% MWCNTs, and its atomic concentration was 18.56%. Comparing with Figure (3-14) which shows the element composition of the wear scar developed by base grease, indicates that the C present on the worn surfaces is from the deposition of MWCNTs during the process of friction. The presence of C gives strong evidence that a lubricating film must be formed and probably contains MWCNTs, which can prevent the steel-to-steel direct contact. To further consolidate the result of MWCNT deposition on the wear surface EDS element mapping was done (Figure 3-16). EDS elemental mapping was performed on the representative box on the SEM image of the wear scar magnified at 500X. Red color circle marked on the 500X SEM image represents the area under discussion. Corresponding marked circle area on

C map shows the presence of C. While the same areas on Fe map reveals carbon is not just adhering on the wear surfaces but it is accumulated in the abrasive grooves. Comparison of the marked areas with the O map rule out the presence of abrasive oxide films in the grooves.
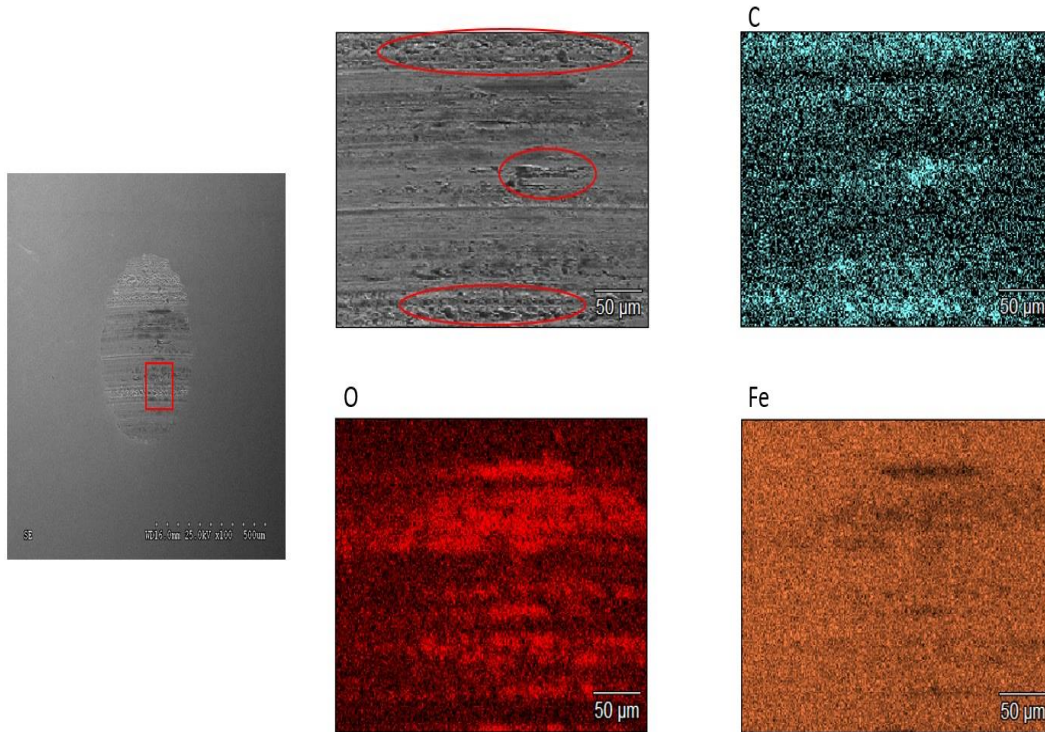
Figure 3-16 EDS mapping of the MWCNT_02 grease blend containing 1wt% MWCNT at 500X.

3.4 Discussion

The following section discusses the effect of MWCNT concentration and functionality of MWCNT on the wear performance of formulated grease blends. The antiwear mechanism of MWCNT and its role in protecting the surface from further abrasion are discussed. A correlation in between concentration of MWCNT and tribological performance of the lithium based lubricating greases is established with the help of friction coefficient, WSD and analysis of wear scar morphology and chemical composition.

Results of friction tests of the grease blends with 0wt%, 0.5wt%, 1wt% and 2wt% MWCNTs as shown in figure (3-3) indicates that the grease blends with MWCNT gave a smaller and more stable friction coefficient than the lithium based grease blend with no MWCNT present in it. The larger friction coefficient of the base grease blends without MWCNT resulted from a real contacting area of the rubbing surface owing to wear. It was observed that coefficient of friction of lithium grease containing MWCNT at 0.5wt% and 1wt% decrease gradually, while it increases again at 1.5wt% of MWCNT. Also, WSD results shown in figure 3-17 suggests that the grease blends with MWCNT in 0-1wt% range resulted in decrease of WSD and increase in WSD at concentration above 1wt%. It is important to note that addition of 1.5wt% MWCNT showed WSD greater than the WSD of base grease blend. A correlation of wear scar diameter with the coefficient of friction is shown in figure 3-17. Using solid lubricant such as MWCNT exists an "optimum concentration" [55]. Less than this concentration, solid lubricant is insufficient to maintain protection against wear.
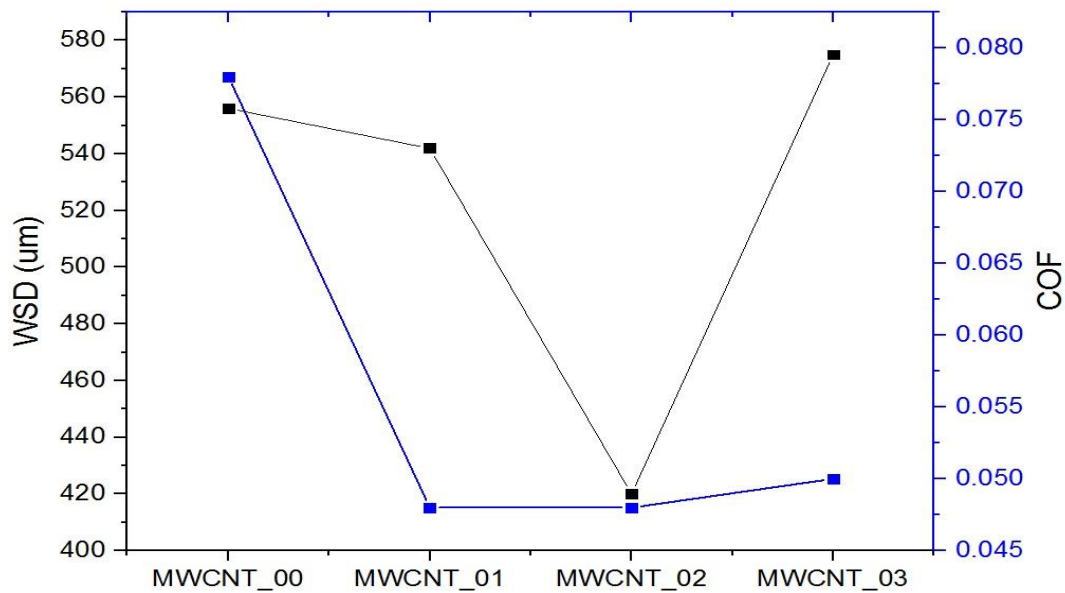
Figure 3-17 Correlation of COF with WSD for the grease blends having different MWCNT concentration

Mohammed et al research work on the tribological behavior of CNTs as an additive in lithium grease also proposed a threshold amount of 1wt%. However, in their study increase in concentration of CNTs upto 3wt% did not resulted in WSD value greater than the base lithium grease blend [53]. In literature, no optimum concentration is reported for MWCNTs as an additive in lubricating greases. It can be seen that optimum concentration of the MWCNT is 1wt% in this study.

Stable coefficient of friction of the MWCNT containing greases can be explained in that at a given concentration, the MWCNT more easily will penetrate the interface with the lubricating grease and form thin film in concave of rubbing face, which can decrease shearing stress, therefore, give a low friction coefficient. These reasoning further validates that the presence of MWCNT increased the wear resistance of the lubricating grease blends. The increase in wear scar diameter at high concentrations of the MWCNT may be explained only by a mutual hindrance of the many particles available. Also, there is possibility of accumulation of MWCNTs at the leading edge of steel ball making it more difficult to penetrate into the interface with the lubricating grease.

The evidence of reducing the friction and wear of MWCNT added in lithium grease blends can also be confirmed by the results of SEM and EDS. Figure (3-9)-(3-12) shows SEM images of the rubbing surface lubricated by the grease blends containing MWCNT in 0-1.5wt%. It can be found that the worn surface lubricated by base grease blend MWCNT_00 is evidently rough with many thick and deep furrows and scuffing but the worn surface lubricated by grease with MWCNT at 1wt% is comparably rather smoother and the furrows are rather shallower. As stated earlier MWCNTs have tendency to form thin dry lubricant film covering the surface asperities and imparting the smooth surfaces. It is possible that the MWCNT in contact of smooth surfaces may undergoes slip and gives protection against high frictional forces. This explains the combined presence of abrasive grooves and polished smooth surfaces on the wear scars developed by grease blends containing MWCNT. EDS spectrum and elemental mapping results as displayed in figure (3-14)-(3-15) suggest that the MWCNT can stably exists on the rubbing surfaces lubricated by

lithium grease. They are capable of forming physically adsorbed films on interacting surfaces and preventing them from direct contact.

This work was also focused on examining the influence of functionalized MWCNTs on the tribological properties of the lubricating greases. It was hypothesized that the modification of MWCNT with covalent carboxylic and hydroxyl functionality may increase the rate of adsorption of MWCNT onto the interacting steel surfaces. However, in the used test conditions grease blends with both carboxylic and hydroxyl functionality showed comparable performance to that of the grease blends having un-functionalized MWCNT.

Many studies have investigated the mechanisms of nano lubrication. The proposed suggestions behind the friction reduction are mending effect, rolling effect, ball bearing effect, colloidal effect, protective film, and third body material transfer. Liu et al. [40] explained the mending effect as a lubrication mechanism. During mending effect, the nanoparticles may deposit on the friction surfaces and form a physical tribofilm to compensate for the loss of mass. Tao et al. discussed the rolling or ball bearing effect of nanoparticles. They proposed that in lubricants the spherical particles act like ball bearings between two friction surfaces. The anti-wear and anti-friction mechanism of the additive was believed to involve the nanoparticles acting as a spacer between the two friction surfaces [73]. Chinas-Castillo and Spikes stated that the mechanism for nano lubrication was mechanical entrapment, where colloidal nanoparticles penetrate elastohydrodynamic (EHD) contacts in thin-film contacts [51]. Qiu, et al. suggested that a thin film is deposited onto contacting regions, which prevents direct contact of the mating surfaces and reduces friction and wear [52]. Rapoport et al reported that three mechanisms contribute to friction properties: the rolling effect due to the spherical shape of the nanoparticle additives, their prevention of direct metal surface contact by acting as spacers, and third-body material transfer [40]. All of these mechanisms were proposed for spherical nanolubricant additives used in oil.

In this work, several hypotheses can be made on explaining the positive effect of MWCNT addition on tribological properties of the lithium grease. First, from the SEM and EDS mapping, it can be proposed that MWCNT exhibits mending effect as the presence of carbon element was detected in the abrasive grooves developed on the worn surface. Second, SEM-EDS spectrum analysis convinces that MWCNT may get adsorbed on the rubbing surfaces and form thin films capable of preventing contact between the interacting surfaces. In addition to this, some MWCNTs can be rupture or deform under such rigorous friction and extreme pressure condition to form small, planar graphene segments reflecting their origin, in effect resembling amorphous carbon. Then this newly formed lamella may strongly adhere to tribosurface. Such films are referred as transfer films. The role of the transfer film is to reduce the shear strength at the interface while maintaining the stiffness of the contact surfaces. In all the cases, the benefit of MWCNT arises from their unique structure and properties. The high young's modulus of MWCNT enables them to shear under action of high normal friction force. The rolling or sliding of MWCNTs between the interacting surfaces aid in friction and wear resistance.

Though the presence of films was detected in this study, it is beyond the scope of this project to characterize the nature of the films. It may be transfer films or physically adsorbed films. But it is safe to state that the MWCNTs can serve as effective spacers, prohibiting contact and wear of the metal surfaces under extreme pressure and load conditions.

3.5 Conclusion

[1] MWCNT was successfully used as extreme pressure antiwear additive in lithium grease. The optimal concentration of 1wt% was determined above which antiwear and antifriction behavior of formulated grease blends degrades.

[2] Addition of un-functionalized MWCNT at 1wt% decreases the coefficient of friction by 39% and wear scar diameter by 25%.

[3] The morphology and chemical analysis of the worn surfaces helped to determine the antiwear mechanism of MWCNT. From the EDX analysis of the corresponding worn steel surface, it can be seen that the boundary film was composed of MWCNTs, Cr, iron oxide, and other organic compounds.

[4] Tribological behavior of the carboxyl and hydroxyl functionalized MWCNT was comparable with un-functionalized MWCNT.

4. Tribological performance of ionic liquid based grease

4.1 Introduction

Most commonly used multipurpose grease, Lithium based grease has a higher melting point (dropping point) at 190˚C to 220˚C and therefore, offers a broad range of operating temperature range and excellent oxidation, thermal, mechanical, and colloidal stabilities. The lubricating performance of the grease depends on the additive package consisting of antiwear, extreme pressure (EP) additives, friction modifiers, oxidation inhibitors, rust and corrosion inhibitors. Extreme pressure lithium greases subjected to high loads, and temperature conditions demand additive package capable of ensuring high thermal stability and grease consistency at such extreme operating conditions [58]. Conventional solid lubricating additives like graphite, molybdenum disulfide, and PTFE are used in EP lithium greases to meet the required lubricating attributes. However, solid lubricating additives faces the greatest challenge of continuous availability between the two sliding surfaces and this problem necessitates the development of new extreme pressure and antiwear liquid lubricants.

Recently, ionic liquids have received attention as the novel functional lubricant [63]. Ionic liquids are the materials with melting points below 100˚C, so they are present as liquids at room temperature and are referred as Room temperature ionic liquids (RTILs). RTILs are of particular interest in the field of tribology because of their favorable physical properties, such as negligible volatility, nonflammability, high thermal stability, and low melting point. Based on these features, there are high expectations for the development of new ionic liquid applications as lubricants in extreme environments, such as high temperatures, where the use of conventional lubricants is limited.

In 2001, the use of RTILs as lubricants was first reported by Liu et al [59]. Since then, there have been numerous studies reporting RTILs as the base lubricants or lubricating additives. Reich et al. determined the base oil properties of 1-ethyl 3-methylimididazolium bis(trifluoro

methane sulfonyl)-imide and 1-butyl-3-methylimidazolium hexafluoro-phosphate and proposed that imidazolium based ionic liquids have potential as EP additives [74]. Qiming Lu [60] evaluated the performance of room temperature ionic liquid 1-ethyl -3-hexyl imidazolium- bis(trifluoro methyl sulfonyl)-imide as a lubricant for steel–steel contact and stated the excellent antiwear and load carrying capacity of the RTILs as compared to conventional lubricant additives. ILs are currently much more costly than traditional base oils, so their use as a neat lubricant is likely to be limited to critical applications. However, as a lubricant additive, where small amounts can markedly improve the performance, ionic liquids find extensive use. Jimenez et al [61] compared the tribological performance of the imidazolium-based ionic liquid as a lubricant additive in the base oil with the neat imidazolium-based ionic liquids on aluminum contacts using the pin on disc tribometer. They suggested that ionic liquid can act as effective antiwear lubricant additive with the adequate miscibility in the base oil. The ionic liquid used directly as lubricant resulted in worst antiwear behavior due to the tribocorrosive mechanism of the fluorine-based anion.

In the studies discussed above, ILs have been used as lubricants and additives in base oils with good results. Many reported studies are focused on imidazolium cation based ionic liquid and trifluoroborate (BF_4) and hexafluorophosphate (PF_6). However, there are limited number of studies describing the potential of ionic liquid as an additive in lubricating grease. Fox et al. found that imidazolium ILs with trifluoroborate and hexafluorophosphate anions as additives considerably improved the lubricating property of commercial grease. They also stated that ionic liquid based greases resulted in the increase of the weld load for the four-ball extreme pressure test. Motivated by the Fox et al. study, Meirong Cai et al. [62] examined the antiwear and friction properties of five imidazolium-based ionic liquid added as 1 wt% additive in polyuria grease using oscillating reciprocating wear and friction tester and four ball wear tester at room and high temperature. They found the tribological properties of ionic liquid based greases were better than the base grease containing 1wt% of zinc dialkyldithiophosphate (ZDDP). They attributed the excellent tribological

properties of ionic liquid based greases to the good miscibility of ionic liquid in grease and formation of a surface protective film composed of FeF_2, nitrides, and compound containing the P–O bonding on the lubricated metal surface by a tribochemical reaction [62].

Ionic liquids are also called designer's liquids because various characteristics can be created by different combinations of anions and cations. Owing to this wide variety of choices, it is important to understand the characteristics of the ionic liquid targeted for use as a lubricant. Selection of a proper combination of anion and cation of ionic liquid is important to achieve considerable lubrication performance. The range of ionic liquids with variety of anion and cation moieties have been investigated and many of them have miscibility issues in non-polar oils such as mineral oil and polyalphaolefin (PAO). Recently, two phosphonium ILs, trihexyltetradecylphosphonium bis(2-ethylhexyl)phosphate and trihexyltetradecylphosphonium bis (2,4,4-trimethylpentyl) phosphinate, were found to be fully miscible in a mineral oil and a PAO and they performed well as anti-wear additives. It has been suggested that ionic liquid should contain long alkyl chain length and have high ion association for miscibility in non-polar oils and good antiwear performance [63,67]. The anions also have a significant influence on the tribological properties of ionic liquids. Hydrophobic anions such as BF_4 and PF_6 occasionally cause corrosion of steel under humid conditions. In contrast, other hydrophobic anions containing nitrogen and phosphorous active species are less corrosive and exhibit excellent tribological properties [65].

The primary aim of this study is to evaluate the potential of ionic liquid as an antiwear and antifriction additive in lithium based grease. Based on the current understanding of the research of ionic liquid as lubricant antiwear additives, four ionic liquids with either phosphonium cation or phosphate anion was selected for this study. Choline bis(2-ethylhexyl)-phosphate, Choline dibutyl-dithiophosphate, Methyl-tributyl-phosphonium dimethyl-phosphate, Tetra-n-butyl-phosphonium O, O-diethyl-dithiophosphate were added in commercial lithium based grease at 0.2 wt% treat rate. The ionic liquid additives were compared to zinc dialkyldithiophosphate, which is typically used in

grease as a friction reducing and antiwear additive, but it is a sulfur and phosphorus containing compound that may pose pollution to the environment.

4.2 Experimental Details

4.2.1 Details of Additive chemistries and grease blend formulation

In this study, grease blends were formulated using different antiwear additives and synthetic base oil. Synthetic base oil and zinc dialkyl dithiophosphate (ZDDP) were commercially purchased. The ZDDP used in this study is a secondary alcohol derived ZDDP with approximately 70% neutral and 30% basic characteristic. Four different ionic liquids used in this study were provided from AC2T Research GmbH Austria. Table 3 details the chemical structure of the antiwear additives used including ZDDP and the four ionic liquids. The four different ionic liquids were selected to provide diversity in the chemistry. This also help to understand the contribution of different cations and anions on the tribological performance of the ionic liquids. Choline bis(2-ethylhexy)-phosphate (N_DEHP) and choline dibutyl-dithiophosphate (N_DBDTP) have the same cation while one anion has phosphate structure and another has a thiophosphate structure. Methyl-tributyl-phosphonium dimethyl-phosphate (P_DMP) and tetrabutyl-phosphonium O,O-diethyl-diphosphate (P_DEDTP) have similar (not same) cations while the anions have either a phosphate or thiophosphate moiety. The tribological behavior of four different ionic liquids is compared with conventional metal based ZDDP antiwear additive.

Grease blends of NLGI grade 2 were formulated by adding lithium complex thickener with synthetic base oil at 100:30 ratio. To this mixture antiwear additives were added at constant phosphorous treat level of 0.2 wt%. Table 4 describes the different grease blends formulations prepared. For the baseline comparison, base grease blend without any additives was also prepared.

Table 3 Structure and chemical names of four ionic liquids and ZDDP

Coded Name	Chemical Name	Chemical Structure
N_DEHP	Choline bis(2-ethylhexyl)-phosphate	
N_DBDTP	Choline dibutyldithiophosphate	
P_DEDTP	Tetrabutyl-phosphonium O,O-diethyldithiophosphate	
P_DMP	Methyl-tributylphosphonium dimethylphosphate	
ZDDP	Zinc dialkyl-dithiophosphate	

Table 4 Details of grease blends formulations with the coded names

Coded Name	Base Grease	Additives
Base Grease	Lithium complex	-
DBDTP	Lithium complex	Choline dibutyldithiophosphate
DEHP	Lithium complex	Choline bis(2-ethylhexyl)-phosphate
DMP	Lithium complex	Methyl-tributylphosphonium dimethylphosphate

DEDTP	Lithium complex	Tetrabutyl-phosphonium O,O-diethyldithiophosphate
ZDDP	Lithium Complex	Zinc dialkyl-dithiophosphate

The blends were formulated using a Kitchen-Aid Mixer. The electrical specifications of the mixer were, 120 Volts, power rating of 250 W. Each formulation was blended for 2 hours with hand mixing at every 25 minutes. Initially calculations were carried out for 100:30 ratio of thickner and synthetic base oil for 100 grams of total blend. Then the base oil and antiwear (ionic liquids/zddp) additive was measured for 0.2 wt% treat level and hand mixed in the steel container. About 30-40gms of base grease was initially added to the mixture of base oil and antiwear additive and hand mixed and later the complete mixture was mixed in the Kitchen-Aid at a speed of 100 rpm. Figure 4-1 shows the Kitchen Aid in the TLCL used for grease blends formulations.

Figure 0-18 Kitchen Aid Mixer

The blended greases are tested further in a Plint Four-Ball Tribometer. They are evaluated for wear and friction performance. If the blended grease is not used over a period of time there is high probability of oil separation. Before every use the grease is mixed using a spatula manually.

4.2.2 Tribological Test Details

ASTM standard D2266 test was used to evaluate the tribological performance of the prepared grease blends. The test was performed using four ball tribometer at 40kg load, 12000rpm and 75˚C temperature condition. The Plint TE-92 Rotary Tribometer provided from Phoenix Tribology (London, UK) shown in figure (4.2) was used. About 10-15gms grease was loaded in the steel cup. Three E52100 ½" steel balls were taken in the cup, which were fixed with the help of a holding cup and a hexagonal nut (Lower Loading assembly). The fourth ball was taken in the chuck and fixed to the top rotating spindle. The spindle ball was normally loaded (0.39 kN) against the three base balls to create a point contact and heated (upto test condition). The spindle and the top ball were rotated at speed of 1200rpm for 72000 cycles. The lubricating medium ran between the top ball and base balls, thus evaluating its tribological properties. The friction coefficient is measured using a load cell attached to the lower loading assembly and another load cell attached such as to measure the torque sensed by the lower assembly which could freely rotate over a centre spindle. All the tests were repeated thrice to ensure repeatability.

Figure 0-19 Four ball tribometer at TLCL facility in UTA.

The friction values after the test are measured by the formula as described in the ASTM D5183 and using the torque and load values generated during tests from the Compend X software assisting the four ball tribometer. After the termination of every test, the three stationary steel balls were retrieved and analyzed to determine the WSD (Wear Scar Diameter) using stereo-optical microscope and image J software.

4.2.3 Stere-optical microscope

Stereo-Optical microscope (model type: Nikon SMZ 1500) was used to image the wear scars formed on the three stationary steel balls after the four ball tests. The steel balls were cleaned using hexane and were mounted on a home-made sample holder; which were then imaged at a

magnification of 100X on the microscope. The images were analyzed using the Image J software. The software comprised of measuring tools & Pixel-counter which was used to document the WSD for all the three steel balls and an average value was reported. Wear Scar Diameter for each blend was determined using an average of 18 readings on 9 samples from a total of three repeat runs. Each reading represents the average value of longest horizontal striation and longest vertical striation. Imaging all the samples ensured machine repeatability and normal loading of the samples by the spindle.

Figure 0-20 Stereo Optical Microscope at CCMB facility in UTA.

4.2.4 Scanning Electron Microscopy (SEM) and Energy Dispersive Spectroscopy (EDS)

SEM (model type: Hitachi S-3000N) was used in the SE (Secondary Electron) mode to image the wear surfaces developed on the stationary steel balls. Images were taken at an accelerating voltage of 15-20 kV was used in all the cases. Carbon tape was used to maintain good electrical contact in between the steel balls and sample holder. The wear mechanism in play on the surface formed on the surface was evaluated by observing images at 100X and 500X. Specific areas on the surface showing distinct wear tracks and surface morphology were imaged at a higher magnification of 1000X to understand the wear mechanism.

EDS spectrums were collected for the wear test samples. The spectrums were for the magnification of the 1000x, the voltage was charged down to 15kV to reduce the penetration depth. The spectrum was collected in order understand the carbon percentage on the worn surfaces. EDS maps were also collected. EDS elemental mapping helps to understand the antiwear protection of antiwear additives towards severe wear of the surfaces.
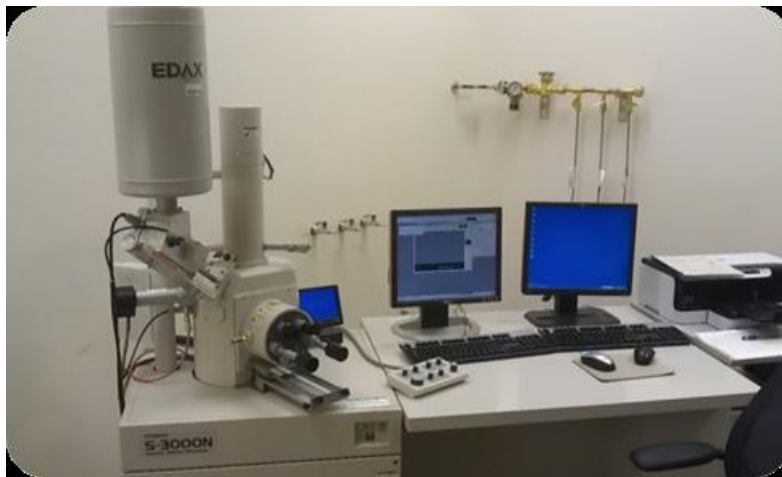
Figure 0-21 SEM-EDS setup at CCMB facility in UTA.

4.3 Results

4.3.1 Friction Results

The coefficient of friction (COF) values are obtained using the procedure described in ASTM D5183-05. The procedure involves use of normalization factor [68]. Coefficient of friction values are derived using following formula:

$$COF = (0.2227*Torque)/Load$$

The absolute torque and load values were received from the tests conducted using the Four-ball tribometer. Figure 4.5 exhibits the change in COF values during the test run for the grease blends containing ionic liquids and ZDDP as antiwear and antifriction additive added at 0.2wt% Phosphorus treat level.
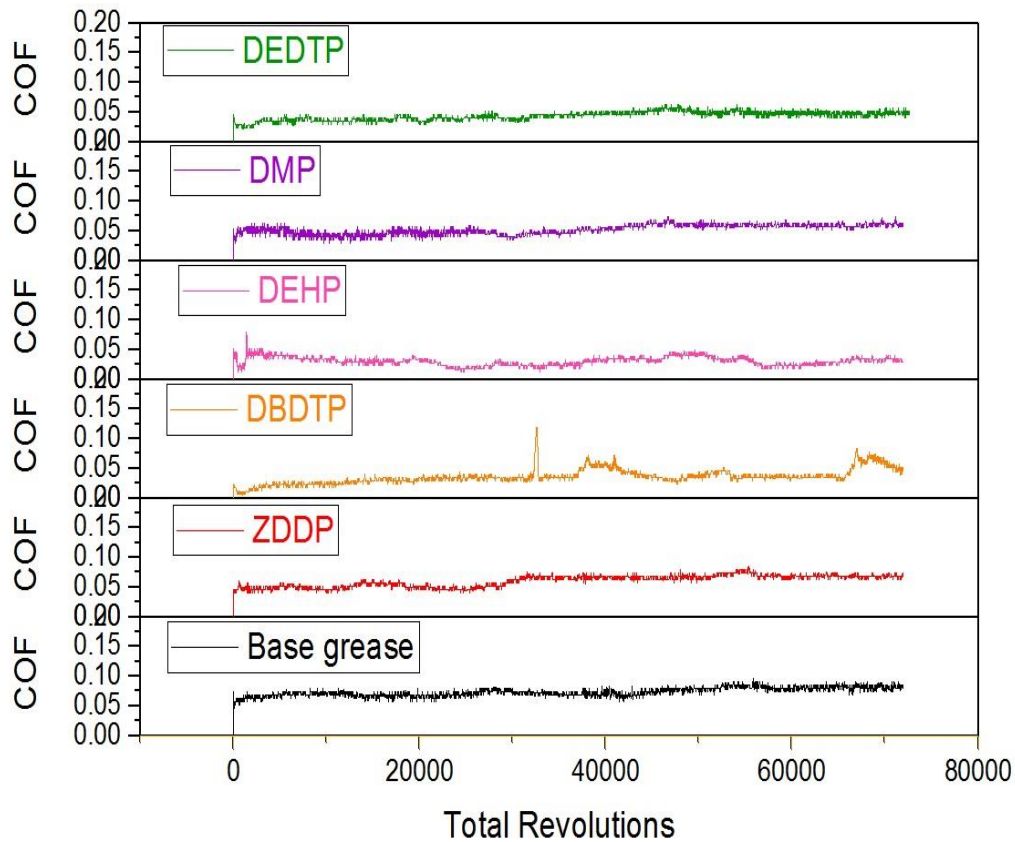
Figure 0-22 Comparison of COF values of four different ionic liquids with ZDDP and Base grease.

All four ionic liquids and ZDDP show improvement in friction response compared to base grease without any additives. Ionic liquid DEHP has the lowest friction coefficient however the COF shows sudden drop at certain revolutions. Ionic liquids DBDTP, DMP and DEDTP also display lower coefficient of friction in comparison to ZDDP for the duration of the test. Careful observation reveals all antiwear additives exhibits some variations in COF values as compared to the base grease. Friction behavior of the grease blends is evaluated in terms of the average coefficient of friction values generated from the three test runs conducted for each grease blends. Figure (4-6) is a plot of the average coefficient of friction generated for four ionic liquids along with ZDDP and base oil.
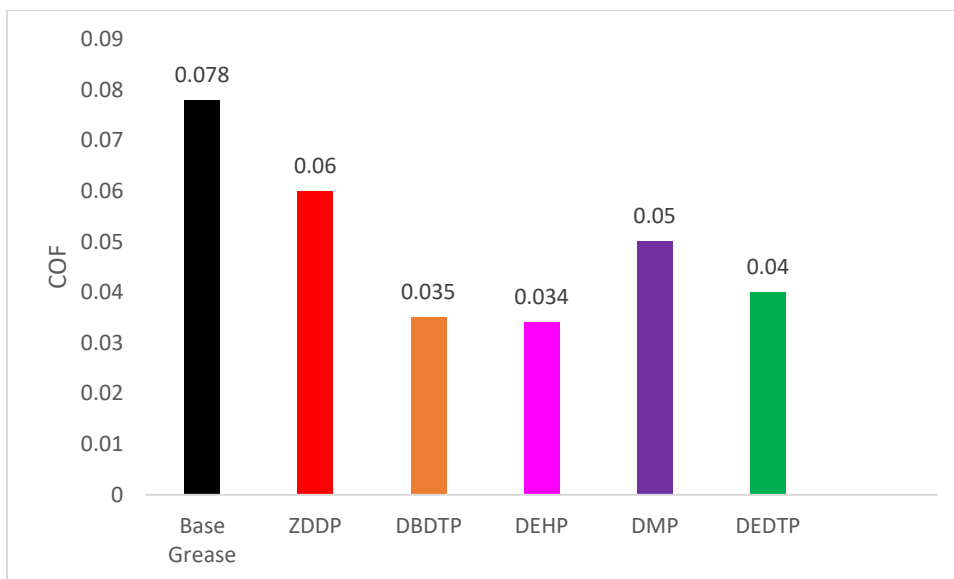
Figure 0-23 Friction results for grease blends with four different ionic liquids and ZDDP.

The high COF value of 0.078 for the base grease blend conveys the need of addition of friction modifier. Comparison of COF values indicates that ZDDP is the poor friction modifier for the extreme pressure grease application. Choline cation based DBDTP and DEHP exhibits excellent antifriction performance. Addition of DEHP at 0.2 wt% P resulted in 57% decrease in coefficient of friction value which evidences the potential of the ionic liquids as antifriction additives. Phosphorus cation based ionic liquids, DEDTP and DMP does not show impressive reduction in coefficient of friction.

4.3.2 Wear Results

Antiwear performance of all the grease blends is determined in terms of the average wear scar diameter developed during four ball tribo-test. Calculation of average wear scar diameter is discussed in section 4.2.3. Figure 4.7 is a column chart of an average wear scar diameter (WSD) for four ionic liquids along with ZDDP and base grease. In comparison with base grease, all ionic liquids showed significant improvement in wear protection in lithium base grease. ZDDP is well known antiwear additive, however, in this study addition of ZDDP at mere 0.2wt% P resulted in

poor antiwear performance. Choline cation based ionic exhibits better antiwear performance than the phosphonium cationic ionic liquids. Figure 4-8 exhibits the correlation between coefficient of friction with the wear results.
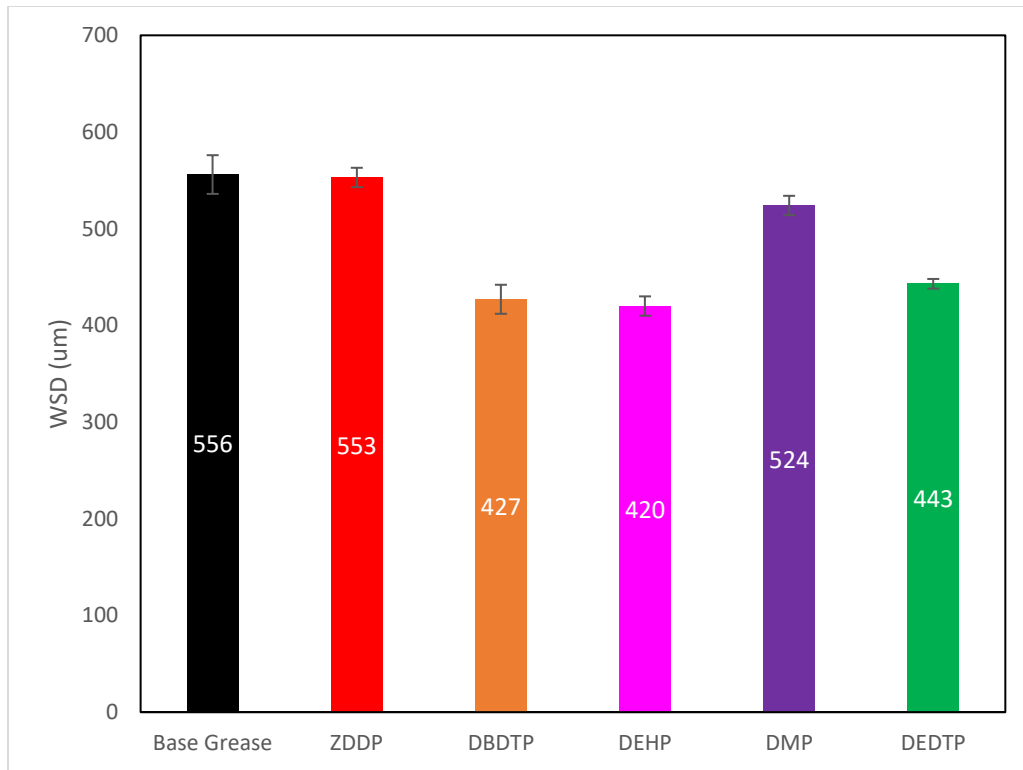
Figure 0-24 Comparison of WSD of four ionic liquids with ZDDP and Base Grease.
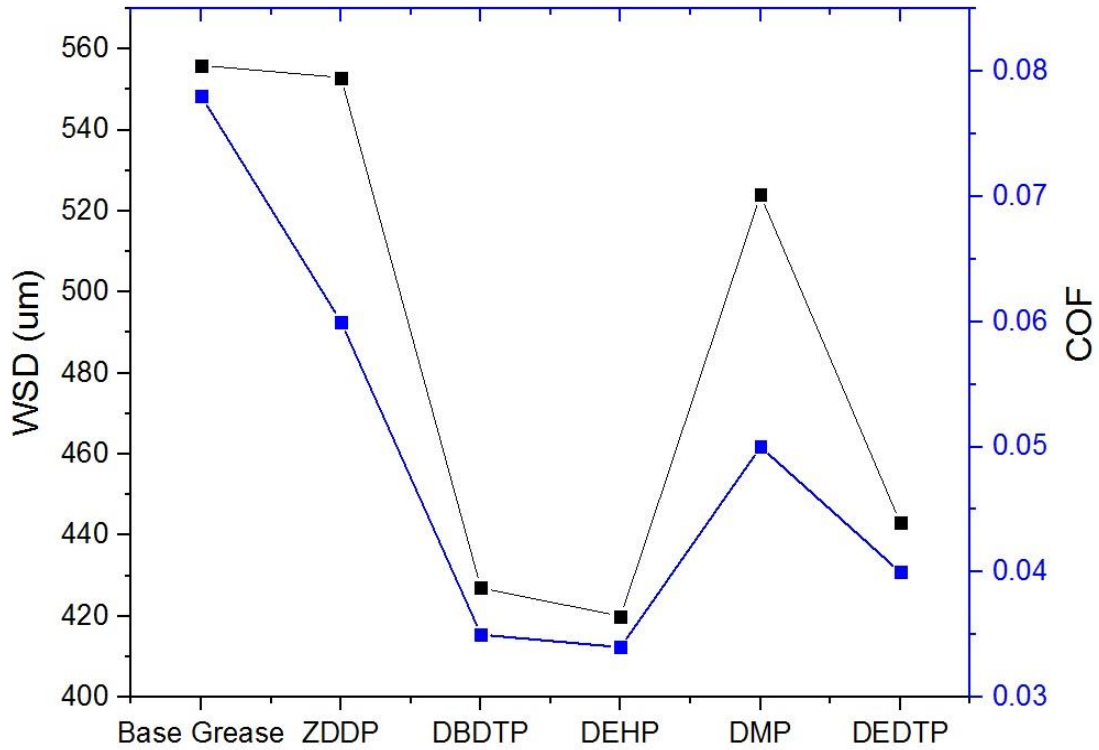
Figure 0-25 Correlation of COF and WSD

4.3.3 Analysis of Morphology of the Wear Surface using Scanning Electron Microscope

The SEM images for the wear surface were obtained for all the tests of base grease, ZDDP and ionic liquids at 100X, and 1000X which correspond to the lower and higher magnification images at an acceleration voltage of around 25 kV and a working distance of 14 mm to 16 mm. Figure (4.9) displays the low magnification images of the wear scar of all the grease blends.
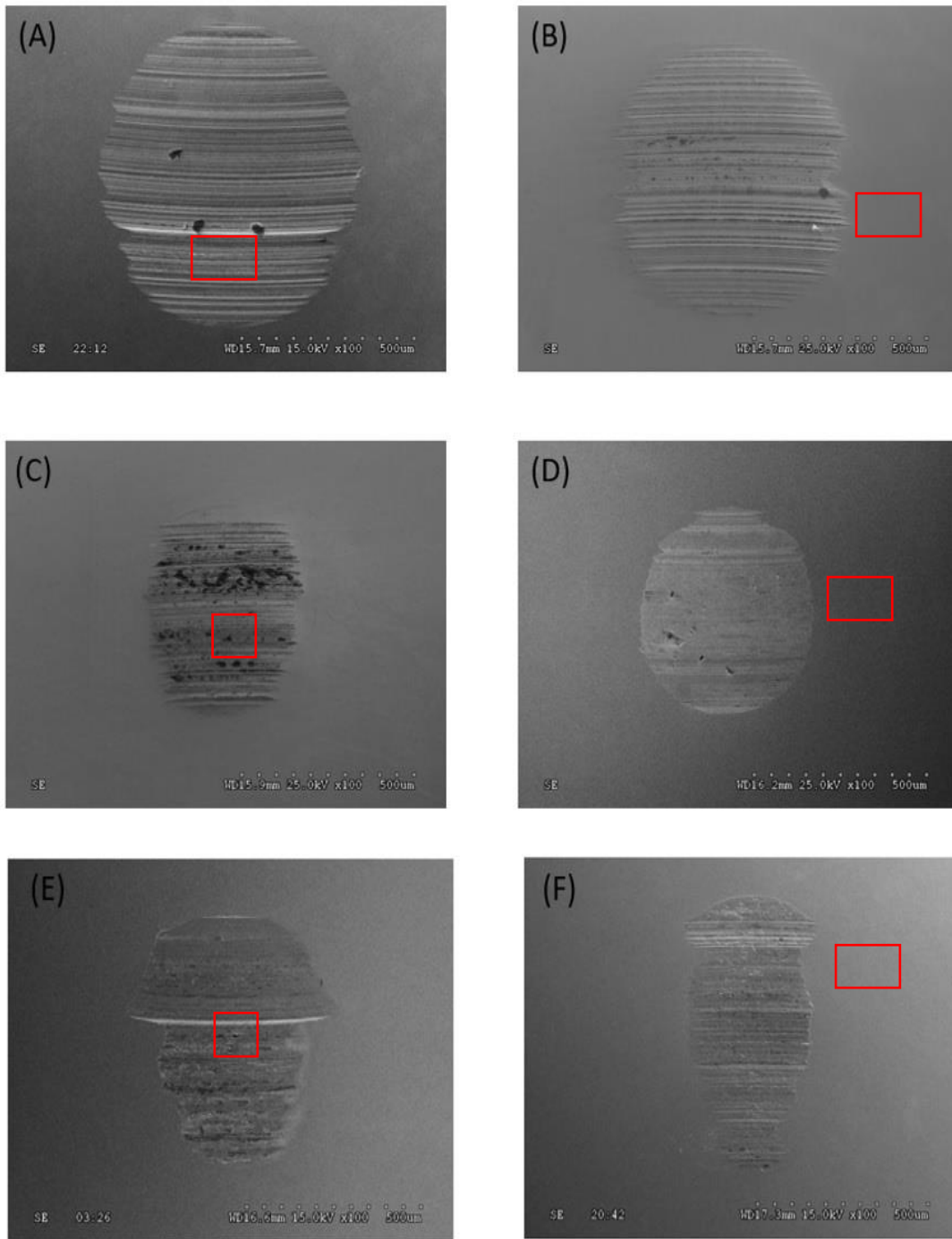
Figure 0-26 Low magnification SEM images of the wear scar at 100X (A) Base Grease (B) ZDDP

(C) DBDTP (D) DEHP (E) DMP (F) DEDTP

SEM images of the wear scar at low magnification gives an idea about the wear scar diameter and overall characterstic features. Wear scars of ZDDP and DEHP appears smooth in nature as compared to DBDTP, DMP and DEDTP. High magnification images at 1000x as shown in figure (4-10) helps to understand the nature of the wear and morphology of the worn surfaces.
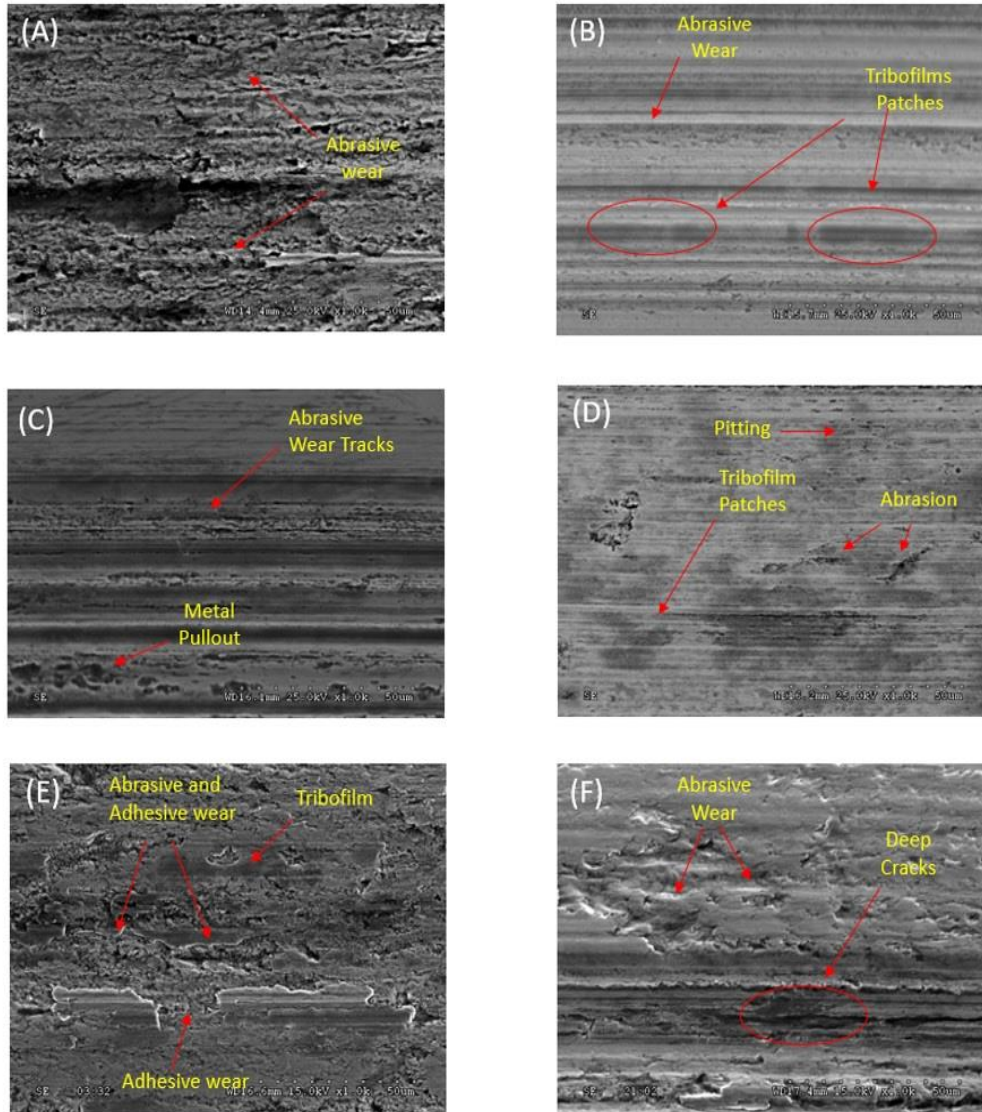
Figure 0-27 High Magnification SEM images of (A) Base grease (B) ZDDP (C) DBDTP (D) DEHP (E) DMP (F) DEDTP

Base grease sample exhibits large wear scar and combined abrasive and adhesive wear throughout the wear scar. As no additive protection was present in the base grease, direct metal to metal contact have resulted in abrasive worn surface. SEM image of ZDDP lubricated surface exhibits regions of abrasive wear with scratches aligned to the sliding direction together with the formation of protective patchy tribofilms. DEHP SEM image exhibits dark patches throughout the wear scar which corresponds to less conductive patchy tribofilms formation. The SEM image of DBDTP worn surface shows slight abrasive wear tracks and patchy tribofilm formation, with patch sizes that are larger than what is seen in DEHP. On the other hand, the wear surfaces observed in the case of DMP and DEDTP exhibit deeper scratches and severe adhesive-abrasive wear compared to DEHP and DBDTP. Also, the wear surface of DMP and DEDTP appears to be rougher than the DEHP and DBDTP. The analysis of the morphology of worn surfaces thus correlates to the wear results discussed earlier. DEHP and DBDTP showed smaller WSD value than the DMP and DEDTP. In order to further understand tribological behavior of the ionic liquids, chemical composition analysis of the wear scar is done by using EDS.

4.3.4 Energy Dispersive (EDS) Analysis of the Wear Scar Surfaces

EDS spectra were obtained to elucidate the tribo-chemistry of the worn surface. Wear scar areas magnified at 1000X showed in the figure 4-10 was subjected to EDS spectrum analysis. Element spectrum analysis determines the type and amount of element present on the worn surfaces of the stationary ball. Figure 4-11 exhibits elemental spectrums for four ionic liquid compared with ZDDP. All spectrums were obtained with acquisition of approximately 1,20,000 net count. Table (4) details the amount of antiwear forming elements phosphorus and sulfur comprised in the tribofilms formed by ionic liquids and ZDDP.
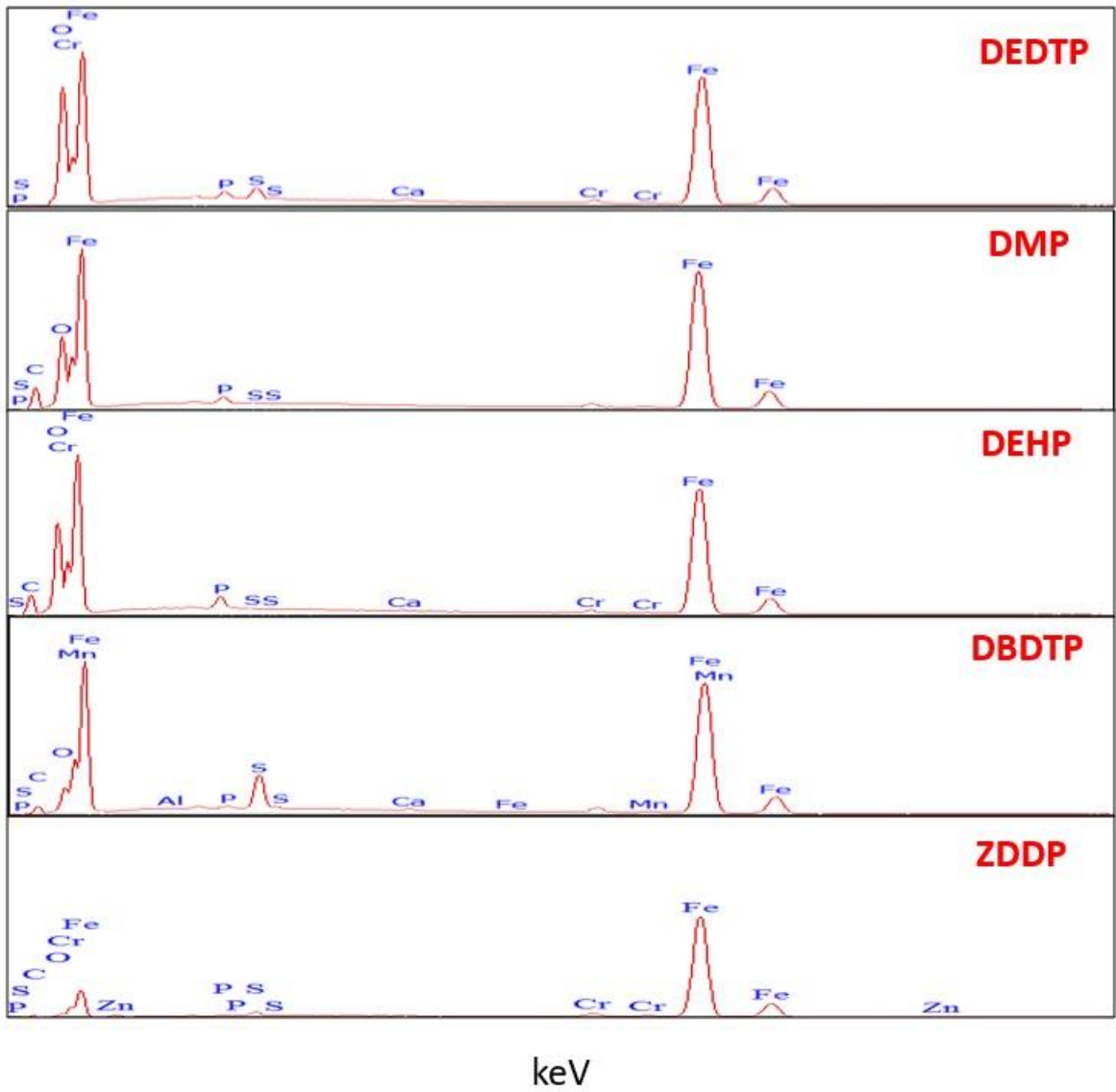
Figure 0-28 Comparison of EDS spectra of four ionic liquids with ZDDP.

Table 2 Phosphorus and sulfur element concentration

Grease Blend	Phosphorus atom wt%	Sulfur atom wt%
ZDDP	0.29	1.60
DBDTP	0.38	5.48
DEHP	1.60	-
DMP	0.76	-
DEDTP	0.36	2.22

ZDDP is well known to form antiwear tribofilms consisting of zinc phosphates, zinc sulfides/sulfates, iron phosphate and iron sulfides/sulfates. EDS spectra and concentration table suggests less amount of ZDDP tribofilms formed in this study. DBDTP wear surface shows the presence of good amount of sulfur based films and less amount of phosphorus films. DEHP results in formation of iron phosphate based tribofilms and provides excellent protection against the rubbing process. As the sulfur is not present in the original structure of DEHP and DMP, no sulfur peaks were determined from their lubricated worn surfaces. DMP EDS spectra demonstrate shorter peak of phosphorus than DEHP and hence correlates well with the wear results of higher WSD than DEHP. DEDTP has the phosphonium cation and dithiophosphate anion which results in detection of phosphorus and sulfur peaks.

4.4 Discussion

The potential of ionic liquid as extreme pressure antiwear additive under boundary lubrication regime was assessed in terms of wear scar diameter (WSD), coefficient of friction (COF), wear surface morphology and chemical analysis using SEM-EDS. Figure (4-6) and (4-7) represents the average coefficient of friction and average wear scar diameter resulted from four ball tribometer test performed with lubricating greases containing four different ionic liquids and ZDDP.

Addition of ionic liquids at 0.2wt% P enhances the antifriction and antiwear properties of the lithium complex base grease. Ionic liquids exhibited better tribological performance than the ZDDP and base grease. Choline base ionic liquid, DEHP resulted in reduction of coefficient of friction by 57% and wear scar diameter by 25%.

Figure (4-8) correlates the friction and wear results of ionic liquid and ZDDP. ZDDP showed adverse antifriction and antiwear behavior as compared to all ionic liquids used in this study. DBDTP and DEHP original structure has the same choline cation, however, there is difference in anionic moiety, DBDTP has thiophosphate anion while DEHP has phosphate anion. Out of DBDTP and DEHP, DEHP exhibited better performance. In the case of phosphonium cation based DMP and DEDTP, DEDTP showed better tribological performance. DEDTP has the longer chain length than the DMP. And also, there is a difference in their anionic moiety, DEDTP has phosphate while DMP has thiophosphate anion. This indicates that the functional group in the ionic liquid molecules plays an important role in increasing the antiwear and antifriction ability. Interestingly, both the anions and the length of the alkyl chains of the ionic liquid molecules have a significant effect on the tribological properties.

The good tribological performance of the ionic liquids could be attributed to their unique dipolar structure. Owing to that ionic liquids could be very easily adsorbed on the friction contact pairs to form an effective boundary film. These adsorbed films cover the rough surface asperities of the interacting surfaces and contributes towards the reduction of coefficient of friction. In addition, the reduction of WSD is due to the tribofilms formed by the reaction of adsorbed antiwear additive films with the rubbing surface. Antiwear additive tribofilms mainly contribute to improve the friction-reduction and antiwear performance under relatively high loads.

The formation of the lubricating and protective film on the contacting surface can be further confirmed by the corresponding SEM-EDS analysis. From the figure (4-9), it can be seen that the SEM image of the wear scar of only DEHP appeared to be smoother than other ionic liquids, which

advocates the least WSD and COF value of DEHP grease blend. Morphological study of the wear scar surfaces of DBDTP, DMP and DEDTP exhibited the rough wear surfaces with the adhesive wear, deep scratches and abrasive grooves in the direction of sliding. The tribofilms formation by ionic liquids and ZDDP was evident from the dark patches observed on the SEM images of the worn surfaces. To confirm the presence of tribofilms, EDS analysis was carried out. EDS spectrum analysis (figure 4-11) successfully displayed that the chemistry of the wear surfaces lubricated with ionic liquid based greases mainly consists of phosphorus and sulfur based compounds. From the EDS concentration table (4-3), it can be seen that the presence of the antiwear element on the worn surface is related to the original structure of the ionic liquid. DEHP and DMP didn't showed the presence of sulfur element while DBDTP and DEDTP exhibited the presence of both phosphorus and sulfur. This hints that the tribofilm composition is dependent on the original structure of ionic liquids and anionic moiety plays some role in the tribofilm formation.

The analyses of the worn surface by SEM-EDS showed that complicated tribochemical reactions were involved in the sliding process. It is well known that during the sliding process, there is low-energy electrons emitted from contact convex points on metal surface and the positive charge formed at the surface of tiny convex volume commonly. The anion part of ionic liquid can easily adsorb onto the positive charged sites of metal worn surface. Under the boundary lubrication regime (used in this study), points at the surface asperity contacts generate very high temperature and pressure, which induces thermo-mechanical decomposition of the physiochemically adsorbed ionic liquid. The final byproduct of this reaction is deposited on the rubbing surface which ultimately provides the protection against the continued sliding condition. Therefore, it is safe to reason out that the ionic liquids undergo decomposition and forms the tribofilm comprising of iron phosphate, iron sulfides/sulfates. The tribofilms act like a sacrificial film which periodically form and break-down due to the shearing action during the process. Many authors have proposed that the ionic liquids form the tribofilm similar to ZDDP [60,63,66,67]. It is important to note that in this study

ZDDP didn't exhibited the comparable tribological performance to that of ionic liquids. There are several possibilities for this performance, first may be the rate of film break down was higher than the rate of film formation by ZDDP. Secondly, it is possible that the concentration of ZDDP was insufficient to maintain the film formation throughout the test.

As stated earlier, in this work functional group and alkyl chain length are having influence on the tribological performance of the ionic liquids. Comparison of the friction and wear results of the ionic liquids having same cation helped to determine phosphate as the beneficial anion moiety (i.e the tribological performance was in this order: DEHP >DBDTP and DEDTP>DMP). Similarly, comparison of the ionic liquids with same anion directed that the choline cation based ionic liquid resulted in better antiwear ability (i.e the tribological performance was in this order: DEHP >DMP and DBDTP>DEDTP). It is reported by many authors that the coefficient of friction and wear volume decreases as the alkyl chain length of the room temperature ionic liquid increases. In this study, two ionic liquids DMP and DEDTP were selected with the same phosphonium cation but with different chain length. The DEDTP having longer alkyl chain length showed the better tribological performance than DMP. The ionic liquids of longer alkyl chain have stronger adsorption on the sliding metallic surfaces and chemisorbed films are easier to form and hence they show better antiwear ability than the ones with shorter alkyl chain. However, though the DEDTP has the longer alkyl chain length than the DEHP and DBDTP, it showed poor antiwear performance. This behavior can be explained by referring to the Vibhu et al comparative study of the chemical and mechanical properties of the tribofilms formed by six different ionic liquids using cylinder on flat tribometer. They proposed that the DEHP and TFSI ionic liquid showed the comparable antiwear performance to that of ZDDP at 0.1wt% P treat level. They also studied the chemical composition of the tribofilms using XANES characterization technique and suggested that the ionic liquids formed short chain polyphosphate with the length of polyphosphate in decreasing order of DEHP>DBDTP>DEDTP [66]. Longer alkyl chain length will facilitate the film formation by physio-chemical adsorption, but,

the antiwear protection at higher stress conditions is due to the presence of tribofilms instead of adsorbed films. Thus, the additive capable of forming tribofilms with the longer chain of polyphosphates will contribute more towards the improvement of the antiwear and antifriction property. Therefore, in this study, the antiwear performance of ionic liquids used as an antiwear additive is correlated with the length of chain of polyphosphates instead of the alkyl chain length.

4.5 Conclusion

[1] As the extreme pressure antiwear additives in lubricating lithium based grease, the four-different phosphorus and sulfur based ionic liquids show excellent tribological behavior and are superior to the conventional antiwear additive, ZDDP. The addition of DEHP at 0.2wt% P treat level resulted in decrease of coefficient of friction by 57% and wear scar diameter by 25%. Choline cation based ionic liquid, DBDTP and DEHP showed better antifriction and antiwear performance than the phosphonium cation based ionic liquids, DEDTP and DMP.

[2] The SEM/EDS results indicated that the ionic liquids as the lubricants experienced tribochemical reaction in the sliding of steel against steel, with the formation of a surface protective film composed of iron phosphates and iron sulfides/sulfates on the worn surface. This helps to improve the friction and wear behavior.

[3] Physical adsorption and complicated tribochemical reactions both play an important role in antiwear protection mechanism. Namely, the tribological behaviors of all the four ionic liquids were dependent on both the anions moiety and the length of short chain polyphosphate.

5. Tribological Performance of the grease with the combined additive mixture of MWCNT and ionic liquid

5.1 Introduction

The quest of developing advanced grease lubricating additives capable of meeting modern mechanical systems harsh operating conditions has been expanded with the advent of new nanomaterials. Numerous nano-particles as the solid lubricant additives in oil or greases have been investigated in the recent years [35,55]. Solid lubricant additives are always preferred for the applications demanding excellent tribological performance under rigorous conditions involving very high temperatures, ultra-high vacuum, radiation, extreme contact pressure, very low or high speeds, etc. Moreover, solid lubricant additives are capable of providing protection against high frictional forces at such interfaces where liquid lubricants squeezed out. Over the last two decades, molybdenum disulfide (MoS_2), graphite, hexagonal boron nitride, boric acid and poly-tetrafluoroethylene (PTFE) have been used as the friction modifier and extreme pressure additives in the lubricating greases. The lubricity and durability of all solid lubricants are controlled by mechanisms that may involve interfilm sliding, intrafilm flow, and film/substrate or interface slip (with and/or without third body or transfer layer formation.

Carbon based materials have attracted tremendous attention in tribology field Because of their high load-bearing capacity, high chemical stability, weak intermolecular and strong intramolecular bonding, particle size and chemical stability. Several studies have reported the potential of carbon nanotubes as the lubricating additives in the oil [18,20,26,39,47]. However, very limited research has been done on the carbon nanotubes as an additive in lubricating greases. Our companion study evaluated the tribological performance of multi-walled carbon nanotubes (MWCNT) at different concentration in the lithium grease. It was observed that MWCNT at optimal concentration of 1wt% can effectively reduce the coefficient of friction by 39% and wear

scar diameter by 25%. The lubrication mechanism of MWCNT was proposed using SEM-EDS analysis of the worn surfaces developed by lubricated grease containing 1wt% of MWCNT. SEM-EDS analysis showed the presence of carbon element on the wear tracks and ploughing grooves. Based on the observation, it was proposed that MWCNTs formed a thin layer at the surface through physio-adsorption and intervene the contact of the interacting surfaces. This layers impart smooth surface for the continued sliding process and enhances the antiwear and antifriction protection. Also, because of the unique structure and high young modulus, adsorbed MWCNT undergoes low shearing and minimizes the high friction forces. It was assumed that due to extreme pressure and stress conditions, shearing or deformation or even breaking of MWCNT can lead to the formation of transfer films/lamellar films of amorphous carbon on the rubbing surface. The tribological performance of MWCNT can be increased by the achieving adequate degree of dispersion and stability in the lubrication system.

In addition to solid additives, liquid lubricant additives containing phosphorus and sulfur also find application at extreme operation conditions. Liquid lubricant additives undergo decomposition under boundary lubrication condition and forms the protective interfacial layers at contacting surface. The most well-known example of liquid additive is zinc dialkyldithiophosphate (ZDDP). Excellent antiwear performance of ZDDP is attributed to the formation of amorphous glass like tribofilms comprising of phosphates, sulfides/sulfates of iron and zinc. Lot of efforts have been carried out by researchers to replace ZDDP due to its environmental concern. Recently, ionic liquids have attracted considerable interest because of their favorable physical properties, such as negligible volatility, nonflammability, high thermal stability, and low melting point [62]. These attributes are essential to an ideal lubricant. Because of the excellent performance of ionic liquids, they are good candidates for high performance lubricants [62].

Our companion research work on the novel ionic liquids convinced that ionic liquids are superior to ZDDP and can be used as an effective antifriction and antiwear additive in lithium grease. The comparative study of four different phosphorus and sulfur based ionic liquids with the ZDDP was carried out using four ball tribometer test. All ionic liquids showed better tribological performance than ZDDP. Addition of the ionic liquid having choline cation and phosphate anion, DEHP at 0.2wt% P treat level showed decreased the coefficient of friction by 57% and wear scar diameter by 25%. Based on the comparison of the tribological performance of four different ionic liquids it was concluded that the anionic moiety and alkyl chain length plays important role in the antiwear ability of ionic liquid. It was proposed that the ionic liquid capable of forming long chain polyphosphates can exhibit better tribological performance under boundary lubrication test conditions.

From the perspective of complimenting the respective tribological properties of liquid and solid lubricants, it would appear advantageous to combine them. Together the two materials could provide lubrication over a wider spectrum of loads and speeds than either component separately. In this work, the preliminary tribological tests of the lithium grease blends containing additive mixture of MWCNT and ionic liquid are reported. It is hypothesized that addition of ionic liquid and MWCNT will result in synergetic effect, i.e. the ionic liquid will form sacrificial tribofilms on rubbing surfaces while MWCNT will contribute towards the wear protection by forming adsorbed layer on the wear tracks and grooves. The coefficient of friction of MWCNT is higher than that of ionic liquid, their combined mixture may enhance the antifriction performance. We postulate that the ionic fluid may form a strong physisorbed layer upon the SWNTs due to their strong dipole moment and separate the formation of bundles of MWCNTs. More numbers of bundles with fewer nanotubes will provide a larger solid-phase contribution to the lubrication system.

This chapter deals with the effect of MWCNT interaction with ionic liquid on the antifriction and antiwear properties of the lithium greases. Initially, the effect of mixing temperature and functionality of MWCNT is studied. The findings from the initial study is then used to prepare the grease blends at the adequate temperature with the suitable functionalized MWCNT. Also, the effect of different ionic liquid cationic and anionic moieties on the interaction with MWCNT is studied by using stereo-optical microscope, scanning electron microscopy and energy dispersive.

5.2 Experimental Procedure

5.2.1 Details of Additive Chemistries
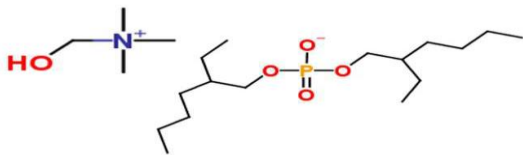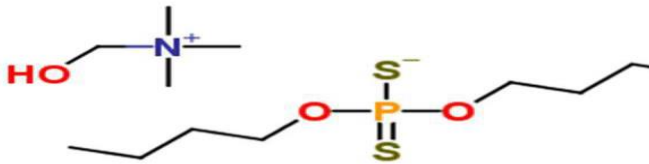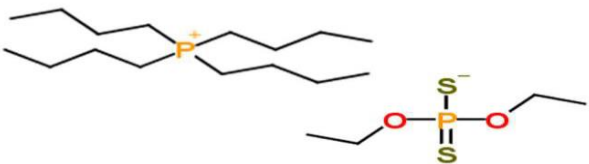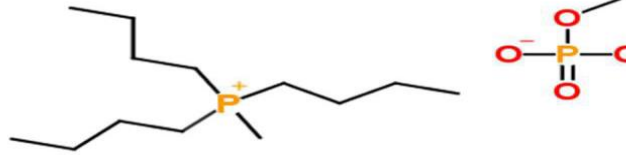
In this study, the grease blends with the additive mixture of MWCNT and ionic liquid was prepared. Base grease used was lithium complex thickener. This grease was obtained from the supplier by removing a pail during the grease making process before adding any type of additives. This helped in understanding of the role additives and getting control test data showing tribological effects of only the test additive. Since the test base grease had been pulled out early in the process, remaining base oil (added at the end of the process to achieve desired consistency) had to be added manually. The base grease of NLGI grade 2 was obtained by adding the synthetic base oil in the lithium thickner.

Base oil used was product of Shell manufactured under brand name Shell 46 Rotella T Triple Protection 15W-40. It is basically used as engine oil. It is highly refined mineral oil. It has outstanding shear stability for viscosity control.

The unfunctionalized MWCNT, carboxyl functionalized MWCNT and hydroxyl functionalized MWCNT additives were commercially purchased from the cheap tubes inc. USA. This MWCNTs were made by combustion chemical vapor deposition (CCVD) and purified using concentrated acid chemistry. Both type and diameter are important for MWCNTs selection. The wider the diameter of the carbon nanotube (CNTs), the more it behaves like graphite. The narrower the diameter of the Carbon Nanotubes (CNTs), the more its intrinsic properties depends upon its

specific type. The diameter of MWCNTs used was 20-30nm and the length was 10-30 nm. Along

with the MWCNTs, second additive was ionic liquid. To check the effect of different cation and

anion moieties on the interaction with MWCNT, four different ionic liquids were used. Ionic liquids

were were provided from AC2T Research GmbH Austria. Table 5 details the chemical structure of

the antiwear additives used including ZDDP and the four ionic liquids. Choline bis(2-ethylhexy)-

phosphate (N_DEHP) and choline dibutyl-dithiophosphate (N_DBDTP) have the same cation while

one anion has phosphate structure and another has a thiophosphate structure. Methyl-tributyl-

phosphonium dimethyl-phosphate (P_DMP) and tetrabutyl-phosphonium O,O-diethyl-diphosphate

(P_DEDTP) have similar (not same) cations while the anions have either a phosphate or

thiophosphate moiety. The tribological behavior of four different ionic liquids is compared with

conventional metal based ZDDP antiwear additive.

Table 3 Structure and chemical name of four ionic liquids and ZDDP

Coded Name	Chemical Name	Chemical Structure
N_DEHP	Choline bis(2-ethylhexyl)-Phosphate	
N_DBDTP	Choline dibutyldithiophosphate	
P_DEDTP	Tetrabutyl-phosphonium O,O-diethyldithiophosphate	
P_DMP	Methyl-tributylphosphonium dimethylphosphate	

ZDDP	Zinc dialkyl-dithiophosphate	

5.2.2 Grease Blend Formulations

As no literature is available on the synergetic concentration of MWCNT and Ionic liquids, it was very crucial to form a mixing protocol with the optimum concentration. In the previous study, MWCNT was proved to act as an effective antiwear and antifriction additive at 1wt% concentration in lithium based lubricating greases. Similarly, ionic liquids at 0.2wt% P treat level exhibited good tribological properties. Hence, for the preliminary study grease blends were prepared by adding MWCNT at 1wt% and ionic liquid at 0.2wt% P concentration in the lithium thickener and base oil mixture.

At first, both the additives were weighed carefully and mixed with the Base oil. To achieve adequate mixing, the weighed mixture was subjected to ultrasonication for 30 mins. Ionic liquids are known to be immiscible in the non-polar solvents like synthetic base oil. Therefore, the mixture was subjected to the proper mixing by using pulse ultrasonicator with D.I water bath. Ultrasonication heat is not sufficient to trigger the interaction between MWCNT and Ionic liquid. So, the mixing was carried out at different temperature and time using the magnetic stirrer at constant 150 rpm. After the mixing, additives were added into lithium based thickener and the mixture was blend in a kitchen aid blender for about 2 hours. After an interval of 15 to 20 min, the blender was stopped and a spatula was used to manually mix the content in the steel bowl of the blender which ensured homogeneity and adequate blending of the grease. For the study of mixing temperature and time MWCNT_COOH and ionic liquid DEDTP were selected. It was assumed that the longest alkyl chain length of the DEDTP phosphonium cation will effectively act as the barrier

between stacking interactions among the nanotubes. The effect of additive mixing temperature and time was assessed from the friction and wear results of the grease blends. Details of the time and temperature selection is discussed in the section 5.3.1. The details of the grease blend formulations were prepared for the study of mixing temperature and time is given in the following table 6.

Table 4 Details of the grease blend formulations for the study of mixing temperature and time

Coded Name	Base Grease	Additives used	Mixing Temperature (˚C)	Time
Blend_01	Lithium Complex	MWCNT_COOH & DEDTP	Room Temperature	30 min
Blend_02	Lithium Complex	MWCNT_COOH & DEDTP	50	120 min
Blend_03	Lithium Complex	MWCNT_COOH & DEDTP	50	12 Hrs.

After selection of proper mixing time and temperature, effect of the functionality of MWCNT on its interaction with DEDTP was examined. For this set of experiments the grease blends were prepared by using ionic liquid DEDTP at 0.2wt% P and different MWCNT at 1wt%. The procedure for grease blend formulation is the same. First additives are mixed thoroughly by using ultrasonication and magnetic stirrer. Then the mixture is added in lithium base thickener in kitchen aid and is blended for 2 hours. Table 7 details the grease blends chemistry used for studying the effect of functionality of MWCNT.

Table 5 Details of the grease blend formulations for the study of functionality of MWCNT

Coded Name	Base Grease	Additives used	Mixing Temperature (˚C)	Time
Blend_04	Lithium Complex	MWCNT_OH & DEDTP	50	120 min
Blend_05	Lithium Complex	MWCNT & DEDTP	50	120 min

The effect of ionic liquid cation and anion functionality is also believed to play significant role in the interaction with MWCNT. Grease blends for this study were prepared using four different ionic liquids having phosphorus and sulfur in either the cation or anion moieties. Ionic liquids were added at 0.2wt% P and MWCNT at 1wt%. Grease blend preparation is the same as described above. Also, the tribological performance of ZDDP-MWCNT additive mixture was evaluated for the comparative study with ionic liquids. Table 8 describes the grease blend chemistries prepared at specific temperature along with the coded name.

Table 6 Details of grease blend formulations for the study of influence of cation and anion moieties of ionic liquids on the interaction with MWCNT.

Coded Name	Base Grease	Additives used	Mixing Temperature (˚C)	Time
Blend_06	Lithium Complex	MWCNT_OH & DMP	50	120 min
Blend_07	Lithium Complex	MWCNT_OH & DEHP	50	120 min

Blend_08	Lithium Complex	MWCNT_OH & DBDTP	50	120 min
Blend_09	Lithium Complex	MWCNT_OH & ZDDP	50	120 min

The blended greases were tested in a four ball tribometer to evaluate the wear and friction performance. Before testing the greases, they were stirred using a micro-spatula so as to ensure the consistency of the grease.

5.2.3 Four Ball Tribometer Tests

The four ball wear tests were conducted in a continuous sliding mode under boundary lubrication regime. The procedure for all the tests was in accordance to ASTM D2266 standards. The ASTM method describes the test using three steel balls placed in a chuck that is locked using a cage and a fourth ball is rotated against the three stationary balls with the lubricating medium in between as shown in the figure 5.1. The four balls are made up of E52100 steel (Bearing quality aircraft grade steel) & are ½ inch diameter. The Plint Four Ball Tribometer was used to conduct the tests. It allows loading to be done at 40kg as well as 80kg. Being pneumatically operated, changing the load during the test is easier and viable option. The friction values on the test are measured by the formula as described in the ASTM D5183 and using the torque and load values [68]. Once the tests are performed the wear samples are studied using the Optical Microscope, Scanning Electron Microscope (SEM) and Energy Dispersive Spectroscopy (EDS). This help us determine the wear scar diameter (WSD) and also study the morphology and chemistry of the wear surface.
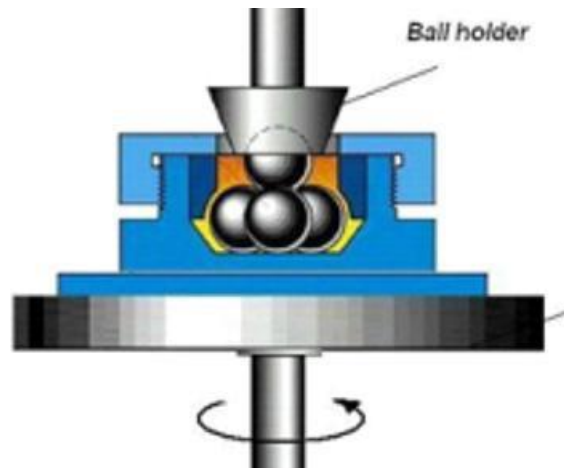
Figure 5-1 Schematic of the four ball geometry [75].

5.2.4 Characterization Techniques

Stereo-optical microscope (Nikon SMZ 1500) was used to take optical images of the wear scar developed on the stationary ball at 100X magnification. This images were used to determine average wear scar diameter using image J software. Average wear scar diameter for each wear scar is the average value of the longest horizontal striation and longest vertical striation. Therefore, average wear scar diameter for each blend is the average of 18 reading obtained from 9 steel balls. SEM (model type: Hitachi S-3000N) was used to in the SE (Secondary Electron) mode to image the wear surfaces at a higher magnification of upto 1000X & an accelerating voltage of 15-20 kV was used in all the cases. Carbon tape was used to maintain good electrical contact in between the steel balls and sample holder. The wear mechanism in play on the surface as well as the tribofilm formed on the surface was evaluated. Specific areas on the surface which were of interest were imaged at a higher magnification to understand the wear mechanism. For some samples EDS elemental spectrum analysis was done to understand the chemistry of the wear surface.

5.3 Results and Discussion

5.3.1 Effect of mixing temperature and time on interaction of additives

The grease blends formulated in this study comprised of mixture of MWCNT_COOH and ionic liquid DEDTP. The formation of the lubricant system with two different phases, solid and liquid requires precision mixing so that stable interactions can be formed between additives. To study the effect of mixing temperature and time, three grease blends were prepared. The following figure 5-2 shows the effect of varying temperature and time of mixing additives on coefficient of friction (COF). COF values of the blends containing DEDTP and MWCNT_COOH is also shown in the following bar chart.
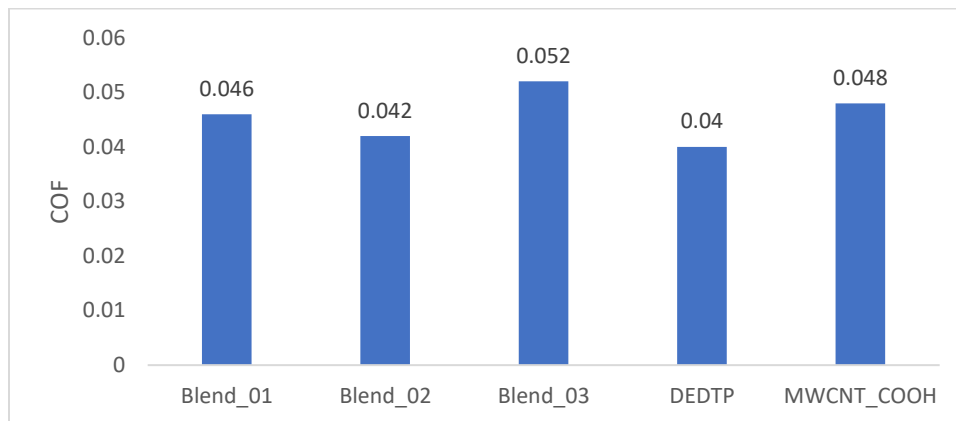
Figure 5-2 COF of the grease blends formed at different additive mixing temperature and time.

Blend_01 is formed by mixing additives at room temperature for 30 mins of magnetic stirring. Blend_01 shows the COF of 0.46 which is lesser than COF of MWCNT_COOH but greater than DEDTP. Blend_02 which is prepared by mixing additives at temperature 50˚C and 120 mins of magnetic stirring shows the similar trend but it's COF value is lesser than Blend_01. Blend_03 which is prepared at temperature 50˚C and 12 hrs of magnetic stirring exhibit worst performance of all with the COF of 0.052. The COF behavior with respect to temperature variation indicates the mixing at 50˚C is advantageous.

Figure 5.3 demonstrate the change in wear scar diameter (WSD) with the temperature and time of mixing the additives. At the room temperature and the minimum time of mixing of 30mins the WSD is 524 µm (Blend_01) and with the increase in temperature and time to 50˚C and 120 mins respectively, the WSD drops to 454 µm (Blend_02). Further, increase in time of mixing to 12 Hrs. leads to the increase in WSD to 558 µm. From the overall COF and WSD behavior it is clear that MWCNT_COOH and ionic liquid are not having synergetic effect. To further understand the reduction in WSD and COF for Blend_02, SEM characterization of the wear surfaces was carried out.
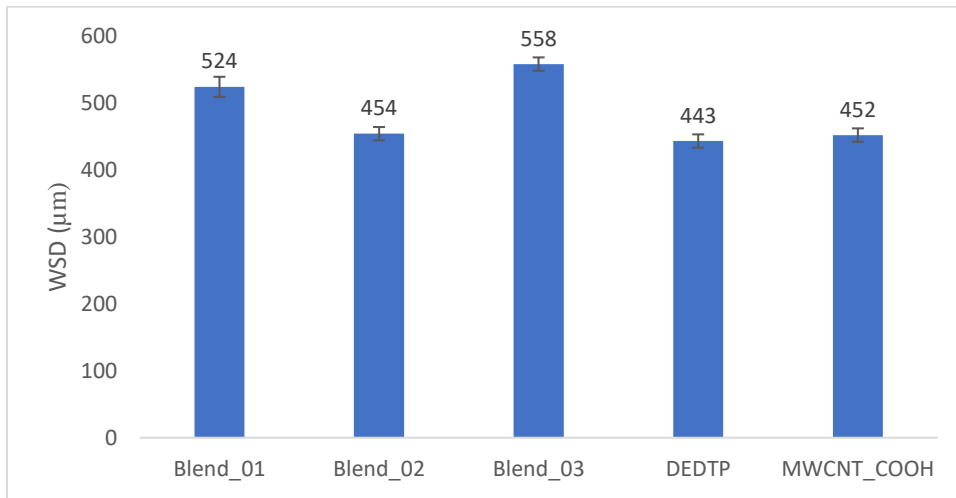
Figure 5.3 WSD of the grease blends formed at different additive mixing temperature and time.

SEM images of the wear scars of Blend_01, Blend_02, Blend_03 helps to determine that the influence of only ionic liquid DEDTP is resulting in the controlled frictional wear behavior of the lubricating greases. Blend_01 shows the pitting on the surfaces along with the formation of tribofilms, which are the characteristics of ionic liquid. Some amount of MWCNT accumulation on the wear tracks can be seen on the SEM image of blend_02. However, it looks like MWCNTs were simply accumulated in the grooves, no combined contribution of ionic liquid and MWCNT towards wear protection is observed for Blend_02. SEM image of blend_03 exhibits the polishing wear with

some amount of abrasive wear. The wear scar morphology doesn't show the presence of ionic liquid tribofilm and MWCNT deposition.
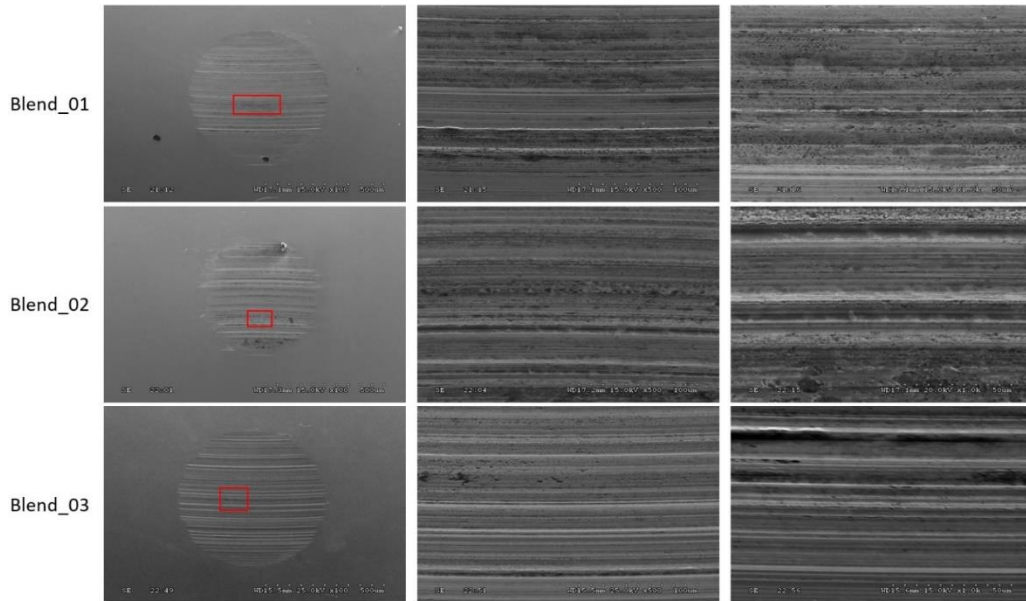
Figure 5-4 SEM images of the wear scar of the grease blends formed at different additive mixing temperature and time.

The COF and WSD results of all the grease blends were comparable with the results of DEDTP alone and MWCNT_COOH used alone. The SEM-EDS results reveals the better performance of the grease blend having additive mixture of MWCNT_COOH and DEDTP is due to the effective performance of the ionic liquid, DEDTP. This set of results help to set the constant temperature and time for mixing the additives to 50°C and 120 mins respectively. It was also concluded that the COOH functionalized MWCNT is not forming any surface interactions with the ionic liquid and hence, the effect of functionality of MWCNT and ionic liquid on the tribological performance of the combination MWCNT-ionic liquid was further studied.

5.3.2 Effect of the polarity of MWCNTs

This work focuses on the evaluation of extreme pressure characteristics of lubricating grease blends containing additive mixture of un-functionalized, carboxyl functionalized and hydroxyl functionalized MWCNT with the DEDTP. Figure 5-5 details the coefficient of friction value for the different MWCNTs containing grease blends. Also, the COF values for the grease blends containing only MWCNT and only DEDTP are shown for the baseline comparison.
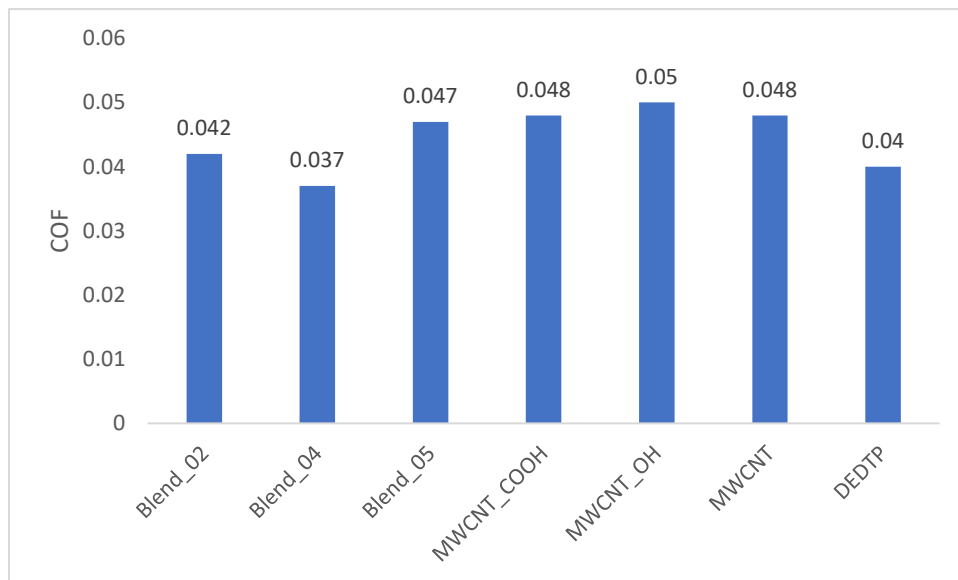
Figure 5-5 COF results of the grease blends used for the study of the effect of MWCNT polarity on the tribological

It can be seen that the presence of carboxyl functionalized MWCNT is not having any significant reduction in the COF value as compared to the blends MWCNT_COOH and DEDTP. Unlike carboxyl functionality, hydroxyl functionalized MWCNT is exhibiting comparable or even better COF results than the baseline grease blends. The un-functionalized MWCNT is showing the highest COF of 0.047.

Antiwear performance of the grease blends formulations formed by mixing un-functionalized and functionalized MWCNT with DEDTP is illustrated in terms of wear scar diameter (WSD) in the figure 5-6. The wear scar diameter of 615 µm for un-functionalized MWCNT combination mixture is observed. Also, the WSD for the carboxyl functionalized MWCNT with DEDTP is greater than the WSD of grease blends containing MWCNT_COOH and DEDTP alone. We can observe that the good COF result of the Blend_04 can be correlated with its WSD result. WSD of the hydroxyl functionalized MWCNT exhibited lowest value of 415 µm indicating the synergy between MWCNT_OH and DEDTP ionic liquid.

SEM images at 100X, 500X and 1000X of the worn surface developed during four ball testing of the lubricating greases is shown in the following figure 5.7.
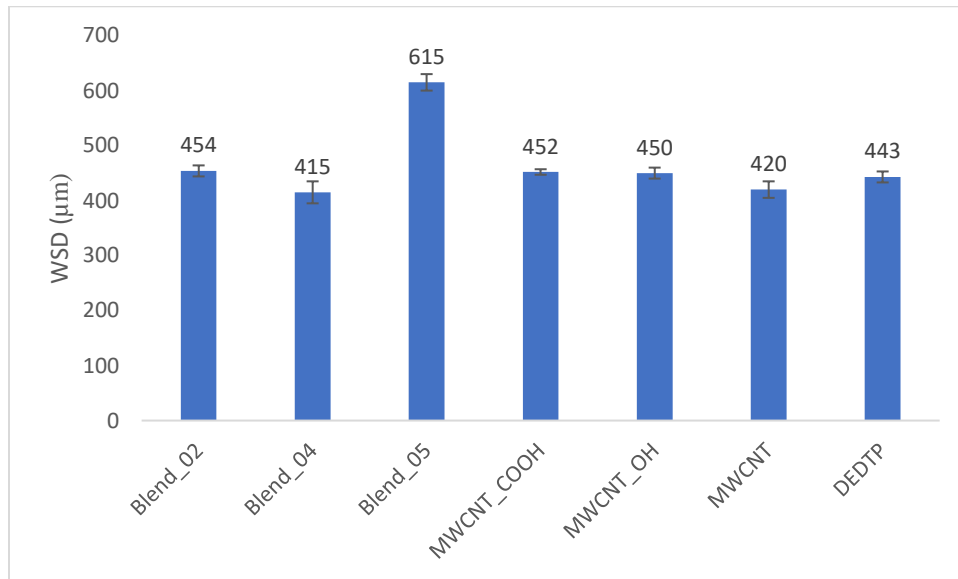
Figure 5.7 WSD results of the grease blends used for the study of the effect of MWCNT polarity on the tribological

Red box on the low magnification image is the representative area which is further magnified at the magnification of 500X and 1000X.
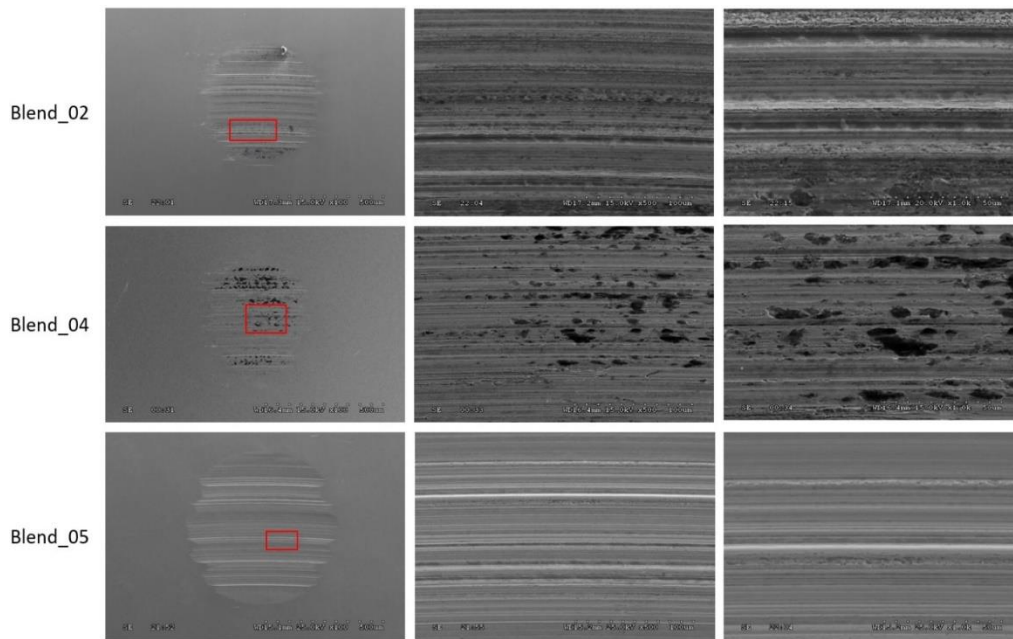
Figure 5.8 SEM images of the wear scar lubricated by grease blends used for the study of the effect of MWCNT polarity on the tribological

Low magnification SEM images of all the three grease blends shows the smooth polished wear surfaces. Deposition of the MWCNTs in the ploughing grooves can be seen in the low magnification image itself. Higher magnification image at 1000X details the nature of wear mechanism taking place. The SEM image of Blend_02 shows the characteristic adhesive wear combined with the abrasive grooves in the direction of sliding. Blend_04 wear surface shows the presence of continuous thin layer tribofilm evident from the dark patches seen on the SEM images. Also, the SEM image shows layers of the carbon deposition on the wear tracks. This explains the lower COF and lower WSD value for blend_04. Worn surface of the blend_05 exhibits combine abrasive wear and polishing wear.

From the WSD, COF and SEM results, it is safe to say that un-functionalized MWCNT doesn't undergoes a synergetic interaction with the ionic liquid DEDTP. It is important to note that the tribological behavior of the grease blends containing only un-functionalized MWCNT was better than the other additive combinations. It is assumed that the non-polarity of the MWCNT hinders the

positive surface interactions with the ionic liquid. The presence of hydroxyl functionality showed the positive contribution in enhancing the friction and wear resistance of the combination grease blend. During the mixing of MWCNT_OH with ionic liquid showed change in the viscosity of the mixture. This increase in viscosity was characteristic of the forming gels. It was proposed by Wang et al [69] that Imidazolium ion-based room temperature ionic liquid grounded with pristine single-walled carbon nanotubes (CNTs) form gels by physical cross-linking of the nanotube bundles, mediated by local molecular ordering of the ionic liquids. The overall organization of ionic liquids is not remarkably altered by single-walled carbon nanotubes. However, ionic liquids disperse the CNTs by shielding the stacking interaction among them. The ionic liquids interact with CNTs through weak van der Waals interaction without influence on their electronic structure and properties [69,70].

5.3.3 Effect of the cation and anion moieties of the ionic liquid

Four different ionic liquids namely, DEHP having choline cation and phosphate anion, DBDTP having choline cation and dithiophosphate anion, DMP having phosphonium cation and phosphate anion and DEDTP having phosphonium cation with longer alkyl chain length than DMP and dithiophosphate anion were selected for this study. In reference to our previous results on the effect of functionality of MWCNT, hydroxyl functionalized MWCNT was added at 1wt% with these four ionic liquids separately. In addition to ionic liquids, the grease blends with the conventional liquid lubricant ZDDP were also prepared, so as to understand the synergy between MWCNTs and already existing lubricant additive. The effect of cation and anion moieties on the tribological behavior of the combined additive mixture of MWCNT-ionic liquid was assessed through four ball boundry lubrication test. The COF result of these grease blends is shown in the following figure 5.9.
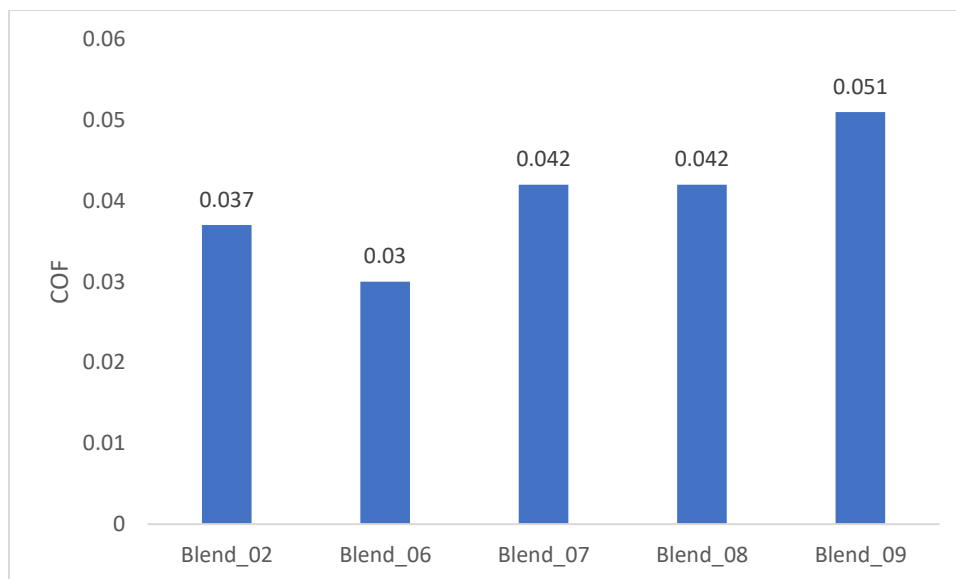
Figure 5.9 COF results for the study of the effect of different cation and anion moieties of ionic liquids.

The grease blend containing phosphonium cation based ionic liquid, DMP exhibits the lowest COF of 0.033, while the another phosphonium cation based ionic liquid, DEDTP shows almost comparable COF value of 0.037. The blend with the choline based cation ionic liquid shows the COF value in the same range of 0.042. The ZDDP and MWCNT_OH grease blend exhibits the higher coefficient of friction of 0.051.

The effect of different cation and anion moieties of ionic liquids on the wear performance of the lubricating grease formulations prepared for this study is demonstrated in figure 5.10. The WSD value of phosphonium cation based ionic liquid is lesser than the choline based cation based ionic liquids. The wear performance of the DBDTP is slightly better than the DMP. The WSD value of the ZDDP and MWCNT_OH combined grease is greater than the grease blend of only ZDDP.
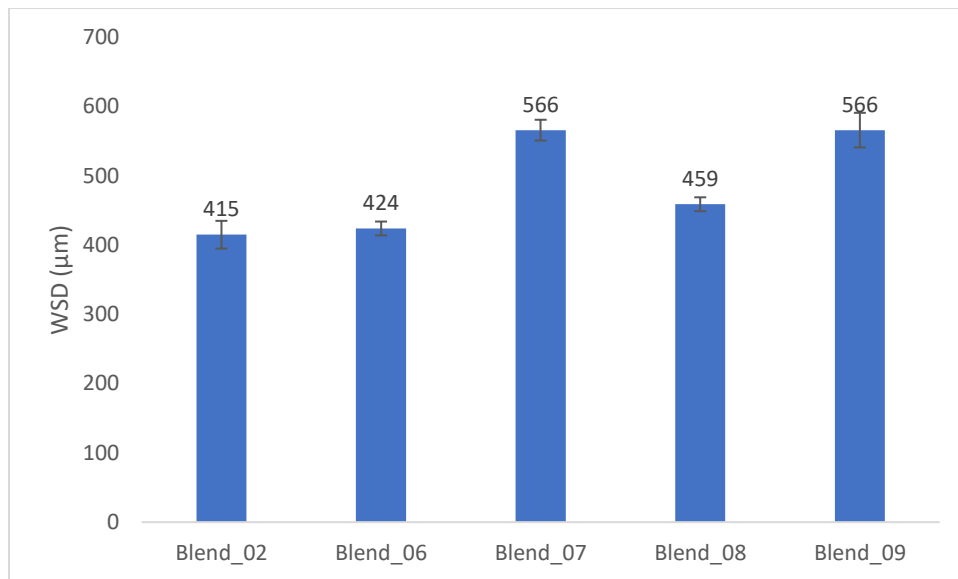
Figure 5.10 WSD Results for the study of the effect of different cation and anion moieties of ionic liquids.

SEM images of the grease blends containing different ionic liquids is shown in the following figure. Except the wear surface of DEDTP (Blend_04) all other worn surfaces lack the presence of carbon deposition. The lubricating grease containing DMP ionic liquid (Blend_06) exhibits the smearing type of adhesive wear all over the worn surface. This type of wear was also observed on the wear surface developed by grease containing only ionic liquids. The grease Blend_07 having DEHP shows no evidence of the tribofilm formation or carbon deposition and hence correlates with the higher WSD results of 566 µm. The worn surface of DBDTP (Blend_08) shows the severe abrasive wear with the deep scratches in the direction of sliding.
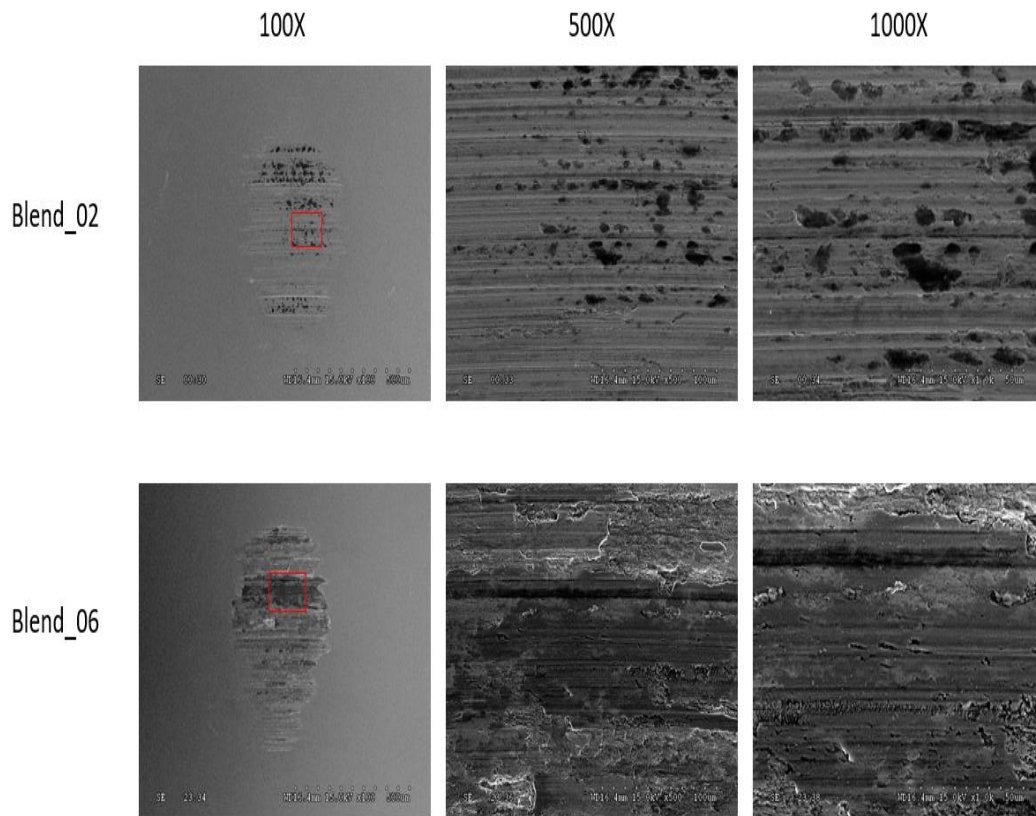
Figure 5.11 SEM images of the grease blends formed to study the effect of cation and anion moieties of ionic liquids, Blend_02 and Blend_06.
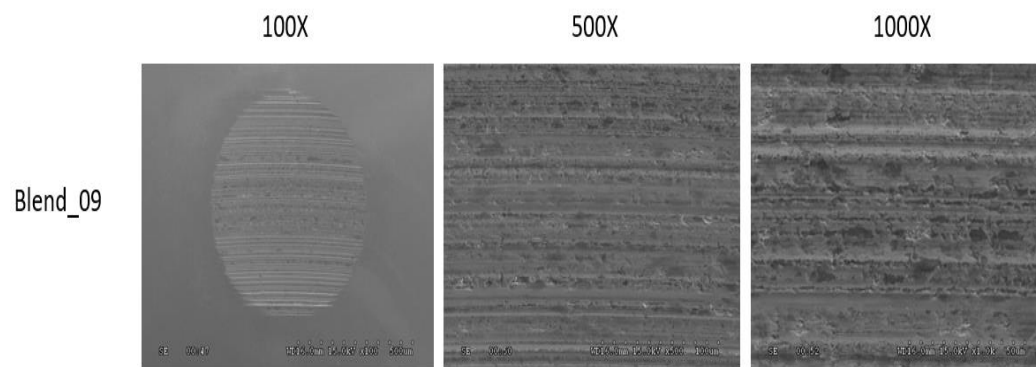
Figure 5.12 SEM images of the grease blends containing ZDDP and MWCNT_OH
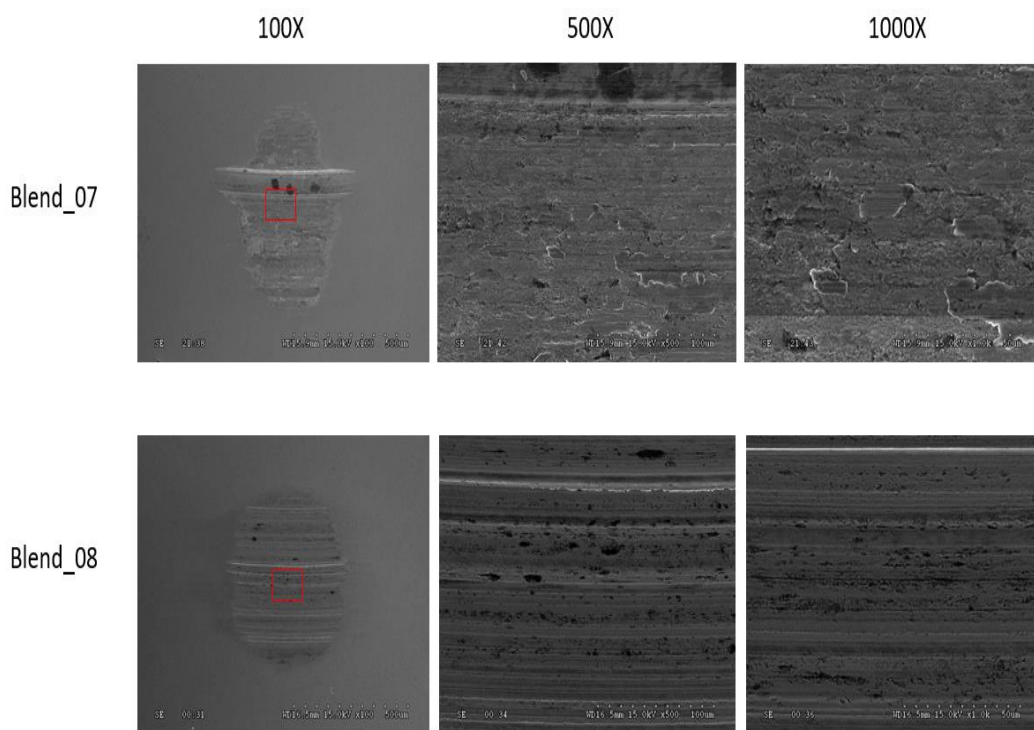
Figure 5.13 SEM images of the grease blends formed to study the effect of cation and anion moieties of ionic liquids, Blend_07 and Blend_08.

Out of all the ionic liquids, DEDTP exhibits better tribological performance. So, the wear scar lubricated by the combined additive grease of DEDTP and MWCNT_OH was further analyzed by using EDS spectrum. Figure 5.14 shows the comparison of EDS spectrum of the 1000X magnified SEM image of the Blend_04 and Blend DEDTP.

Element	Atom %
Phosphorus	1.27
Sulphur	2.12

Element	Atom %
Phosphorus	0.36
Sulphur	2.22
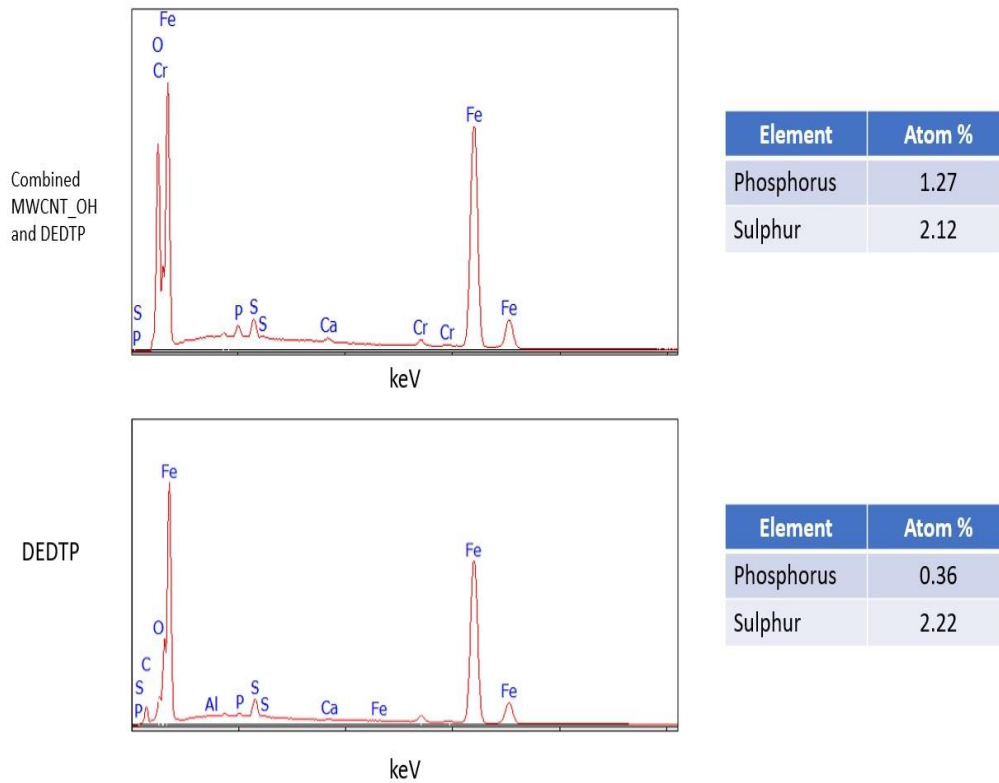
Figure 5.14 Comparison of EDS spectra of combined MWCNT_OH and DEDTP with DEDTP grease blend.

Comparison of spectra shows that addition of solid MWCNT additive results in decrease of phosphorus element. As the MWCNT hardness is greater than the hardness of the tribofilm, it may result in peeling of the phosphate layers formed by ionic liquid on the interacting surfaces. Also, there is a possibility that the larger concentration of MWCNT may hinders the adsorption of ionic liquid molecules on the contacting surfaces and affects the formation of phosphate tribofilms. Comparison of the combined MWCNT_OH and ionic liquids antiwear and friction results with the greases having only MWCNT_OH reveals that addition of only 0.2wt% of ionic liquids enhances the tribological properties of the single solid phase lubricant. It was hypothesized that 0.2wt% of ionic liquid will provide a larger solid phase contribution to the lubrication system by physically

adhering to MWCNTs and maintain their stability in the system. It was expected that ionic liquid will provide protection against wear by forming both physisorbed and tribofilm layer on the contacting surface, while the high tensile strength and elastic modulus of MWCNTs will contribute complimentary lubricant properties to the binary lubricant system. However, the comparison of the combined MWCNT_OH and ionic liquids results with the greases having only ionic liquids indicates that the major contribution towards the antiwear protection is from the ionic liquid.

5.4 Conclusion

1. The combination of MWCNT-ionic liquid additive grease blend showed a comparable tribological performance with the grease blend having only MWCNT and only ionic liquid.

2. The ionic liquid was identified as the superior antiwear and antifriction additive as compared to MWCNT in the formed two phase lubricant additive system.

3. The phosphonium cation based ionic liquid with the longer cation chain length exhibited better tribological performance than the choline cation based ionic liquids.

4. It was concluded that high concentration of the MWCNT may result in the removal of tribofilms formed by ionic liquid.

Section II

1. Introduction

Since the discovery of the first compression ignition engine in 1983, diesel engines have been looked in as the vital workhorse for road transportation. Heavy-duty diesel engines are the most favored engines for larger vehicles like trucks, locomotives, ships, and submarines, while spark driven gasoline engines have been dominating the personal transportation sector [76]. Diesel engines are much better than gasoline engines because of the several advantages, including high efficiency, low maintenance cost, and good fuel economy [77]. Incomplete combustion in both types of internal combustion engines results in the emission of carbon monoxide (CO), carbon dioxide (CO_2), nitric oxides (NO_x), sulfur compounds like (SO_x) and Particulate matters (PMs). Diesel engine exhaust contains the lower amount of CO and greenhouse gas CO_2 as compared to the gasoline engine, but, the amount of NO_x is negligible in the case of direct injection gasoline engines while diesel engine has 30% of NO_x in the form of NO_2. This makes diesel engine exhaust more harmful and hazardous to the environment and human health [78].

Diesel engine exhaust is carcinogenic in nature and as an attempt to minimize its detrimental effect environmental protection agency (EPA) introduced the Tier 3 emission standards where the maximum limit has been put on the emission of NO_x to 0.2 gram/BHP hr and PMs to 0.01 gram/BHP hr [79,80]. To fulfill the requirements of the stringent emission norms modification of the engine design like retarded timing, raised piston rings and development of the effective after treatment like Exhaust gas emission (EGR) and catalytic converters were employed by the engine manufacturers. The implication of after treatment EGR resulted in a decrease of NO_X emissions but also affected engine efficiency and life expectancy [81].

Exhaust gas emission (EGR) recirculates the incomplete combustion byproducts of the hydrocarbon fuel back into the combustion chamber to be burned for the second time. This method

involves displacing some of the oxygen introduced into the engine with inert gases, which absorbs heat during the combustion process, thus lowering the combustion temperature and hence reducing NO_x emissions. However, application of EGR leads to certain penalties. Exhaust recirculation associated with EGR system leads to the contamination of diesel engine oil with the soot particles. EGR system results in a reduction of flame temperature which reduces the rate of soot oxidation/re-burning. As a result, in EGR system, more soot is formed during combustion and remains un-oxidized eventually accumulating in the lubricating engine oil. Soot loading in the engine oil causes degradation of the lubricating properties of the engine oil and results in considerable wear of the various engine parts such as cylinder liner, piston rings, valve train and bearings. The application of EGR adversely affects the engine durability [82,83].

In parallel with the emission standards for heavy-duty diesel engines, the EPA announced regulation known as SAPS where chemical limits have been imposed on the amount of phosphorous (0.1wt%), sulfur (0.12wt%), sulfated ash (1wt%). This pressurized the lubrication engineers to develop oil formulations for diesel engines with exhaust gas after treatment to meet American Petroleum Institute (API) oil specification of CJ4 and CJ5 category having the capability to handle optimum soot concentration with the reduced amount of sulfated ash, phosphorous and sulfur. It is challenging for lubrication professionals to maintain the lubrication oil and emission standards of EPA and increase the efficiency of diesel engines by minimizing friction and wear losses. This challenge is overtaken by the use of new engine technology and development of new ashless and green lubricant additives like ionic liquids. A quest to improve efficiency and fuel economy of the automotive system has enforced to discover the new generation of environment-friendly lubricant additives having a potential to combat against harsh soot induced diesel engine environment.

1.1 Motivation of the Research

Diesel engine soot is a microscopic carbonaceous particle, which is a product of incomplete combustion of hydrocarbons. It has been shown that, of the soot produced within the engine, only 29 per cent reaches the atmosphere through the exhaust pipe [84], with the remainder being deposited on the cylinder walls and piston crown. Of the soot that is retained in the engine (mainly in the lubricant), 3 per cent is attributable to blow-by gases; the remainder results from piston rings scraping away soot deposits in the cylinder, which then end up in the sump [85].

Considerable amount of research has been done to understand the formation of diesel soot inside the engine using simulations and other characterization methods. Various characterization techniques like X-ray Diffraction, Raman Spectroscopy, Electron Energy Loss Spectroscopy (EELS), Scanning Transmission X-ray Microscope (STXM), Near Edge X-ray Absorption Fine Structure have been employed to study the structure and composition of "exhaust soot" obtained from exhaust tail pipe.

Soot accumulated in the engine oil is one of the major cause of wear in engine components. Over the years, various soot induced wear mechanism has been proposed by researchers. These mechanisms include (a) Abrasion of anti-wear film by soot [86,87,88] (b) Competition between soot and anti-wear additives to adsorbed on metal surface [89] (c) Accumulation of soot at inlet and cessation of oil supply to metal contact [90,91] (d) Adsorption of active anti wear product of lubrication oil by soot [92,93] (e) Inducing transition of metal surface from anti-wear Fe_2O_3 film to pro wear FeO film. [94] (f) EGR re-circulate SO_x which promote corrosive wear [95]. Although several mechanisms have been suggested, there is still no general agreement. To help formulate soot-wear resistant lubricants, it is important to have fundamental understanding of the mechanism by which soot in engine oils promotes wear.

1.2 Objective of research work:

It is well known that the increased level of soot in engine oils can result in severe wear of engine parts. Several different soot induced wear mechanisms have been proposed, out of which the most widely accepted is the abrasion by soot particles, either by direct excoriating the metallic parts in the motion or by scraping of the anti-wear additive films formed on rubbing metal surfaces. However, it is still not clear that how soot promoted abrasive wear leads to the high wear of engine parts.

The objective of this thesis is to gain a fundamental understanding of the soot elevated abrasive wear in diesel engine and to study the influence of the combination of anti-wear additive and soot on engine wear. To seek this goal, first approach is to elucidate the effect of the interaction of engine oil additives and soot on the chemistry, composition, structure, oxidation characteristics and nature of the soot. The soot used in this study is extracted from the drain interval used oil of dynamometer engine test Mack T12 which represents realistic field conditions that soot experience during engine operation. The chemistry of the diesel engine soot is analyzed by using higher spatial resolution analysis technique, X-ray absorption near edge spectroscopy (XANES). Transmission Electron Microscope (TEM) is utilized to characterize soot structurally and morphologically. High temperature XRD is used to learn the changes in the phase, crystal structure with the increase in the temperature, further incombustible inorganic residue after soot oxidation was characterize using Energy Dispersive X-ray spectroscopy (EDX).

Second part of this research study involves the detail evaluation of the effect of diesel engine soot on the lubrication characteristics of the three different anti-wear additives. In the recent years, new environment friendly "Ashless" additives were developed, which have comparable or better anti-wear properties than the conventionally used "Ashed" anti-wear additive ZDDP (Zinc Dialkyldithiophosphate). It is important to understand the anti-wear performace of these novel additives in the presence of soot so as to develop new formulation capable of mitigating the adverse

effect of soot on engine wear. Hence, two ashless anti-wear additives, Phosphonium based ionic liquid and metal free dithiophosphate with diesel engine soot are scrutinize under mixed to boundary lubrication condition using four ball tribometer test and wear results are compared with formulation having ZDDP anti-wear additive at same identical test conditions. An in-depth characterization of the worn surface morphology as well as chemical properties of formed tribofilms shed insight into the mechanism of wear. In the final approach, a phenomenological model of wear mechanism induced by diesel engine soot is proposed by combining the knowledge gained from the earlier approaches.

<div align="center">Hypothesis….</div>

Author postulate that soot which is known to be abrasive in nature, abrades the anti-wear films formed by lubricant additives rapidly and might lead to severe wear of engine parts. Decomposition of anti-wear additives results in the formation of films primarily of metal phosphates and metal sulfide/sulfate. These films are softer than steel and thus should be much more susceptible to abrasion by soot. There are two possible suggestions of this, one is that soot results in direct removal of anti-wear films by mechanical action. A second suggestion is that soot hinders the continued formation of the tribofilm by absorbing active film forming species and disturbs the equilibrium between film formation and film removal.

Zinc dialkyldithiophosphate is the classic anti-wear additive considered ideal for the study of tribochemical reactions. Many studies have proved that ZDDPs breakdown in a combustion engine to create reaction products which reacts with the metallic surface under high temperature and pressure, create sacrificial films that are responsible for minimizing wear. Initially, ZDDP undergoes thermo-oxidation reaction and forms zinc polyphosphate and zinc sulfides/sulfates. This decomposition byproducts get adsorbed and reacts chemically with the rubbing metallic surfaces and forms iron phosphates and iron sulfides/sulfates. These anti-wear films act like a sacrificial film which periodically form and break-down due to the shearing action during the process. The rate of

film formation depends mainly on the availability of the active anti-wear film forming cations i.e. availability of Zn^{+2} contributed from ZDDP decomposition and Fe^{+2} from the Fe_2O_3 layer on the steel substrate.

Author speculate that the novel anti-wear additives (composed of phosphorous and sulfur) used in this thesis work will form the protective glassy anti-wear films of phosphate and sulfur compounds like ZDDP on the rubbing surfaces under used tribological conditions (i.e. high temperature and shearing forces). As these are "Ashless" metal free anti-wear additives the only source of metal cation contributing towards anti-wear films is the Fe^{+2} from Fe_2O_3 layer existing on steel substrate. It is expected that chemical interaction of additives with rubbing metallic surfaces will result in faster rate of film formation in comparison to rate of film removal by soot and will eventually lead in improved wear protection than the ashed based ZDDP anti-wear additive.

Hence, to consolidate the proposed hypothesis tribological performance evaluation of the test formulations containing ashless anti-wear additive with diesel engine soot are compared with the performance of test formulations having ashed anti-wear additive (ZDDP) with diesel engine soot. Tribological performance evaluation is carried out in terms of wear scar diameter measurement using stereo-optical microscope and image J software. Scanning Electron images of the wear scar developed on the steel ball will help to understand the morphology of the worn surfaces and interpret the possible soot induced wear mechanism. Also, an effort is carried out to apprehend the effect of increased soot levels in engine oil on the severity of wear by performing tribological test with the test formulation having soot content in increasing amount of 2%, 5%, 10%.

To advocate the proposed speculation, chemical composition analysis of the worn surfaces is performed using energy dispersive x-ray spectroscopy (EDX). Detailed analysis of EDX elemental maps and spectrum will help to elucidate the removal of tribofilms formed by three anti-wear additives. It will also help to understand the effect of dispersant additive interaction on the chemistry of the tribofilms formed by anti-wear additives.

1.3 Structure of this research

This section of the research study consists of four chapter. An outline and summary of each chapter are presented here.

Chapter 1, introduction: This chapter introduces the readers to the field of interest, tribology and lubrication of diesel engine. It also provides the motivation and objectives behind this thesis work and brief about the soot induced problems in diesel engine along with the necessity to study the wear mechanism.

Chapter 2, background: This chapter includes a detailed background on diesel engine trends in technology, soot formation and various soot resulted wear mechanism proposed by previous researchers. In addition, this chapter encompass the information on lubricant and lubricant additives, anti-wear additives such as ZDDP, ashless anti-wear additives and ionic liquids, lubrication mechanism and in-situ formed tribofilms.

Chapter 3, studied the morphology, structure and chemistry of extracted diesel soot from Mack T-12 dynamometer engine test using X-ray Absorption Near Edge Spectroscopy (XANES) and High-resolution Transmission Electron Microscopy (HR-TEM).

Chapter 4, focuses on the anti-wear additive performance of zinc dialkyldithiophosphate, ashless dialkyl dithiophosphate and phosphonium based ionic liquid on the detrimental effect of the diesel engine oil soot extracted from the dynamometer Mack T12 test. It also discusses the effect of increased level of soot concentration and interaction of dispersant-additive on the aggravation of the wear of metallic rubbing surfaces.

2. Background

Internal combustion engine produces soot because of the incomplete fuel combustion. Excessive soot formation occurs in diesel engines as compared to the gasoline engines because of the difference in the way fuel/air mixture is injected and ignited in them. In a gasoline engine, fuel is mixed with air, compressed by pistons and ignited by sparks from spark plugs [106]. However, in a diesel engine, the air is compressed first and then the fuel is injected. Heat energy stored in the air due to compression helps to ignite the fuel. Higher compression leads to higher efficiency of diesel engines as compared to gasoline engines. However, there is a disadvantage to the compression injection combustion of diesel engines. The fuel and air mixture in diesel engine do not mix as thoroughly as they do in gasoline engines. This leads to the formation of fuel dense pockets which produce soot when ignited. This soot escapes from exhaust or gets mix up in the lubricating engine oil [107].

The major disadvantage of the diesel engine is the emission of harmful pollutants like nitrogen oxide (NOx), hydrocarbons (HCs) and particulate matter (PM). These emissions have the adverse effect on human health, so as to reduce exhaust gas emissions, technology changes like engine modification, use of exhaust gas recirculation (EGR) was carried out by diesel engine manufacturers. EGR controls the emission of NOx by recirculating the exhaust gas back into the combustion chamber to be burned the second time. In doing this many of the contaminants from the exhaust gas end up in engine oil, thereby affecting the lubrication performance of the motor oil. Increasing soot amount with the use of EGR is the major concern of lubrication engineers. So as to combat with the soot related problems in the diesel engine, it is important to understand how soot is formed in the engine, how soot affects the engine performance and what measures should be taken to mitigate harmful soot effects [108,109].

2.1 Soot Formation

Soot formation occurs in the high temperature, fuel-rich reaction zone around individual fuel droplets, where fuel hydrocarbons are oxidized under stoichiometric oxygen conditions [110]. In this reaction zone the oxidation reaction is limited by the oxygen concentration. Oxygen transport occurs by diffusion through the flame front, and this type of reaction zone is therefore called a "diffusion flame". Another flame type which occurs in combustion processes is the "premixed flame"; the combustion of a premixed amount of fuel and air. Temperatures in premixed flames are higher than in diffusion flames. As NO, formation depends strongly upon temperature and oxygen concentration, premixed flames give rise to much larger NO, emissions than diffusion flames [111]. Figure 2.1 shows the conceptual model first proposed by Dec and co-workers and followed by other studies [112-115]. It clearly shows the combustion process and emissions taking place in direct injection compression ignition engine. In the conventional diesel combustion process, piston compression stroke rises combustion air above diesel fuel autoignition temperature. Fuel injection takes place during combustion stroke with fuel ignited when fuel vaporization achieves ignition equivalence ratio producing lifted, partially premixed turbulent jet surrounded by a diffusion flame. Stoichiometric mixture is oxidized and combusted with high temperature diffused flame resulting in NOx formation and reduces the available oxygen for remaining fuel entrained in the flame resulting in soot formation.
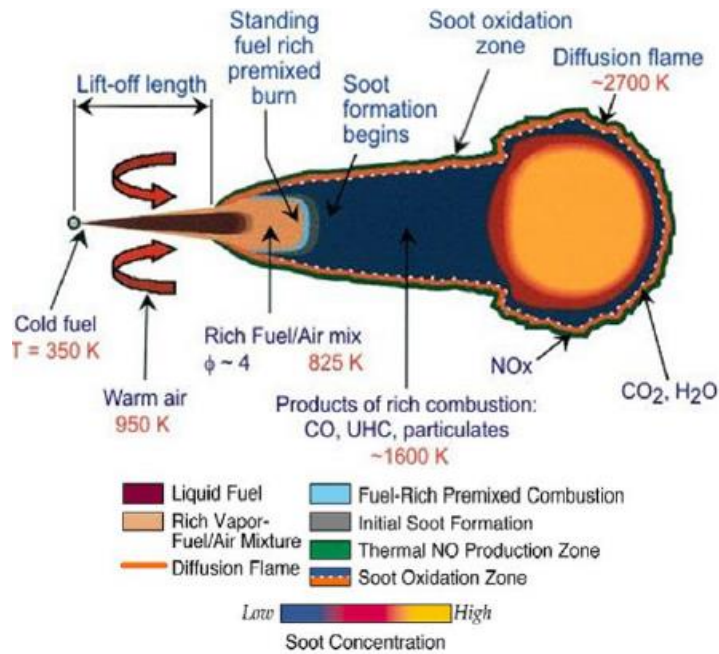
Figure 0-1 Conventional direct injection diesel spray combustion schematics [114,116,117]

2.2 Soot Processes

Many researchers have studied the fundamental of soot formation, the review by smith et al and Haynes et al remains one of the best sources for a full description of this phenomenon. Formation of soot is a complex process. It is the conversion of a hydrocarbon fuel molecule containing few carbon atoms into carbonaceous agglomerate containing some millions of carbon atoms. Soot formation steps can be summarized as (1) formation of molecular precursors of soot, (2) nucleation or inception of particles from heavy polycyclic aromatic hydrocarbon molecules, (3) mass growth of particles by addition of gas phase molecules, (4) coagulation via reactive particle-particle collisions, (5) carbonization of particulate material, and, finally, (6) oxidation of polycyclic aromatic hydrocarbons and soot particles [118,119].
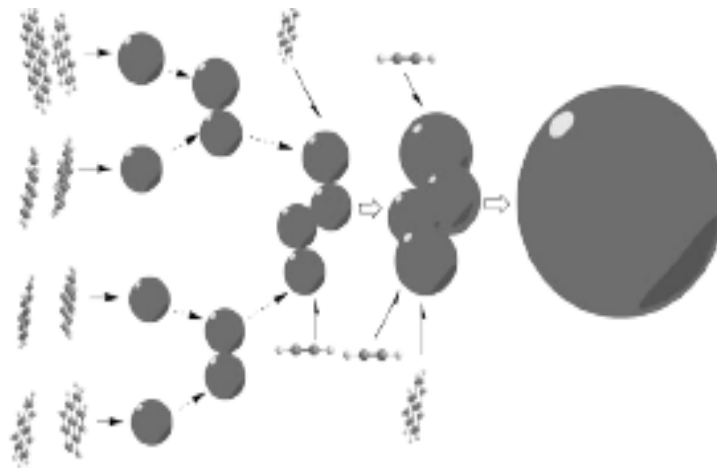
Figure 0-2 Soot formation process: Particle inception ⟶ Coagulation ⟶ Surface growth

Particles rounding due to surface growth [113].

2.2.1 Particle Inception Process:

Pyrolysis of hydrocarbon fuel results into small hydrocarbon radicals, in particular acetylene. The initial step in the production of soot is the formation of the first aromatic species from these aliphatic hydrocarbons. The aromatic species grow by the addition of other aromatic and smaller alkyl species to form larger polyaromatic hydrocarbons (PAH). Polycyclic aromatic hydrocarbon (PAH) molecules are considered as the precursors in the soot formation process. Continued growth of the PAH leads eventually to the smallest identifiable soot particles with diameters of the order of 1 nm and with masses of around 1000 amu [110].

An excellent example of the importance of the inception/nucleation process and its attendant rate to modeling soot formation under conditions of light soot loading is the thorough analysis performed by Markatou et al [111] in their examination of sooting limits in premixed flames. Using a detailed chemical kinetic model of gas-phase chemistry, of soot particle nucleation and of surface growth, they were able to predict the thresholds (i.e. critical equivalence ratio) at which visible (radiant) soot first appeared over a range of flame temperatures and fuels. By showing

that the rates of surface growth, oxidation, and coalescence varied slowly in the regime of the critical sooting limit, while also showing a dramatic rise in the computed concentration of the incepting or nucleating species, they were able to conclude that soot particle inception and hence the sooting limit is determined by particle nucleation.

2.2.2 Coagulation and Surface growth:

Once soot particles are formed through the inception process, they can grow by two mechanisms, collisional coagulation and surface growth. Interaction of precursors prior to the formation of the first primary particle were studied by Miller et al and Graham et al [112,113]. It was concluded that nanometer size precursor particles, consisting of polycyclic aromatic hydrocarbons (PAHs), undergo coalescence collisions forming larger singlet particles rather than chained aggregates irrespective of their liquid-like or solid nature. Meanwhile, it was noted in other studies that high reactivity of young solid particles results in continued surface growth that eliminates asymmetries caused by non-coalescent collisions. As a result of this argument, no aggregates will form during the early stage of soot formation because all collisions are either coalescence or result in single spherical particles because the surface reactions ultimately eliminate asymmetries caused by non-coalescent collisions.

Surface growth of particles proceeds in conjunction with coagulation. Surface growth is the addition of mass to the surface of a nucleated soot particle. As shown in the figure (2-3), both the process, surface growth and nucleation takes place concurrently. During the process, hot reactive surface of soot particles readily accepts gas- phase hydrocarbons which are mostly acetylenes. This leads to an increase in soot mass, while the number of particles remains constant. Surface growth continues as the particles move away from the primary reaction zone into cooler and less reactive regions, even where hydrocarbon concentrations are below the soot inception limits. The majority of the soot mass is added during surface growth and thus, the residence time of the surface growth process has a large influence on the total soot mass or soot volume fraction. Surface growth rate are

higher for small particles than for larger particles because small particles have more reactive radical sites [114].

2.2.3 Agglomeration

Agglomeration, the sticking of particles to one another or to solid surfaces, is a natural phenomenon. Agglomeration occurs when individual or primary particles stick together to form large groups of primary particles, and then the primary particles maintain their shape. Typically, the combined soot particles form chain- like structures, but clumping of particles has also been observed in some cases.

Soot is found to be in the form of necklace-like agglomerates, which are around 100 nm in size. These agglomerates are composed of collections of smaller, basic particle units that are spherical or nearly spherical. Soot clusters may contain as many as 4000 spherules. The size of the spherules varies in diameter from 10-80 nm, but mostly lies between 15-50 nm. Spherules are called as primary particle of soot and this particle agglomerate further to form chain like structures of 100 nm-2um.
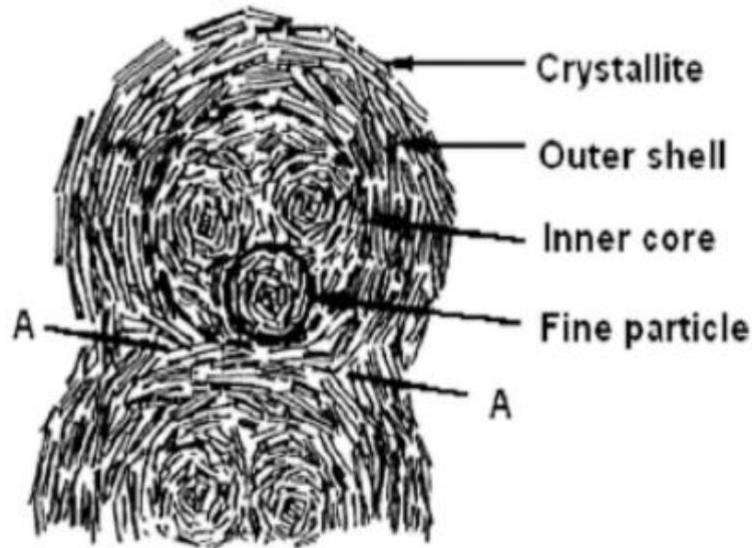
Figure 0-3 Schematic of primary soot particles [115]

2.2.4 Soot Induced Wear Mechanism

Rounds et al. was the first to suggest adverse effect of soot contaminated lubrication oil on engine wear [92,93]. His study suggest that soot particles get adsorbed on surfaces, consequently preventing the adsorption of anti-wear additives and formation of anti-wear tribofilm. He also examined the abrasive action of soot particles in lubricating oil by performing hardness tests to compare soot and alumina (which are known abrasive), and disagreed with the concept that soot removed the surface coating by abrasive action, since the hardness of soot is lower than the hardness of alumina. He believes that engine load and EGR have a large effect on the pro-wear characteristics of soot. Several authors have disputed the adsorption theory proposed by Rounds. Corso and Adamo et al. proposed that adsorption of soot on surface may restrict the amount of oxygen reaching the contact surface resulting in the formation of FeO oxide instead of Fe_3O_4. As Fe_3O_4 has better anti-wear properties than FeO, surfaces become more prone to direct abrasive wear by soot particles [94].

Ryason et al. work on diesel engine soot surrogate carbon black using ball on flat disc tribometer and he suggested that soot could act as abrasive by creating polishing wear [116]. Berbeizer et al. evaluated special test blends of different types of commercial carbon black and concluded that bore polishing is influenced more by the size, nature, and concentration of carbon black rather than by the products of oil degradation. They suggested that decreasing the amount of carbon black reaching the piston or suspension in the lubricant could reduce bore polishing and that bore polishing can be reduced by reducing the elementary carbon black particles, or by completely changing the microstructure of graphitized carbon. They also suggested that abrasive wear is not the sole factor contributing to increased wear, but two other phenomena also play important roles; decreased surface coverage rate by ZDDP molecules due to physical adsorption of carbon black on the surface and subsequent modification of physical and mechanical properties of the reaction film by the introduction of carbon in their composition [89].

Needelman and Madhavan et al. [117] suggested that soot wear could occur because of starvation of lubricant in the contact. This phenomenon is observed when soot agglomerates to a particle size greater than the oil film thickness. Similar relationship between soot particle size and lubricant film thickness was examined by Narita et al. [118]. His work suggests that the wearing agents were secondary soot particles with a size similar or greater than the oil film thickness.

Alajah et al. [119] studied the effect of exhaust gas recirculation (EGR) on wear of diesel engine. In this work the impact of the oil degradation on the wear of steel surfaces was evaluated by comparing results of bench friction and wear laboratory test with the results of measured wear in the cross-head component during the Cummins M-11 engine test. Unlike the crosshead wear measurements, bench test wear data showed no correlation of wear with increase in the soot content. The successfully concluded that the EGR results into degradation of engine oil in terms of increase soot particle loading (7-12% compared to about 4% without EGR) and increased acid content (TAN

133

by 2-3 times). However, they failed to advocate the direct relationship of increased soot particles with the wear of steel surfaces. George et al. [111] examined the lubricant oil thickening issue associated with heavy-duty diesel engines using EGR. He confirmed that presence of high soot level and dispersant results into increase in viscosity of oil. This increase in viscosity could result in engine wear because of pumpability problems.

Gautam et al. [121,122,123] exhaustive study on diesel engine oil soot contamination implied that soot particles are trapped between two surfaces in relative motion may result into three body wear. He also suggested that wear increases with higher concentration of soot and decreases with higher phosphorus concentration. S.George et al. [124] performed tests on three body wear testing machine and ball-on-flat disc to evaluate three body wear mechanism of soot. They analyzed the results using the general linear model (GLM) procedure of the statistical analysis system (SAS) and concluded that wear increased non-linearly as the amount of soot increased.

Fundamental understanding of soot induced wear mechanism of diesel engine is investigated by Patel et al. [125,126]. He studied the interaction of diesel engine soot with lubricating additive chemistry and evaluated these interactions by using laboratory bench tests like SRV friction test and four ball wear test, realistic field operation diesel engine and controlled diesel engine dynamometer engine test. He observed using XANES analysis that tribological by products and decomposition products were present in form of zinc phosphate ($Zn_3(PO_4)_2$), calcium phosphate ($Ca_3(PO_4)_2$), calcium sulfate ($CaSO_4$), zinc sulfate ($ZnSO_4$) on the soot structure. Also, high resolution transmission electron microscopy (HRTEM) with energy dispersive spectroscopy (EDS) reveals the presence of crystalline nano-particles of Ca as well as Fe_2O_3 embedded on the periphery of the turbostratic structure of soot. These compounds have a hardness of around 5-6 on the Moh's scale and can contribute to polishing wear under three boundary lubrication conditions.

Salehi et al. [127] investigated the effect of soot levels and temperature on the wear mechanism of soot in boundary lubrication conditions. They concluded that the corrosive-abrasive mechanism was responsible for the high wear in fully formulated oil. They also suggested that the interaction of phosphorus based anti-wear additive (ZDDP) with carbon black (soot surrogate) resulted in enhancing the wear.

2.3 Significance of the lubrication and lubrication chemistry

Engine lubricants / engine oil performs diverse functions which helps to increase life expectancy of an engine. Lubricants must possess attributes to perform following tasks effectively:

1. Lubrication (reduce friction and wear): Lubrication is the primary function of lubricants. It helps to mitigate the problems of the friction among the moving parts, if friction is not controlled it can lead to wear and surface damage, and ultimately to catastrophic failure of the equipment. Parts such as pistons, bearing exhibits direct metal to metal contact. Lubricants form a lubricating film which minimizes direct metal to metal contact and reduces the wear and energy loss. Without lubrication, engine will fail within minutes.

2. Protection: Lubricants prevent metal damage due to oxidation products, corrosion and wear. It achieves this by forming physical layer which is impervious to oxygen, water and acids or by forming chemical protective film by additives like rust and corrosion inhibitors, anti-wear agents, extreme pressure additives etc.

3. Cooling: During engine operation, parts in relative motion gets heated because of the frictional heat. Also, the parts in the proximity of combustion chamber gets heated due to conduction or radiation of heat from the combustion source. Lubricants act as a heat sink and dissipates the heat away from the critical parts, thereby decreasing the possibility of the machine component deformation and wear.

4. Cleaning and Suspending: Lubricating oil can effectively carry the external and internally generated contaminants like sludge (form by accumulation of combustion by products like soot), varnish and corrosive acids to the filter system where they can be removed. Lubricants consists of additives like dispersants and detergents which help to suspend contamination particles present in the oil thereby facilitating smooth operation of engine parts.

5. Sealing and noise reduction: Thin lubricating oil films provide the necessary gas tight seals between piston rings and cylinder walls preventing gas blow-by. Lubricating oil on the valve train cushions the valves which open and closes at 20 times per second at 2400 RPM cruise power reducing this valve noise.

Lubricating oil's performance and effectiveness mainly depends on its chemistry and composition. Generally, Lubricant consists of 90% base oil and 10% additives. Additives serves many roles like anti-wear and anti-corrosive agents, antioxidants, extreme pressure (EP) additives, dispersants and detergents, rust and corrosion inhibitors, friction modifiers, foam depressants, viscosity index improvers etc.

2.3.1 Basestock:

Lubricating oils basestock is referred as Base Oils and are usually mineral (Petroleum) or Synthetic. The American Petroleum Institute (API) has categorized base oils into five categories (API 1509). The first three groups are refined from petroleum crude oil. Group IV base oils are full synthetic (polyalphaolefin) oils. Group V is for all other base oils not included in Groups I through IV. Before all the additives are added to the mixture, lubricating oils begin as one or more of these five API groups.

Group Ⅰ Base Oils:

Oils which has less than 90 percent saturates, greater than 0.03 percent sulfur and a viscosity-index range of 80 to 120 are classified as Group I base oils. Group I Base oils are the cheapest in the market because they are produced by the simple solvent-refining method. These are the old high paraffin base oils and no longer used for modern engine oils.

Group II Base Oils:

Oils are classified as group II based on its more than 90 percent saturates quantity, less than 0.03 percent sulfur and a viscosity index of 80 to 120. Group II oils are produced by a complex process, hydrocracking which is different than the group I base oil production method. Group II base oils have better antioxidation properties as all the hydrocarbons of these oils are saturated. They also have a clearer color and cost more in comparison to group I base oils.

Group III Base Oils:

Group III base oils are purer than group II base oils and have more than the 90 percent saturates, sulfur less than 0.03 percent and viscosity index above 120. They are produced by severe and longer process of hydrocracking with higher pressure and heat. Though group III base oils are made from crude oil, sometimes they are referred as synthesized hydrocarbons.

Group IV Base Oils:

Group IV base oils are polyalphaolefins (PAOs). These oils are true synthetic lubricants, made through a process called synthesizing. They have a much broader temperature range and are great for use in extreme cold conditions and high heat applications. They also have higher shear strength, and are less prone to oxidation at higher operating temperatures. These oils are little more expensive than other groups but they do have extended life and don't degrade as rapidly as others. They are also more energy efficient, resulting in further operating cost savings.

Group V base oils:

Group V base oils include all other base stocks not included in the I, II, III, IV API oil groups. These include silicone, phosphate ester, polyalkylene glycol (PAG), polyolester, biolubes, etc. Sometimes these base oils are mixed with other base stocks to enhance the lubricant's properties. An example would be a PAO-based compressor oil that is mixed with a polyolester. Esters are common Group V base oils used in different lubricant formulations to improve the properties of the existing base oil. Ester oils can take more abuse at higher temperatures and will provide superior detergency compared to a PAO synthetic base oil, which in turn increases the hours of use.

Table 9 API Base Stock Classification [128]

API group	% Saturates	% Aromatics	% Sulfur	Viscosity index	Noack %
I	<90	>10	>0.03	<120	30
II	≥90	<10	≤0.03	80–120	25
III	>90	<10	<0.03	>120	11
IV		All polyalphaolefins			11
V		All stock not included in group I–IV			<11

2.3.2 Lubricant Additives:

For lubricants to perform effectively, they must possess certain properties, which include suitable viscosity, low corrosivity, low pour point, good cleansing and dispersity ability, non toxicity, low oxidation and low flammability. Base oil serves many functions like maintain of viscosity, density, color and heat dissipation, however, to achieve certain performance specifications lubricating oils are formulated by blending base oils with different additives. The function of additives is either to enhance the original properties of base fluids or to impart new properties which they lack. Each lubricant has its own primary purpose, table (9) shows functions of each additives used in automotive lubricating oils.

Table 10 Lubricant additives and their roles with common examples

Lubricant Additive	Key Role	Examples

Antioxidants	Preventing peroxides and stabilizing radicals (enhancing oxidation stability of oil)	Alkylated Diphenol Amine, Hindered Phenol
Antiwear Additives	Preventing wear in mild condition	Zinc Dialkyl Dithiophosphate (ZDDP), Tricresylphosphate (TCP)
Extreme Pressure Additives	Preventing wear in severe condition	Dibenzyldisulphide, Sulfurized Derivatives, Moly-bdenum Disulphide.
Adsorption or Boundary Additives	Preventing slip-stick phenomena	Sulphurized Fatty Acid Derivatives, Phosphonic Acids
Detergents	Protecting oils against sludge formation	Calcium Sulfonate
Dispersants	Dispersing particles	Sulphurized Fatty Acid Derivatives, Phosphonic Acids
Corrosion and Rust Inhibitors	Preventing corrosion or rust of engine surface and bearings	Barium Sulfonates, Calcium Phenates
Viscosity Index Improvers	Reducing difference in viscosities at different temperatures	Olefin Co-polymers, Polymethacrylates
Friction Modifiers	Performing lower friction behavior on surfaces	Organomolybdenum, Molybdenum Dithiocarbonates

Pour Point Depressants	Preventing the generation of wax crystals at low temperatures	Polymethacrylates
Foam Inhibitors	Retarding the formation of foam in oil	Hydrogen and Silicon compounds

2.3.3 Detergents and Dispersants:

Diesel engine oil are regularly exposed to the fuel and combustion products contamination such as soot from inefficient fuel combustion, wear debris, unburned fuel, breakdown products of the base oil, corrosion products, organic debris from microbiological decomposition of the oil, etc. Without a proper control of contamination, the oil will lose its lubricating performance and will be unsuitable for operation. Also, the agglomeration of these products can be very harmful to engine operation as it will block the oil supply pipelines or filters. To mitigate this deleterious effect Dispersants and Detergents are added in engine oil formulations. The additive package is dominated by dispersants and detergents contributing to 55-70 percent of the total performance package.

Dispersants are metal free additive which helps to suspend the insoluble corrosion and contamination products in the bulk oil and prevents the sludge formation, particulate-relative abrasive wear, lubricant viscosity increase, and oxidation-related deposit formation. Dispersants perform these functions implicitly because of the following attributes:

1. They include polar contaminants in their micelles
2. They associate with unstable particles and prevents them from colloidal agglomeration
3. They also suspend aggregates in the bulk lubricant
4. They lower the surface/ interfacial energy of the polar products to decrease their tendency to adhere to surfaces.

5. They surround soot particles and minimizes its agglomeration, thereby, prevents soot related thickening.

A dispersant molecule structure consists of a hydrocarbon group, a polar group and a connecting group or link. Figure (2-4) shows a graphical representation of a dispersant molecule. The hydrocarbon group is polymeric in nature and usually has molecular weight ranging between 3000 and 7000 g/mol. Variety of poly-olefins, like polyisobutylene, polypropylene, polyalphaolefins can be used to make polymeric dispersants but polyisobutylene-derived dispersants are the most common. Popularity of polyisobutylene is because of its good thermal stability, low cost and large volume availability in the proper molecular weight range. However, industry is striving hard to develop new olefins which will be chlorine and amine free so as to avoid dispersant assisted corrosion of engine parts. Besides the amine and oxygen based dispersants, oxygen derived phosphonate ester dispersants were also used. Now their usage is restrained because of the phosphorus limit set by API CJ 4 oil category.
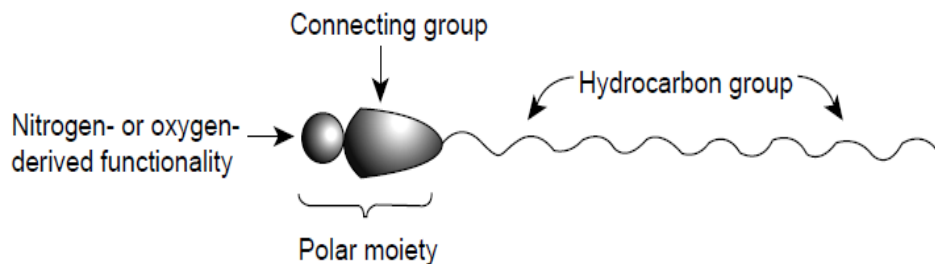
Figure 0-4 Graphical representation of a dispersant molecule [129].

Dispersing soot and deposits are the primary role of dispersants. This discrepancy is achieved by separating secondary soot particle and hindering coalescence assisted agglomeration. Smaller particles remain in oil for longer time than lager particles. That mean growth of particles occurs before separation. Growth of primary soot particles takes place because of the adsorption of polar impurities present in the oil. Dispersant suppress the agglomeration of soot particles further by

141

enveloping around them and minimizing their interaction with each other. Dispersant molecules surround the soot particle by the polar ends and remain suspended by keeping oleophilic hydrocarbon functional group in the bulk lubricant as shown in the figure (2-5). The polar interaction between dispersant molecules and soot particles is because of their own polar nature or adsorption of polar impurities to their surfaces. The inability of particles to coalesce with each other can be explained by two theories, steric stabilization and electrostatic stabilization.
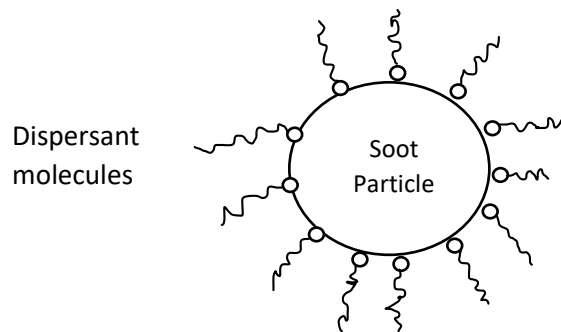
Figure 7-5 Mechanism of dispersant and soot interaction

The discrepancy is the important characteristic of dispersants and depends on all the three of its structural features: the hydrocarbon chain, the connecting group, and the polar moiety. The molecular weight of the hydrocarbon group in a dispersant determines its ability to associate with undesirable polar species and suspend them in the bulk lubricant. For dispersants that have the same connecting group and the polar moiety, the lower the molecular weight, the higher the ability to associate with polar materials and the lower the ability to suspend them. Because of the trade-off between the two properties, the hydrocarbon chain must have the correct size and branching.

Detergents

In addition to suspending contaminant particles like dispersants, detergents play variety of roles like inhibiting rust and corrosion, preventing high temperature deposits by neutralizing acids.

Detergent structure is composed of metal hydroxide or metal carbonate with a colloidal inorganic core which not only helps to stabilize the polar impurities in the oil but also helps to neutralize the acidic combustion and oxidation products. The organic portion of the detergents is similar to that of dispersants i.e polar functional group is linked to the oleophilic moiety through a connecting group. Unlike dispersants, detergents don't have the great ability to suspend the polar particles in the oil. They have less molecular weight than dispersants typically in the range of 500-1500 g/mol. The moiety which contributes to the suspending property has a molecular weight of around 600g/mol or less. The remaining balance molecular weight is because of the metal hydroxide or metal carbonate, which provides excellent acid-neutralizing ability but does not add to polar suspending ability. Calcium and magnesium derived detergents find most extensive use as lubricant additive, with a preference for calcium based due to its low cost.

In addition to the suspending insoluble oil oxidation and combustion product activity (shown in figure (2-6)), detergents also act as oxidation inhibitors, depending upon the nature of their functional group. For example, phenates, sulfurized phenates, and salicylates possess oxidation-inhibiting properties because of the presence of phenolic functional group and sulfur. Also, basic detergents act as a corrosion inhibitors. This because they not only neutralize corrosive acidic products but also form surface films that isolate the material surfaces from the corrosive agents. The carbonate portion of the detergents performs the acid neutralization action while the soap portion provides surface films.
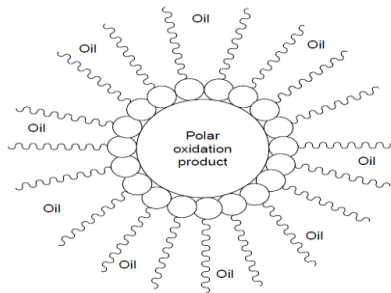
Figure 0-5 Oil suspension of polar oxidation products [130]

2.3.4 Anti-wear and Extreme pressure additives

Anti-wear and extreme pressure (EP) additives are used to provide protection against the friction and wear of the parts which are in continuous motion. In boundary lubrication condition, surface asperities contact each other even though the lubrication is sufficient to support the loads and friction takes place because of the shearing force cleaving these adhered asperities. EP and anti-wear additives can reduce the friction and wear in these conditions and thus sometimes called as boundary lubrication additives. Common additives that are used to provide EP/antiwear protection include metal-free and metal-containing dialkyl dithiophosphates; alkyl phosphites, alkyl phosphates and their salts; sulfurized hydrocarbons, fats, oils, and fatty carboxylic acids; phosphorized and phospho-sulfurized fats and olefins; organic molybdenum compounds, molybdenum disulfide, graphite, and borate dispersions.

Both anti-wear and EP additives provide protection by similar mechanism, except EP additives requires higher temperature and loads than the anti-wear additives. In simple terms, Anti-wear additives are designed to reduce wear when the sliding surfaces are exposed to low or moderate pressures, while extreme pressure additives work in a more severe pressure environment.

Anti-wear and extreme pressure additives function by thermal decomposition and by forming products that react with the metal surface to form a solid protective layer. This solid metal film fills the surface cavities and facilitates effective film formation, thereby reducing friction and preventing

welding and surface wear. The film formation by these additives is a multi-step process. The steps involved are as follows:

1. Adsorption of the chemical onto the metal surface.

2. Formation of the chemically reactive species due to thermal decomposition or hydrolysis and their chemical reaction with the metal to form a sacrificial protective film.

3. Removal of this film by mechanical wear, exposing fresh metal surface.

4. Readsorption of the EP/ anti-wear agent on the freshly exposed surface.

5. Repetition of steps 2-4.

This sequence follows the temperature profile of the contact zone. An increase in the temperature causes the sequence of events to proceed in the order listed. There are several different types of antiwear additives that are currently used in oil formulations. Usually phosphorus additives like zinc diakyl dithiophosphate (ZDDP), ashless dialkyl dithiophosphate, and other phosphate esters are used as antiwear additives. Of all antiwear additives, zinc dialkyl dithiophosphate has so far been the most commonly used in the engine oil due to its excellent antiwear and anti-oxidant properties while ashless dialkyl dithiophosphates, phosphates esters, and amine phosphates have recently been used as possible replacements to ZDDPs

2.3.4.1 Zinc dialkyl dithiophosphate (ZDDP):

Zinc dialkyl dithiophosphate commonly referred as ZDDP is the dominant lubricant additive almost from 60 years. ZDDP having the structure shown in figure (2-7) serves as a classic anti-wear and anti-oxidant additive for engine lubricants. Willermet and co-workers [130-133] did extensive research on the role of ZDDPs as antiwear agents. The work included studying the degradation products of ZDDP to assess the antiwear properties of these products; the products were found to be less effective as antiwear agents than ZDDP. One of the principal degradation products was found to be the disulphide, which on subsequent synthesis and wear testing was shown to be inferior to the ZDDP.
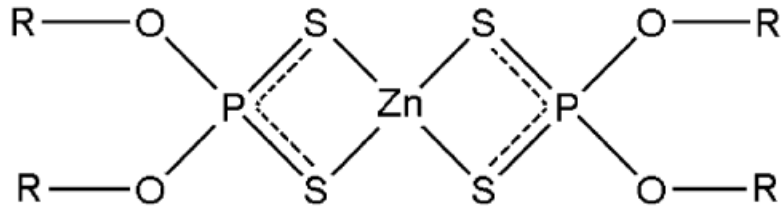
Figure 0-6 shows ZDDP structure where R group dictates whether it is alkyl or aryl dithiophosphate [134].

ZDDP acts as an excellent anti-wear agent by forming anti-wear sacrificial films from its own decomposition products. A great deal of research has been carried out on the mechanism of film formation and protection by ZDDP. Two types of surface films are formed by ZDDP: thermal films and tribofilms. Thermal films are formed when oils containing ZDDP are in contact of certain metallic surfaces (like steel or copper) at high temperature around 150˚C. Transparent and solid thermal films are formed in the absence of rubbing surfaces [135]. However, when surfaces rub together in a ZDDP-containing lubricant, ZDDP films are generated rapidly and at much lower temperatures, at least as low as 25˚C. These are called ''tribofilms''. Fujita et al. [136] studied the ZDDP thermal and tribofilm formation mechanism on steel surface and concluded that negligible amount of thermal film is formed below 110˚C but tribofilm is generated even at the room temperature. They also suggested that tribofilm formation is dependent upon extent of direct solid to solid contact during rubbing and can't be explained in terms of flash temperature and contact pressure. They proposed tribofilm formation reaction is catalysed by the species released during rubbing, like Fe^{II} or Fe^{III} [137]. Researchers have suggested different controlling factors which drives the ZDDP tribofilm formation on the rubbing surfaces. Possible factors include flash temperature rise [138], pressure [139], triboemission and surface catalysis [140], and stress related thermal activation [141].

In the literature, there exist several possible mechanisms for the formation of ZDDP antiwear films: thermal degradation [142,143] surface adsorption [144,145] oxidation by hydroperoxide [146,147], radical reactions [130], hydrolysis [148], chemical reaction with FeO [149] and oxygen in air [150] The mechanism which got considerable appreciation involve the ZDDP thermal decomposition and chemical reaction of degradation products. Willermet et al proposed detailed step by step mechanism of anti-wear film formation by chemical reaction of degradation products with the metal surface [131-133]:

1. Adsorption of ZDDP on metallic surface.

2. Reaction of ZDDP with the metallic surface to form species of phosphates and phosphothionic moieties bound to metal surface.

3. Formation of phosphate precursor from anti-oxidant reactions of ZDDP.

4. Condensation of the phosphates/phosphothionates species occur and are then terminated by zinc containing compounds or other metal ions in the solution.

Ferrari et al. [151] also proposed a similar mechanism of film formation. They also suggested further step in which zinc polyphosphate undergoes an oxidation process leading to the formation of Zn–O and Fe–O bonding and finally to the formation of a glass network. The authors propose a simple two-step pathway by which the metallic surface is responsible for the decomposition of ZDDP:

1. The removal of iron oxide.

2. Reaction of ZDDP with nascent iron substrate.

ZDDP's excellent properties partly contribute to the P, S and Zn elements contained in its molecule structure. Unfortunately, the phosphorus element would make the catalysts, equipped in the exhaust gas converter of the automobile, be poisoned and finally lose their efficacy. Moreover, the zinc salts produced by ZDDP in tribological condition might cause the electrolytic corrosion. These problems have forced engine oil manufacturer to develop new anti-wear additives as a replacement to ZDDP.

2.3.4.2 Ashless dialkyl dithiophosphate:

Since 1940 ZDDP is widely used as anti-wear and anti-oxidant additive by automative industry. Recently though, environmental implications of using ZDDP have been addressed and the use of more environmentally friendly additive has become necessity. This has aggravated the pressure engine oil formulators to look for alternatives to ZDDP that are both ashless and contain reduced amount of phosphorus and sulfur. It is challenging to eliminate three elements entirely from an oil formulation, there are many alternatives to ZDDP that are metal free. Ashless dithiophosphates are the metal free phosphorus containing additive which are gaining attention as a replacement of ZDDP from last 10 years [152].

Sarin et al. [153] showed that ashless dialkylphosphorodithioic acids has comparable anti-wear and antioxidant properties to those of ZDDP in bench tests. They found that the absence of zinc did not affect their tribological properties. In contrast to the ZDDP film chemistry, XANES analysis showed that DDP gave short chain polyphosphates throughout the film and the sulphide formed was largely FeS. In opposed to Sarin et al., Zhang et al [154] proposed that ZDDP serves as better anti-wear agent than ashless dialkyl dithiophosphate and a combination of ZDDP and ashless dialkyl dithiophosphate can provide very good wear protection. Vibhu et al [155] also examined the tribological performance of the combined ZDDP and ashless anti-wear additive formulations by using cylinder on flat test setup and showed that combined formulation has much better wear protection than ZDDP alone. They also studied wear surface morphology and chemistry using SEM and XANES surface characterization technique and found the presence of the ashless fluorothiophosphates and/or ashless thiophosphates assist the formation of Zn phosphates and ZnS in the tribofilm and enhances its anti-wear properties.

Ashless anti-wear additive forms tribofilms of phosphorus and sulfur similar to that of ZDDP. Nichollas et al proposed detailed three step tribofilm formation mechanism of ashless dialkyldithiophosphate (DDP) [156]. At initial step adsorption reaction between DDP and steel

surface takes place, second step involves thermal oxidation aided decomposition of additive and last step involves the formation of long and short phosphates by reaction between active P and S species with the iron oxide surface. This three-step mechanism is similar to Yin et al proposed mechanism of ZDDP tribofilm formation [157]. Kim et al [158] briefly studied the morphology, chemical composition, thickness and mechanical composition of tribofilms formed by ZDDP and dialkyl dithiophosphate (DDP). They found that the thickness of the ZDDP tribofilm is about 100nm while thickness of DDP is around 400nm (shown in figure (2-8)). Both films have same chemical structure of short chain pyrophosphate and iron sulfates with small amounts of iron and zinc sulfide. They proposed that tribofilms formed by DDP and ZDDP have an outside harder crust and complaint bulk which imparts good anti-wear characteristics. In addition, Kim et al. [159] also characterized the wear debris from the ball on cylinder wear test ran under extreme pressure conditions of several ashless dithiophosphates based additives and reported Fe_3O_4 nanoparticles embedded in the amorphous structure of tribofilms. The wear performance was correlated to the number of nanocrystalline oxide particles with the one with smaller number of oxide particles exhibiting the best wear performance.
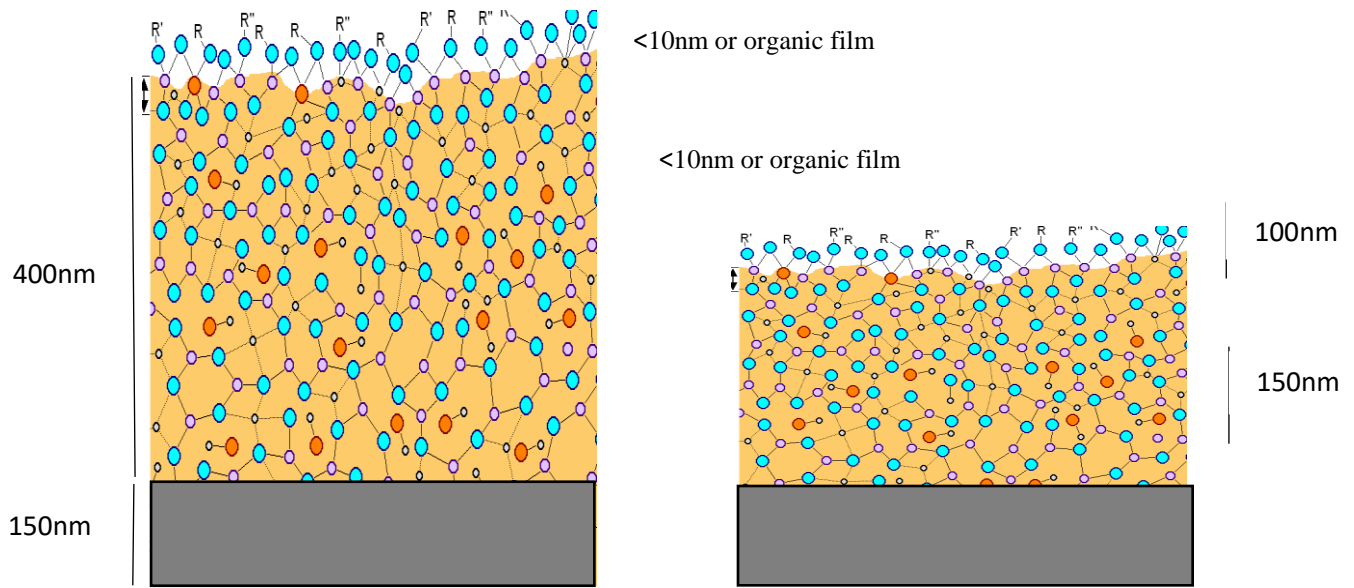
      (a) Ashless DDP Tribofilm   (b) ZDDP Tribofilm

Figure 0-7 Phenomenological Model of Tribofilms Constructed Based on SEM, EDS, FIB, Nano-Indentation, Nano-Scratch, Nano-Wear, and XANES Spectroscopy Data: (a) Ashless DDP Tribofilm and (b) ZDDP Tribofilm [160].

2.3.4.3 Ionic Liquid (IL)

The unique properties of ionic liquids (IL) enable versatility and efficiency across many industrial applications. The adaptability of IL to countless combinations of cations and anions provide vast array of uses such as electrolytes in batteries, as supercritical and heat transfer fluids, solvents for chemical synthesis and engineering fluids [161]. Recent studies have shown good potential of ILs in tribology [162,163].

Room temperature ionic liquids (RTILs) refers to the organic salts which are liquid below 100˚C. RTILs have gained considerable attention these days because of their outstanding properties like non-volatility, non-flammability, excellent thermal stability, low melting point, controlled

miscibility with organic compounds and a wide temperature range for liquid phase [162]. In the field of tribology, research in development of different RTILs as lubricant additive or base lubricant is in boom nowadays. Though various anions and cations have been used as precursors to synthesize ILs, following four types of cations based ILs (Figure (2-9)) found common applications in tribology: 1) alkylammonium [163,164] 2) dialkylimidazolium [164,165], 3) phosphonium [166] and 4) N-alkylpyridinium [167].

$[NR_xH_{4-x}]^+$ $[PR_xH_{4-z}]^+$
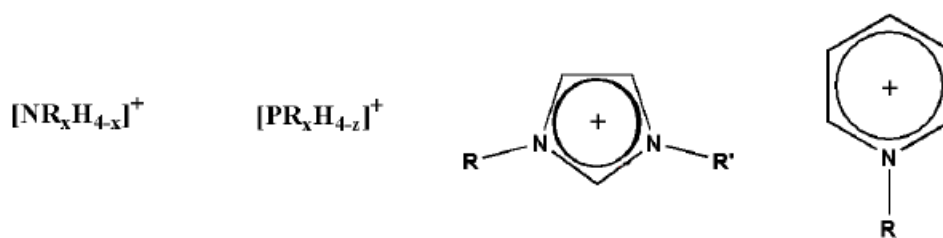
Figure 0-8 Alkylammonium, phosphonium, dialkylimidazolium and N-alkylpyridinium cations

[152]

Also, there are many studies dealing with the BF_4^- [158] and PF_6^- [159] anion based ionic liquids. Features of ionic liquid make them attractive additives for engine lubrication but they do possess some disadvantages. It is challenging to maintain optimum performance of lubricating oils having ionic liquid as an additive because of their low miscibility in non-polar oils and corrosion attack on lubricated surfaces [160]. Some studies have shown phosphonium and imidazolium cation based ILs can overcome this problem when used as a neat lubricant. However, due to high cost of ILs it's not economically beneficent to use IL in bulk as a neat lubricant, but can certainly use as a lubricant additive in small quantity.

Phosphonium based ionic liquids are more efficient than the imidazolium and pyridinium because of their excellent thermal stability and presence of active phosphorus element. The organic phosphorus has an important role in the lubricant chemistry, no matter being used as additive, such

as ZDDP, or as the synthetic fluid lubricants, such as phosphate esters and phosphazenes [161]. Moreover, phosphonium salts generally are not attacked by most organic compounds and are compatible with most commonly used lubricant additives. Bo Yu et al [159] and Jun Qu et al [162] both showed that phosphonium based ILs can show outstanding oil miscibility, thermal stability and non-corrosivity in both synthetic and mineral base oil. Jun Qu et al [162] also compared the anti-wear performance of DEHP (phosphonium IL) and ZDDP with the temperature increase using reciprocating sliding bench tribotest. They observed that at room temperature conditions IL performed as effectively as ZDDP, however, at 100˚C when base oil viscosity is low, ZDDP failed to prevent the surface from scuffing and resulted in high wear and high friction, while, the IL additive maintained a stable boundary lubrication friction coefficient and a low wear rate without scuffing throughout the test. Minami et al. [163] studied the tribo-chemistry of ionic liquid having tetraalkyl phosphonium cation under boundary lubrication condition using Auger electron spectroscopy (AES) and XPS surface characterization techniques. They suggested that the reactions of the phosphate anion and thiophosphate anion leads to a formation of a phosphate boundary film which exhibited better tribological properties than those of the fluoride boundary film. M. Anand et al [164] showed that addition of phosphonium based ionic liquids to in-service and used fully formulated diesel engine lubricants enhances their tribological performance. They also studied the interaction of ILs with the existing additives present in fully formatted oils using XPS. They suggested that ILs in the tribofilm formation of phosphate layers gets interfered by ZDDP and Ca detergents active elements and results in high wear.

Gabler et al. [165] analyzed the tribolayer chemistry using XPS depth profiling as well as XPS imaging techniques for bis(trifluoromethanelsulfonyl)imide ionic liquid with various cationic moieties. They suggested that cations did not lead to the formation of the tribolayer. However, it was observed that depending on the presence of cation, degradation of anionic moiety varied in the order of phosphonium > imidazolium > pyrrolidinium > sulfonium > ammonium. Vibhu et al.

[160,161] briefly examined the tribofilm formation of choline based phosphorus and sulfur ILs using XANES analysis technique. They proposed that tribofilm formation mechanism of ILs are similar to that of ZDDP, However, there is difference in the chemical structure of their tribofilms. IL tribofilm showed the presence of long chain polyphosphates while ZDDP tribofilm showed short chain polyphosphates. They suggested that the formation of long chain polyphosphates may impart better anti-wear properties to the ionic liquids. In another study, Vibhu et al also reported the relationship between ionic liquid chemistries and tribological properties. They used six different phosphorus based ionic liquids and examined the role of different cations and anions on the tribological performance. They found the wear results for DEHP and TFSI were better than ZDDP. Tribofilm mechanism for six different ionic liquid was also proposed, where IL undergoes decomposition and decomposition products reacts with the steel substrate resulting in the formation of anti-wear tribofilm. Figure (2-10) shows the difference in the chemical structure of tribofilm formed by choline based ionic liquid in base oil and ZDDP in base oil. a/c ratio up to 0.3-0.4 represents short chain polyphosphate while > 0.6 indicates the presence of long chain polyphosphate. It can be seen from the figure that choline based IL-P (representing thiophosphate) and IL-TP (representing dithiophosphate) forms relative longer chain polyphosphates than the ZDDP.
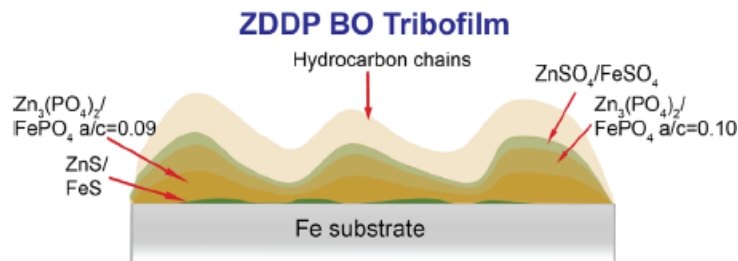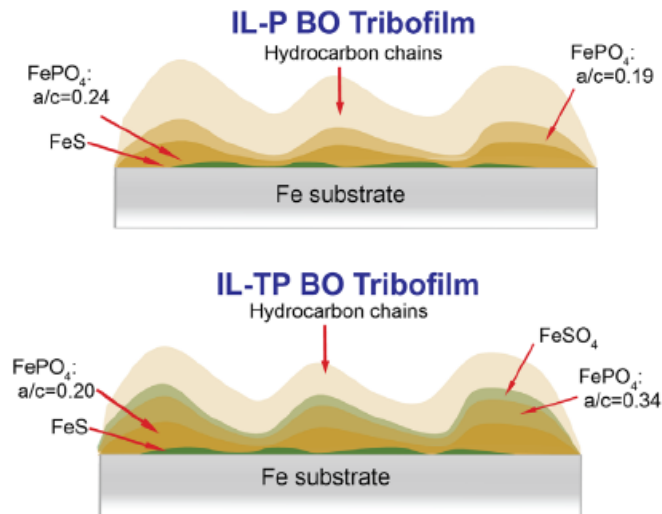
Figure 0-9 Phenomenological modelofthetribofilms generated using choline based ILs and ZDDP

in base oil [161].

2.4 Tribofilms

Tribology is the science and technology of interacting surfaces in relative motion and deals with the study of friction, wear and lubrication. Study of the mechanical systems in relative motion is important to improve its efficiency and life expectancy. The resistance force associated with the interacting surfaces called as friction force, results into loss of energy of the system and loss of the material. The losses due to friction and wear can be minimized by the use of effective lubrication, which forms a thin protective layer between the surfaces in contact. Thus, the basic concept of tribology is that friction and wear are best controlled with a thin layer or intervening film of material separating, sliding, rolling and impacting bodies. This protective layer is called as "tribofilm".

The continuous supply of lubricant is necessary to maintain effective lubricant film between the bodies in relative motion so as to avoid direct interfacial contact of the surfaces and reduce severe friction and wear. However, in the cases like mixed film lubrication and boundary lubrication surfaces run together under thin film conditions and a part of the load is carried by fluid film and a part by contact between surfaces. Under such conditions a thin film is subjected to high

shear conditions and the rubbing contact is made between the surface irregularities called as asperities. When sliding takes place, the friction occurs over the very small contact area and surface temperatures at the rubbing asperity contacts reach very high values. These local temperatures, which are of short duration, are known as flash temperatures. This heating effect may cause micro-structural changes to asperities as well as local melting. To help minimize the friction and wear under boundary conditions, lubricants containing anti-wear additives and extreme pressure additives are used. These additives get adsorbed at surfaces in contact and undergoes decomposition by thermo-mechanical chemical reaction because of the high temperature present at the minute asperity contact area. The additive decomposition byproduct either directly forms a protective thin film or it chemically reacts with the sliding surfaces to form a strong surface films. The surfaces in motion tend to wear away the surface films rather than the metal surface. Thus, the tribofilms formed due to decomposition of lubricant anti-wear and extreme pressure additives are sacrificial in nature. It is important to notice, tribofilms are the results of the decomposition reaction triggered by rise in temperature due to rubbing action. Additive decomposition byproduct protective films are also formed between the stationary contacting surfaces operating at the high temperature conditions, such films are called as thermal films.

Tribofilms formed by anti-wear additive ZDDP are investigated by many researchers from a long time. According to various authors, different models of tribofilm generation can be drawn. Lin et al. proposed three step formation of tribofilm by ZDDP:

1. At the specific oil temperature, ZDDP added to the base oil undergoes the process of decomposition.

2. Decomposition products are absorbed onto the rubbed surfaces to form the chemisorbed film.

3. Some elements or compounds in the chemisorbed film reacts with the iron based undergoing rubbing action to form anti-wear tribofilm.

A survey of the literature helps to understand the nature and chemistry of the tribofilms formed by ZDDP. ZDDP thermal films are usually formed by solution decomposition above 150˚C while ZDDP tribofilms can form at relatively lower temperature, also at room temperature in some cases. Average thickness of ZDDP is Fuller et al. compared the chemistry of ZDDP thermal film formed at preheating of ZDDP solution at 150˚C with the ZDDP tribofilm formed by using high frequency wear tester. Using XANES analysis they proposed that the chemistry of both the films is similar and the rate of formation of films is temperature dependent and increases with increase in temperature. They found out that thickness of the film increases with the increase in ZDDP decomposition in the solution.

Many research studies have used surface characterization techniques such as X-ray photoelectron spectroscopy (XPS), Auger electron spectroscopy (AES), energy dispersive spectroscopy (EDS), X-ray absorption near edge spectroscopy (XANES) and have showed that ZDDP tribofilms mainly consist of short chain zinc/iron phosphates and zinc/iron sulfides/sulfates. It has been proposed that initially ZDDP forms pad like patches on steel surface and gradually grows into a continuous film. The structure of these pads is schematically shown in figure (2-11). The pads consist mainly of amorphous and glassy polyphosphates, with a thin, outer layer of zinc polyphosphate (≈10 nm thick) grading to pyro- or orthophosphate in the bulk. The outer parts of the pad have mainly zinc cations; however, the amount of iron cations increase deeper in the film and closer to the metal substrate surface. Within the pads there is negligible thiophosphate but sulfur is present as zinc and iron sulfide. On the metal surface below these pads there may be a sulfur-rich layer of zinc or iron sulfide.
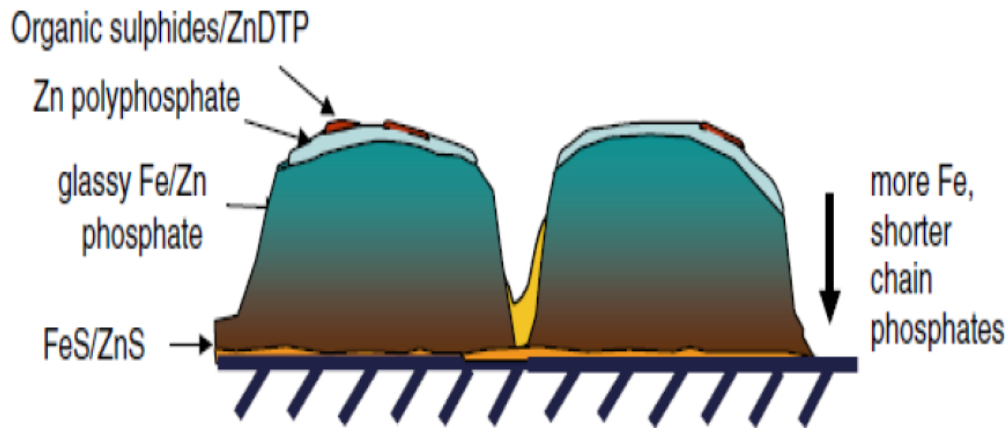
Figure 0-10 Schematic diagram of ZDDP tribofilm chemical structure [182].

Other popular anti-wear additives like ashless dithiophospates, phosphonium ionic liquids also forms similar protective tribofilms at the surface contact under boundary lubrication conditions. Najman et al. studied the mechanism of film formation and spatial distribution of chemical species in thermal and tribofilms derived from ashless antiwear chemistries using X-ray absorption near edge structure spectroscopy (XANES), Photo-emission electron microscopy (PEEM) and X-ray photoelectron spectroscopy (XPS) and concluded that the films contain short or long chain iron polyphosphates and iron sulfates. Also, the topographic study using Atomic force microscopy (AFM) showed that the films were composed of elongated short and large antiwear pads oriented in the sliding direction. Studies on ionic liquids showed that phosphorous containing ILs do participate in the tribochemical reaction during the rubbing action and form antiwear phosphate films on tribosurfaces under mixed to boundary lubrication conditions by interacting with Fe substrate. XANES analysis also showed that these findings further develop a strong understanding of the ability of ILs to interact with the rubbing surface and form glassy antiwear films composed of phosphates of Fe [183].

2.5 Dynamometer Engine Tests

American petroleum institute (API) commercial "C" diesel engine oil categories are developing considerably from 1950 to meet emission control set by Environment Protection Agency (EPA). Changes in design of diesel engine and consumer requirement for long life fuel lead to significant modification in the engine oil formulations. To assess the engine oil performance several qualification tests were developed which are named as dynamometer engine tests. These tests simulate the actual infield operating conditions of the diesel engine and hence have been accepted by the oil formulators as a standard procedure for engine oil evaluation.

Dynamometer engine tests procedures were undergoing several changes alongwith the design of diesel engine and API lubricant oil categories. In early 1970s, Mack engine oil tests were developed to evaluate engine lubricant capabilities in high speed operating environment. Mack T7 was introduced to assess soot related viscosity increase in low speed, high BMEP engines with reduced oil consumption. In 1980, as EPA imposed stringent limits on the emission of NOx, diesel engine manufacturers shift from retarded timing injection to cooled EGR. With the time, several lubricant testing procedures were introduced for evaluating lubricants against standards formed by API and various engine manufacturers like Caterpillar, Cummins, Mack and Volvo.

The aim of the dynamometer engine tests is to evaluate the standard API category oil ability to control valve train on ring and linear wear under severe operating conditions like use of EGR, high load duty cycle and high level of soot loading. The API CH-4 category requires various tests that include analysis of soot loading and viscosity measurement, like Caterpillar 1 K Lubricant test, Caterpillar 1 M-PC lubricant test, Mack T-8 A and Mack T-9 test. Various qualification tests like GM Roller Follower Wear Test (RFWT), Mack T-12, Cummins ISM and Cummins ISB are set to check ability of an engine lubricant to minimize camshaft lobe, sliding cam, cylinder liner, ring and bearing wear. While Mack T8A and Mack T 11 evaluate lubricant's ability to limit viscosity increase with soot loading [162].

2.5.1 Mack T12 (ASTM -D7422)

The Mack T 12 is part of the API CJ-4 performance category of engine oil procedures and it simulates heavy duty, on highway truck operations after 2007. This 300 Hr test uses much the same hardware as the Mack T10 test, except for variable geometry turbocharger and production EGR cooling heat exchangers. Mack T12 test aims at assessing lubricant ability to limit viscosity increase with high soot loading. The Mack T12 test uses a Mack E TECH V-MAC III diesel engine with Exhaust gas recirculation (EGR). A warmup and 1 Hr break in are followed by a two-phase test consisting of 100 Hr at 1800 r/min and 200 Hr at 1200 r/min, both at constant speed and load conditions. The operating parameters of the Mack T12 test are summarized in the Table (2.5)

Table 7 Operating Parameters for Mack T 12

Parameter	Phase 1	Phase 2
Time, hours	100	200
Speed, rpm	1800	1200
Fuel rate, Kg/hr	59.2	63.5
Torque, N-m	1349	2576
Oil Gallery Temperature, ˚C	88	116
Oil Sump Temperature, ˚C	93	129
Coolant Outlet Temperature, ˚C	66	108
Intake Manifold Temperature, ˚C	90	80
EGR Rate, %	35	15
Air/Fuel Ratio	23.6	21.1
Soot, weight %	4.3 ± 0.3 at 100 hours	6.0 at 300 hours

3. Experimental Approach

3.1 Diesel Engine Oil Soot Extraction

Soot used in this study is extracted from the drain interval oil of the standardized dynamometer MackT12 engine test. This test is developed to evaluate the wear performance of engine oils in turbocharged and intercooled four cycle diesel engines equipped with EGR and running on ultra-low sulfur level. EGR soot is extracted from the series of extraction process as described in the following subsection.

3.1.1 Oil dissolution

Test engine oil was mixed with industrial solvent hexane in about 1:1 weight ratio. Approximately 500 ml of total oil and hexane mixture was prepared in glass container so that it will be sufficient to extract higher yield of soot. This mixture was then ultra-sonicated to ensure thorough mixing of the soot in the oil which might have settled down at the bottom of the glass container. Weighted dissolved used oil in hexane and laboratory ultrasonicator is shown in Figure (3-1) below.

Figure 0-1 Weighed mixture of dynamometer engine test oil and hexane

3.1.2 Centrifuge Process

Ultrasonicated mixture was then further subjected to "SORVALL SS-34" centrifuge machine in the tribology and coating laboratory lab at UTA. Eight numbers of 32mm * 100mm centrifuge tubes encompassing total 250ml volume of mixture can be accommodated in this centrifuge machine. All the centrifuge bottles were filled to the same volume which ensured a proper balancing of the centrifuge disc. To fill the centrifuge bottle, a standard volume of oil sample mixture was measured for all the bottles using a measuring cylinder. Figure (3-2(a)) below shows a typical centrifuge and centrifuge bottle holder (disc). After balancing of centrifuge bottles in the disc, centrifuge parameters were set for operations to give optimal soot sediment. Operating conditions for optimal extraction was set at 12000 rpm for 2 hours duration. The supernatant from each bottle were carefully removed into a glass tube to remove the soot particles settled at the bottom of the tube. Solid soot particle settled at the bottom of the bottle which can be scooped out with a spatula. The process is repeated for all centrifuge bottles to extract soot particles.

Figure 0-2 (a) Sorvall SS34 centrifuge (b) Centrifuge bottle holder

3.1.3 Soxhlet Process

Soot obtained after centrifuging was subjected to the soxhlet extraction process which gives an oil free soot of high purity with minimal foreign impurities in it. Hexane was used as a solvent in the process which cleans the soot of all the oil and other impurities. Cellulose thimble containing soot was inserted into the Soxhlet extractor tube. Allihn condenser was kept above the soxhlet extractor tube and hexane was placed in round bottom flask connected to thermowell induction heater. This forms a close system where only hexane is circulated throughout the extractor assembly as shown in the figure 3-3.

The soxhletting process removed oil still attached to soot particles to give oil-free soot. The process was carried out for 24 hours period. Cleaning was achieved by heating up hexane to boiling point and leaving it to condense into the soot sample to wash out oil through the pores of the thimbles in which soot is placed; thimbles size of 8μm pore size was used in the process. The whole soxhletting process was carried out in an experimental fume hood to ensure safety precautions.

(a)   (b)

Figure 0-3 (a) Soxhlet setup in an experimental fume hood (b) Cellulose thimble

3.1.4 Drying and Grinding

On completion of soxhlet process, the thimble is removed from the extractor assembly and left in the fume hood for soot to dry up. Dried soot should be carefully removed from the thimble to maximize extraction and minimize waste. The dried soot is ground to fine powder using an experimental mortar and pistil. The final weight of soot is obtained using the weigh balance and recorded before storage in a glass tube properly closed in a dry environment. The soot samples are then stored for further analysis.

3.2 Characterization Techniques

3.2.1 X-ray Absorption Near Edge Spectroscopy (XANES)

XANES experiments were carried out at Canadian Light Source, Saskatoon, Canada, using the 2.9 GeV storage ring and at The Synchrotron Radiation Center, Wisconsin, Madison, using the 800 MeV storage ring. Three beam lines were used at Canadian Light Source to obtain K and L shell absorption edge spectra. Phosphorous, sulfur and calcium K absorption edges were recorded using the Soft X-ray Micro-Characterization Beam line (SXRMB) covering region of 1700–10,000 eV with photon resolution of 0.2 eV and beam spot size of 4 mm 300 μm. Phosphorus and sulfur L-edge spectra were obtained using the Variable Line Grating-Plane Grating Monochromator (VGM-PGM) beam line covering region of 5–250 eV with photon resolution of 0.2 eV. The PGM beam spot size is 500 μm 500 μm. Zinc L edge spectra were obtained using the Spherical Grating Monochromator (SGM) beam line that covers the energy range between 250 and 2000 eV with photon resolution of 0.2 eV in 100 μm 100 μm spot size. XANES spectra were acquired using a Total Electron Yield (TEY) mode and a Fluorescent Yield (FY) mode. Calcium L edge was obtained at the Synchrotron Radiation Center (Wisconsin, Madison) using HERMON beam line covering 64–1400 eV with 0.2 eV resolution.

3.2.2 High-Resolution Transmission Electron Microscopy (HR-TEM)

High-resolution transmission electron microscopy of the diesel soot was conducted using a Hitachi H-9500 microscope at an accelerating voltage of 300 kV with a lattice resolution of 0.18 nm. High-resolution lattice images of crystalline nanoparticles were acquired. Selected area diffraction patterns were acquired from selected regions coupled with energy dispersive spectra using x-rays to determine the chemical makeup of different regions within the soot particles.

3.2.3 High Temperature X-Ray Diffractometry (HT-XRD)

Oxidation behavior of diesel soot samples was studied using a Rigaku Smart Lab Diffractometer. Samples were placed on a fused silica glass slide capable of withstanding up to 1300 °C. The soot surface was flattened to get good X-ray reflection from its surface. The sample holder was placed in a heating furnace, and the temperature was ramped up from room temperature to 700 °C at a rate of 30 °C/min. X-ray scans were taken at increments of 50 °C. Changes in phase or composition were mapped for every scan obtained. An additional scan was taken at 50 °C after the sample was cooled from 700 °C to check for final composition of the sample. Bragg−Brentano reflection geometry was employed in the XRD. Cu Kα radiation ($\lambda = 1.5425$ Å) was used for diffraction with tube voltage and current at 40 kV and 44 mA, respectively. Scan range for 2θ was 10−90°. Interplanar spacing (d_{002}) was calculated using Bragg's law for each temperature step from the position of the (002) peak. Phase identification of residue left behind after soot oxidation was done using the "search-match" function wherein peak positions and peak RIR (reference intensity ratio) values of model compounds in the ICDD crystal structure database are matched. Samples were weighed before and after subjecting them to high temperatures to calculate the amount (in wt %) of residue left behind after soot oxidation.

3.2.4 Energy-Dispersive Spectroscopy (EDS)

A Vega 3SB electron microscope with a fully integrated EDS Microanalyzer from TESCAN Instruments was used for elemental analysis of residue originating from all samples after HT-XRD

studies. EDS clarified the possible compounds originating from inorganic engine-oil additive species, dirt, wear, and foreign contaminants. Aluminum stubs with carbon tape were used as sample holder. Carbon tape eliminated the possibility of surface charging of the sample, and there was no necessity for sputtering the sample for enhanced conductivity. Microscope parameters such as acceleration voltage, working distance, acquisition time, magnification, etc., were maintained constant for all the samples.

4. Influence of Soot on Antiwear Additives Performance Part I: Characterization of Extracted soot

4.1 Introduction

Diesel engines are important part of our present economy. Diesel engines are considered as the most efficient prime movers available today because of their higher efficiency and low maintenance cost. But they are also major contributors to environment pollution problems worldwide. Diesel engine emissions like particulate matter (PM), nitrogen oxided (NO_x), carbon monoxide (CO) has adverse effect on human health and environment [76,79]. Stringent emission controls implied by Environment Protection Agency (EPA) have resulted into technology changes such as engine modification, use of Exhaust Gas Recirculation (EGR) and catalytic after treatment which eventually result in significant emission reduction. However, use of EGR result in contamination of lubricant oil by a highly carbonaceous material known as soot.

Diesel engine soot is the byproduct of incomplete fuel combustion. Increased level of soot in lubrication oil has detrimental effect on engine efficiency as it led to increase in viscosity of oil, degradation of lubricating oil performance and severe wear of engine components.

Over the years, several researchers have addressed the effect of soot on engine wear and studies by Rounds et al. [92,93], Gautam et al. [119,120,121] , Rayson et al. [184], George et al.[122] , Ratoi et al. [185], Salehi et al. [125], give summaries of previous work done to illuminate soot induced wear mechanisms. List of these different wear mechanisms is indicated in table (11).

Table 8 List of the different proposed wear mechanism

No.	Proposed Soot Mechanisms
1.	Soot competes with anti-wear additives for adsorption sites at metal surfaces.
2.	Soot adsorbs active anti-wear component from the oil phase.
3.	Soot induces a transition of metal surfaces from anti-wear Fe_3O_4 to pro-wear FeO.

4.	Soot accumulates in the contact inlet and restricts oil supply.
5.	Corrosive wear is caused by increased SO_x recirculated by exhaust gas recirculation And there is a correlation between soot level and SO_x.
6.	Soot abrades protective anti-wear films.
7.	Soot abrades rubbing metal/metal oxide surfaces.
8.	Soot results into three body wear.
9.	Soot agglomerates greater than the film thickness result in starvation of lubricant in the contact.
10.	Interaction of lubricant additives and soot particles.

Out of all the suggested wear mechanism, the mechanism which has received good acceptance is that the soot has detrimental effect on anti-wear protective tribofilm formed by additives in lubricating oil. There have been two different interpretations, one is that the soot causes direct mechanical abrasion of tribofilm and secondly soot hinders the active tribofilm formation which indirectly decrement the positive contribution of additive for wear protection.

One quite widely proposed wear mechanism in recent year is that the interaction of dispersants and anti-wear additives with carbon black (commonly used as a surrogate for soot) result in antagonistic behavior which enhances wear of metal surface. Olomolehin et al. [176] and Salehi et al. [125] suggested that wear increase considerably when P and S containing anti-wear additives / EP additives are present in mineral base oil with carbon black. They also suggested that the wear at the tribological contact takes place by the continuous removal of the anti-wear additive tribofilm. Although several mechanisms have been proposed, still there is no accord on the mechanism responsible for high wear of diesel engine. So, there is a need of further fundamental understanding of the underlying wear mechanism.

In addition to the stringent emission norms API CJ 4, EPA imposed a regulation known as SAPS where chemical limits have been decided on the amount of phosphorus (0.1 wt%), sulfur (0.12 wt%) and sulfated ash (1wt%). This aggravated the stress on the lubricating additives manufacturers to optimize their products to sustain he challenging and conflicting demands of chemical limits of main anti-wear elements while also maintaining EPA pollution norms.

For years, anti-wear additives for high performance oils have been phosphorus and Sulphur compounds, especially ZDDP which work by forming a polyphosphate film on engine parts that reduces wear. However, the phosphorus element would make the catalytic converter to be poisoned, reducing their effectiveness and life span. So, from long-time researchers have been searching for ways to replace or reduce the use of ZDDP.

Metal free ashless lubricant additives have been proposed as a replacement of ZDDP with better or comparable anti-friction, anti-wear, anti-oxidant properties. Commonly used phosphorus based ashless additives are alkyl/ azyl mon and di-hydrocarbyl phosphates, amine salts of di-hydrocarbyl thiophosphates, alkylthioperoxydiphosphate and alkylphosphorofluoridothioates. Kim et al. compared the wear protection and tribofilm formation of ashless dialkyl dithiophosphate with the ZDDP. They characterize the wear debris from the ball on cylinder wear test of several ashless dithiophosphates based additives and reported Fe_3O_4 nanoparticles embedded in the amorphous structure of tribofilms. The wear performance was attributed to the number of oxide particles, the one with the smaller number of oxide particles, the one with the smaller number of oxide particles, the one with the smaller number of oxide particles exhibited the best wear performance. They also reported the thickness of the films derived from the ashless dialkyl dithiophosphates to be significantly thicker (400 nm) and similar to ZDDP triboflims in chemical structure [158,159].

Another family of anti-wear additives which is gaining attention of the researchers this days is ionic liquids. The versatility of ionic liquids make them promising candidate in the

competition to replace ZDDP. In tribology, most commonly studied IL's include cation's such as imidazolium, ammonium/ aromatic amine and phosphonium and anions those are, tetrafluoroborate, hexaflorophosphate, sulfonates and bis (fluoroalkyl amides) [163]. Sharma et al. examined the performance of P and S based ionic liquids. They reported that tribofilms formed by ionic liquid in oil comprised of glassy polyphosphates with a chain length greater than that formed with ZDDP in oil [161].

The aim of this study is to evaluate the influence of interaction diesel engine oil soot with various anti-wear lubricant additives on the wear mechanism. Study is also focused on understanding tribological wear and friction performance of anti-wear additives ZDDP, ashless alkyl dialkyl dithiophosphate and phosphonic cation based ionic liquid with soot containing lubricating oils.

This chapter is split into two parts. This part details the structured, morphological and chemistry of extracted diesel soot from Mack T12 dynamometer engine test. X-ray absorption near edge spectroscopy (XANES) and High resolution transmission electron microscopy (HRTEM) have been employed to chemically and structurally characterize diesel soot and any other constituents of the decomposition products that are incorporated into soot. XANES is used in determining the local co-ordination, valence and chemical bonding of individual elements, coupled with HRTEM it is possible to characterize the crystalline and amorphous phases in diesel soot.

<div align="center">4.2 Results</div>

4.2.1 XANES Results

4.2.1.1 P L-edge XANES spectra analysis:

The Phosphorus L- edge XANES spectra of diesel soot in both TEY and FY mode is compared with model compounds of iron phosphate ($FePO_4$), zinc phosphate ($Zn_3(PO_4)$), tri-calcium phosphate ($Ca_3(PO_4)_2$) and calcium pyrophosphate ($Ca_2P_2O_7$) in figure (4-1).
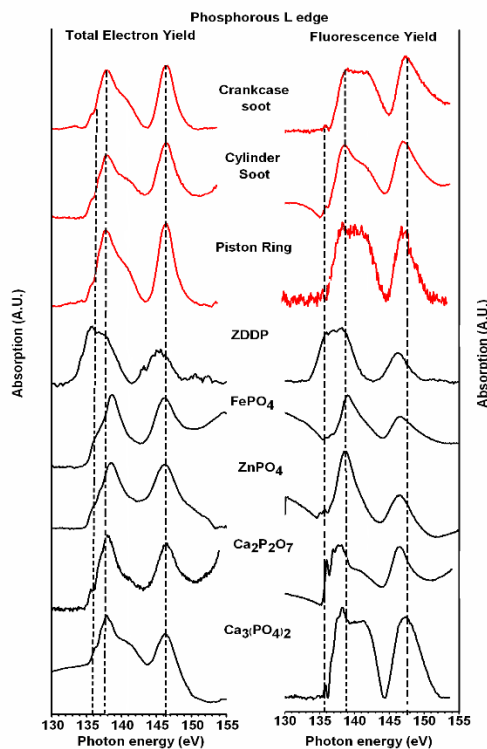
Figure 0-1 Normalized Total Electron Yield (TEY) and Fluorescent Yield (FY) phosphorous L

Phosphorus L-edge spectra is characterized by spin-orbit splitting of phosphorus 2p electrons and excitation to the antibonding orbitals. Transition of spin orbit split of 2p electrons between $2p^{3/2}$ (L_3 edge) and $2p^{1/2}$ (L_2 edge) is shown by peaks a and b. Peak labelled as c is assigned to transitions to 3p orbitals, which are sensitive to the presence of other elements such as oxygen and other cations like Fe or Zn. Peak d is the shape resonance peak characteristic of all phosphates regardless of structure, whether crystalline or glassy [153]. The phosphorus L-edge spectra gives better information of the oxidation and chemical environment than the P-edge spectra [164].

Many studies have proved the significance of XANES spectroscopy in chemical characterization of anti-wear tribofilm formed by ZDDP on metal surface [165]. Kasrai et al. and Zhang et al. examined the tribochemical nature of ZDDP tribofilm on the rubbing surface under air

and inert atmosphere using Phosphorus and Sulphur L-edge XANES spectroscopy [157,154]. They proposed ratio of peak a/c or b/c can be used to estimate the chain length of polyphosphate glass. A quantitative calibration curve has been proposed by Yin et al., which can be used to determine the number of phosphorus atoms in different chain-length phosphate glasses assigned at respective a/c ratios. For an a/c ratio of less than 0.44, polyphosphate glasses are termed to be of short chain length with about 10 or fewer phosphorus atoms present in each chain [157].

A film with an a/c ratio between 0.44 and 0.60 indicates the medium chain length of polyphosphate with phosphorus atom number between 10 and 25. An a/c ratio greater than 0.60 is termed as a long-chain polyphosphate glass with P atom number 25 or more. Unlike the above deconvolution method, in this study linear background subtraction was used instead of arctangent function. This has resulted into the change of a/c ratio and hence new standard of chain length of polyphosphate is applied here [157]. The phosphorus L-edge spectra shown in figure (4-1) confirmed the presence of polyphosphate glasses. The a/c ratio for the soot sample extracted from dynamometer engine test Mack T12 is 0.22, which is suggestive of short chain polyphosphate.

4.2.1.2 Sulphur L-edge XANES spectra analysis

The TEY and FY of Sulphur L absorption edge spectra of Mack T12 soot is shown in figure (4-2). This spectrum was compared using model compounds of $ZnSO_4$, $CaSO_4$, $FeSO_4$, $Fe_2(SO_4)_3$, ZnS and FeS. $FeSO_4$ and $Fe_2(SO_4)_3$ have characteristic distinctive spectra. Sulfides of Iron and Zinc have distinctive peaks at lower energy and that's what distinguishes them from sulfates. Diesel soot spectra is closely aligned to the $ZnSO_4$ characteristic spectra.

Figure 0-2 Normalized Total Electron Yield (TEY) and Fluorescent Yield (FY) sulfur L edge

spectra of crankcase soot, cylinder soot and piston ring of Mack T 12 engine test and model

4.2.1.3 Zinc L-edge

Information of chemical state of Zn can be derived from TEY and FY mode of soot extracted from dynamometer engine test oil. These spectra were compared with model compounds of oxides, sulfides, sulphates and phosphates of zinc as shown in figure (4-3). Absorption spectra of $ZnSO_4$ and $Zn_3(PO4)_2$ are almost similar but they have distinctive white line energy peak at 1024 ± 1 ev which is absent in ZnS and ZnO. The absorption spectra of soot closely align with $Zn_3(PO_4)_2$.
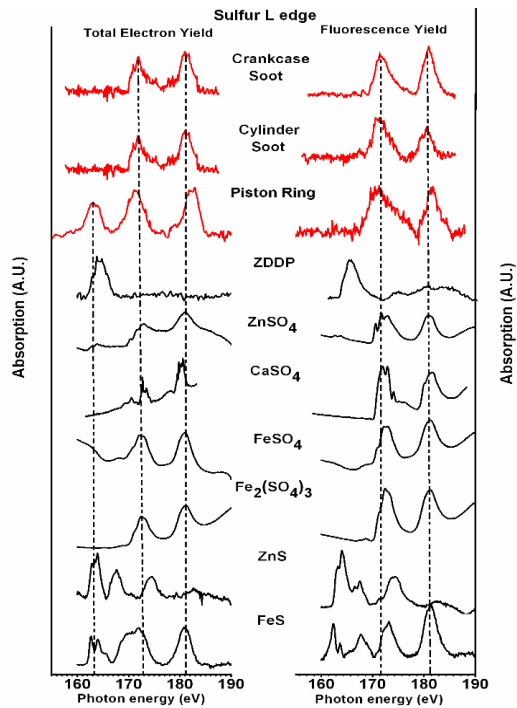
Figure 0-3 Normalized Total Electron Yield (TEY) and Fluorescent Yield (FY) zinc L edge spectra of crankcase soot, cylinder soot and piston ring of Mack T 12 engine test and model compounds

4.2.1.4 Calcium L-edge

Calcium has electronic configuration of $2p^6 3d^{10}$ with a high priority of transition of electron from the 2p to the 3d shells. Earlier studies on calcium L $_{2,3}$ edge using density of states and other approaches have taken into account the 2p-3d spin-orbit interactions as well as 3d-3d Coulomb and exchange interactions [157]. Shown in figure (4-4) is the calcium absorption edge recorded in TEY and FY compared with model compounds of calcium sulfate ($CaSO_4$), calcium hydroxide ($Ca(OH)_2$), calcium phosphate ($Ca_3(PO_4)_2$) and hydroxyapatite ($Ca_{10}(PO_4)_2$) and hydroxyapatite ($Ca_{10}(PO_4)_6(OH)_2$). The two primary peaks in the spectra located at 350 eV and 353 eV correspond to the L_3 and L_2 absorption edges [156]. The other minor peaks before the L_3 and L_2 edges correspond to various 2p transitions. Absorption edges of $Ca(OH)_2$ and $Ca_{10}(PO_4)_2$ are at slightly

lower energy state than $CaSO_4$ and $Ca_3(PO_4)_2$. The diesel soot spectrum slightly resembles to the spectra from $CaSO_4$ and $Ca_3(PO_4)_2$
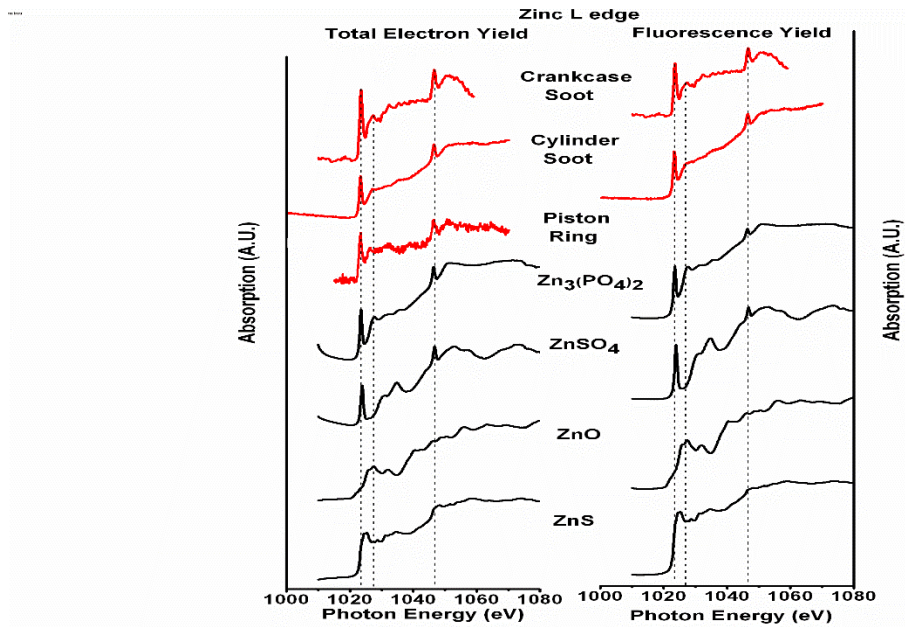

Figure 0-4 Normalized Total Electron Yield (TEY) and Fluorescent Yield (FY) calcium L edge spectra of crankcase soot, cylinder soot and piston ring of Mack T 12 engine test and model compounds

4.2.1.5 Phosphorus K- edge

Figure 4-5 shows the P K-edge spectra recorded in the FY and TEY modes with model compounds like $Zn_3(PO_4)_2$, $Ca_3(PO_4)_2$, $FePO_4$. Excitation of electrons from phosphorus 1s orbital to unoccupied 2p orbital results into strong peak which is characteristic of P k-edge spectra. Absorption peak for $Zn_3(PO_4)_2$ is almost similar to $Ca_3(PO_4)_2$. $FePO_4$ has absorption peak at 2154.5eV, higher than that of $Zn_3(PO_4)_2$ and $Ca_3(PO_4)_2$. Also, $FePO_4$ has distinctive pre-edge peak which is absent in $Zn_3(PO_4)_2$ and $Ca_3(PO_4)_2$.

The unreacted ZDDP has P K-edge peak at 2149.4 eV while $Zn_4P_6O_{19}$ has at 2152 eV. This difference of 2.5eV is because of the difference in the atom co-ordination of phosphrous in ZDDP and zinc phosphates. In ZDDP the phosphorus atom is co-ordination with 2 oxygen and 2 sulfur atoms while phosphorus in zinc polyphosphate is co-ordinated with four oxygen atoms. Moreover, high electronegativity of oxygen as compared to sulfur induces peak shift to higher binding energy. The similarity in peak shape and position of the phosphorus K-edge spectra in both FY and TEY mode suggests the presence of zinc polyphosphate which is the decomposition product of anti-wear ZDDP additive. Possibility of $FePO_4$ is not likely due to absence of pre-edge in soot spectrum. The phosphorus K edge spectra shows similar behavior to the phosphorus L edge spectra.
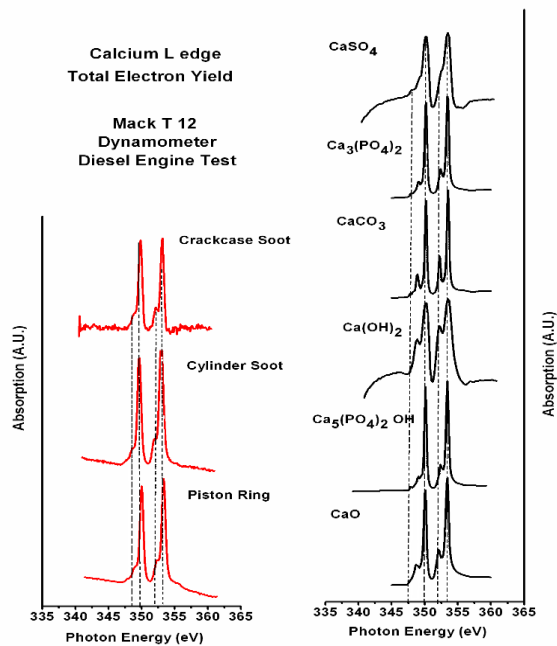

Figure 0-5 Normalized Total Electron Yield (TEY) and Fluorescent Yield (FY) phosphorus K edge spectra of crankcase soot, cylinder soot and piston ring of Mack T 12 engine test and model compounds

4.2.1.6 Sulfur K-edge:

The TEY and FY mode of sulfur K-edge spectra for dynamometer engine Mack T12 test oil soot sample is shown in figure 4-6. This spectrum was compared with sulphates of zinc, calcium and

iron and with sulfides of zinc and iron. Sulfates have their white lines at higher energies than the sulfides. FeS has characteristic absorption edge at 2482eV while ZnS has strong peak at 2470eV. $FeSO_4$ has higher energy state at 2482.3eV which differentiate it from zinc and calcium sulfate. Zinc sulfate and calcium sulfate can be differentiated by the presence of a post edge at 2484.8eV in the case of $CaSO_4$, which is absent in the case of $ZnSO_4$.

An assessment of both TEY and FY mode of the spectra of diesel soot shows that there is the sharp absorption edge at 2481.2 eV which is characteristic peak of $ZnSO_4$ and $CaSO_4$. Also an additional peak at 2472 eV indicates the presence of ZnS.

S K-edge spectra can also be used to quantify the relative proportion of sulfur compounds in diesel soot. This quantification was carried out by deconvoluting the sulfur K edge spectra in TEY mode. Analysis of relative amount of sulfide and sulfate compound was done by calculating height ratio of sulfide to sulfate peak. The sulfide/sulfate ratio for diesel soot is 0.37.
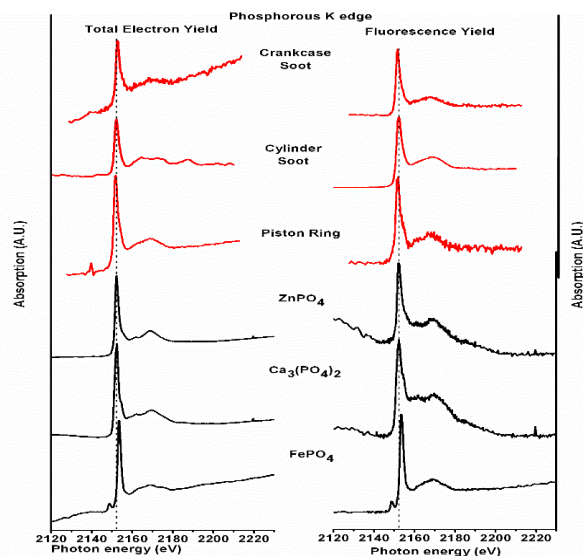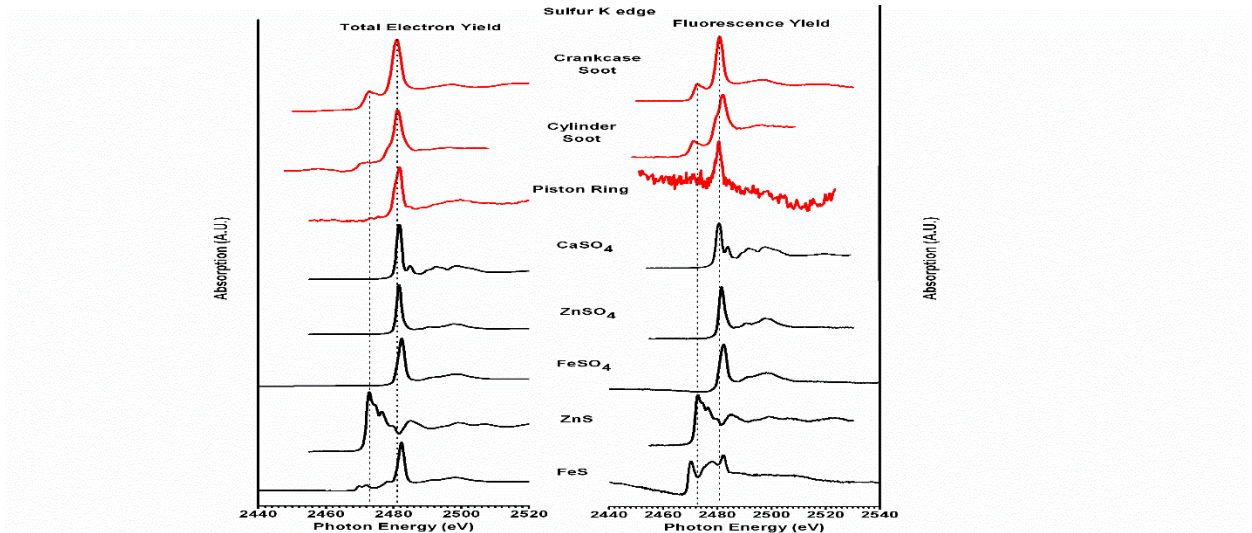

Figure 0-6 Normalized Total Electron Yield (TEY) and Fluorescent Yield (FY) sulfur K edge spectra of crankcase soot, cylinder soot and piston ring of Mack T 12 engine test and model compounds

4.2.1.7 Ca K-edge:

The calcium K-edge spectra taken in the TEY and FY mode is shown in figure (4-7). Spectra of soot samples is compound with model compounds of $CaSO_4$, $Ca_3(PO_4)_2$, $CaCO_3$ and CaO. CaO has a distinguish pre-edge at 4043 eV and strong peak at 4049.8 eV. While calcium sulfate and $Ca_3(PO_4)_2$ has an intense absorption edge at 4050 eV and 4049.4 eV respectively. Also, calcium sulfate has more fine structure compared to $Ca_3(PO_4)_2$.

A careful examination and comparison of the soot spectra and model compounds clearly indicates that the spectra appears to be close to both calcium sulfate ($CaSO_4$) and $Ca_3(PO_4)_2$. There is absence of CaO. However, the soot spectra is noisy which might indicate the lesser amount of calcium compound on the soot structure.
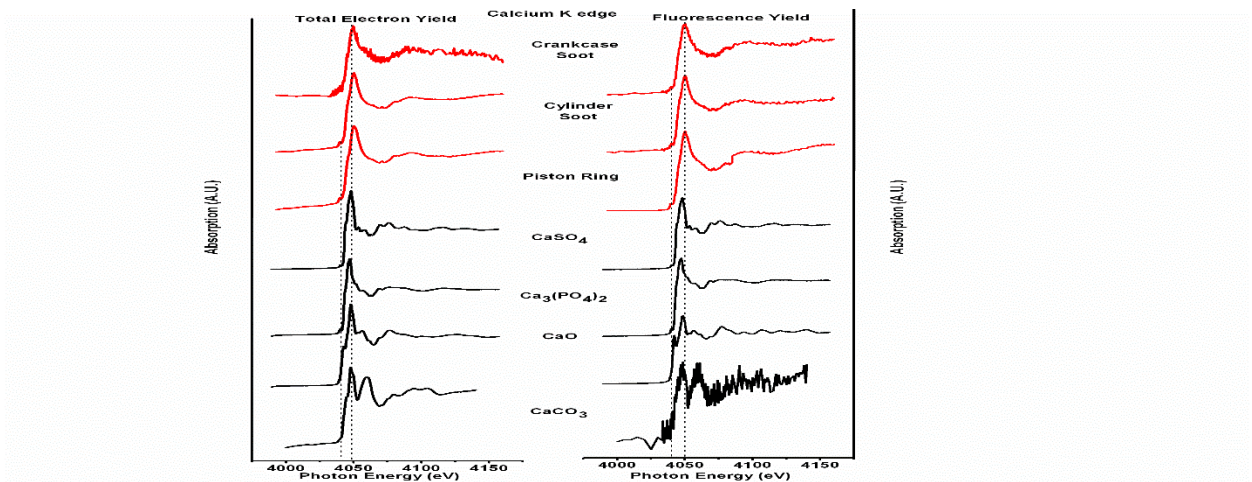
Figure 0-7 Normalized Total Electron Yield (TEY) and Fluorescent Yield (FY) calcium K edge spectra of crankcase soot, cylinder soot and piston ring of Mack T 12 engine test and model compounds

4.2.2 High Resolution Transmission Electron Microscopy (HRTEM)

Figure (4-8) is high-resolution bright field transmission electron microscopic image of Mack T12 soot that shows typical turbostratic structure of diesel soot. In addition, several nano crystalline

177

regions identified that are embedded with turbostratic structure of soot. Careful observation of the HRTEM images of the soot imply that the crystalline region is present on the edge of the primary particle of soot. Moreover, they appear as embedded on the outer periphery of the primary particle rather than loosely incorporated between the soot primary particles as wear debris. The crystalline phase of nano crystalline particles is continuous with crystalline domain of turbostratic soot structure. This continuity of crystalline phase on the surface of diesel soot primary particle suggests that possibility of mechanical embedding or chemical bonding of nano crystalline particle on surface of diesel soot primary particles and hence cannot be removed by washing, ultra-sonication and centrifuging the soot.
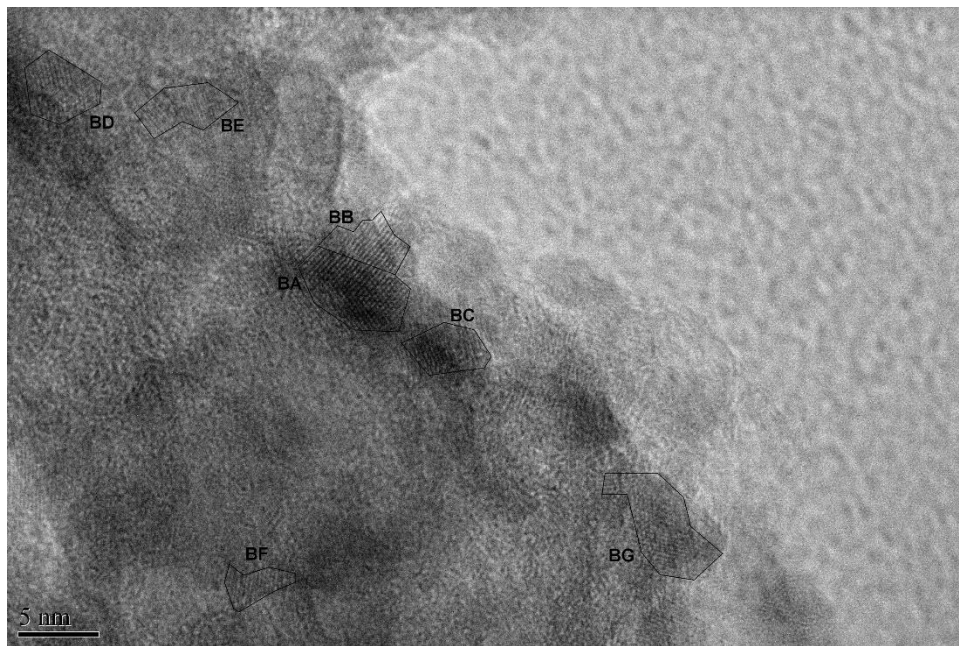
Figure 0-8 High-resolution bright field transmission electron micrograph of cylinder soot showing nano crystalline particle, turbostratic and amorphous regions

A corresponding energy dispersive spectrum (EDX) was recorded on the region that suggest the presence of P, S, Ca, Fe, Zn and O as shown in Figure 7.9. Peak for the Cu corresponds to the sample

holder. An associated XANES spectra on the soot revealed the presence of tricalcium phosphate, zinc phosphate and iron sulfide on the soot structure. EDX results bolster the XANES analysis data. Correlation of XANES and EDX results indicates that the interaction between soot particles and antiwear additives tribofilms results in embedment of zinc phosphates and iron sulfide. In addition, the high peak of oxygen in the EDX spectrum indicates the possibility of zinc oxide or iron oxide crystalline compounds present in the soot structure. Also, the good concentration of calcium in EDX spectra and the detection of tricalcium phosphate (which is the part of detergent chemistry) clearly suggest the interaction between detergents and diesel engine soot.
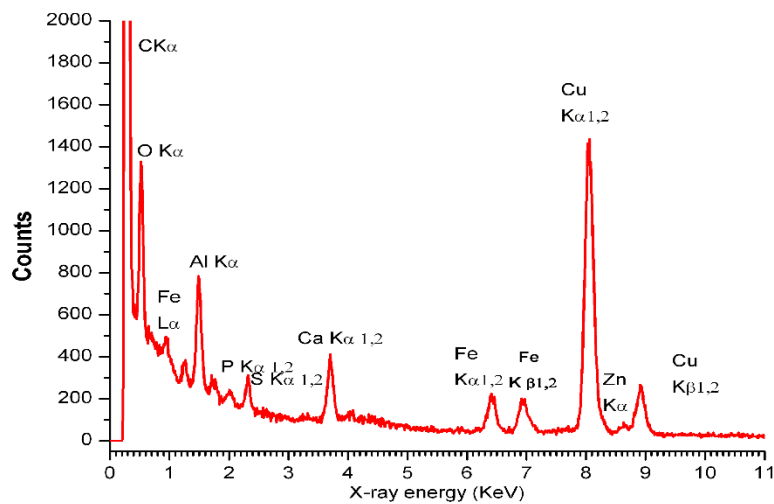
Figure 0-9 EDX spectrum for Mack T12 soot
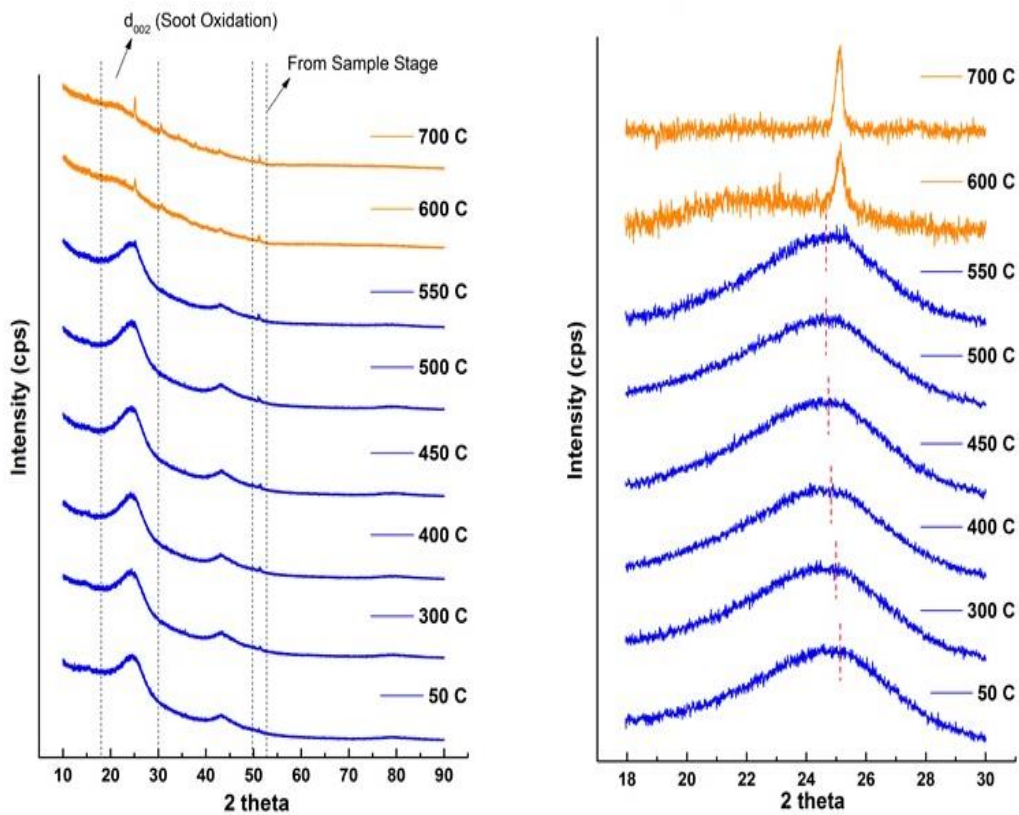
Figure 0-10 Variation in the X-ray diffraction spectra of soot with temperature

4.2.3 High Temperature X-Ray Diffraction

Figure 4-10 displays the XRD spectra for Soot extracted from the dynamometer engine test

Mack T12. The figures are divided into two sections that present the data acquired for the entire

scan range of $10-90°$ 2θ and the "d_{002} range" of $18-30°$ 2θ. The plot on the left side of the figure

(4.10) shows the data acquired at those specific temperatures where the significant changes such as

phase transitions, peaks from embedded or adsorbed nanocrystalline species etc. are noticeable. The

peak originating from all samples (before oxidation) around $24-26°$ 2θ originates from the basal

plane (002) of the disordered graph/itic lattice in the soot structure. Observing the changes in the

interplanar lattice spacing of the (002) family of planes with temperature can provide valuable

insight into the degree of disorder, crystallite height, width, and number of graphene layers per crystallite which can be correlated to combustion conditions, fuel type, ease of oxidation, etc. Spectra marked in the blue color shows the XRD spectra of the soot in the process of oxidation while the spectra in orange color is from the oxidized soot. Changes in the turbostratic structure can be seen from the onset of oxidation. Oxidation of soot sample takes place around 575˚C.

Looking at d_{002} regions, it is observed that with increase in temperatures, the intensity maxima (dotted red lines) shifts towards lower 2Θ values, indicating bigger d_{002} Inter-planar spacing. Higher the d_{002} spacing, easier it is for oxygen to access internal soot core structure and oxidize the soot at relatively lower temperatures. There is a marked increase in d_{002} after 150°C, which is a characteristic of higher disorder in the soot structure. The lattice rapidly expands in the [002] direction, presumably increasing the ease of oxygen access to the highly disordered core of the soot particle. XRD spectra at 700˚C indicates the diffraction peaks from the polycrystalline inorganic incombustible remain after soot oxidation. It is evident from figure (4-11) that peak from characteristic turbostratic carbon in the soot nanostructure vanishes at 700˚C. Peaks originating from the residue are indexed. Residue from the Drain Interval soot sample was primarily composed of Ca based compounds, namely, $CaSO_4$. $CaSO_4$ in the engine oil soot originates from detergents in oil and this could result in DPF ash accumulation in the long run affecting catalytic activity, filtration efficiency by sintering to the substrate.
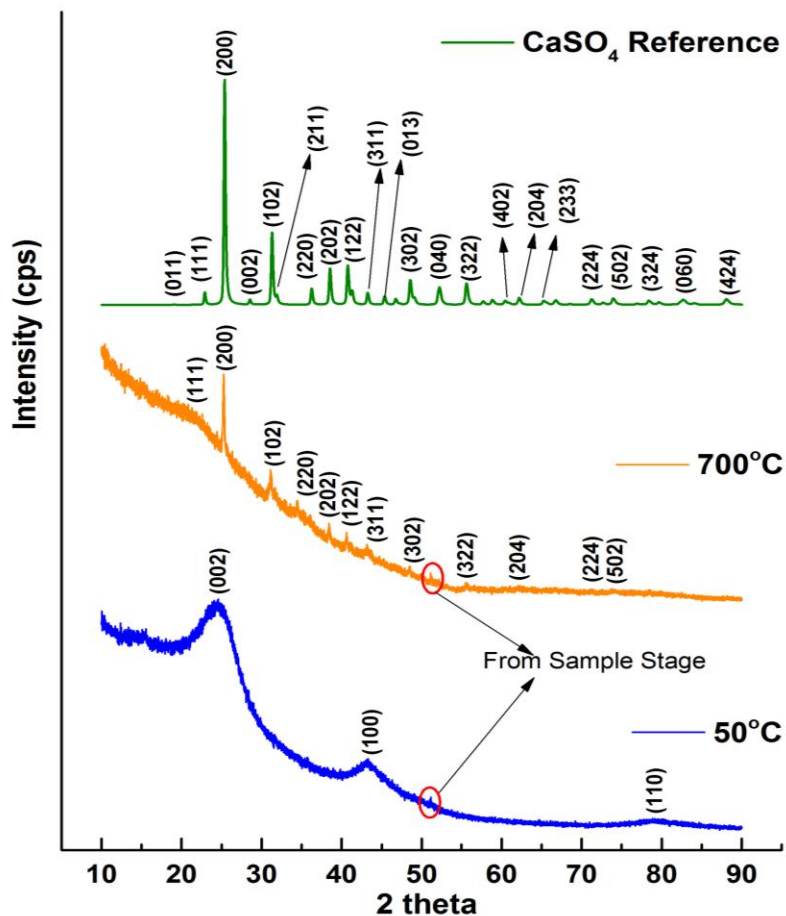
Figure 0-11 XRD spectra of oxidized soot and phase identification

Soot samples were oxidized during high temperature XRD to 700°C and the remaining residue amount was calculated. The residue that remains after soot oxidation exhibits a yellowish to gray appearance as shown in figure 4-12. Residue of soot samples was further quantified by normalizing them as a percentage of their initial weights; following equation was used to calculate weight percentages (wt %) of residue. "W_{soot}" and "$W_{residue}$" correspond to weight of the soot sample before oxidation and the weight of residue left behind after oxidation; they were measured on a precision scale in milligrams with two decimal accuracy.

$$\text{Residue (wt \%)} = \{(W_{\text{soot}} - W_{\text{residue}})/W_{\text{soot}}\} \times (100)$$

Polar species in engine oil get adsorbed onto the surface of soot agglomerates along with wear/corrosion byproducts embedded in the soot structure is left behind as incombustible residue after oxidation of soot. Soot sample showed 64 wt% of the residue left after oxidation at 575˚C.
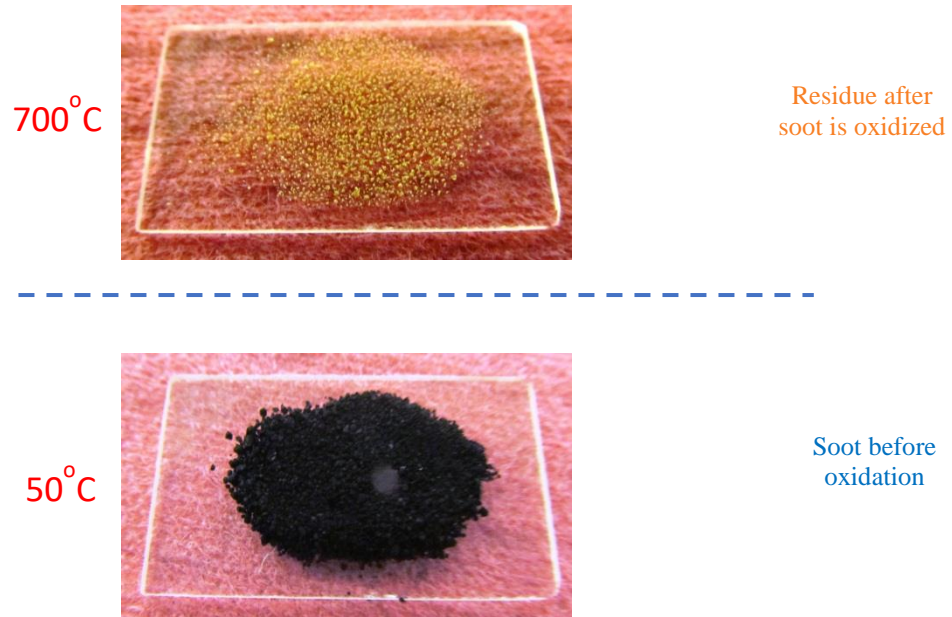
Figure 0-12 Soot appearance before oxidation at 25 ˚C and after oxidation at 700˚C

Energy dispersive spectroscopy (EDS) was used to analyze the elemental composition of the residue; EDS uses the ZAF method for quantification of elements in the sample. The atomic number (Z), absorption coefficient (A) for every element is calculated. Table 12 gives details of elements detected in all samples as detected in the spectra. Two categories for possible sources are also described in table, elements such as Zn, Mg, P, S, and Ca originate from oil additive, whereas Fe originate from the wear of engine components. Figure 4-13 shows the EDS spectra for residue from all diesel soot sample.

EDS spectra from the residue left over after oxidation resembles with the EDS spectra associated with HRTEM (mentioned in section 4.2.2). Correlation between both results indicates that additive decomposition or additive antiwear tribofilm compounds get adhere or embedded in

the drain interval soot during the engine operation. Also, the phase identification of the remains after oxidation by XRD shows the presence of $CaSO_4$. However, there was no identification of P, S, Zn peaks in the XRD spectra because may be the compounds formed by P, S, Zn were amorphous in nature.

Table 9 Elements detected by EDS analysis in diesel engine soot and possible sources

Element	Weight Percentage	Possible source
C	64.56	Multiple
O	19.08	Multiple
Mg	0.30	Oil Additive
P	1.51	Oil Additive
S	3.13	Oil Additive
Ca	6.68	Oil Additive
Fe	1.40	Wear Metal
Zn	3.35	Oil Additive
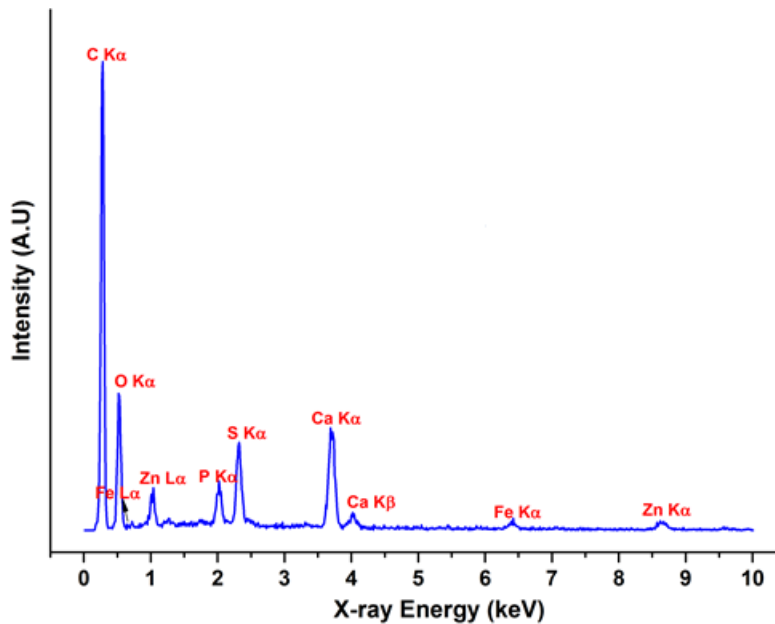
Figure 0-13 EDS spectrum of residue left after soot oxidation

4.6 Discussion

The Mack T12 test uses a Mack E-TECH V-MAC III diesel engine with Exhaust Gas Recirculation (EGR). It is operated in two steps format where a dedicated lubrication degradation phase is followed by high load phase. Also, the use of EGR increases ignition delay and thereby increases soot formation. The soot formation occurs later in the combustion cycle when more of the lubricants film on the cylinder wall is exposed. Hence, soot is trapped in the larger oil film surface and carried into the crankcase lubricants. During this operation, trapped soot between piston and cylinder wall represent typical three-body wear condition. During second phase of T-12 test, the ring and liner wear rate is maximized using combination of low speed and high load that create boundary lubrication condition [182,188]. It has also been reported that the impact of Mack T 12 test promotes changes in the lubricant formulation such as optimized detergency, increased antioxidants and sulfates ash.

It has been reported that as the soot enters in the crankcase, it interacts with reactive degradation compounds or polar additive species in the engine oil additive package, which are responsible for adsorption of inorganic decomposition products on the soot structure. In addition, there also exists the possibility of modification in the crystalline structure of diesel soot. There are several studies that indicate the presence of three body wear mechanisms where engine oil soot trapped between two opposing surfaces in the engine experiences extremely high local temperature and pressure conditions that might induce modifications in crystalline and/or amorphous domains of carbonaceous soot. Patel et al. briefly examined the chemistry and the structure of the dynamometer MackT12 test soot and found that soot extracted from cylinder walls goes through severe interaction environment than the crankcase soot. They suggested that during engine operation trapped soot agglomerates interact with the lubricant additive decomposition byproducts under high hertzian contact pressure and results into mechanical embedment or chemical bonding of nano crystalline particles of Fe_2O_3, hydroxyapatite ($Ca_5(PO_4)_3OH$) and carbonate hydroxyl apatite ($Ca_5(PO_4CO_3)_3OH$ [182]. Presence of these nano crystalline particles makes soot particle more abrasive in nature and results in catastrophic failure under extreme conditions.

XANES results reveals the presence of various decomposition products such as zinc phosphates, zinc sulfide, calcium sulfates, calcium phosphates, iron sulfates/sulfides. In addition, EDS and HRTEM results on the crankcase soot also showed the appearance of nanocrystalline particles contributed from lubricant additive and soot interaction. HRTEM images suggested that nanocrystalline particles are just not adhering to soot structure, they are mechanically embedded in the periphery of the turbostratic structure of the soot. XRD phase analysis showed that the residue from diesel soot samples was primarily composed of crankcase oil additive species and wear debris from engine hardware components. Crystalline compounds such as $CaSO_4$ and amorphous compounds of P, S, Zn, Fe was also identified by EDS results.

It can be postulated that the highest amount of wear debris element might have come from the tree body wear mechanism of the trapped soot particles. Also, the good amount of Zn, P originated from the ZDDP tribofilm indicates the interaction of soot particles with the antiwear additives decomposed byproducts.

Sharma et al. [172] and Patel et al. [173] also studied the presence of embedded nano crystallites originating from engine oil additives or wear debris in the soot turbostratic structure. It is postulated that nanocrystallites present on the soot structure could create higher disorder, resulting in an increased number of graphene edges and thereby more active sites favoring easy oxygen attack. Samples that contain wear debris in the form of Fe (or their oxides) could also catalyze oxidation of carbon in the soot structure when subjected to higher temperatures (above 300 °C) and in an oxygen environment. Yehliu et al [181] studied the impact of fuel on the soot reactivity and nanostructure by using three fuels : an ultra low sulfur diesel fuel, a pure soybean methyl-ester, and a synthetic Fischer-Tropsch fuel and generated soot by using A 2.5 L, 4-cylinder, turbocharged, common rail, direct injection light-duty diesel engine. They suggested using XRD and HRTEM that soot oxidation reactivity was dominated by the disorder of the carbonaceous nanostructure and the increase of accessible carbons on the edge sites. They also proposed that the basal plane diameter obtained from XRD was inversely related to the apparent rate constants for soot oxidation. In accordance to this studies, HT-XRD results also showed the influence of the nano crystalline species on the variation of oxidation behavior. Change in the d_{002} interplanar spacing with the temperature indicates the extent of disorder in the turbostratic structure of carbon and the ease with which oxygen access the internal soot structure and results in oxidation at lower temperature.

XANES, HR-TEM and HT-XRD results reveals that the interaction of soot particles with the lubricant additive decomposition products at high temperature and shearing stress conditions leads to mechanical embedment of nano crystalline particles which affects the chemistry, structure and oxidation stability of the soot. The hardness of the nano crystalline particles of Fe_2O_3, ZnO and

phosphates/sulfates of calcium is in the range of 4.5-6 in the Moh's scale, which is much larger than the 2-3 for gypsum and basanite. It can be speculated that the trapped soot with such nano crystalline particles may result in polishing wear in three body lubrication conditions and also may result in abrasive under extreme conditions.

5. Influence Of Soot On Antiwear Additives Performance Part II: Tribological Evaluation

5.1 Introduction

Severe wear due to soot oil contamination was always a concern for the automotive industry. The diesel engine soot is the by-product of incomplete fuel combustion. Use of exhaust gas emission (EGR) aggravates soot contamination in lubricating oil. Over the years, many researchers have addressed this issue and studies were carried out to get a thorough understanding of soot induced engine wear mechanism. This helped lubrication engineers to formulate newer engine oils with a better soot handling capabilities. However, it is challenging for lubrication professionals to develop oil formulations with anti-wear additives which will not poison the catalytic converter and will also help to mitigate the harmful effect of soot contamination on diesel engine wear.

This second part of chapter aims at understanding the effect of soot on the anti-wear performance of three different additives namely zinc dialkyl dithiophosphate (ZDDP), ionic liquid Tetrabutyl-phosphonium O, O-diethyl dithiophosphate (DEDTP), ashless dialkyl dithiophosphate (DDP). Standard ASTM D2266 test procedure designed for four ball tribotest was used to assess the tribological parameters. The wear scar diameter (WSD) was calculated for each test from each of the three stationary balls using a stereo-optical microscope. The coefficient of friction (COF) values were reported directly from four-ball machine. This study also focusses on understanding the effect of concentration of soot and the effect of dispersant-additive surface interaction on the wear of test steel samples. To apprehend the mechanism of wear, morphology, and chemistry of the tribofilms was studies using secondary electron microscope (SEM) and energy dispersive X-ray spectroscopy (EDX).

5.2 Experimental Details

5.2.1 Description of additive chemistry and oil formulations

Extraction of soot particles from the Mack T12 dynamometer engine test was done according to the procedure described in (section 3.1). Group III base oil, ZDDP and DDP were purchased from commercial vendors. The phosphonic ionic liquid named as DEDTP was provided from AC2T Research GmbH Austria. In this study, sorbitan monoleate was used as dispersant. Table 13 details the structure and coded name of additives used in the test oil formulations.

Table 10 Chemical structure of the additive compounds

Coded Name	Chemical Name and Function	Chemical Structure
ZDDP	Zinc dialkyl dithiophosphate	
DEDTP	Tetrabutyl-phosphonium O, O- diethyl Dithiophosphate	
DDP	Dialkyl dithiophosphate	
Dispersant	Sorbitan Monoleate	

Bench test oil formulations were prepared by adding all the anti-wear additives at 700 ppm phosphorus treat rate in group III base oil. Dispersant was also kept constant at 5wt% in all the formulations. The maximum amount of phosphorus according to API CJ 4 SAPS norms is 0.1 wt%, so an optimum amount of 0.07 wt%. To understand adverse effect of increased soot level in lubricating oils on engine wear, soot was added in test oil formulations in increasing order of 2 wt%, 5wt%, 10wt%.

Previous studies have suggested that presence of additive and dispersant in lubricating oil promotes engine wear. Baseline test oil formulations were formed to apprehend the effect of certain interactions like antiwear additive-dispersant, antiwear additive-dispersant-soot on the wear of tribological contact. Table 14 details the bench test oil formulations composition and coded name which will be used further as a reference name.

Table 11 Details of the bench test oil formulations

Coded Name	Bench Test Oil Formulations
A	Base Oil
B	Base Oil + 5% Dispersant
C	Base Oil + 0.07% ZDDP
D	Base Oil + 5% Dispersant + 0.07% ZDDP
E	Base Oil + 5% Dispersant + 0.07% ZDDP + 2% Soot
F	Base Oil + 5% Dispersant + 0.07% ZDDP + 5% Soot
G	Base Oil + 5% Dispersant + 0.07% ZDDP + 10% Soot
H	Base Oil + 0.07% DEDTP
I	Base oil + 5% Dispersant + 0.07% DEDTP
J	Base Oil + 5% Dispersant + 0.07% DEDTP + 2% Soot
K	Base Oil + 5% Dispersant + 0.07% DEDTP + 5% Soot
L	Base Oil + 5% Dispersant + 0.07% DEDTP + 10% Soot
M	Base Oil + 0.07% DDP
N	Base Oil + 5% Dispersant + 0.07% DDP
O	Base Oil + 5% Dispersant + 0.07% DDP +2% Soot
P	Base Oil + 5% Dispersant + 0.07% DDP + 5% Soot
Q	Base Oil + 5% Dispersant + 0.07% DDP + 10% Soot

Bench test oil formulation was carried out by thorough mixing of additives, dispersant and soot by using pulse ultrasonication for 15 min in DI water bath. Tribological test were carried out for each oil formulation immediately after mixing.

5.2.2 Tribological Test Procedures:

To evaluate the tribological behavior of all the test formulations four ball tribotester was used. Tests were carried out using the Plint TE-92 Rotary tribometer procured from Phoenix Tribology (London, UK). The four ball tribometer arrangement consists of three stationary balls held together in a clamp and the fourth ball is fixed in a ball holder at the top. This fourth ball slide over the three balls resulting in a wear scar over the three balls and a circular wear mark over the top ball. The boundary lubrication regime is active throughout the test as the interacting surfaces make contact and asperities interact to produce wear scar.

ASTM standard D2266 was used for making evaluation of the antiwear properties of blended lubrication test oils in sliding contact by means of four balls. According to ASTM standard, three E52100 chrom steel balls of ½ inch diameter were clamped together at the bottom and covered with the formulation to be evaluated. A fourth steel ball held in ball holder was pressed with force of 40 Kgs into the cavity formed by the three clamped balls. The temperature of the test was regulated at 75˚C and the top ball was rotated at 1200 rpm for 60 min and 72000 cycles. All the tests were repeated thrice to avoid any discrepancy in the data. After termination of each test, three balls were removed and cleaned thoroughly using hexane to observe wear scar. Wear scar diameter was determined by using stereo optical microscope (SOM). The comprehensive understanding of the wear mechanism was studied by examining the wear surface morphology and chemistry using secondary electron microscope (SEM) and energy dispersive X-ray spectroscopy (EDX).

5.2.3 Stereo-Optical Microscopy (SOM)

SOM (model type: Nikon SMZ 1500) was used to image the wear scars formed on the three stationary balls after the fourth ball tests. The balls were cleaned with hexane and were placed on homemade fixture under the microscope. Samples were imaged at 100x magnification and saved with a 300μ marker using software provided by quartz imaging corporation. These images were further analyzed using image J software and WSD was calculated for each ball.

Measured WSD for each ball is the average of longest horizontal striation and longest vertical striation. WSD for each bench test oil formulation was determined using an average of 12 readings on 6 ball samples from a total of 2 repeat runs.

5.2.4 Scanning Electron Microscopy (SEM)

SEM model type (Hitachi S-3000N) was used in the SE (Secondary electron) mode to image the wear surfaces at magnification highest upto 1000x and an accelerating voltage of 15-25 kV was used in all the cases. Two ball samples per each test were selected for SEM study by carefully analyzing their optical images for better defined wear tracks or material pull out. The sample is cleaned and placed on the fixture using carbon tape. Carbon tape was used to ensure good electrical contact between the steel balls and sample holder. Secondary electron images were taken at three magnifications 70x, 500x, 1000x. Images at higher magnification was used for the understanding of wear mechanism and study of the tribofilm formed on the surface.

5.2.5 Energy Dispersive X-ray Spectroscopy (EDX)

EDX element maps and spectrum were collected for the wear test samples at higher magnification of the 1000X and at the acceleration voltage of 15 kV. The spectrum analysis of the selected wear scar area gives the information of element weight percent like Phosphorus and Sulfur. EDX maps were used to understand the abrading of anti-wear tribofilm by soot particles.

5.3 Results

5.3.1 Wear Results

The wear scar diameter was obtained for all the test balls using the method described in the section (5.2.3) and average value was reported (referred to as AWSD further). The following figure shows average wear numbers for all the test oil formulations in the form of bar chart. All the AWSD values are in µm with their exact value in the center. The error bars represent the corresponding variation in the AWSD values for each test.

Figure 5-1 shows the AWSD values for all the oil formulations having ZDDP as primary anti-wear additive. For the sake of baseline comparison AWSD value for base oil is also added in the bar chart. When ZDDP anti-wear additive was mixed with the base oil, AWSD was decreased from 773 µm to 618 µm. Thermal decomposition of ZDDP results in formation of anti-wear tribofilm mainly comprising of phosphorus, zinc and sulfur. This thin tribofilm layer adheres to the surfaces in contact and further protects them from wear. That's why the addition of ZDDP have resulted into decrease of AWSD. Addition of the dispersant results in increase of the AWSD value to 745 µm. AWSD for the oil formulations E, F, G displays the effect of increase amount of soot levels. As the amount of soot dispersed in the oil increases the AWSD also increases. This shows that presence of soot in the lubricating oil results into severe wear of the surfaces in contact.
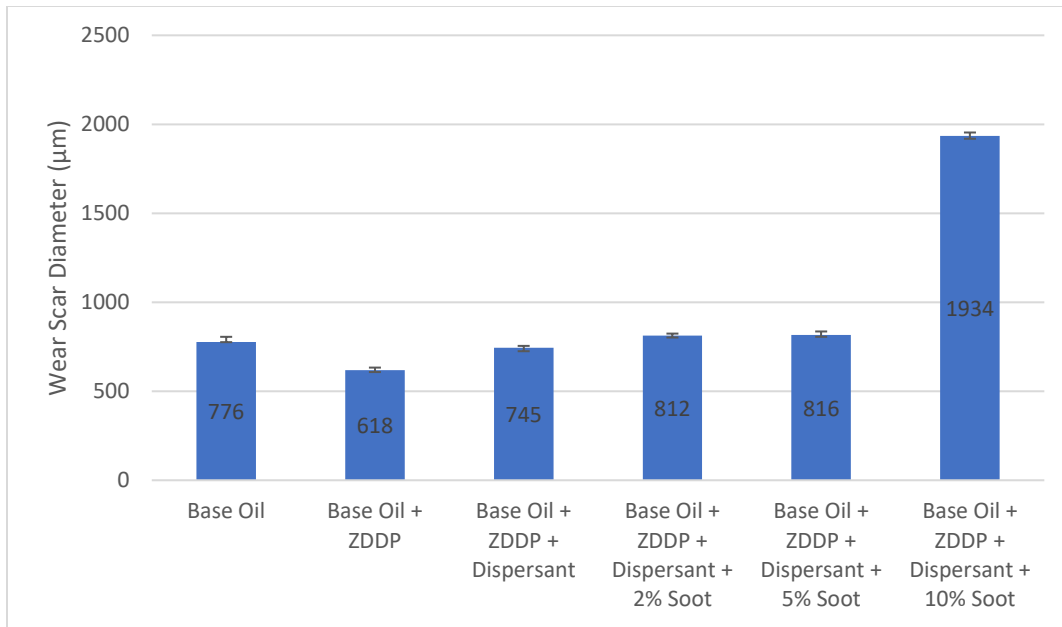
Figure 0-1 ASWD values for the test formulations having ZDDP as primary antiwear additive
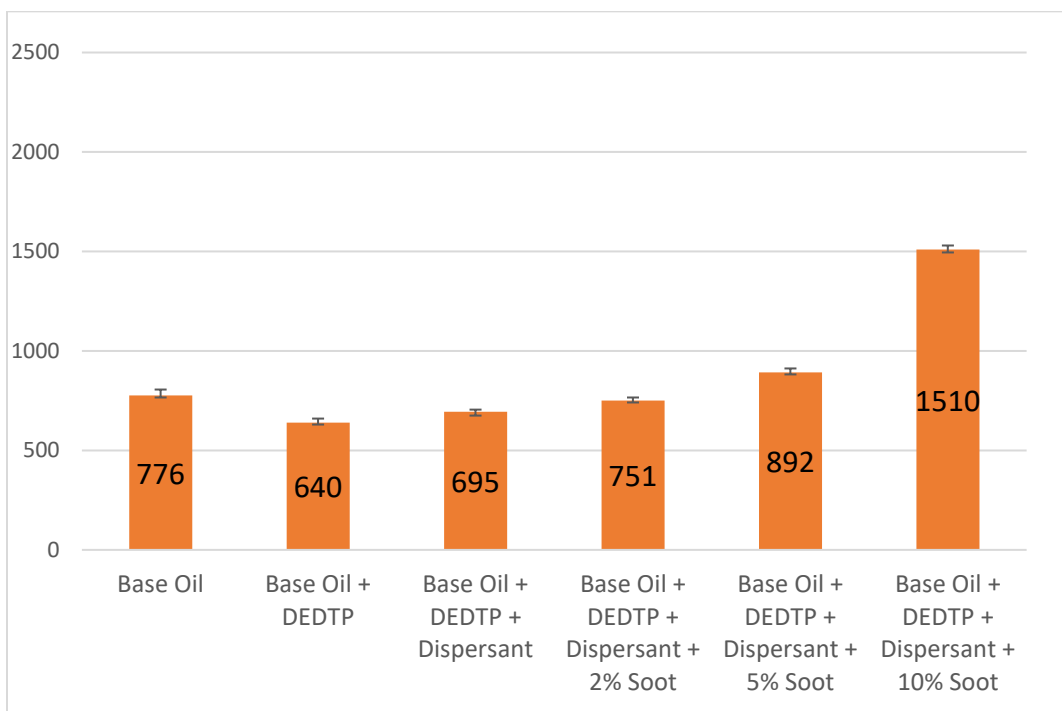

Figure 0-2 AWSD values for the test formulations having DEDTP as primary additive

Figure 5-2 shows the AWSD bar chart for all the oil formulations having DEDTP as the anti-wear additive. Addition of the ionic liquid DEDTP results in decrease of AWSD value by 133 µm. Phosphorus and sulfur based ionic liquid forms tribofilms similar to those formed by ZDDP. Ionic liquids form anti-wear tribofilm composing of short chain and medium chain polyphosphate during the rubbing action under mixed to boundary lubrication regime. The ionic liquid formed tribofilms adhere onto the wear prone surfaces and enhances the wear protection. It can be seen from the increased AWSD value of formulation I that addition of dispersant has detrimental effect on the anti-wear behavior of DEDTP. DEDTP formulations with increasing amount of soot shows the similar trend of increasing AWSD values with the increase in soot concentration. However, the comparison of AWSD value of formulation G and formulation L indicates that the ionic liquid DEDTP shows better anti-wear performance than ZDDP at increased10% soot concentration.

Ashless anti-wear additive DDP based test oil formulations wear performance is shown in the figure 5-3. Mixing of DDP in base oil results into decrease of AWSD value from 773 µm to 695 µm. Anti-wear additives enhance the wear performance of lubricating oil by undergoing decomposition forming and protective film or layer between the contact surfaces. DDP forms the stable amorphous tribofilm of phosphorus with very few of the crystalline oxide particles suspended in it. AWSD values of oil formulations O, P, Q shows that addition of soot deteriorates the anti-wear performance of lubricating oil. Diesel engine soot is abrasive in nature and results in heavy wear of contacting surfaces.
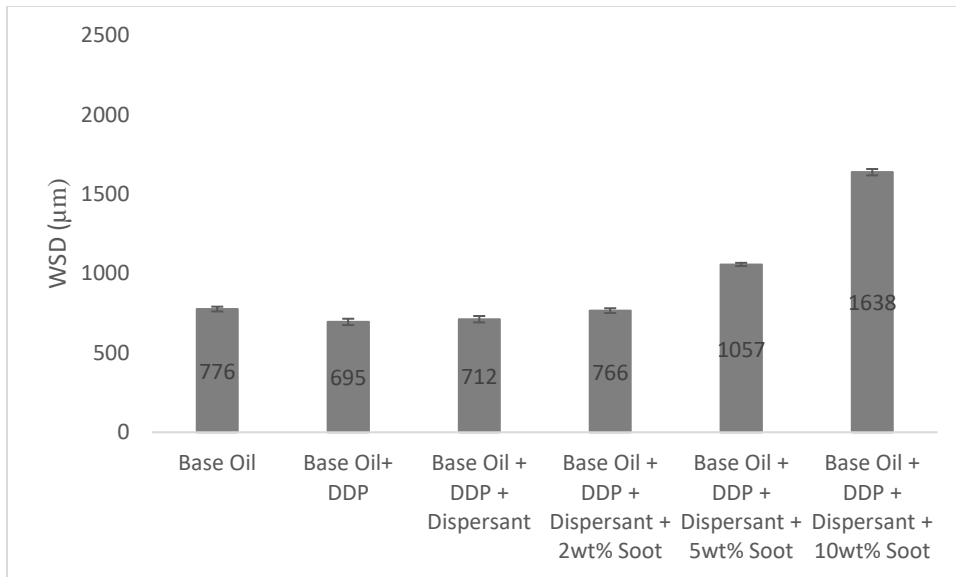
Figure 0-3 AWSD values for the test formulations having DDP as primary antiwear additive

5.3.2 SEM Results

Scanning electron microscopic (SEM) images of the wear scars formed on the stationary balls by the test oil formulations with 0%, 2%, 5%, 10% soot along with three different anti-wear additives is analyzed in this section. Figure 5-4 shows lower magnification SEM images and Figure 5-5 shows higher magnification SEM images of the wear scar formed by the test oil formulation having ZDDP as primary anti-wear additive.
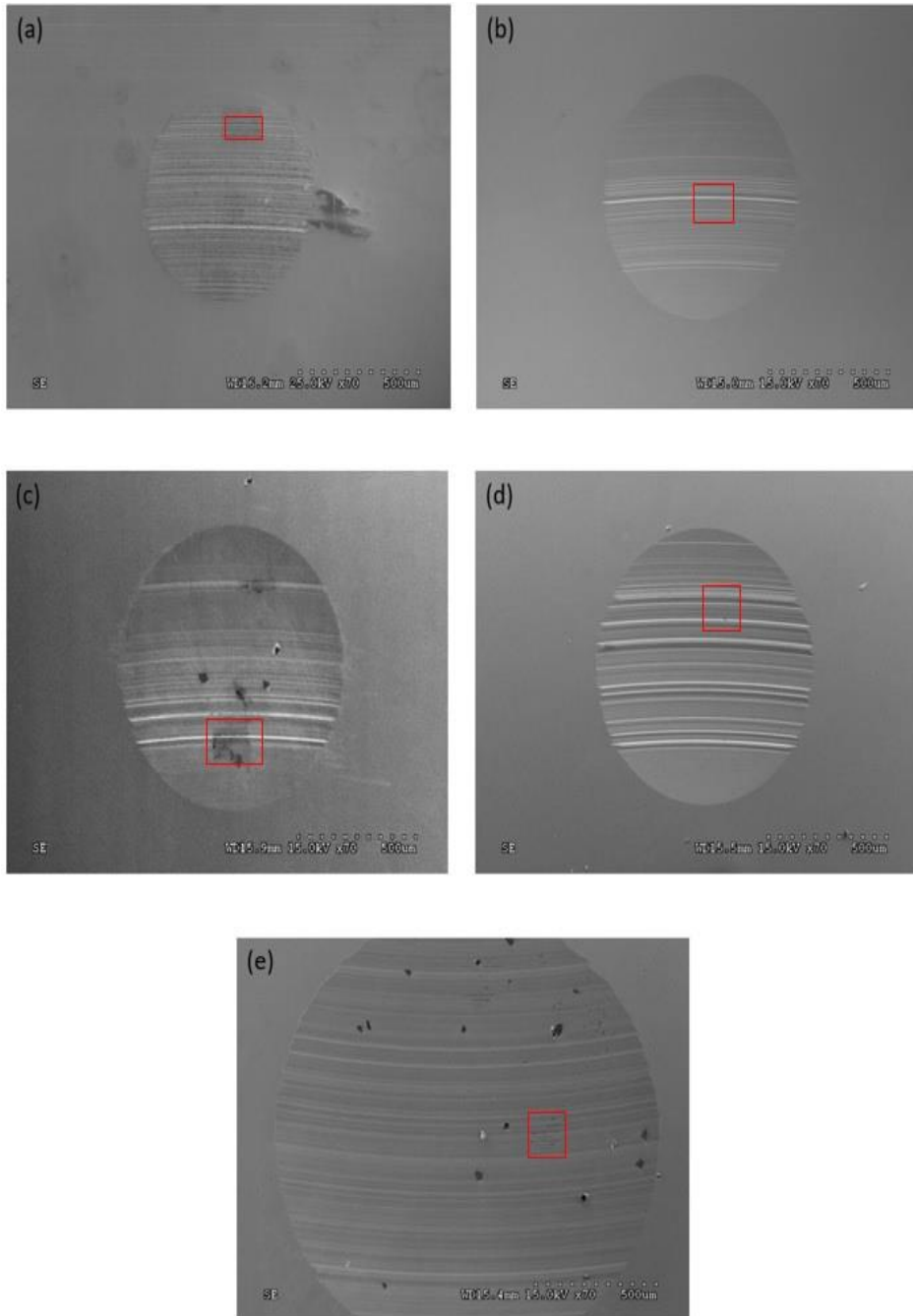
Figure 0-4 Low magnification SEM images for the test oil formulations (C-G) having ZDDP as antiwear additive.
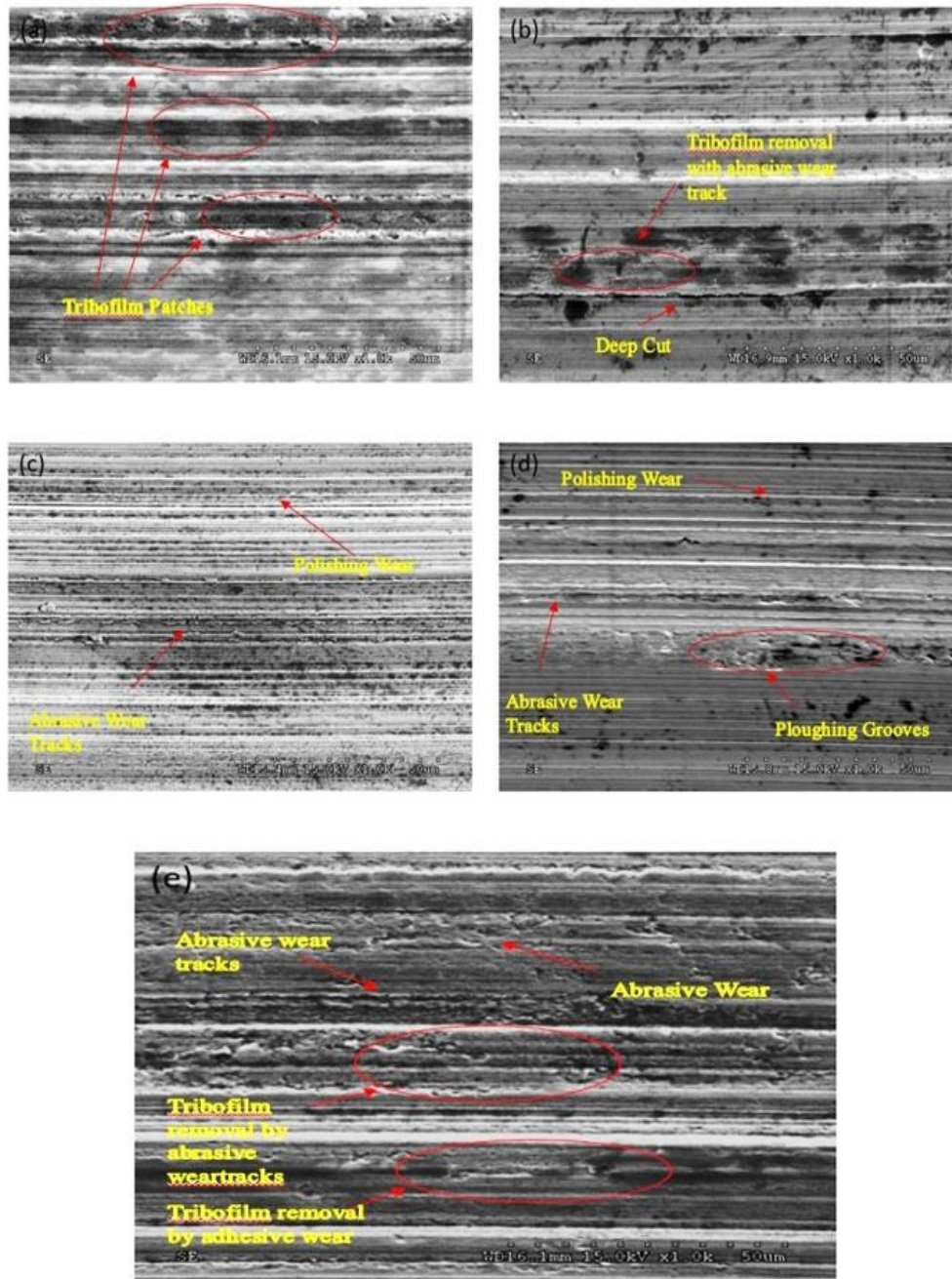
Figure 0-5 High magnification SEM images of the test oil formulations having ZDDP as antiwear additive (a) only ZDDP (b) ZDDP and Dispersant (c) ZDDP, Dispersant and 2wt% soot (d) ZDDP, Dispersant and 5wt% soot (e) ZDDP, Dispersant and 10wt% soot.

The boxes marked in figure 5-4 are the representative of the area under consideration which is further magnified to study the wear mechanism. Wear scar of the test formulation having just ZDDP antiwear additive and no soot particles shows some dark patches of tribofilms throughout the scar width. SEM image of the test formulations E i.e with 5wt% dispersant shows very few dark patches of tribofilm and presence of polishing wear tracks. This indicates addition of dispersant may have affected the tribofilm formation and resulted in increase of WSD as shown in figure 5-5. For the wear scar of test formulation having 2wt% soot, combined abrasive and polishing wear can be observed in the direction of sliding. The surface morphology from the surfaces of the samples having 5wt% and 10wt% soot display furrowed wear tracks with fine cracks indicating significant abrasive wear. Also, tribofilm removal by abrasive and adhesive wear can be seen clearly in high magnification images. SEM analysis advocates the severe wear resulting because of the increased levels of soot. Soot agglomerates leads to the rapid removal of ZDDP tribofilms and promotes the wear at higher rates.

Figure 5-6 shows the wear images for test oil formulations having DEDTP as antiwear additive. At 70x it is seen that the WSD increases as the concentration of soot increases. To better understand the cause and nature of increased wear, higher magnification images at 1000X were taken. As shown in figure 5-7, at 1000X we can see more details of the wear scar features.
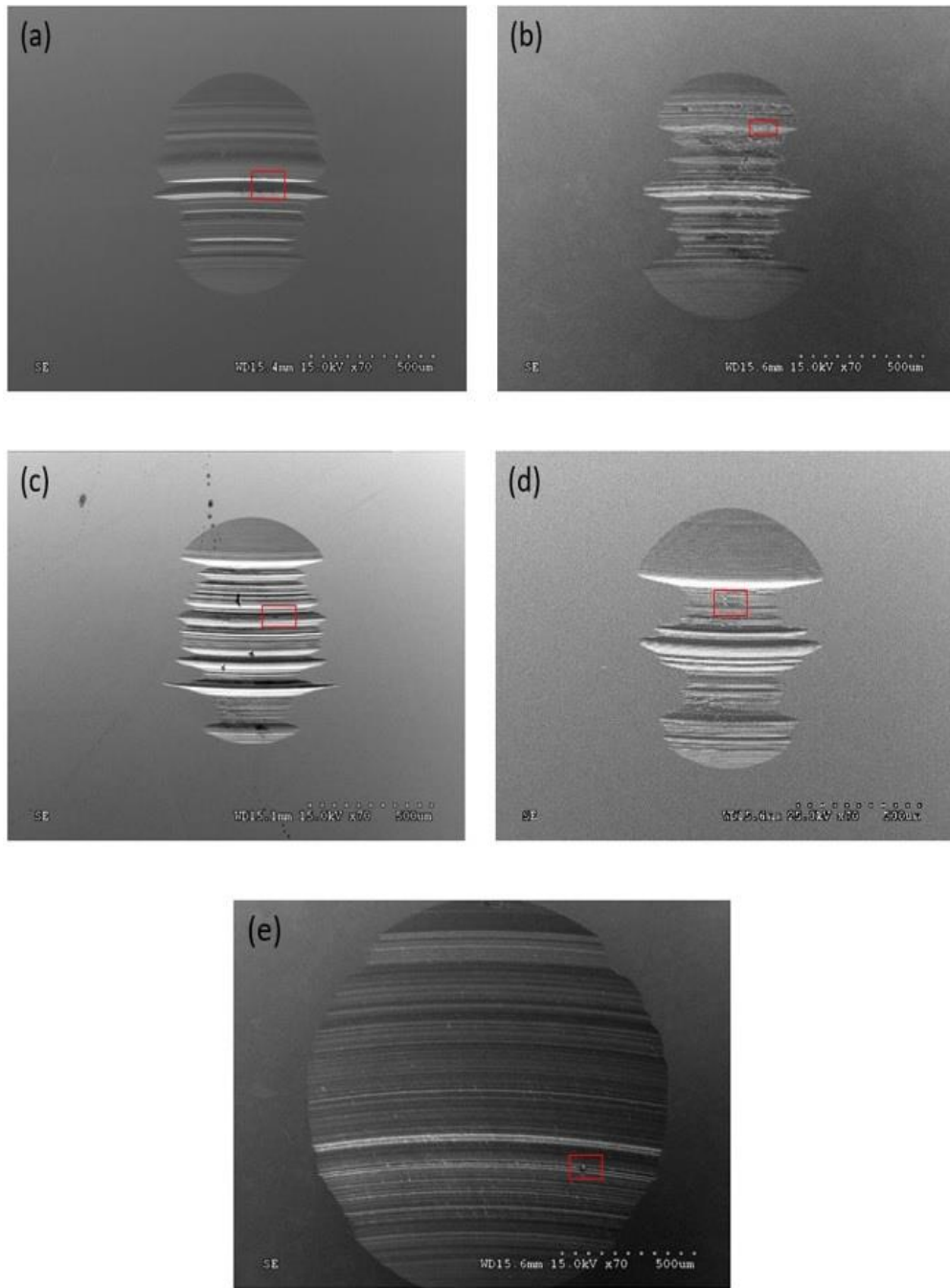
Figure 0-6 Low magnification SEM images of the test oil formulations having DEDTP as antiwear additive.
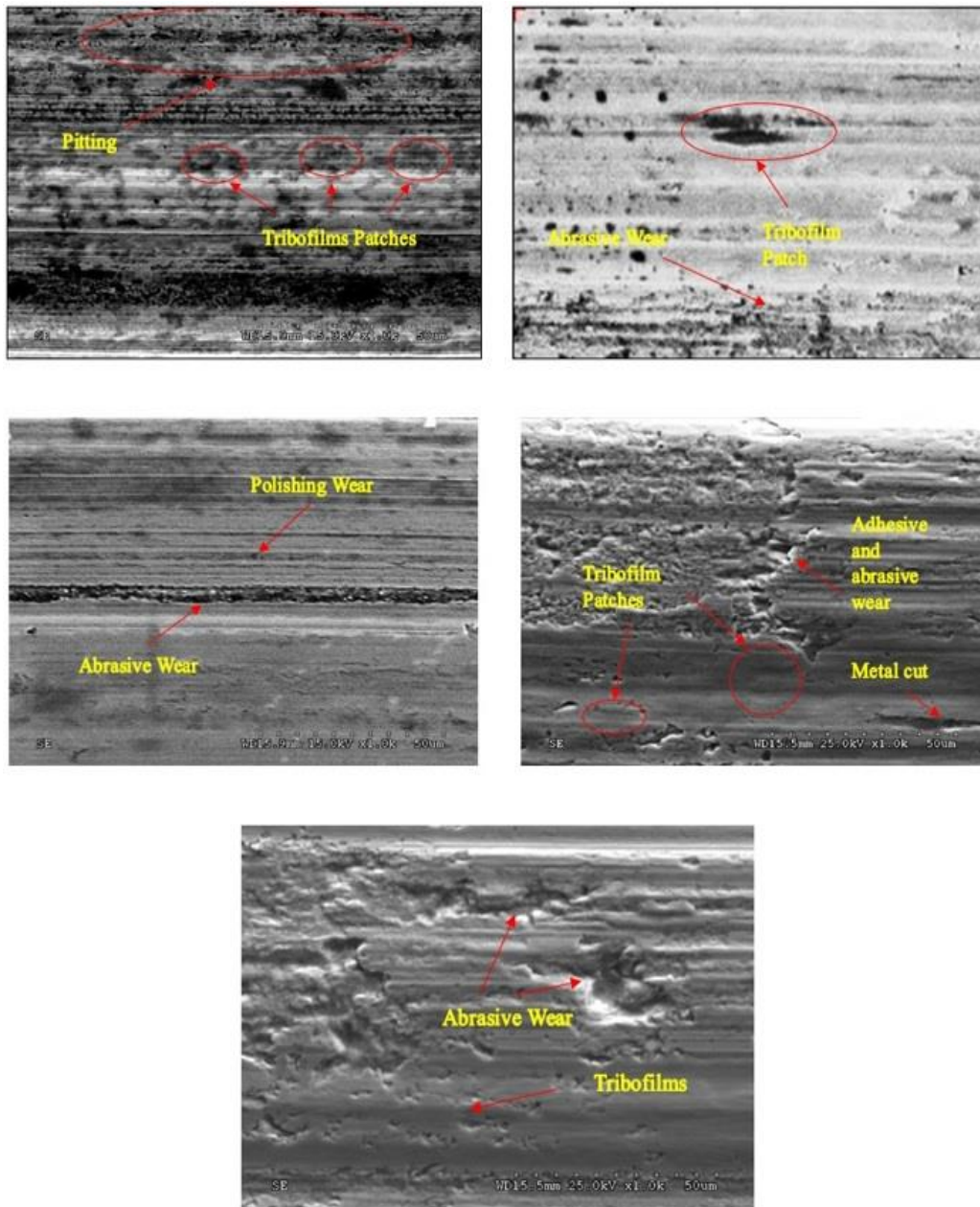
Figure 0-7 High magnification SEM images of the test oil formulations having DEDTP as antiwear additive. (a) only DEDTP (b) DEDTP and Dispersant (c) DEDTP, Dispersant and 2wt% Soot (d) DEDTP, Dispersant and 5wt% Soot (e) DEDTP, Dispersant and 10wt% Soot.

SEM image of test samples with 0.07wt% DEDTP showed wear scar with the dark patches of tribofilms. Some amount of pitting can also be seen. Ionic liquids are reported to have corrosive effect on the steel surfaces. As the amount of DEDTP is less, the pitting effect was not dominant. Also, the wear scar appears to be rough as compared to other test formulations wear scar. Addition of dispersant results in reducing the tribofilms patches and smooth wear scar as evident from figure (5.7 (b)) SEM image. Wear scar surface morphology of samples having 2wt% soot shows some amount of abrasive wear track. Samples with 5wt% shows combination of adhesive and abrasion wear. Also, deep scratches and metal pullout can be seen. SEM images of the wear scar formed on the stationary four ball by test formulation blended with 3 wt.% diesel soot has areas that are smooth with patches of tribofilm as well as areas with severe abrasion indicating the deleterious effects of the presence of diesel soot in the formulation. Higher magnification SEM image at 4000X of the test oil formulations containing 10wt% displays the abrasive groove on the scar surface (figure 5-8).
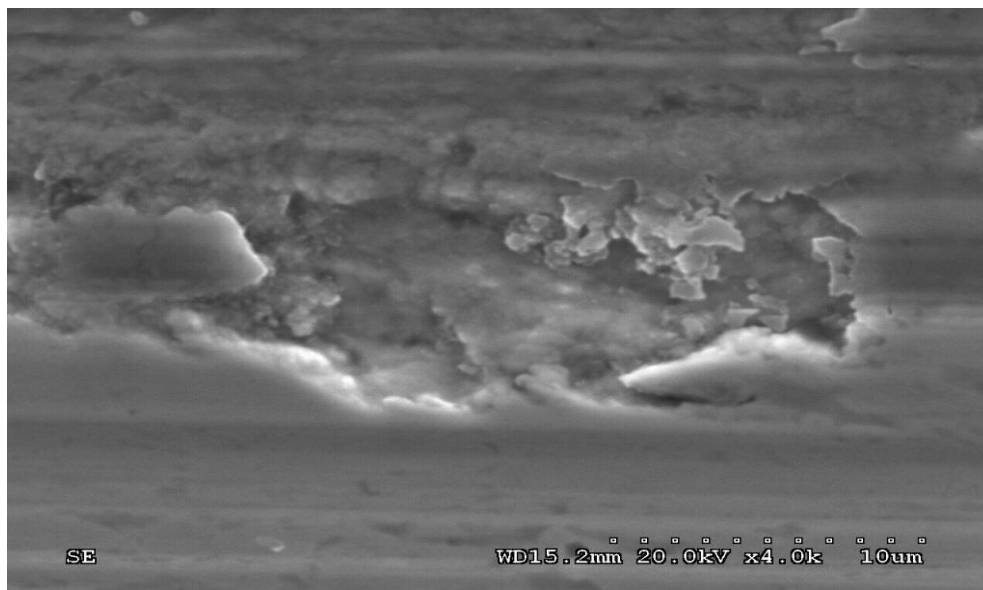

Figure 0-8 High magnification SEM image of the wear scar formed on the stationary four ball by test formulations blended with 10wt% diesel soot.

Scanning electron images of wear scar developed on the stationary steel balls during four ball tribometer test of oil formulations having DDP as the antiwear additive with increasing amount of diesel engine soot as 0wt%, 2wt%, 5wt%, 10wt% is shown in the figure 5-9. Wear scar of the test oil formulation have DDP as the primary antiwear additive and no soot exhibit large tribofilm patch and smooth worn surface with some amount of polishing wear. Thin tribofilms on the wear scar shown in SEM image (c) confirms the effect of dispersant on tribofilm formation and adsorption of decomposition products of DDP. SEM images (d) and (e) depicts the detrimental effect of increasing soot concentration in the test formulations. Soot addition causes deep ploughing grooves in wear track indicating abrasive wear.

Figure 0-9 High magnification images of test formulations having DDP as antiwear additive (a) Only DDP (b) DDP and Dispersant (c) DDP, Dispersant and 2wt% Soot (d) DDP, Dispersant and 5wt% Soot (e) DDP, Dispersant and 10wt% Soot.
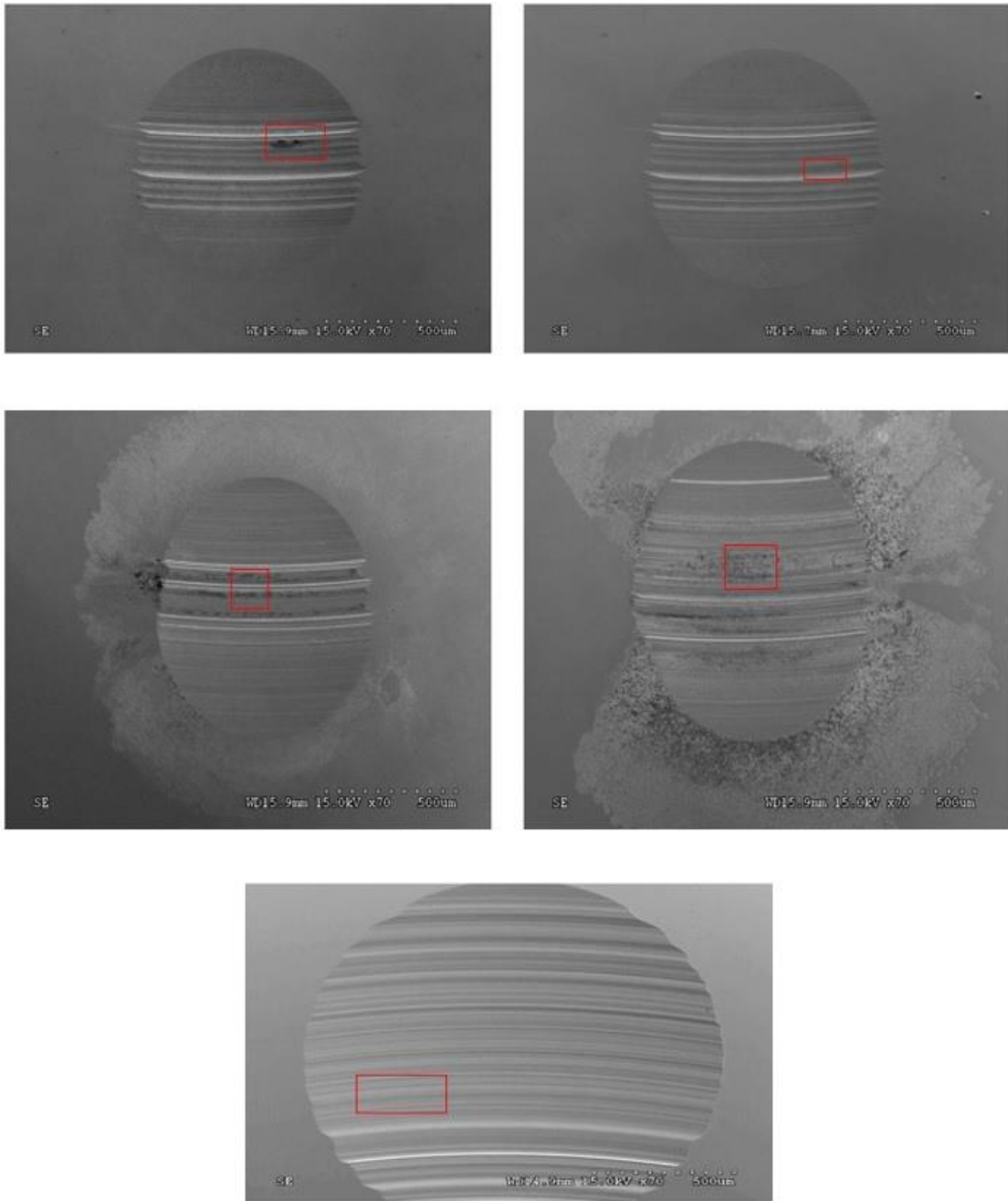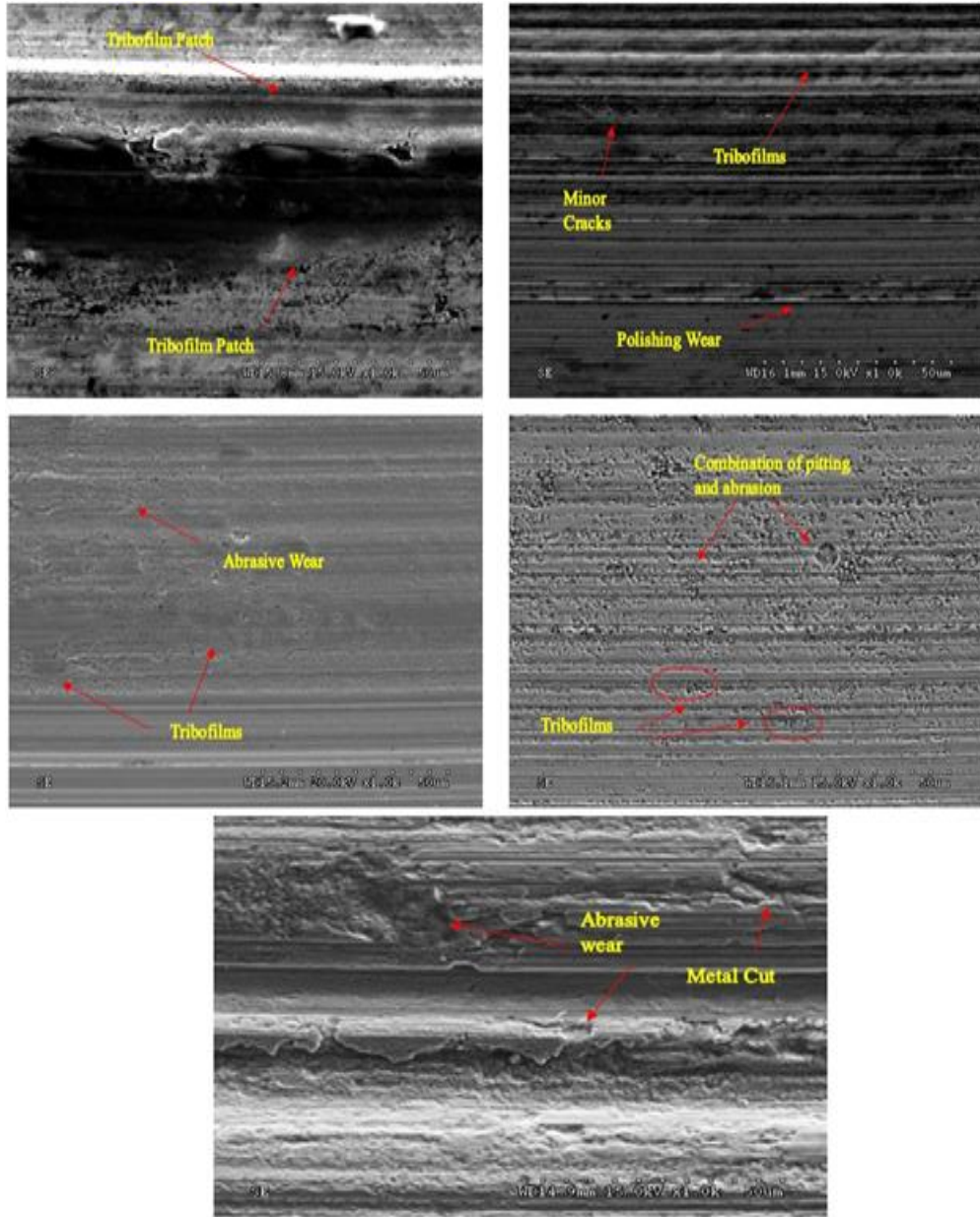
Figure 0-10 High magnification images of test formulations having DDP as antiwear additive (a) Only DDP (b) DDP and Dispersant (c) DDP, Dispersant and 2wt% Soot (d) DDP, Dispersant and 5wt% Soot (e) DDP, Dispersant and 10wt% Soot.

5.3.3 EDS Results

5.3.3.1 Oil Formulations with ZDDP as antiwear additive

SEM-EDS results show the elemental composition and elemental maps, which will help to understand the chemical composition of tribofilms present on the wear surfaces of the test steel balls.

Figure 5-11 shows the EDS elemental mapping of the worn surface of the test formulation with no soot particles. SEM image clearly shows ZDDP tribofilm patches spread throughout the wear scar. ZDDP forms complex antiwear films of short and long chain polyphosphates co-ordinated by zinc cations and most probably a mixture of zinc and iron cations at the film metal substrate interface. Sulfur species are diminished in the film and exist primarily as sulfate or sulfides. EDS spectra helps to assume the ZDDP tribofilms composed of Zn, P, S, O elements. Zhang et al [157] examined the low load and friction tribofilm formed by ZDDP using XANES and found that predominant cations were of Zn as compared to Fe. However, in this study more amount of Fe is observed. Stron Fe peaks may have been originated from the substrate. As the penetration depth of the electron beam is deeper than the thickness of the tribofilm on the surface, the amount of Fe can be from both the tribofilm and the substrate.
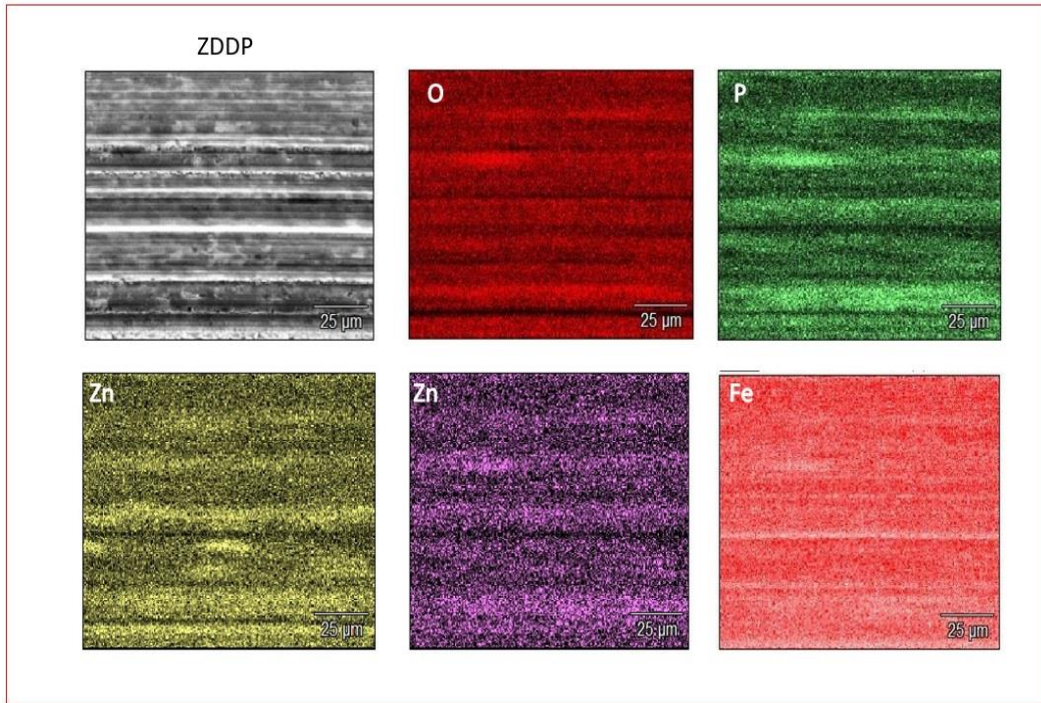
Figure 0-11 EDX Map of test formulation C having 0.07wt% ZDDP.
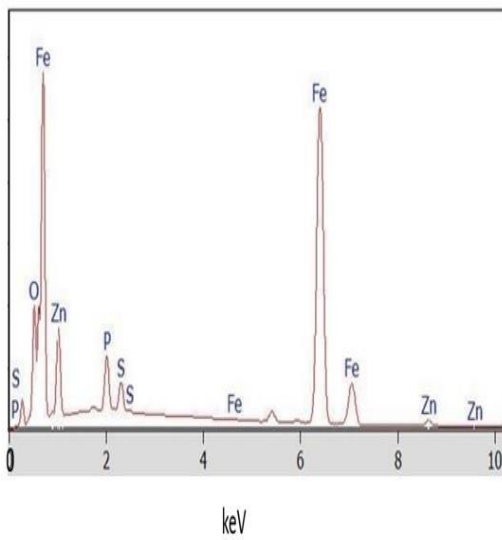
Element	Atomic Weight%
Phosphorous	3.93
Sulphur	2.01
Zinc	3.99

Figure 0-12 EDS Spectrum and concentration table for the test formulation C having 0.07wt% ZDDP

Morphology and chemical composition of the wear scar of the formulation containing ZDDP and
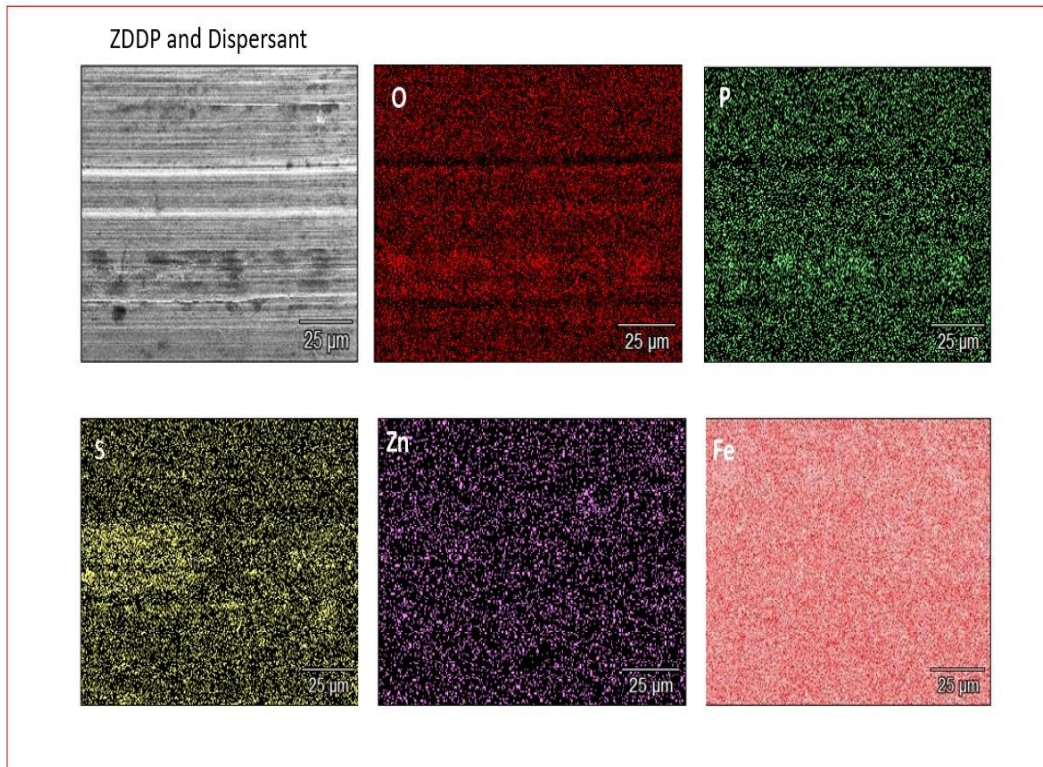
Dispersant is displayed in figure (5-13).

Figure 0-13 EDX Map of test formulation D having 0.07wt% ZDDP and Dispersant.

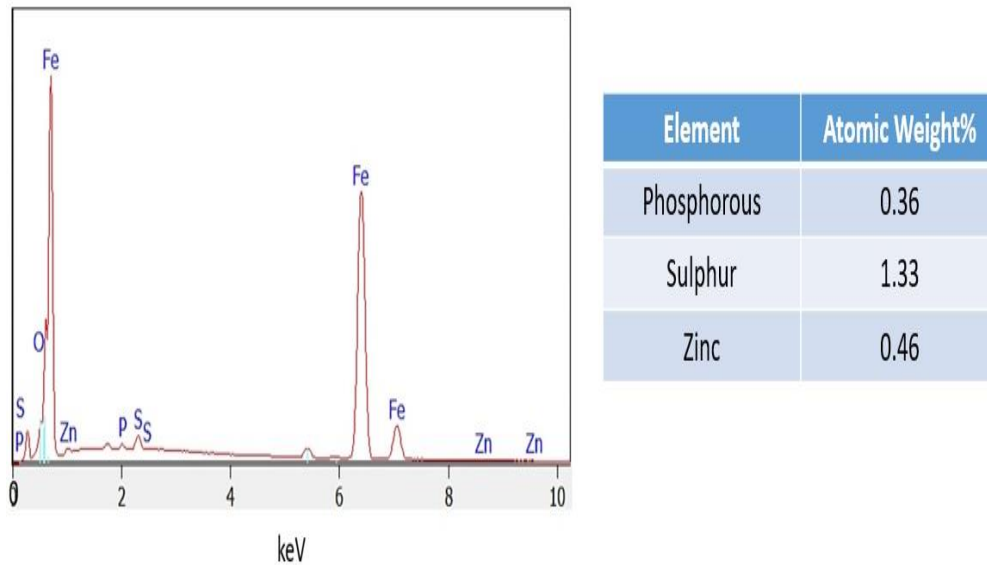| Element	Atomic Weight%
Phosphorous	0.36
Sulphur	1.33
Zinc	0.46

Figure 0-14 EDS Spectrum and concentration table for the test formulation D having 0.07wt%

ZDDP and Dispersant

SEM image shows tribofilm patches. Also, the EDS spectra shows less amount of Phosphorous and Zinc as compared to previous sample. This suggest the added dispersant is having negative effect on the anti-wear performance of ZDDP. Based on this observation, we think that the dispersant is may be interacting with the active antiwear species formed by the initial ZDDP decomposition. This interaction is further hindering the formation of ZDDP tribofilm. This is in agreement with Ratoi et al [184], who reported the rate of reaction film build up by ZDDP. The deleterious effect of dispersant on antiwear additive film formation explains the increase in WSD for sample as shown in figure (5.1).

Figure 5-15 and 5-16 shows SEM-EDS results for test formulation E with ZDDP, Dispersant and 2wt% soot. Corresponding SEM image show high concentration of Sulphur layers above or below the wear track. However, these Sulphur layers are not continuous. By comparing S K map with the Fe K map we can observe, the area of Sulphur layer discontinuation has the presence

of Fe. This indicates the peeling of sulfur based films formed by the decomposition of ZDDP antiwear additive. Diesel engine soot dispersed in this test formulation is proved to be abrasive in nature (as discuused in companion study of this chapter) and may have resulted in removal of tribofilms. This supports the poor tribological performance of formulation E as showed in figure (5-1).
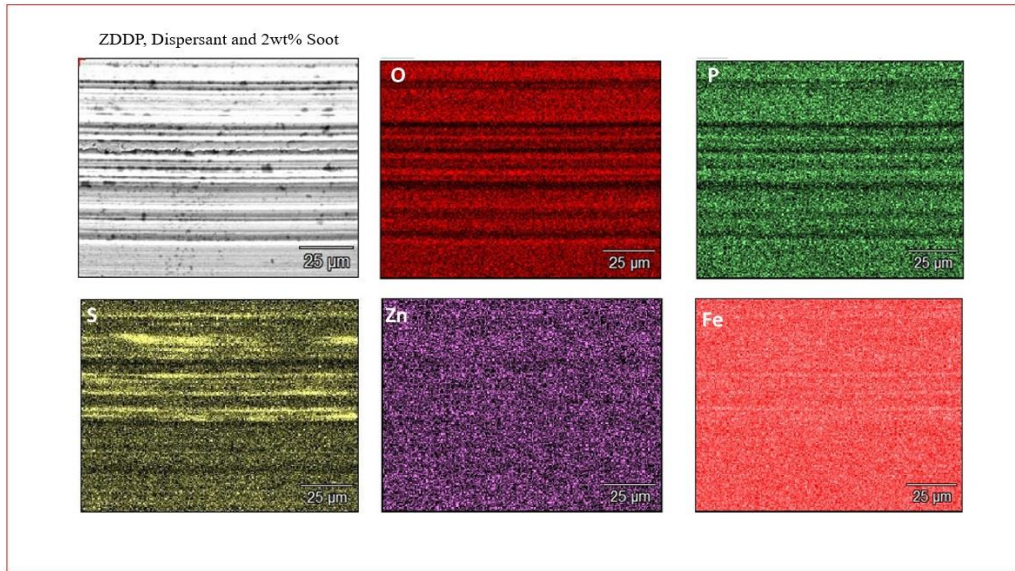
Figure 0-15 EDX Map of test formulation E having ZDDP, Dispersant and 2wt% Soot
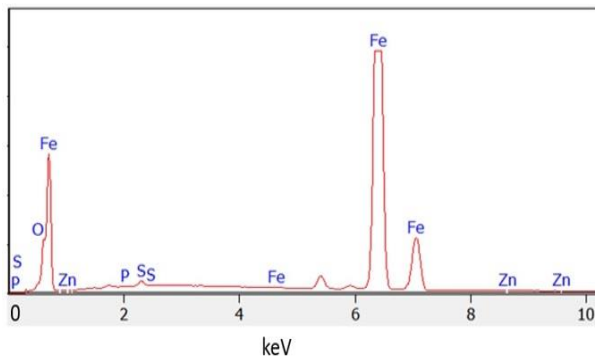
Element	Atomic Weight%
Phosphorous	0.28
Sulphur	0.98
Zinc	0.08

Figure 0-16 EDS Spectrum and concentration table of the test formulation E having ZDDP, Dispersant and 2wt%Soot

SEM-EDS results for sample of formulation F is displayed in figure (5-17). The representative box (A) and (B) on the elemental box is the area under discussion.
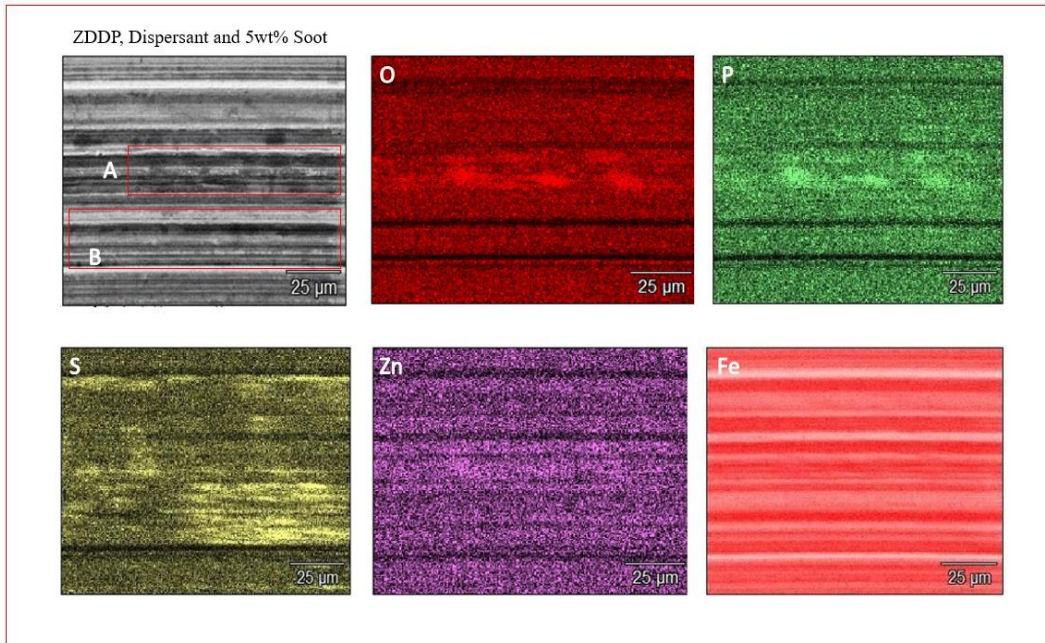
Figure 0-17 EDX Map of test formulation F having ZDDP, Dispersant and 5wt% Soot
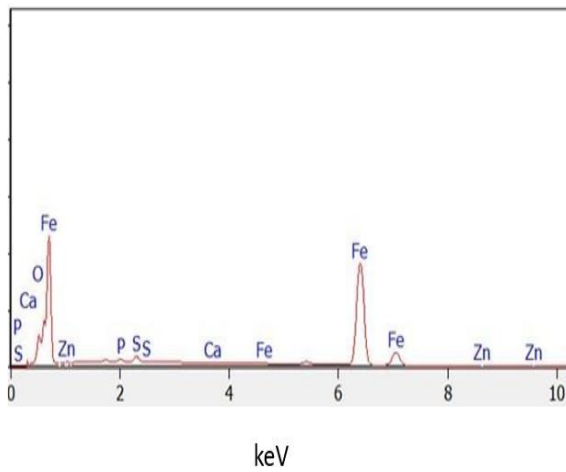
Element	Atomic Weight%
Phosphorous	0.25
Sulphur	0.89
Zinc	0.08

Figure 0-18 EDS Spectrum and concentration table of the test formulation F having ZDDP,

Dispersant and 5wt%Soot

Comparison of O K, P K and Zn K maps area corresponding to the representative box (A) indicate that the films were discontinued at the left corner, middle part and right corner. This hints the presence of zinc polyphosphate films formed by decomposition of ZDDP is removed by soot particles at the areas of the discontinuity. The representative box (B) area corresponding to the S K, Zn K and Fe K elemental maps explains the presence of zinc sulfides/zinc sulfates and iron sulfates/sulfides. Careful observation reveals the removal of sulphur layers at the middle part of the representative box (B). Removal of the tribofilms can be confirmed by comparing elemental composition concentration of the samples of the test formulations E and F. Amount of antiwear tribofilm elements like P, S, Zn, O decreases as the amount of soot dispersed in the formulations E and F increases. This validate the soot induced abrasive wear by removal of tribofilms. EDS elemental maps for the test formulations having 10wt% of soot is shown in figure (5-19).
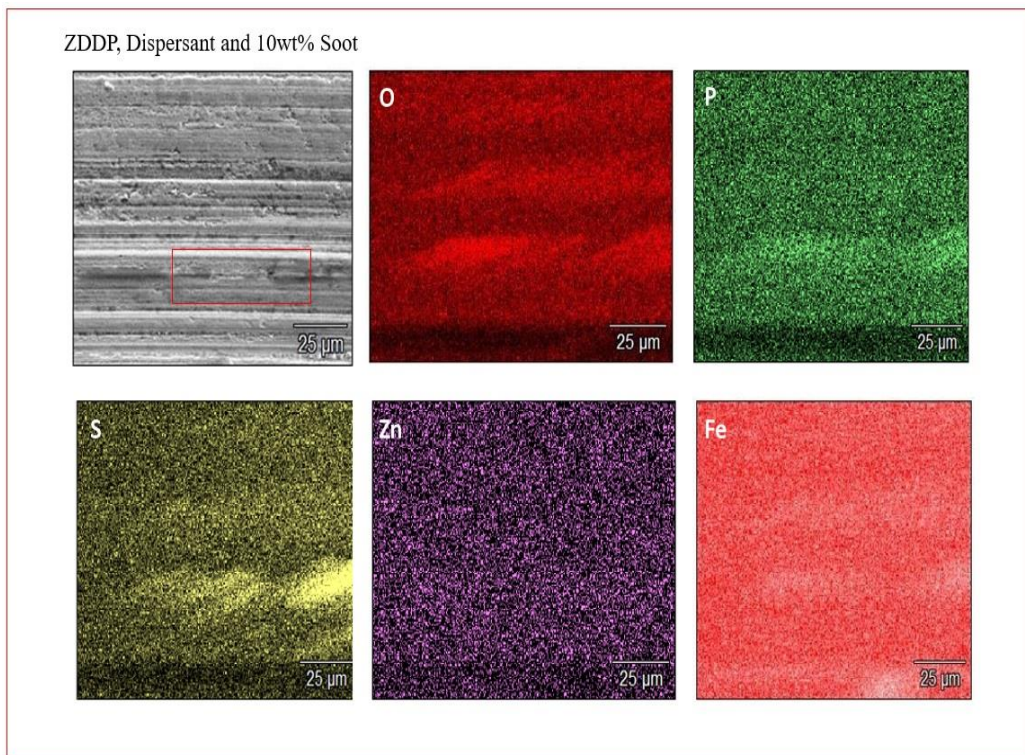
Figure 0-19 EDX Map of test formulation G having ZDDP, Dispersant and 10 wt% Soot

SEM image shows severe abrasive wear track. Tribofilms on the SEM image corresponds to the Fe depletion region. Representative boxes on the SEM image indicates the area of abrasive wear formed by removal of tribofilm. EDS mapping is slightly noisy for this sample because of the weak signal from the antiwear elements present in the tribofilm. Comparison of the marked area on O K, P K, S K, Zn K and Fe K maps show that oxygen, phosphorous and sulfur layers are abraded of the surface.
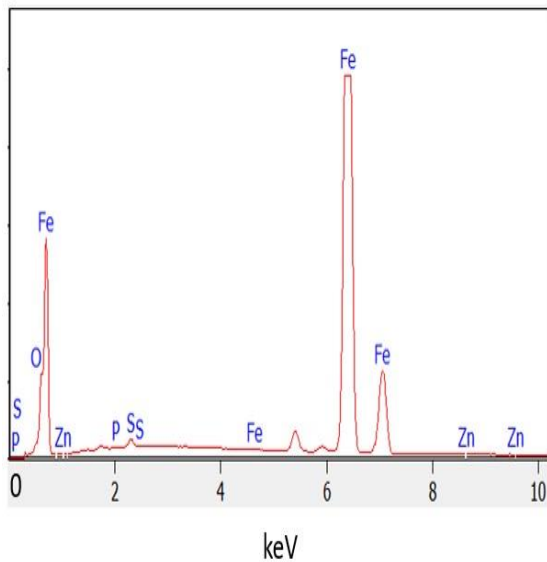
Element	Atomic Weight%
Phosphorous	0.12
Sulphur	0.57
Zinc	0.05

Figure 0-20 EDS Spectrum and concentration table of the test formulation G having ZDDP, Dispersant and 10wt%Soot

Element concentration table indicate great decrease in the P, S, Zn and O concentration as compared to the formulations of E and F. Formulation G has the highest amount of soot dispersed in it. Increased soot results in agglomeration. Large Agglomerates of soot may act as a third body and assist the ongoing wear by rapid removal of protective antiwear films. This rules out the worst tribological performance of the test formulation G among all the ZDDP based oil formulations.

5.3.3.2 Oil formulations with DEDTP

Figure (5-21) is the SEM-EDS result of the test formulation H. Black portions on the SEM image corresponds to the area where tribofilms can be seen. EDS mapping images for this sample are noisy because the tribofilms formed by ionic liquid, DEDTP is not stable. However, the presence of tribofilms can be confirmed by the EDS pectrum analysis. It can be seen that the tribofilm developed by DEDTP consists mainly of phosphorous, sulfur and oxygen. This is in accordance with the study by Sharma et al, who reported that ionic liquid form tribofilms of polyphosphates and sulfates similar to ZDDP. Also, the element concentration table shows the good amount of phosphorous and oxygen element on the wear surface. Phosphorous and oxygen layers provide antiwear protection to the test sample of formulation H. This result assists the better performance of formulation H among all the formulations of DEDTP.
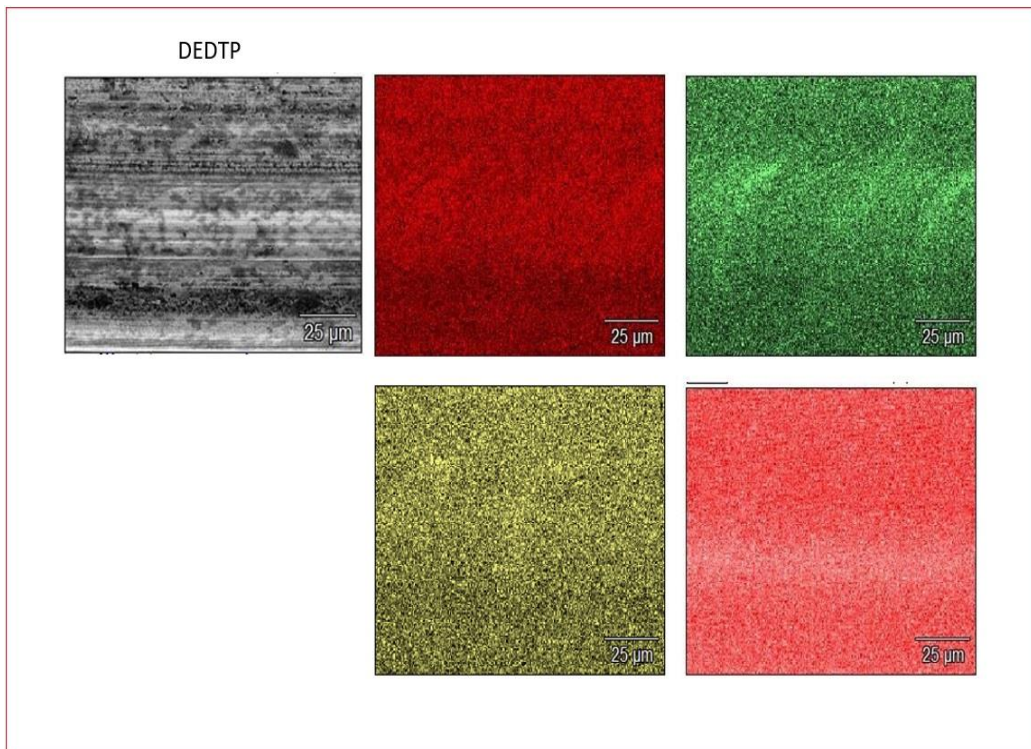
Figure 0-21 EDX Map of test formulation H having DEDTP as antiwear additive.
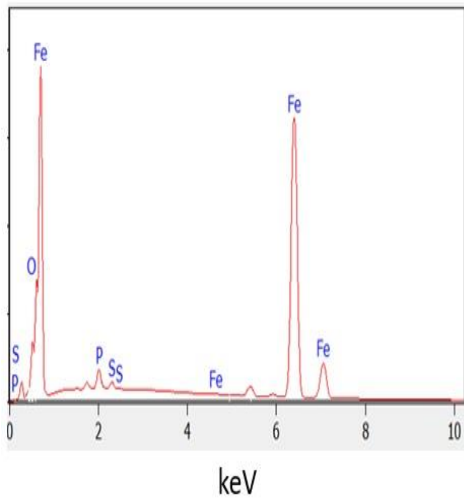
Element	Atomic Weight %
Phosphorous	1.71
Sulphur	0.44

Figure 0-22 EDS Spectrum and concentration table of the test formulation H having DEDTP as

antiwear additive

Figure (5-23) shows the SEM results with its corresponding EDS elemental spectra and mapping for the sample of the test formulation I. Elemental maps and concentration table shows higher amount of oxygen and sulfur. Comparison of this test formulation element concentration with the previous concentration table (5-22) indicates that the addition of dispersant has resulted into decrease of phosphorous element. This decrease in antiwear element lead to increase WSD by 55 µm as shown in figure (5-2). However, addition of dispersant result into increase in WSD by 127 µm. Thus, dispersant have much more adverse effect on ZDDP than DEDTP.
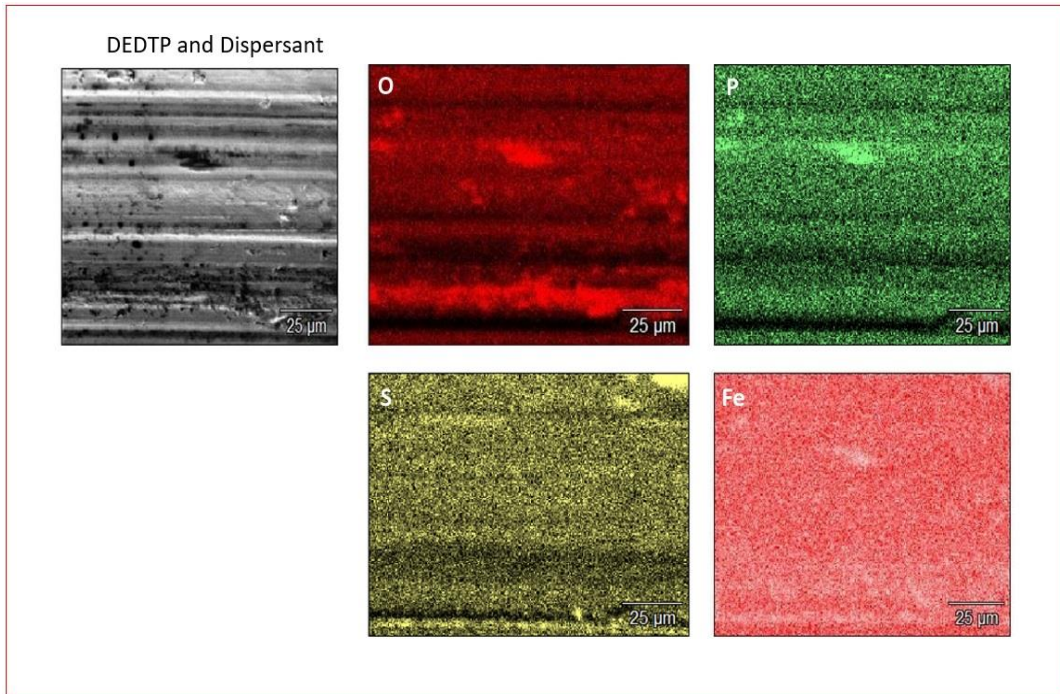
Figure 0-23 EDX Map of test formulation I having DEDTP and Dispersant.
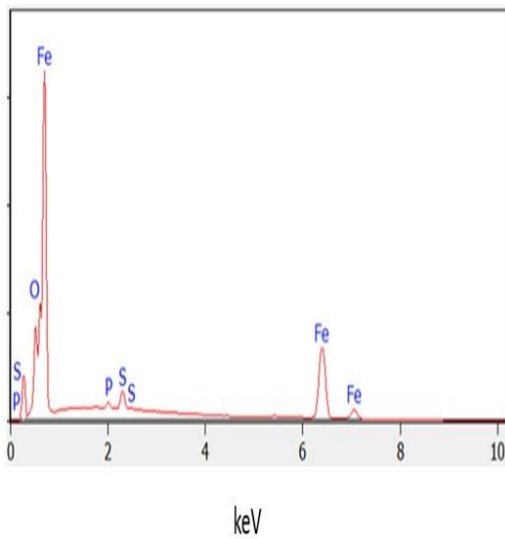
Element	Atomic Weight %
Phosphorous	0.89
Sulphur	3.60

Figure 0-24 EDS Spectrum and concentration table of the test formulation I having DEDTP and

Dispersant

Figure (5-25) shows SEM image of the formulation J test sample with its cooresponding EDX element composition mapping and spectrum. Severe abrasive wear can be seen at the upper left corner of the SEM image.
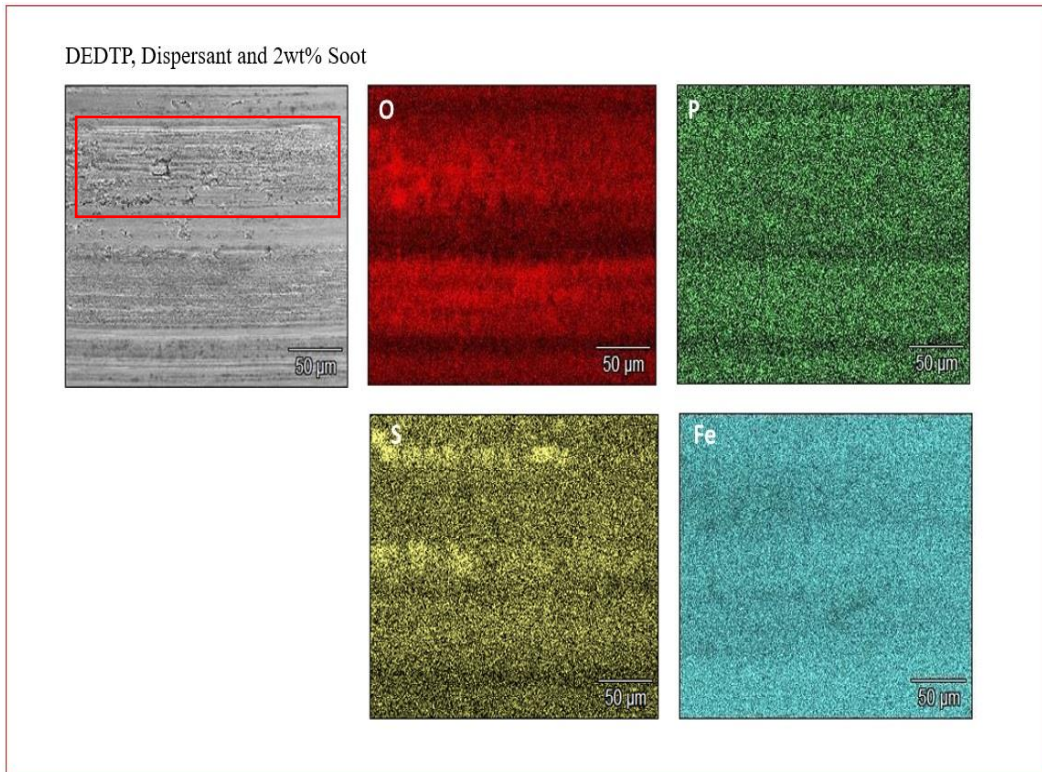
Figure 0-25 EDX Map of test formulation J having DEDTP, Dispersant and 2wt% Soot.
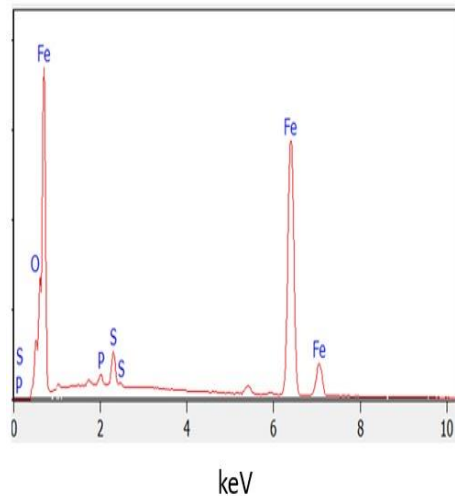
Element	Atomic Weight %
Phosphorous	0.85
Sulphur	3.41

Figure 0-26 EDS Spectrum and concentration table of the test formulation J having DEDTP, Dispersant and 2wt% Soot.

EDS mapping results shows clearly the presence of oxygen and sulfur layers on the wear surface. Careful observation of SEM image with the corresponding O K, S K, Fe K image shows the depletion of tribofilm on the abrasive wear tracks developed in the direction of rotation. Removal of the oxygen and sulfur layers by soot particle can be clearly seen in the right corner of the representative box. Comparison of SEM-EDS results of the test formulation J and I reveal the negative influence of the soot. When soot is absent in the oil, formed wear surface is relatively smooth and well protected by tribofilms. However, addition of only 2wt% of soot resulted in removal of tribofilms and abrasive wear track. Tribofilm removal is also suggested by element concentration table as shown in Figure (5-26). Some amount of sulfur patches is evident from EDS mapping which justifies the mere decrease in WSD by 56 µm as shown in figure (5-2).

Figure (5-27) exhibits the chemical composition of the wear scar developed during four ball tribotest of the test formulation having 5wt% soot dispersed in it. Combined adhesive and abrasive wear mechanism can be implied from the SEM image. EDX map of O K hints the presence

of abrasive iron oxide present on the wear surface. Iron oxides films might act as a sacrificial and provide protection against the abrasive wear. The beneficiary effects of the iron oxide mainly depend on the type of iron oxide compound present on the wear surface. Fe_3O_4 is known to provide protection while FeO and Fe_2O_3 are abrasive in nature and can promote the wear. Some amount of sulfur and phosphorous layers can be seen at the bottom part. This observation suggest that phosphorous and sulfur patches cover the inevitable wear surface asperities and provides relatively smoother surface to slide against the contact area.
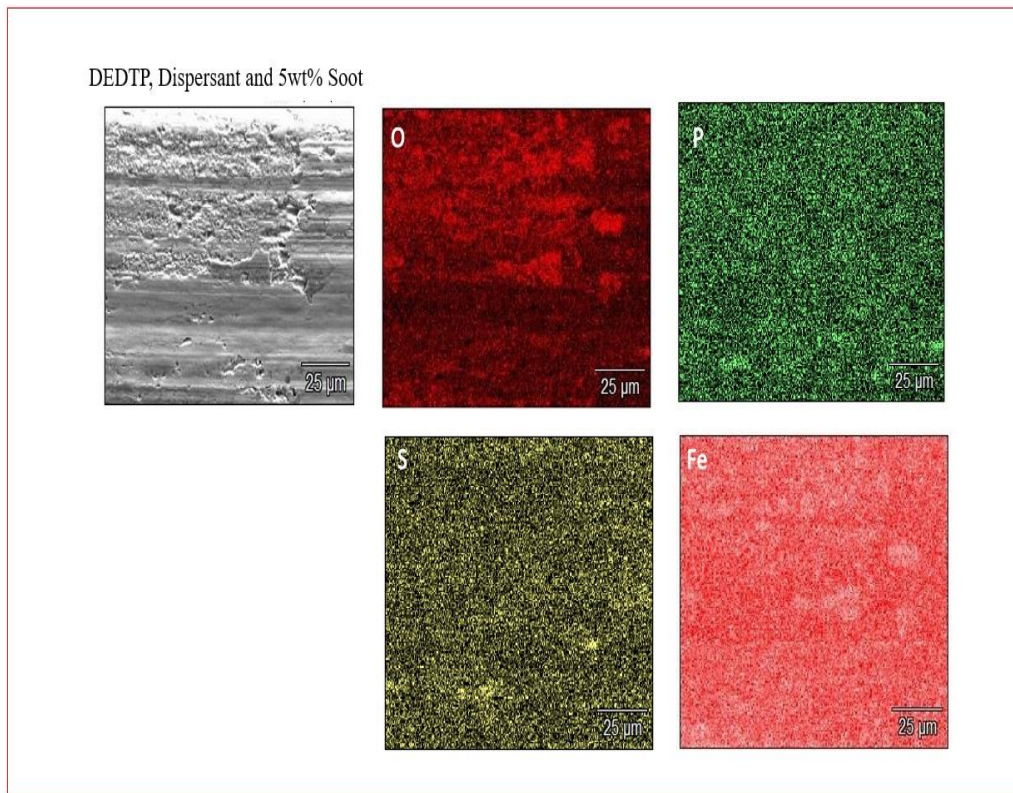
Figure 0-27 EDX Map of test formulation K having DEDTP, Dispersant and 5wt% Soot.

Element	Atomic Weight %
Phosphorous	0.33
Sulphur	0.93
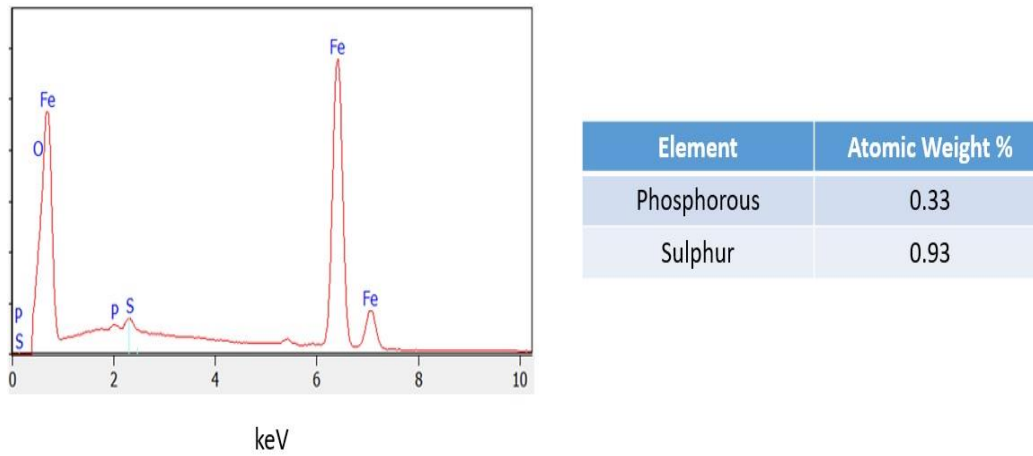
Figure 0-28 EDS Spectrum and concentration table of the test formulation K having DEDTP,

Dispersant and 5wt% Soot.

The element concentration table of the antiwear elements shown in figure (5-28) witness the considerable removal of antiwear tribofilms by soot particle.

Figure (5-29) exhibit SEM-EDS results of the formulation L. SEM image indicate the scratches running in the direction of rotation and abrasive wear track with deeper grooves. Corresponding EDS spectra shows some patchy features of oxygen film in the grooves indicating the formation of abrasive iron oxide. Also, there are low traces of Phosphorous on the wear scar of this sample.
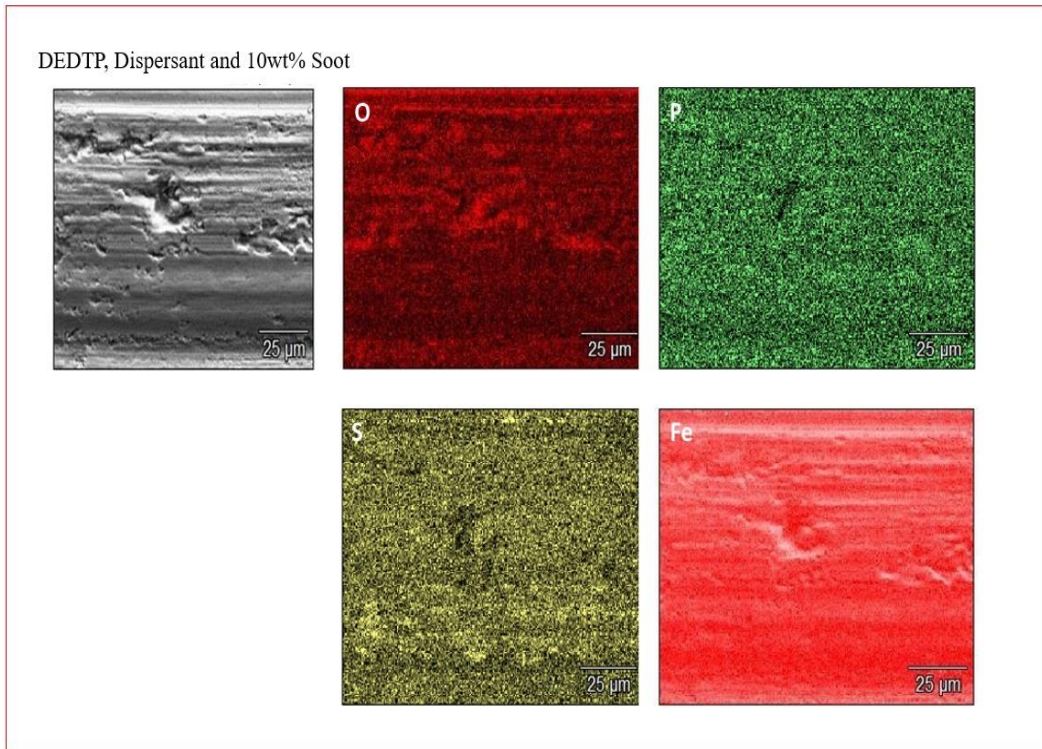
Figure 0-29 EDX Map of test formulation L having DEDTP, Dispersant and 10wt% Soot.
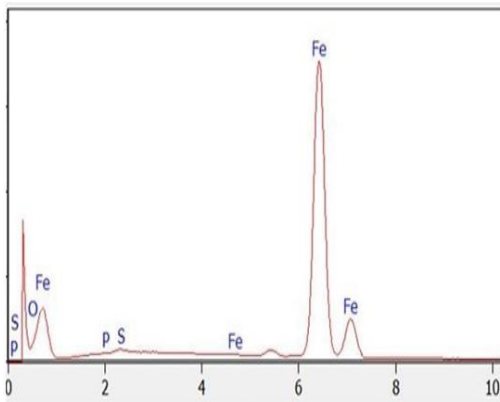
| Element	Atomic Weight %
Phosphorous	0.07
Sulphur	0.90

Figure 0-30 EDS Spectrum and concentration table of the test formulation L having DEDTP,

Dispersant and 10wt% Soot.

Formulation L has the highest amount of soot as compared to the other formulations having DEDTP as antiwear additive. Higher soot content in oil tends to form agglomerates known as sludge. Soot agglomerates results in heavy abrasive wear of the surface and rapid removal of tribofilm. Either it directly abrades the surface or act as a blockage at the surface contact leading to lubrication starvation and severe wear. This helps to understand the large WSD of 1510 µm.

5.3.3.3 Oil formulations with ashless DDP as antiwear additive

EDX elemental composition spectra and mapping for the formulation M with 0.07wt% of DDP is shown in the figure 5-31. Dark patches in the SEM image are the tribofilms evident from the corresponding EDS spectra. EDS maps clearly show the high concentration of oxygen and phosphorous layers formed by decomposition of ashless DDP additive. Kim et al [158,159] studied the wear debris resulting from the ball on cylinder tribotest of the lubricating oil containing DDP. They proposed that DDP wear debris were rich in iron oxides and consist mainly of Fe_3O_4 and some amount of FeO and Fe_2O_3. This supports the presence of high amount of oxygen seen on the O K maps. Formation of iron phosphates is evident from the O K, P K, and Fe K maps.
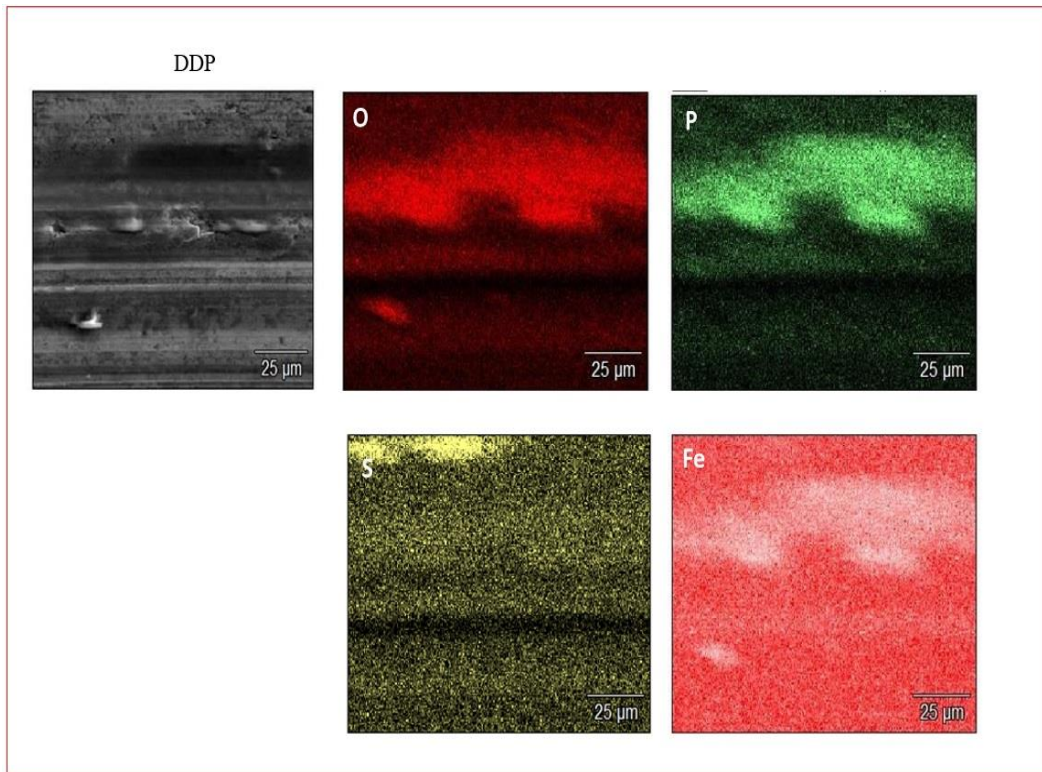
Figure 0-31 EDS Map of test formulation M having DDP as antiwear additive.

EDS mapping displays the continuous and thick tribofilm patch formed by DDP. Comparison of EDS maps of the test formulation C having only ZDDP with these EDS maps signals the strong and thick tribofilm formation of DDP. However, it is important to note that the wear performance of DDP was not better than the ZDDP in this study. It may be because the zinc phosphates, zinc sulfides/sulfates, iron phosphates, iron sulfides/sulfates bolster the ZDDP tribofilm protection while DDP tribofilms consists only of iron phosphates and iron sulfides/sulfates. So, the less amount of tribofilm formation on the surfaces in motion may result in poor wear performance of DDP as compared to ZDDP. This reasoning can also be consolidated from the low magnification SEM image shown in figure (5-8). The image clearly shows one dark big patch developed on the entire wear scar while the SEM image of ZDDP test oil formulation (figure 5-4) displays thin and

continuous patches throughout the wear scar. The antiwear tribofilm formed by DDP on the steel surface leads to the small WSD of 695 µm.
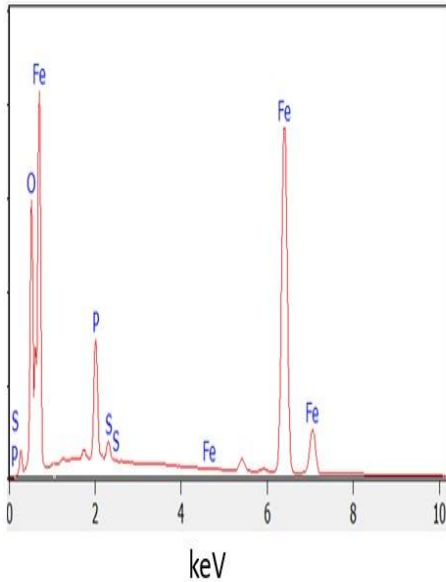
Element	Atomic Weight %
Phosphorous	6.79
Sulphur	0.88

Figure 0-32 EDS Spectrum and concentration table of the test formulation M having DDP.

SEM-EDS data of the test formulation N shows the effect of dispersant on the DDP tribofilm chemical composition. SEM image has the smooth tribofilm patches on the wear surface. EDS O K, P K, S K maps confirm the presence of oxygen, phosphorous and sulfur layers on the wear scar surface. EDS spectrum and composition table (5-32) indicates the high concentration of sulfur. So, he addition of dispersant affects the DDP tribofilm chemistry and results in decrease of Phosphorous concentration and increase of sulfur concentration. Decrease in antiwear element concentration ultimately results in increase of WSD for formulation N. However, WSD is increased by only 17 µm [Figure 5-5]. This may be because of the good antiwear protection of the sulfur films.
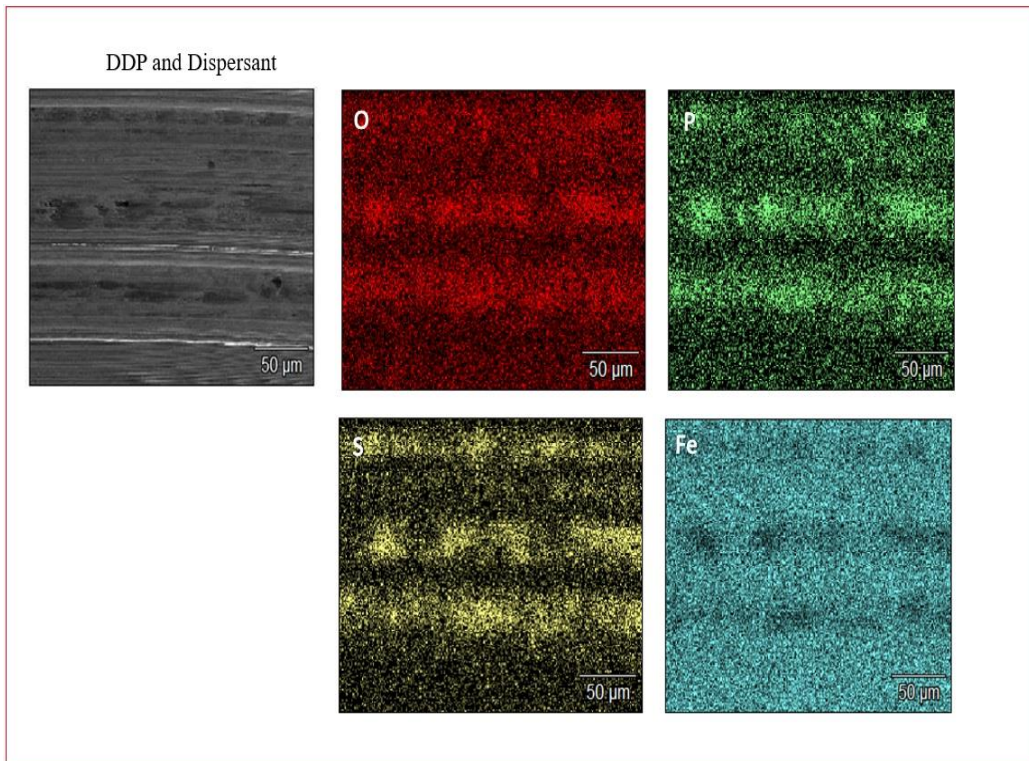
Figure 0-33 EDS Map of test formulation N having DDP and Dispersant.
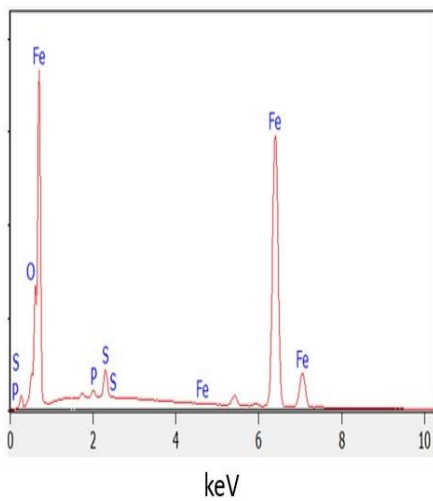
Element	Atomic Weight %
Phosphorous	0.68
Sulphur	2.71

Figure 0-34 EDS Spectrum and concentration table of the test formulation N having DDP and
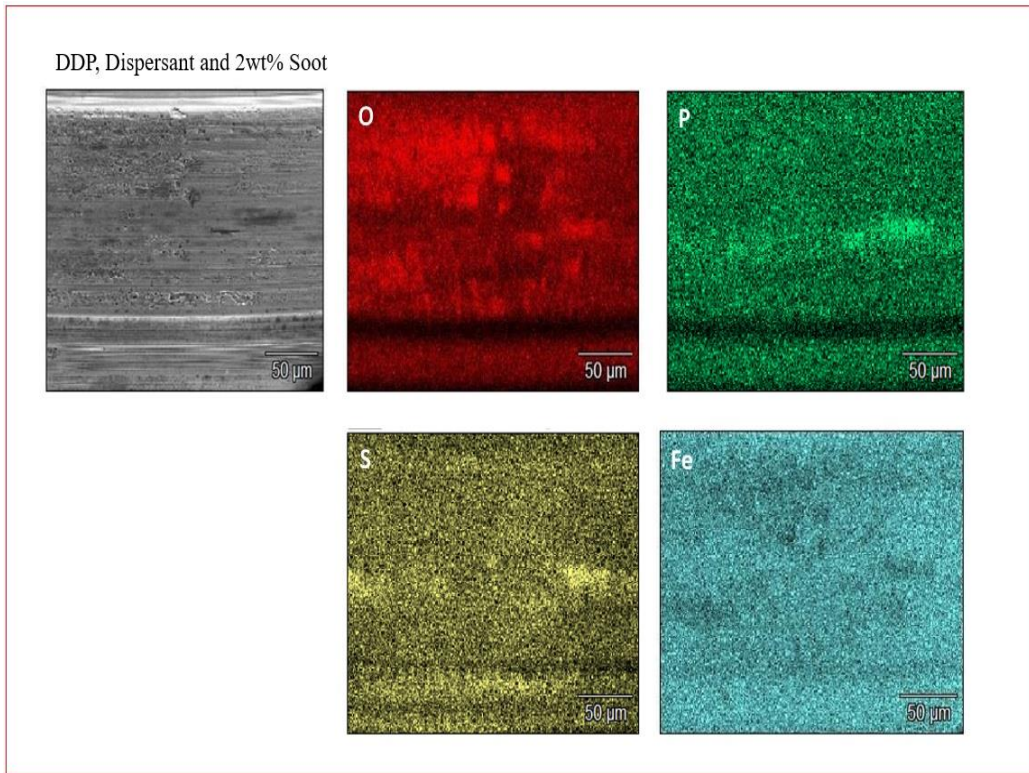
Dispersant.

Figure 0-35 EDS Map of test formulation O having DDP, Dispersant and 2wt% Soot
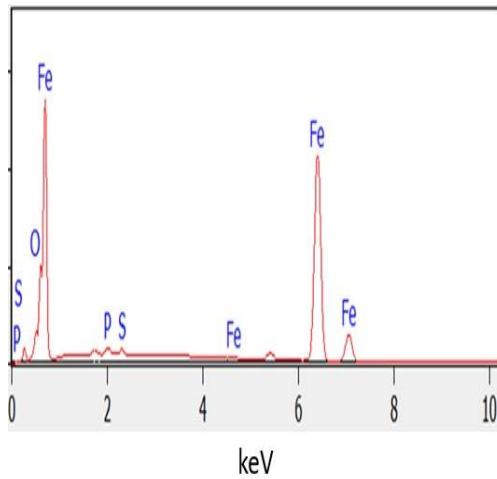
Element	Atomic Weight %
Phosphorous	0.60
Sulphur	0.53

Figure 0-36 EDS Spectrum and concentration table of the test formulation O having DDP,

Dispersant and 2wt% Soot

SEM-EDS results for the formulation O having 2wt% soot illustrates the decrease in antiwear elements comprising DDP tribofilms because of the diesel engine soot and DDP interaction. Combined abrasion and pitting can be seen in the left top corner. Corresponding area in the O K maps exhibits the presence of high amount of oxygen. Smooth surfaces on the SEM image relates to the tribofilm formation of the iron phosphates and iron sulfates/sulfides.
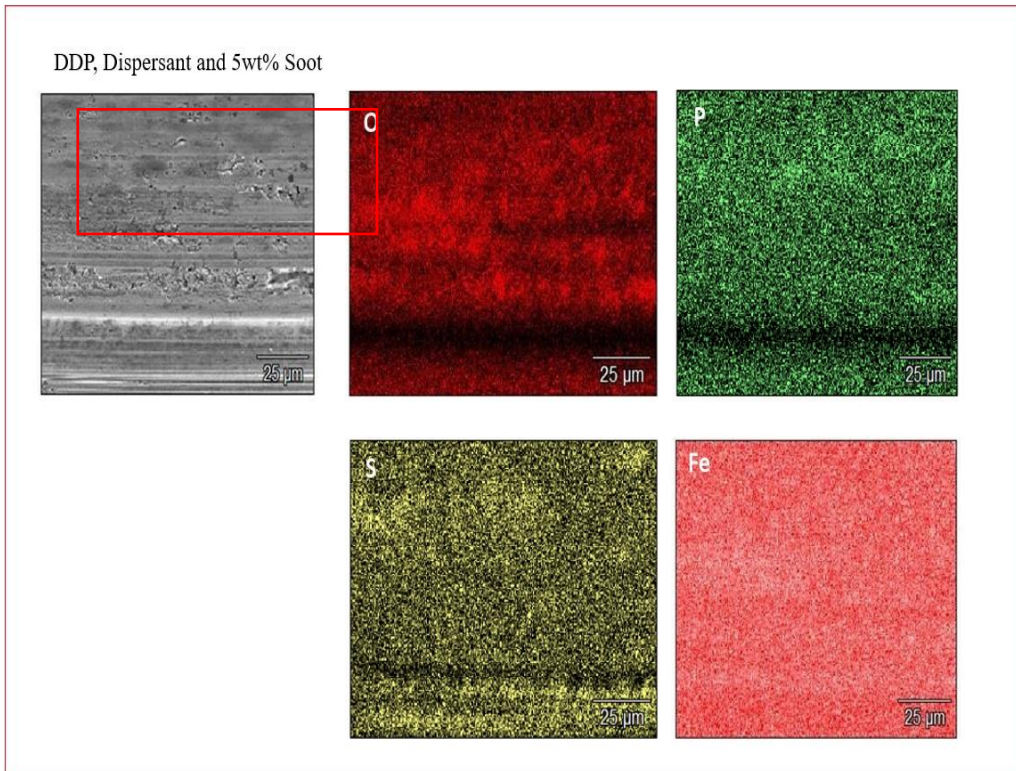
Figure 0-37 EDS Map of test formulation P having DDP, Dispersant and 5wt% Soot
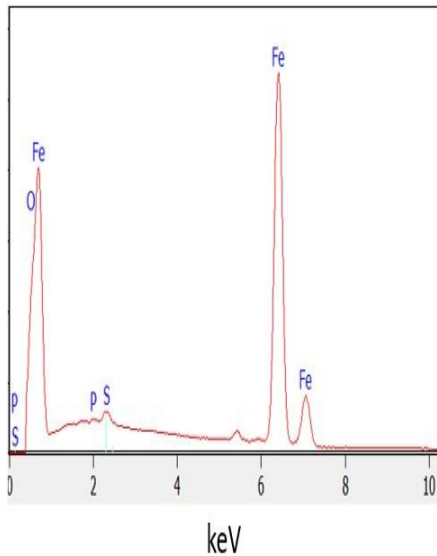
Element	Atomic Weight %
Phosphorus	0.32
Sulfur	0.69

Figure 0-38 EDS Spectrum and concentration table of the test formulation P having DDP,

Dispersant and 5wt% Soot

SEM-EDS results for the test oil formulation having 5wt% of soot is shown in the figure (5-38). It is evident from the SEM image that addition of 5wt% soot results in more severe abrasive wear than 2wt% soot. Representative box marked on the SEM image displays the area of dark tribofilm patches protecting the slight abrasive and pitted wear tracks. Corresponding area on P K and S K maps confirms the formation of iron phosphates and iron sulfates/sulfides formed on the wear tracks. Area below the representative box shows abrasive tracks with the presence of oxides on it. Observed sulfur films are imparting smooth surfaces and protection against the effect of sliding or abrasive action of soot particles.
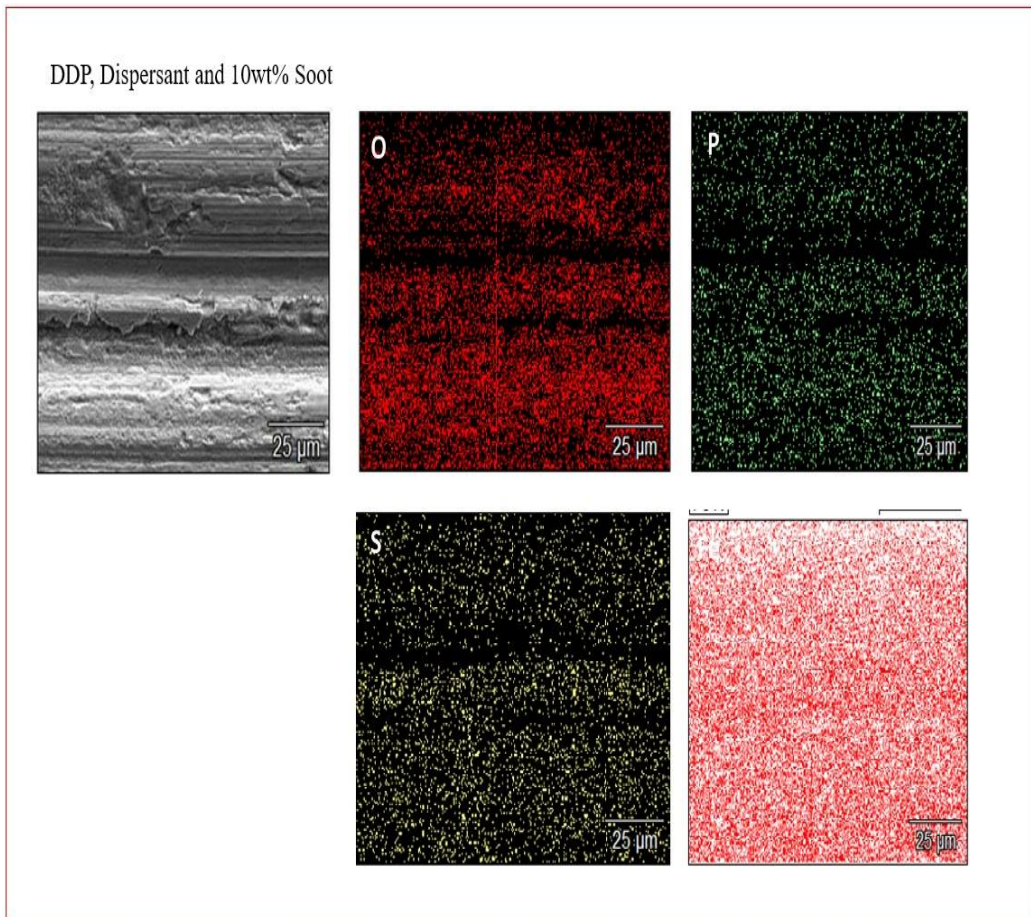
Figure 0-39 EDS Map of test formulation Q having DDP, Dispersant and 10wt% Soot

Figure 5-39 shows the EDS mapping and spectrum results of the wear scar developed for test oil formulation containing 10wt% soot in it. SEM shows the deep ploughing grooves with the severe abrasive wear. EDS mapping and corresponding concentration results clearly indicates the failure of DDP antiwear performance against the effect of 10wt% soot.
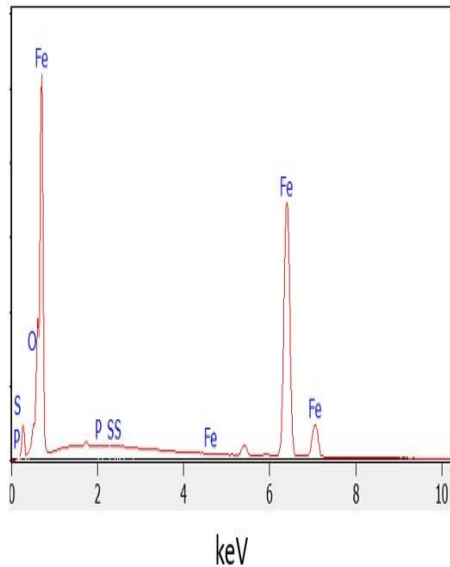
Element	Atomic Weight %
Phosphorus	0.19
Sulfur	0.24

Figure 5-40 EDS Spectrum and concentration table of the test formulation Q having DDP,

Dispersant and 5wt% Soot

5.4 Discussion

5.4.1 Effect of soot concentration on wear

Soot extracted from dynamometer engine test Mack T12 was dispersed in base oil and various formulations were prepared as mentioned in Table (5-3). Figure (5-41) shows the effect of soot concentration on the tribological performance of the test formulation formed with three different anti-wear additives. For all the test formulations WSD was increased with the soot content. Increased soot level of 2 wt% and 5wt% is not affecting the WSD to a greater extent, however, soot level of 10wt% result in significant increase in WSD. This decrement in the anti-wear property can be attributed to the agglomeration phenomenon of the soot particles. Soot particles are attracted to one another by van der Waals forces. They collide and agglomerate to form larger particles. Large soot agglomerates cause the problem of pumpability and lubrication starvation at the tribological contact which leads to the severe wear of engine parts. Gautam et al. [119] study on effect of diesel soot contamination on engine wear using pin on disc tester suggested that soot is abrasive in nature

and increasing soot concentration increased wear. This was also supported by Bardasz et al. [185], who reported that wear in a GM 6.5 L test roller follower was mainly caused by abrasive action of agglomerated soot particles. Sato et al. proposed that, when soot particles aggregate within the lubricant, starvation may occur as the diameter of soot agglomerates is much larger than the oil-film thickness. Green et al. used the reciprocating wear testing designed to replicate an elephant's foot valve train contact and showed that specimen wear increases with increase in carbon black content. He also suggested that the abrasion is the dominant soot related wear mechanism, but, at increased levels of soot content in the lubricant, can result in starvation of the contact and increase wear further [187].
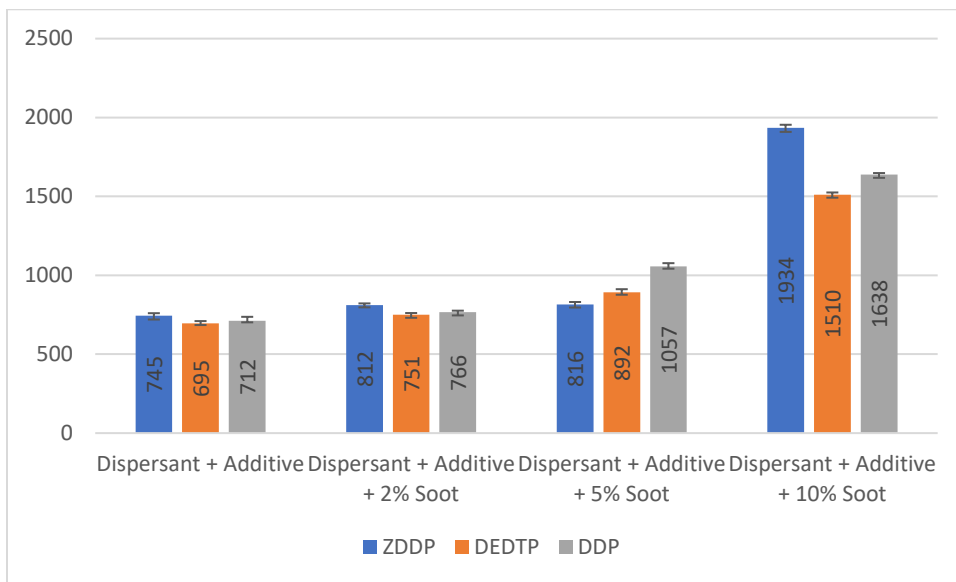
Figure (5-41) Effect of soot concentration on wear

At minimum soot concentration levels (2wt% and 5wt%) soot particles act as a third body. Soot particles trapped between two surfaces results into three body abrasive wear of diesel engine [122]. In three body abrasion, particles are present in the interface between the surfaces, and are either free to slide or roll or embedded in one of the surfaces. In this case, soot particles are acting as a third

body abrasive particles generating local wear to the stationary ball surface by sliding or rolling motion as shown in figure (5-42). Patel et al. [182] examined the dynamometer test Mack T12 soot using XANES and HRTEM coupled with EDX. He suggested that the nano-crystalline particles of Fe_2O_3 and phosphates of Ca gets mechanically embedded at the periphery of turbostatic soot structure. These particles have hardness of 5-6 on Moh's scale and can result in polishing wear of the surface. It can be speculated in that nano-crystalline particles embedded in the extracted soot can act as a third body and contribute to polishing wear. Nano-crystalline particles assisted three body wear may have also resulted in increase of WSD. It is important to note that soot particles do not undergo direct abrasion of the stationary steel ball surface through three body wear mechanism. Soot particles primarily tend to scrape off the tribofilms formed by anti-wear additives on the steel ball surface and further promotes abrasive wear.
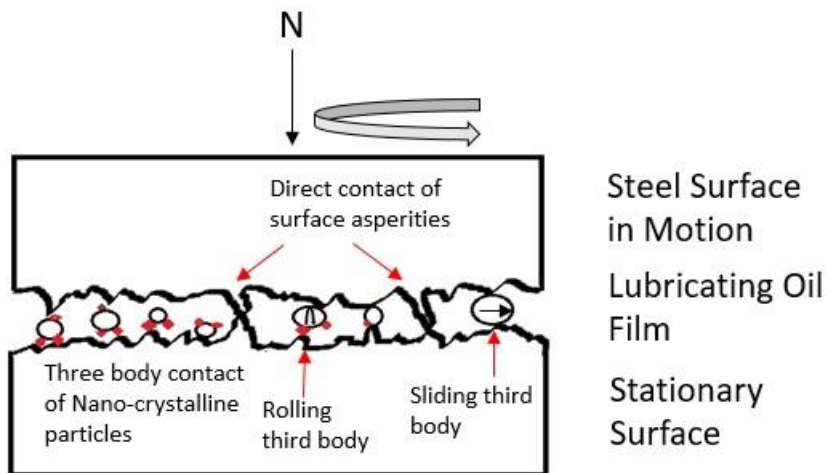
Figure 5-42 Three body wear mechanism taking place at 2wt% and 5wt% soot concentration.

Test formulations having 10 wt% of soot showed sudden increase in the WSD because of the soot agglomeration effect. Soot related agglomeration can indirectly ascribe to the effect of dispersant. The job of the dispersant is to limit the strength of agglomeration of secondary particles and to stabilize the individual primary particle. Increasing soot concentration does not necessarily result in

increase in the wear if discrepancy is maintained in the oil. In this study, discrepancy was effective till soot concentration of 5wt%, however, loss of discrepancy at 10wt% resulted in agglomeration assisted severe wear. Figure (5-43) gives the details of the effect of soot concentration on the wear.
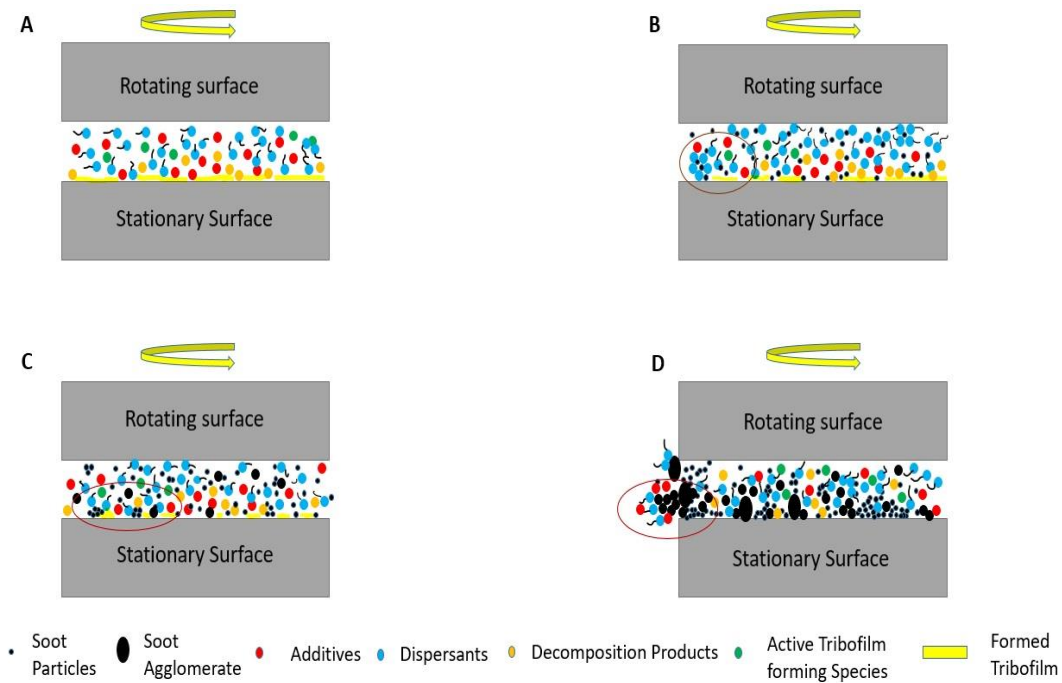
Figure (5-43) Effect of soot concentration (a) No soot (b) 2wt% soot (c) 5wt% soot (d) 10wt% soot

5.4.2 Effect of Dispersant-Additive interaction

Dispersants are added in diesel engine lubricants to improve their soot handling capabilities. Dispersants can interact with the additives present in the oil and affect the anti-wear performance of the lubricating oil. The effect of the dispersant-additive interaction on the wear can be examined from the figure (5-41). Dispersant-additive interaction is explained with the help of Phosphorous concentration ratio calculated from the EDX element composition data. Figure (5-45) shows the Phosphorous concentration for the test formulations developed by adding 0.07 wt% of anti-wear additive and 5 wt% of dispersan. Addition of dispersant in all the test formulation resulted

in decrease of phosphorous concentration. Decrement in the beneficial anti-wear element phosphorus confirms the deleterious effect of dispersant-additive interaction on the wear of steel ball.
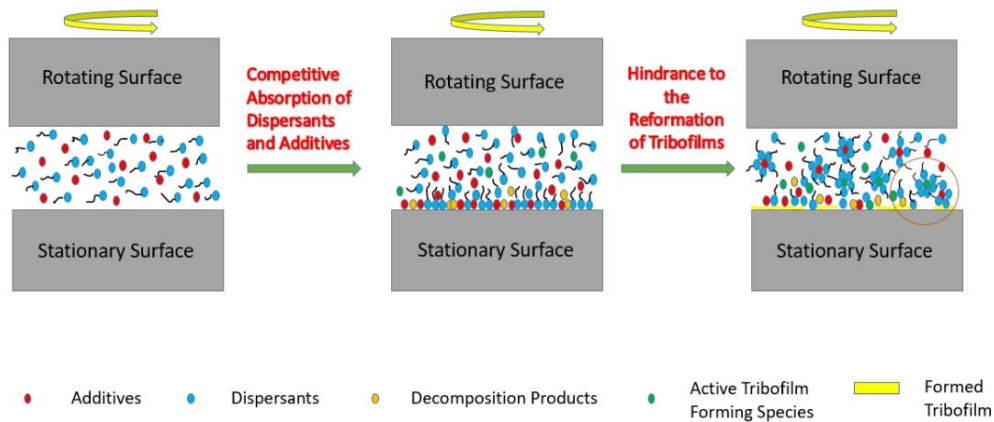
Figure (5-44) Schematic diagram explaining Dispersant-Additive interaction.

Dispersants include polymer backbone component (oleophillic in nature) connected to the polar group. The polar head of the dispersant molecule clings to the particle in the oil directing its tail outwards. Dispersant molecules forms micelle by enveloping the particle and stabilize it in the oil. Figure (5-44) displays the postulated schematic diagram of dispersant-additive interaction. It can be hypothesized that the dispersant molecules can surround the additive particles or active anti-wear film forming element (like Zn cations in ZDDP formulations) and hinders their adsorption on the surface (Shown by marked red circle). Deceleration in the rate of adsorption can affect the tribofilm growth. Also, dispersant can get quickly adsorbed to the surface than the anti-wear additive. Competitive absorption of dispersant and additives may result in reduction of tribofilm formation. This hypothesis is manifested by the findings of Fujita et al. [189] who reported that the dispersant has detrimental effect on formation and removal of ZDDP tribofilms. Also, Yamaguchi et al [190] studied the interaction of dispersant and ZDDP by using pin on disc tribometer and

XANES spectroscopy. They suggested that the presence of dispersants in the oil blend decrease the chain length of polyphosphate in the tribofilms.
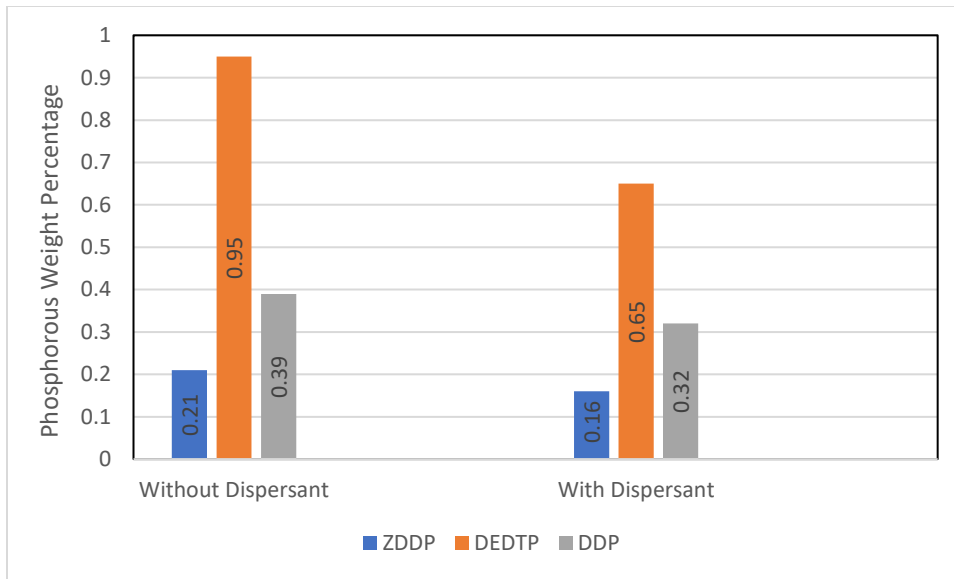
Figure (5-45) Phosphorous Weight Percentage for test formulations without dispersant and with dispersant

5.4.3 Antagonistic behavior of antiwear additives and soot

Figure (5-46) shows the WSD values for the test formulation containing dispersant and 5%soot compared with the test formulation having antiwear additives, dispersant and 5% soot. With soot, it was not possible to study reliably blends without dispersant because of problems in keeping the particles fully suspended. With dispersant and soot test formulation results we can study the effect of interaction between soot and antiwear additive.
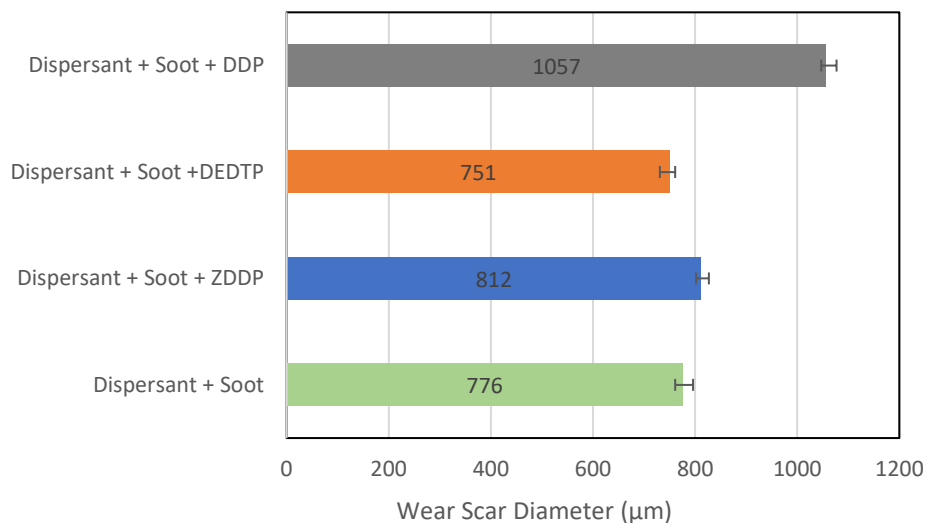
Figure (5-46) WSD comparison of test formulation having soot without antiwear additive and test formulations with antiwear additive having soot

It can be observed from the plotted data in figure (5-48) that soot dispersed in lubricating oil without antiwear additive contributes positively towards tribological performance. This suggests (i) that the soot disrupts to some extent the boundary film formed by the dispersant solution and (ii) the dispersant (or the soot) provides some protection for the surfaces. It can be speculated that the diesel engine soot acts as the third body between the interacting steel ball surfaces. As the hardness of the soot is relatively lesser than the steel substrate, soot particles can't directly abrade the steel ball surface. However, soot particles/soot agglomerates can result in three body polishing wear.

WSD results in figure (5-46) indicates the adverse effect of soot on the antiwear performance of all the additives. EDX and SEM results suggests that the addition of the soot results in very rapid film removal formed by antiwear additives. There are two possible suggestions of this. Either the soot causes direct film removal by mechanical action or the CB

inhibits the continued formation of the tribofilm by adsorbing active film-forming species. This work clearly suggests the direct removal of antiwear tribofilms by the abrasion wear mechanism of the soot particles/agglomerates. Antiwear tribofilms formed by all the additives composed of metal polyphosphate and metal sulfates/sulfides. These films are considered to be less harder than the steel substrate and can get easily removed by abrasive soot particles. Rapid removal of antiwear films can overcome the rate of film formation by antiwear additives and result in high wear of the steel substrate. The rate of wear thus becomes directly dependent on the rate of film formation by antiwear additive.

It is important to note that the combination of soot and antiwear additive result in severe wear than the soot alone. According to the proposed wear mechanism for the soot and antiwear formulation, phosphorus-based tribofilms which are formed on the steel substrate are removed through abrasion by soot particles/agglomerates. Since the formation of the tribofilm involves intermixing of the substrate (Fe) with the additive, the removal of the antiwear films also results in the removal of the substrate. A new tribofilm forms on the newly generated surface and is then removed by soot particles. The rapid tribofilm formation by the additives and removal by soot particles results in severe wear. The mechanism is also explained with the help of phenomenological model as shown in figure (5-47).
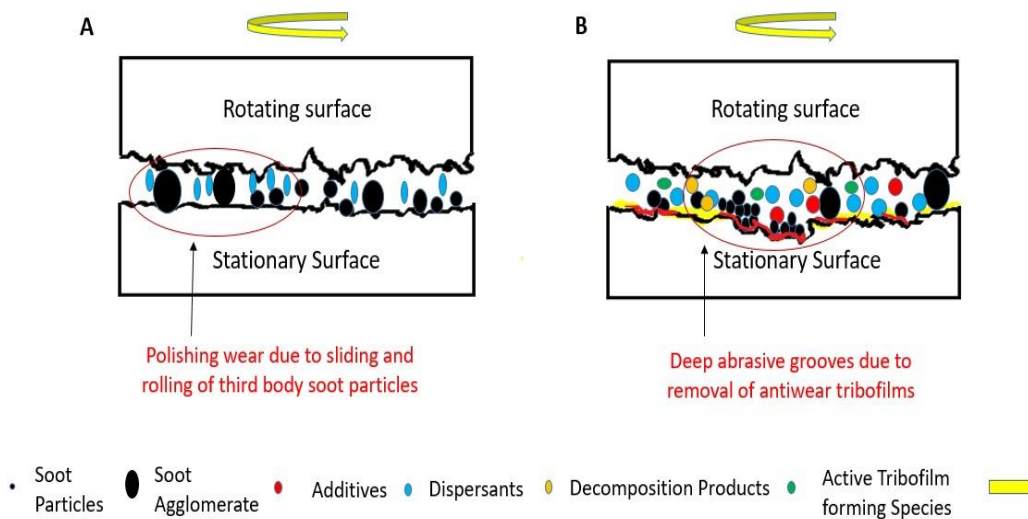
Figure (5-47) Schematic diagram explaining soot induced wear mechanism in the presence of antiwear additive.

Antagonism between ZDDP and soot is proposed by many authors, Beshouri et al refers to soot ''completely disabling'' ZDDP [191]. Recently Booth et al. [192] have also suggested a similar corrosion–abrasion mechanism to that outlined above and identified iron sulphide as the species most likely to be controlling this process. However other work has found that ZDDP plays a strong role in reducing wear of sooted oils and that secondary ZDDP is more effective at this than primary ZDDP. The discrepancy may depend on the differing rubbing conditions. In support to this, Yoshihara found with formulated oils that soot decreased wear in cam lobes but increased it in rocker arm contacts [193].

From Fig. (5-46) it is evident that the antagonism between soot and antiwear additives is a universal one. In all cases the combination of antiwear additive and soot gave more wear than antiwear additive without soot or soot without antiwear additive. This helps support the proposed abrasion mechanism, as opposed to there being some specific chemical interaction between soot and the ZDDP tribofilm. Figure (5-46) also shows that the deleterious effect of soot is much greater with

the ZDDP than the other ashless antiwear additives. Initially, the wear performance of ZDDP is almost comparable with ashless additives. However, increase in soot content results in increase in degradation of antiwear property of all the three additives. ZDDP showed the worst performance as compared to ashless dialkyl dithiophosphate and phosphonium based ionic liquid. There are two possible interpretation for the ZDDP behavior, one is that the interaction of dispersant and soot with the ZDDP film forming active species like Zn^{+2} may cause hindrance to the adsorption of active species onto the metallic surface ultimately resulting in the slow rate of tribofilm formation. Second interpretation is that the dispersant molecule and soot particles may result in faster adsorption on the metallic surface than the decomposition products / active species of ZDDP, minimizing the rate of film formation. In the case of ashless antiwear additives, the active metal cation species contributing to continuous film formation is Fe from the Fe_2O_3 which is present on the abrasive wear track of the steel substrate. Finally, it should be noted that the essential observation of this study, that the combination of soot and antiwear additives gives much more wear than soot in the absence of antiwear additive. Antagonistic effect is not specific to ZDDP, it is common to all the antiwear additives used in this study. This confirms removal of the antiwear film by soot as the most likely mechanism by which the presence of soot in engine oil promotes high wear.

5.5 Conclusion

This study was mainly focused on understanding the mechanism by which abrasive soot promotes high wear in boundary lubrication conditions. The results of this study suggested that the direct rubbing action of abrasive soot particles doesn't result in severe wear. Author believe that the antagonistic behavior of soot present with phosphorous containing antiwear additives enhances the wear of steel substrate i.e blends containing both antiwear additives and soot give much higher wear than ones containing antiwear additives without soot or soot without antiwear additives. The

240

proposed wear mechanism is the abrasion wear due to rapid removal of the protective antiwear tribofilms by the abrasive soot particles/agglomerates.

XANES, HR-TEM and HR-XRD characterization helped to understand the effect of lubricant additive interaction and the soot during actual operation field condition was examined for soot extracted from dynamometer engine test MackT12. XANES analysis showed the presence of zinc polyphosphate, calcium sulfate and phosphate, and iron sulfate and phosphate. Identification of short chain zin polyphosphate suggested the interaction of soot with the ZDDP decomposed byproduct antiwear tribofilm. HR-TEM image and its associated EDS spectra showed the nano crystalline particles originated from lubricant additive chemistry embedded in the periphery of the turbostratic carbon structure of the soot. HR-XRD results supported the existence of nano crystalline particles embedded in the soot structure and also reveals that the presence of these particles results in disordering of the turbostratic structure of carbon and affects the oxidation stability of the soot particle. It was concluded that the mechanical embedment of the nano crystalline particles during the three body contact of soot particles in the crankcase oil affects its structure and make it more abrasive in nature. This study also help to understand the detrimental effect of increased soot levels in the lubricating oil on the enhancement of the engine wear. Amount of soot concentration dispersed in engine oil showed a linear relationship with the wear scar diameter i.e on the degradation of antiwear performance of engine oil. In addition to this potential of novel ashless antiwear additives to alleviate the adverse effect of soot on engine wear was examined using standard four ball tribometer. ZDDP showed worst performance at higher level of soot while ionic liquid exhibited better anti-wear performance. This study helped to evaluate the capability of ashless additives to serve as a improving additive for in-service and used fully formulated diesel engine lubricants.

References

[1] Bhushan B Modern tribology handbook. CRC Press 2001: Boca Raton, FL, London 2.

[2] Rudnick LR. Synthetics, mineral oils, and bio-based lubricants: chemistry and technology.: CRC, 2005.

[3] Minami I. Ionic liquids in tribology. Molecules 2009;14:2286-305

[4] Qu J, Luo H, Chi M, Ma C, Blau PJ, Dai S. Comparison of an oil-miscible ionic liquid and ZDDP as a lubricant anti-wear additive. Tribol Int 2014;71:88-97.

[5] Totolin V, Minami I, Gabler C, Dörr N. Halogen-free borate ionic liquids as novel lubricants for tribological applications. Tribol Int 2013;67:191-8.

[6] Sharma V, Gabler C, Doerr N, Aswath PB. Mechanism of tribofilm formation with P and S containing ionic liquids. Tribol Int 2015;92:353-64.

[7] J. Qu, P.J. Blau, S. Dai, H.M. Luo, H.M. Meyer III, J.J. Truhan, Tribological characteristics of aluminum alloys sliding against steel lubricated by ammo- nium and imidazolium ionic liquids, Wear 267 (2009) 1226–1231.

[8] C.M. Jin, C.F. Ye, B.S. Phillips, J.S. Zabinski, X.Q. Liu, W.M. Liu, J.M. Shreeve, Polyethylene glycol functionalized dicationic ionic liquids with alkyl or polyfluoroalkyl substituents as high temperature lubricants, Journal of Materials Chemistry 16 (2006) 1529–1535.

[9] K.F. Ma, B.S. Somashekhar, G.A.N. Gowda, C.L. Khetrapal, R.G. Weiss, Induced amphotropic and thermotropic ionic liquid crystallinity in phosphonium halides: ''Lubrication'' by hydroxyl groups, Langmuir 24 (2008) 2746–2758.

[10] J. Qu, J.J. Truhan, S. Dai, H.M. Luo, P.J. Blau, Lubricants or lubricant additives composed of ionic liquids containing ammonium cations, U.S. Patent #7,754,664, 2010.

[11] J. Qu, M.F. Chi, H.M. Meyer III, P.J. Blau, S. Dai, H.M. Luo, Nanostructure and composition of tribo-boundary films formed in ionic liquid lubrication, Tribology Letters 43 (2011) 205–211.

[12] Sharma V, Christoph G, Doerr N, Aswath P. Mechanism of tribofilm formation with P and S containing ionic liquids. Tribology international 2015;92:360:364.

[13] M. Zhu, Y.F. Mo, W.J. Zhao, M.W. Bai, Micro/macrotribological properties of several nano-scale ionic liquid films on modified silicon wafers, Surface and Interface Analysis 41 (2009) 205–210.

[14] B.G. Wang, X.B. Wang, W.J. Lou, J.C. Hao, Rheological and Tribological Properties of Ionic liquid-Based Nanofluids Containing Functionalized Multi-Walled Carbon Nanotubes, Journal of Physical Chemistry C 114 (2010) 8749–8754.

[15] Shubrajit Bhaumik*, S.Prabhu, VarunKarpurapu and Nihit Uppala. Extreme pressure property of carbon nanotube (CNTs) based nanolubricant. Journal of chemical engineering and material science 2013;4:123-127.

[16] Fukushima T, Aida T. Ionic liquids form soft functional materials with carbon nanotubes. Chem-Eur J 2007;13:5048–58.

[17] Fukushima T, Kosaka A, Ishimura Y, Yamamoto T, Takigawa T, Aida IshiiN, et al. Molecular ordering of organic molten salts triggered by single-walled carbon nanotubes. Science 2003;300:2072–4.

[18] Yu B, Liu Z, Zhou F, Liu W, Liang Y. A novel lubricant additive based on carbon nanotubes for ionic liquids. Mater Lett 2008;62:2967–2969.

[19] Wang B, Wang X, Lou W, Hao J. Rheological and tribological properties of ionic liquid-based nanofluids containing functionalized multi-walled carbon nanotubes. J Phys Chem C 2010;114:8749–54.

[20] Chang-Gun Lee, Yu-Jin Hwang, Young-Min Choi, Jae-Keun Lee, Cheol Choi and Je-Myung Oh. A study on the tribological characteristics of graphite nano lubricants. International journal of precision engineering and manufacturing 2009;10:85-90.

[21] J. Gansheimer, R. Holinski, Molybdenum disulfide in oils and greases under boundary conditions, ASME J. Lubric. Technol. 95 (1973)242–248.

[22] Hengzhou Wo, Kunhong Hu, Xianguo Hu, Tribological properties of MoS_2 nanoparticles as additive in a machine oil, Tribology 24 (1) (2004)33–37.

[23] Savage,R,H, Graphite lubrication, Journal of applied physics, 19 (1),1948,1-10.

[24] Bowden, F,P, Tabor, D., The friction and lubrication of solids, Claredon Press, Oxford,1950.

[25] www.substech.com

[26] Yu MF, Files BS, Arepalli S, Ruoff RS. Tensile loading of ropes of single wall carbon nanotubes and their mechanical properties. Phys Rev Lette 2000 Jun 12;84(24):5552-5

[27] Rabinowicz, E., Friction and wear of materials. Vol. 2. 1965: Wiley New York.

[28] Woldman M. An experimental and theoretical investigation into three-body abrasive wear. 2014.

[29] P Suh, N., The delamination theory of wear. Wear, 1973. 25(1): p. 111-124.

[30] Dowson, D., A generalized Reynolds equation for fluid-film lubrication. International Journal of Mechanical Sciences, 1962. 4(2): p. 159-170.

[31] Christensen, H., A theory of mixed lubrication. Proceedings of the Institution of Mechanical Engineers, 1972. 186(1): p. 421-430.

[32] Blok, H., Fundamental mechanical aspects of boundary lubrication. SAE Journal, 1940(2). 46. Lindsay, N., et al., Characterization of films formed at a lubricated cam/tappet contact. Spectrochimica Acta Part A: Molecular Spectroscopy, 1993. 49(13): p. 2057-2070

[33] Woydt M, Wäsche R. The history of the Stribeck curve and ball bearing steels: The role of Adolf Martens. Wear 2010;268:1542-6.

[34] Zhang, Y., Boundary lubrication—An important lubrication in the following time. Journal of Molecular Liquids, 2006. 128(1–3): p. 56-59.

[35] Zhang Y, Hu T, Ning X, and Ding Q. Advanced Nanomaterials and Nanostructures for Tribological Applications. Journal of nanomaterials 2014;2.

[36] Great Britain. Dept. of Education. Lubrication (tribology), education and research: a report on the present position and industry's needs: HM Stationery Off., 1966.

[37] www.cefic.org/Nano-Fact-Sheet-Multiwalled-carbon-nanotubes.

[38] www.cefic.org/application-benefits-nanotubes.

[39] Chang-Gun Lee, Yu-Jin Hwang, Young-Min Choi, Jae-Keun Lee, Cheol Choi and Je-Myung Oh. A Study on The Tribological Characteristics of Graphite Nano Lubricants. International journal of engineering and manufacturing 2009;10:85-90.

[40] Liu, G., Li, X., Qin, B. et al. Investigation of the mending effect and mechanism of copper nano-particles on a tribologically stressed surfaceTribology Letters 2004;17: 961.

[41] A. Hernández Battez, R. González, J.L. Viesca, J.E. Fernández, J.M. Díaz Fernández, A. Machado, R. Chou, J. Riba, CuO, ZrO2 and ZnO nanoparticles as antiwear additive in oil lubricants. Wear 2008;265, 422-428.

[42] A. Hernandez Battez, J.E. Fernandez Rico, A. Navas Arias, J.L. Viesca Rodriguez, R. Chou Rodriguez, J.M. Diaz Fernandez. The tribological behaviour of ZnO nanoparticles as an additive to PAO6, Wear 2006;261:256-263.

[43] Shuang Chen, Weimin Liu, Laigui Yu. Preparation of DDP-coated PbS nanoparticles and investigation of the

antiwear ability of the prepared nanoparticles as additive in liquid paraffin. Wear 1998;218:153-158.

[44] L Rapoport, Y Feldman, M Homyonfer, H Cohen, J Sloan, J.L Hutchison, R Tenne, Inorganic fullerene-like material as additives to lubricants: structure–function relationship, Wear 1999;225–229:975-982.

[45] Z.S. Hu, J.X. Dong Study on antiwear and reducing friction additive of nanometer Titanium borate. Wear 1998;216:87-91.

[46] H.D. Huang, J.P. Tu, L.P. Gan, C.Z. Li, An investigation on tribological properties of graphite nanosheets as oil additive, Wear 2006;261:140-144.

[47] Zhang Z, Simionesie D and Schaschke C. Graphite and Hybrid nanomaterials as lubricant additives, Lubricants 2014;2:44-65.

[48] Mistry, K.; Fox, M.F.; Priest, M. Lubrication of an electroplated nickel matrix silicon carbide coated eutectic aluminium-silicon alloy automotive cylinder bore with an ionic liquid as a lubricant additive. Proc. Inst. Mech. Eng. J: J. Eng. Tribol. 2009, *223*, 563–569.

[49] E. Fernández Rico, I. Minondo, D. García Cuervo, The effectiveness of PTFE nanoparticle powder as an EP additive to mineral base oils, Wear 2007; 262:1399-1406.

[50] Zefu Zhang *, Laigui Yu, Weimin Liu, Qunji Xue. The effect of LaF3 nanocluster modified with succinimide on the lubricating performance of liquid paraffin for steel-on-steel system. Tribology international 2001;34:83-88.

[51] Kobayashi K et al. Additive effect of carbon nanohorn on grease lubrication properties. Journal of japan petroleum institute 2005;48:121-126.

[52] Cursaru D, Andronescu C, Pirvu C, Ripeanu R. The efficiency of Co-based single-wall carbon nanotubes (SWNTs) as an AW/EP additive for mineral base oils, Wear 2012;290–291:133-139.

[53] Mohammed A, Osman T, Khatab A, Zaki M.Tribological Behavior of Carbon Nanotubes as an Additive on Lithium Grease. Journal of Tribology 2015;137

[54] Available: http://www.epc.shell.com/Docs/GPCDOC_GTDS_Shell_Rotella_T5_15W-40_(CJ-4)_(en)_TDS.

[55] Bartz W. Solid Lubrication additives-effect of concentration and other additives on anti-wear performance. Wear 1971;17:421-432.

[56] Chinas-Castillo, F. and Spikes, H., "Mechanism of Action of Colloidal Solid Dispersions," Transactions of the ASME, Vol. 125, No. 3, pp. 552-557, 2003.

[57] Qiu, S., Dong, J. and Chen, G., "Tribological properties of CeF3 nanoparticles as additives in lubrication oils," Wear, Vol. 230, No.1, pp. 35-38, 1999.

[58] Rudnick LR. Lubricant additives: chemistry and applications: CRC, 2009.

[59] W. Liu, C. Ye, Q. Gong, H. Wang, P. Wang, Tribological performance of room temperature ionic liquids as lubricant, Tribol. Lett. 13 (2002) 81–85.

[60] Qiming Lu, Haizhong Wang, Chengfeng Ye, Weimin Liu _, Qunji Xue. Room temperature ionic liquid 1-ethyl-3-hexylimidazoliumbis(trifluoromethylsulfonyl)-imide as lubricant for steel–steel contact. Tribology international 2004;37:547-552.

[61] A.E. Jiménez, M.D. Bermúdez, F.J. Carrión, G. Martínez-Nicolás, Room temperature ionic liquids as lubricant additives in steel–aluminium contacts: Influence of sliding velocity, normal load and temperature, Wear 2006;261:347-359.

[62] Meirong Cai , Zhu Zhao, Yongmin Liang , Feng Zhou, Weimin Liu. Alkyl Imidazolium Ionic Liquids as Friction Reduction and Anti-Wear Additive in Polyurea Grease for Steel/Steel Contacts. Tribology Letters 2010;40:215-224.

[63] Anthony E. Somers 1, Patrick C. Howlett 1, Douglas R. MacFarlane 2 and Maria Forsyth. A Review of Ionic Liquid Lubricants. Lubricants 2013;1:3-21.

[64] Itoh, T.; Watanabe, N.; Inada, K.; Ishioka, A.; Hayase, S.; Kawatsura, M.; I.Minami, M.; Mori, S. Design of Alkylsulfate Ionic Liquids for Lubricants. Chem. Lett. 2009, 38, 1, 64-65.

[65] Kajdas, Czeslaw. Importance of anionic reactive intermediates for lubricant component reactions with friction surfaces. Lubrication Science 1994;6:203-228.

[66] Sharma V, Doerr N, Aswath P. Chemical–mechanical properties of tribofilms and their relationship to ionic liquid chemistry. The royal society of chemistry advance 2016;6:22341-22356.

[67] Gandhi K. A review of ionic liquids, their limits and applications. Green and sustainable chemistry 2014;4:44-47.

[68] ASTM International. ASTM D5183-05 (2011) Standard Test Method For Determination of Coefficient of Friction of Lubricants Using the Four-Ball Wear Test Machine. DOI: 10.1520/D5183-05R11. In: Anonymous Book of ASTM standards, Weat Conshohocken, PA: ASTM; 2003.

[69] Jinyong Wang, Haibin Chu, and Yan Li. Why single walled carbon nanotubes can be dispersed in imidazolium based ionic liquids. ASC Nano 2008;2540-2546.

[70] Antony J, Mittal B, Naithani K, Misra A and Bhatnagar A. Antiwear/extreme pressure performance of graphite and molybdenum disulphide combinations in lubricating greases. Wear 1994;174:33-37.

[71] Sharma V, Gabler C, Doerr N, Aswath P. Mechanism of tribofilm formation with P and S containing ionic liquid. Tribology international 2015;92:353-364.

[72] Chen C, Chen X, Xu L, Yang Z, Li W. Modification of multi-walled carbon nanotubes with fatty acid and their tribological properties as lubricant additive, Carbon 2005;43:1660-1666.

[73] Tao, X., Jiazheng, Z. and Kang, X. The ball-bearing effect of diamond nano particles as an oil additivie. Journal of Physics 1996,29:2932-2937.

[74] Reich R, Stewart P, Bohaychick J, Urbanski J. Base oil properties of ionic liquid. Lubrication engineering 2003, 59;16-21.

[75] Four Ball sketch

(http://tribolab.mas.bg.ac.rs/english/images/equipment/four%20ball_sketch.jpg). electronic;2012.

[76] Lloyd A, Cackette T. Diesel engines: environmental impact and control. Journal of air and waste management association 2001;51:809-847.

[77] Bhatia, R, Lopipero, P. Smith, A. Diesel Exhaust Exposure and Lung Cancer; Epidemiology 1998;9:84-91.

[78] Sayin C, Metin Ertunc H, Hosoz M, Kilicaslan I, Canakci M. Performance and exhaust emissions of a gasoline engine using artificial neural network. Applied Thermal Engineering 2007;27:46-54.

[79] Ouenou-Gamo S, Ouladsine M, Rachid A. Measurement and prediction of diesel engine exhaust emissions. ISA Transactions 1998;37:135-140.

[80] Erol A, Ismet C. A diesel engine's performance and exhaust emissions. Applied Energy 2005;80:11-22.

[81] Zheng M, Reader G, Hawley G. Diesel engine exhaust gas recirculation-a review on advanced and novel concepts. Energy conversion and management 2004;45:883-900.

[82] Timothy J, Dennis A, Zoran F. The Impact of Exhaust Gas Recirculation on Performance and Emissions of a Heavy-Duty Diesel Engine. Society of automotive engineers 2003.

[83] Ajayi O, Erck R, Erdemir A, Fenske G, Goldblatt I. Effect of exhaust gas recirculation (EGR) on diesel engine oil- Impact on wear. 14th DEER Conference, MI, 2008;4-7.

[84] Daido S, Kodama Y, Inohara T, Ohyama N, Sugiyama T. Analysis of soot accumulation inside diesel engines. Society of automotive engineers of Japan 2000;21:303-308.

[85] Dennis A, Garner C, Taylor D. The effect of EGR on diesel engine wear. SAE technical paper 1999; Paper Number 1999-01-0839.

[86] Cadman W, Johnson JH. Study of the effect of exhaust gas recirculation on engine wear in a heavy-duty diesel engine using analytical ferrography. International Congress and Exposition - Society of Automotive Engineers. 1986; SAE, Warrendae, PA, USA.

[87] Jap T-, Li S, Yatsunami K, Chen SJ, Csontos AA, Howe JM. Soot Characterisation and Diesel Engine Wear. Lubrication Science 2004;16:111-26.

[88] Gautam M, Durbha M, Chitoor K, Jaraiedi M, Mariwalla N, Ripple D. Contribution of soot contaminated oils to wear. Proceedings of the 1998 SAE International Spring Fuels & Lubricants Meeting & Exposition;1372:55-67.

[89] Berbezier I, Martin JM, Kapsa P. Role of carbon in lubricated mild wear. Tribology International 1986;19:115-22.

[90] Yoshida K. Effects of sliding speed and temperature on tribological behavior with oils containing a polymer additive or soot. Tribol Trans 1990;33:221-8.

[91] Colacicco P, Mazuyer D. Role of soot aggregation on the lubrication of diesel engines. Tribol Trans 1995;38:959-65.

[92] Rounds FG. Soots from used diesel engine oils - Their effects on wear as measured in 4-ball wear tests. SAE Technical Paper 1981:Paper Number 810499.

[93] Rounds FG. Carbon: Cause of diesel engine wear? SAE Technical Paper 1977:Paper Number 770829.

[94] Corso S, Adamo R. Effect of diesel soot on reactivity of oil additives and valve train materials. Heavy Duty Diesel Lubrication. Fuels and Lubricants Meeting & Exposition. 1984:41-55.

[95] Akiyama K, Masunaga K, Kado K, Yoshioka T. Cylinder wear mechanism in an EGR equipped diesel engine and wear protection by the engine oil. SAE Technical Paper 1987:Paper Number 872158.

[96] Dairene Uy, Ford M, Jayne D, O'Neill A, Haack L, Hangas J, Jagner M, Sammut A, Gangopadhyay A, Characterization of gasoline soot and comparison to diesel soot: Morphology, chemistry, and wear. Tribology International 2014;80:198-209.

[97] Rocca A, Bonatesta F, Fay M, Campanella F, Characterisation of soot in oil from a gasoline direct injection engine using Transmission Electron Microscopy. Tribology International 2015;86:77-84.

[98] Hussain J, Palaniradja K, Alagumurthi N, Manimaran R. Effect of Exhaust Gas Recirculation (EGR) on Performance and Emission characteristics of a Three Cylinder Direct Injection Compression Ignition Engine. Alexandria engineering journal 2012;51:241-247.

[99] Glassman I. Soot formation in combustion processes. Twenty-second international symposium on combustion 1988; 295-311.

[100] Tree D, Svensson K, Soot processes in compression ignition engines, Progress in Energy and Combustion Science 2007;33:272-309.

[101] Kittelson D, Kraft M. Particle Formation and Models in Internal Combustion Engines. Cambridge Centre for Computational Chemical Engineering, University of Cambridge, Technical Report, 31st January 2014.

[102] Dec J, Espey C. A conceptual model of DI diesel combustion based on laser-sheet imaging. SAE Paper 970873, 1997.

[103] Kitsopanidis I. Experimental and computational study of soot formation under diesel engine conditions. Massachusetts Institute of Technology. Dept. of Mechanical Engineering, Thesis Report, 2004.

[104] Ho R J, Yusoff M Z, Palanisamy K. Trend and future of diesel engine: Development of high efficiency and low emission low temperature combustion diesel engine. 4th International Conference on Energy and Environment 2013.

[105] Dec, J. and Espey, C. Ignition and Early Soot Formation in a DI Diesel Engine Using Multiple 2-D Imaging Diagnostics, SAE Technical Paper 950456, 1995.

[106] Haynes B, Wagner H, Soot formation, Progress in Energy and Combustion Science 1981:229-273.

[107] Smith O, Fundamentals of soot formation in flames with application to diesel engine particulate emissions, Progress in Energy and Combustion Science 1981;7:275-291.

[108] Sander M, Patterson R, Braumann A, Raj A, Kraft M. Developing the PAH-PP soot particle model using process informatics and uncertainty propagation. The combustion institute 2010.

[109] Markatou P, Wang H, Frenklach M. A computational study of sooting limits in laminar premixed flames of ethane, ethylene, and acetylene. Combustion and Flame 1993;93:467-482.

[110] Graham S. The collisional growth of soot particles at high temperatures, Symposium (International) on Combustion 1977;16:663-669.

[111] J. Houston Miller, Anthony Hamins, and Trudy A. Kohout. Soot formation in hydrocarbon diffusion flames. Pages 505-512.

[112] Karataş A, Guilder O. Soot formation in high pressure laminar diffusion flames. Progress in Energy and Combustion Science 2012;38:818-845.

[113] Jun X, Bei-Jing Z. Soot in diesel combustion systems. Chemical engineering technology 2009;29:665-673.

[114] Ryason P, Chan I, Gilmore J. Polishing wear by soot. Wear 1990;137:15–24.

[115] Needelman W, Madhavan P. Review of lubricant contamination and diesel engine wear. SAE 881827, 1988.

[116] Narita, K. The effects of diesel soot on engine oil performance. Japan Journal of Tribology 1997;42:677–683.

[117] Aldajah S, Ajayi OO, Fenske GR, Goldblatt IL. Effect of exhaust gas recirculation (EGR) contamination of diesel engine oil on wear. Wear 2007;263:93-8.

[118] George S, Balla S, Gautam V, Gautam M. Effect of diesel soot on lubricant oil viscosity. Tribology International 2007;40:809–818.

[119] Gautam M, Chitoor K, Durbha M, Summers J. Effect of diesel soot contaminated oil on engine wear investigation of novel oil formulations. Tribology International 1999;32:687–699.

[120] Gautam, Durbha M, Chitoor K, Jaraiedi M, Mariwalla N, Ripple D. Contribution of soot contaminated oils to wear. SAE 981406, 1998.

[121] Gautam M, Chitoor K, Balla S, Keane M. Contibution of soot contaminated oils to wear-part II. SAE 1999-01-1519, 1999.

[122] George S, Balla S, Gautam M. Effect of diesel soot contaminated oil on engine wear. Wear 2007;262:1113-1122.

[123] Patel M, Cristy Leonor Azanza Ricardo, Scardi P, Aswath P. Morphology, structure and chemistry of extracted diesel soot—Part I: Transmission electron microscopy, Raman spectroscopy, X-ray photoelectron spectroscopy and synchrotron X-ray diffraction study. Tribology International 2012;52:29-39.

[124] Patel M, Aswath P. Morphology, structure and chemistry of extracted diesel soot: Part II: X-ray absorption near edge structure (XANES) spectroscopy and high resolution transmission electron microscopy. Tribology International 2012;52:17-28.

[125] Salehi F, Khaemba D, Morina A, Neville A. Corrosive–Abrasive Wear Induced by Soot in Boundary Lubrication Regime. Tribol Lett 2016;63-19.

[126] Gligorijevic R, Jevtic J and Borak D. Engine oil contribution to diesel exhaust emissions. Journal of synthetic lubrication 2006;23:27-38.

[127] Stachowiak GW, Batchelor AW. Engineering Tribology. Butterworth Heinemann, 2001.

[128] Leslie R. Rudnick. Lubricants Additives: Chemistry and Applications. January 29, 2003;143:168.

[129] Leslie R. Rudnick. Lubricants Additives: Chemistry and Applications. January 29, 2003;123:135.

[130] Willermet PA, Kandah SK, Siegl WO. Chase RE. The influence of molecular oxygen on wear protection by surface active compounds. ASLE preprint No. 82-LC-4C-4.

[131] Willermet PA, Kandah SK. Some observations on the role of oxygen in lubricated wear. Lubr Sci 1993;5(5-2):129–47.

[132] Willermet PA, Mahoney LR, Haas CM. The effects of antioxidant reactions on the wear behaviour of a zinc dialkyldithiophosphate. ASLE Trans 1978;22(4):301–6.

[133] Willermet P.A, Kandah S.K. Lubricant degradation and wear V. reaction products of a zinc dialkyldithiophosphate and peroxyradicals. ASLE Trans 1984;27(1):67–72.

[134] Nicholls M, Do T, Norton P, Kasrai M, Bancroft M. Review ofthe lubrication ofmetallic surfaces by zinc dialkyl dithiophosphates. Tribology international 2005;38:15-39.

[135] Fuller M, Kasrai M, Michael Bancroft M, Fyfe K,Tan K. Solution decomposition of zinc dialkyl dithiophosphate and its effect on antiwear and thermal film formation studied by X-ray absorption spectroscopy. Tribology international 1998;31:627-644.

[136] Fujita H, Glovnea R, Spikes H. Study of zinc dialkydithiophosphate antiwear tribofilm formation and removal process, Part I: Experimental. Tribology Transactions 2007;48:558-566.

[137] Fujita H, Spikes H. The formation of zinc dialkyl dithiophosphate antiwear films. Journal of engineering tribology 2004;218:265-278.

[138] Jaeger, J.C. Moving sources of heat and the temperature at sliding contacts. Proc. R. Soc. NSW 1942;56:203–214.

[139] Mosey N.J, Muser M.H., Woo T.K. Molecular mechanisms for the functionality of lubricant additives. Science 2005;307:1612–1615.

[140] Kajdas C, Tummler R., von Ardenne H., Schwarz W. The relevance of negative ion mass spectroscopy to the interpretation of the reaction of metal dialkyldithiophosphates during lubricated rubbing. ZFI Mitteilungen 1986;115: 107–112.

[141] Zhang J, Spikes H. On the Mechanism of ZDDP Antiwear Film Formation. Tribol Lett 2016; 63:24.

[142] Choa SH, Ludema KC, Potter GE, DeKoven BM, Morgan TA, Kar KK. A model of the dynamics of boundary film formation. Wear 1994;177:33–45.

[143] Varlot K, Martin JM, Grossiord C, Vargiolu R, Vacher B, Inoue K. A dual-analysis approach in tribochemistry: application to ZDDP/calcium borate additive interactions. Tribology Letters 1999;6:181–189.

[144] Bovington CH, Dacre B. The adsorption and reaction of decomposition products of zinc di-isopropyldiophosphate on steel. ASLE Transactions 1984;27:252–258.

[145] Dacre B, Bovington CH. The effect of metal composition on the adsorption of zinc di-isopropyldithiophosphate. ASLE Transactions 1983;26:333–343.

[146] Habeeb JJ, Stover WH. The role of hydroperoxides in engine wear and the effect of zinc dialkyldithiophosphates. ASLE Transactions 1987;30:419–426.

[147] Paddy JL, Lee NJC, Waters DN, Trott W. Zinc dialkyldithiophosphate oxidation by cumene hydroperoxide: kinetic studies by raman and 31P NMR spectroscopy. Tribology Transactions 1990;33:15–20.

[148] Spedding H, Watkins R. The antiwear mechanism of zddp's. Tribology international 1982;9-12.

[149] Glaeser WA, Baer D, Engelhardt M. In situ wear experiments in the scanning auger spectrometer. Wear 1993;162–164.

[150] Bell JC, Delargy KM, Seeney AM. The removal of substrate material through thick zinc dithiophosphate anti wear films. Wear particles. Tribology series 1992;21:387–96

[151] Ferrari ES, Roberts KJ, Sansone M, Adams D. A multi-edge X-ray absorption spectroscopy study of the reactivity of zinc di-alkyl-di-thiophosphates anti-wear additives 2. In situ studies of steel/oil interfaces. Wear 1999;236:259-275.

[152] Ng E, Sinha S, Satyanarayana N, Lim C and Narayan A. Effect of ZDDP and ashless triphenyl phosphorothionate (TPPT) as lubricant additives on the tribological performance of Cr-N coatings.Tribology-materials, surfaces and interfaces 2014.

[153] Sarin R, Tuli DK, Sureshbabu AV, Misra AK, Rai MM and Bhatnagar AK. Molybdenum dialkylphosphorodithioates: synthesis and performance evaluation as multifunctional additives for lubricants. Tribology international 1994;27:379-386.

[154] Zhang Z, YamaguchI E, Kasrai M, Bancroft G, Liu X, Fleet M. Tribofilms generated from ZDDP and DDP on steel surfaces: Part 2, chemistry. Tribology Letters 2005;19:221-229.

[155] Sharma V, Erdemir A, Aswath P. An analytical study of tribofilms generated by the interaction of ashless antiwear additives with ZDDP using XANES and nano-indentation. Tribology International 2015;82:43-57.

[156] Nicholls MA, Norton PR, Bancroft GM, Kasrai M, Do T, Frazer BT, Stasio G. Nanometer Scale Chemomechanical Characterization of Antiwear Films. Tribol. Lett. 2004;17:205-216.

[157] Z. Yin, M. Kasrai, M. Fuller, G.M. Bancroft, K. Fyfe, K.H. Tan, Application of soft X-ray absorption spectroscopy in chemical characterization of antiwear films generated by ZDDP part I: the effects of physical parameters. Wear 1991;202:172-191.

[158] Kim B, Mourhatch R, Aswath P. Properties of tribofilms formed with ashless dithiophosphate and zinc dialkyl dithiophosphate under extreme pressure conditions. Wear 2010;268:579-591.

[159] Kim B, Jiang J, Aswath P. Mechanism of wear at extreme load and boundary conditions with ashless anti-wear additives: Analysis of wear surfaces and wear debris. Wear 2011;270:181-194.

[160] Sharma V, Doerr N, Aswath P. Chemical–mechanical properties of tribofilms and their relationship to ionic liquid chemistry. The royal society of chemistry advance 2016;6:22341-22356.

[161] Sharma V, Gabler C, Doerr N, Aswath P. Mechanism of tribofilm formation with P and S containing ionic liquid. Tribology international 2015;92:353-364.

[162] Gandhi K. A review of ionic liquids, their limits and applications. Green and sustainable chemistry 2014;4:44-53.

[163] Qu J, Truhan JJ, Dai S, Luo H , Blau PJ. Ionic liquids with ammonium cations as lubricants or additives. Tribology letters 2006;22:207-214.

[164] Qu J, Blau P, Dai S, Luo H, Harry M. Meyer III, Truhan J. Tribological characteristics of aluminum alloys sliding against steel lubricated by ammonium and imidazolium ionic liquids. Wear 2009;267:1226-1231.

[165] Jimenez AE, Bermúdez MD, Carrión FJ, Martínez-Nicolás G. Room temperature ionic liquids as lubricant additives in steel–aluminium contacts: Influence of sliding velocity, normal load and temperature. Wear 2006;261: 347-359.

[166] LiJun W, XuQing L, YongMin L, QunJi X Effect of tetraalkylphosphonium based ionic liquids as lubricants on the tribological performance of a steel-on-steel system. Tribology letters 2007;26:11-17.

[167] Kinzig B, Sutor P, Sawyer G, Rennie A, Dickrell P, Gresham J. Novel ionic liquid lubricants for aerospace and MEMS. Proceedings of World Tribology Congress III September 12-16, 2005, Washington, D.C, USA.

[168] Weimin L, Zonggang M, Xiaoxuan W, Shuxiang Z. Investigation of Tribological Behavior of Al–Si Alloy Against Steel Lubricated with Ionic Liquids of 1-Diethylphosphonyl-*n*-propyl-3-Alkylimidazolium Tetrafluoroborate. Journal of tribology 2008;130:034501-034505.

[169] Bo Y, Feng Z, Chongjun P, Bo W, Yongmin L, Weimin L. Tribological evaluation of α, ω-diimidazoliumalkylene hexafluorophosphate ionic liquid and benzotriazole as additive. Tribology international 2008;41:797-801.

[170] Anand M, Hadfield M, Viesca J, Thomas B, Hernández Battez A, Austen S. Ionic liquids as tribological performance improving additive for in-service and used fully-formulated diesel engine lubricants. Wear 2015;334–335:67-74.

[171] Jones W, Shogrin B, Jansen M. Research on Liquid Lubricants for Space Mechanisms. JSL 17-2:109-122.

[172] Jun Q, Huimin L, Miaofang C, Cheng M, Peter B, Sheng D, Michael V. Comparison of an oil-miscible ionic liquid and ZDDP as a lubricant anti-wear additive. Tribology International 2014;71:88-97.

[173] Ichiro M, Taketo I, Ryusuke S, Hidetaka N. Tribo-Chemistry of Phosphonium-Derived Ionic Liquids. Tribo Lett 2010;40:225-235.

[174] Gabler C, Doerr N, Allmaier G. Influence of cationic moieties on the tribolayer constitution shown for bis(trifluoromethylsulfonyl)imide based ionic liquids studied by X-ray photo electron spectroscopy. Tribology international 2014;80:90-97.

[175] Shank G, Goshorn K, Cooper M, Dam W, Richards S. A History of mack engine lubricants tests from 1985-2005: Mack T-7 through Mack T-12. SAE Technical Paper 2005;2005-01-3713.

[176] Olomolehin Y, Kapadia R, Spikes H. Antagonistic Interaction of Antiwear Additives and Carbon Black. Tibo Lette 2010;37:49-58.

[177] F. Motamen Salehi F, Khaemba D, Morina A, Neville A. Corrosive–Abrasive Wear Induced by Soot in Boundary Lubrication Regime. Tribo Lette 2016; 63:19.

[178] Mourhatch R, Aswath PB. Tribological behavior and nature of tribofilms generated from fluorinated ZDDP in comparison to ZDDP under extreme pressure conditions---Part 1: Structure and chemistry of tribofilms. Tribol Int 2011;44:187-200.

[179] Mourhatch R, Aswath PB. Tribological behavior and nature of tribofilms generated from fluorinated ZDDP in comparison to ZDDP under extreme pressure conditions-Part II: Morphology and nanoscale properties of tribofilms. Tribol Int 2011;44:201-10.

[180] Kasrai M, Yin Z, Fuller M, Bancroft GM, Fyfe K, Tan KH. Application of XAFS in tribology: P and S L-edge XANES spectroscopy of antiwear films. Journal De Physique IV : JP 1997;7:2-847.

[181] Yehliu, K., Vander Wal, R. L. & Boehman, A. L. Development of an HRTEM image analysis method to quantify carbon nanostructure. Combustion Flame 2011; 158:1837–1851.

[182] Patel, M. Fundamental understanding of soot induced wear mechanism of diesel engines. Ph.D. Thesis, University of Texas at Arlington, Arlington, TX, 2014.

[183] Al-Qurashi, K. & Boehman, A. L. Impact of exhaust gas recirculation (EGR) on the oxidative reactivity of diesel engine soot. Combustion Flame 2008; 155: 675-695.

[184] Ratoi, M., Castle, R., Bovington, C., Spikes, H.A. Influence of soot and dispersant on ZDDP film thickness and friction. Lubrication Science 2004; 17: 25–43.

[185] Bardasz E, Carrick V, Ebeling V, George H. Understanding soot related oil thickening through designed experimentation Part 2: GM 6.5 L. SAE technical paper 1996. Paper number 961915.

[186] Sato T, Saito H, Korematsu K, Tanaka J. Study on wear of piston rings in diesel engines with exhaust gas recirculation. Proceedings of the 2001 Spring Technical Conference of the ASME Internal Combustion Engine Division, April 29, 2001 - May 23 2001;36:39-45.

[187] Green DA, Lewis R. The effects of soot-contaminated engine oil on wear and friction: A review. Proc Inst Mech Eng Pt D: J Automobile Eng 2008;222:1669-1689.

[188] Patel M, Aswath P, Structure and chemistry of crankcase and cylinder soot and tribofilms on piston rings from a Mack T-12 dynamometer engine test, Tribology International 2014,77:111-121.

[189] Fujita H, Glovnea R, Spikes H. Study of zinc dialkyl dithiophosphate antiwear film formation and removal processes, Part I experimental. Tribology transactions 2007,48:558-566.

[190] Yamaguchi ES, Zhang Z, Kasrai M, Bancroft GM. Study of the interaction of ZDDP and dispersants using x-ray absorption near edge structure spectroscopy. Part 2: tribochemical reactions. Tribol Lett 2003;15:385–94.

[191] Beshouri, G.M.: Lubricant additive effects on cam and tappet wear in medium speed diesel engines. SAE Paper 860377 (1986).

[192] Booth, J.E., Nelson, K.D., Harvey, T.J., Wood, R.J.K., Wang, L., Powrie, H.E.G., Martinez, J.G. The feasibility of using electrostatic monitoring to identify diesel lubricant additives and soot contamination interactions by factorial analysis. Tribology International 2006; 39: 1564–1575.

[193] Yoshihara, T., Wakizono, T., Hara, H., Nakagawa, E.: Effects of engine oil additives on valve train wear of diesel engines. SAE Paper 831759 (1983).

Biographical Information

Kimaya Vyavhare was born and raised in western part of India and did her schooling in the state of Maharashtra. She pursued her Bachelors from the autonomous college, College of Engineering Pune in Metallurgy and Material Science. She showcased a strong research aptitude by doing several internships and projects with the organizations like Cummins Inc, Bhabha Atomic Research Center, Shembekar foundary during four years of bachelor term. Her final year project was on the synthesis and characterization of sodium beta alumina, which received well appreciation at the international conference of powder metallurgy association (PMAI). With a strong desire to pursue research carrier, she joined in for material science and engineering master's graduation program at University of Texas at Arlington. She was appointed as a research assistant in the department and worked in the Tribology, Lubrication and Coatings (TLCL) laboratory under the guidance of Dr. Pranesh Aswath. She worked on several projects related to Tribological testing, extreme pressure grease formulation, evaluation of different additive tribological performance in oil and grease, materials characterization lubricant formulation, extreme pressure grease formulation and evaluation, materials characterization, surface analysis and metallography. She considers himself extremely fortunate to have worked under the guidance of Dr. Aswath.